SPACE SCIENCES LABORATORY

INTEGRAL EQUATION FORMULATIONS OF SCATTERING FROM TWO-DIMENSIONAL INHOMOGENEITIES IN A CONDUCTIVE EARTH

By
John Robert Parry

Final Report on
NASA Contract NAS2-5078
Item 324
Part I

August 1969

Space Sciences Laboratory Series 11 Issue 46

UNIVERSITY OF CALIFORNIA, BERKELEY

Space Sciences Laboratory
University of California
Berkeley, California 94720

INTEGRAL EQUATION FORMULATIONS OF SCATTERING FROM TWO-DIMENSIONAL INHOMOGENEITIES IN A CONDUCTIVE EARTH

By
John Robert Parry

Final Report on NASA Contract NAS2-5078
Item 324
Part I

August 1969

Space Sciences Laboratory Series 11 Issue 46

TABLE OF CONTENTS

INTEGRAL EQUATION FORMULATIONS OF SCATTERING FROM TWO-DIMENSIONAL INHOMOGENEITIES IN A CONDUCTIVE EARTH

John Robert Parry

ABSTRACT

The electromagnetic fields scattered by finitely conducting cylinders of arbitrary cross section in a conductive half-space with an arbitrary earth-air profile are calculated. The following conclusions of importance to geophysical exploration are reached: 1) The ratio of real $(\vec{H})$ to imaginary $(\vec{H})$ is a function of traverse position x and ground conductivity σ_1 as well as the cylinder conductivity σ_2; 2) Topography can give rise to a tilt angle of about 5° at an operating frequency of 1000 hz., ground conductivity of 10^{-3} mhos/m and normal incidence of an E_y-polarized plane wave; and 3) In no case was a zero phase observed, even for perfectly conducting scatterers.

The problem is formulated by choosing an integral representation for the electromagnetic fields in each homogeneous region present. By enforcing the boundary conditions on tangential $\vec{E}$ and $\vec{H}$, a set of coupled integral equations results which can be solved numerically for the unknown equivalent surface current densities on the interface bounding each homogeneous region. Once these current densities have been estimated, the fields can be calculated at any point from the general integral representations.

The validity and accuracy of the integral equations are demonstrated by comparing numerical results with analytical results for scattering from circular cylinders in a conductive whole-space assuming plane wave

and line source incident fields. It is shown that three-dimensional source configurations can be considered by expanding the primary current distribution and the field it radiates into a Fourier integral over a continuous mode distribution.

ACKNOWLEDGEMENTS

This research has been conducted under contract NAS2-5078 with the National Aeronautics and Space Administration.

I would like to acknowledge the assistance of S.H. Ward, H.F. Morrison, and A.R. Neureuther who served on my thesis committee. K.K. Mei was helpful in pointing out pertinent literature in the early stages of this research.

I greatly appreciated the discussions with and suggestions from students in Engineering Geoscience. In particular, I would like to thank J.C. Coggon, B.D. Fuller, and G.W. Hohman. I am also indebted to D. Dufalla for his assistance in programming and running the models, especially towards the end of this research.

To the secretaries and my superb draughtswoman, I owe many thanks.

Finally, I would like especially to thank my wife, Julie, whose good nature and encouragement helped to make this research the pleasure it was.

CHAPTER 1

INTRODUCTION

The determination of the electromagnetic fields scattered by conducting inhomogeneities reduces to the solution of a vector Helmholtz equation. Unfortunately, the classical method of solution yields analytical results only for those inhomogeneities whose surfaces coincide with coordinate surfaces of orthogonal coordinate systems in which the vector Helmholtz equation is solvable by the method of separation of variables. In these special cases, which include wedges, spheres and circular, elliptic and parabolic cylinders, the fields in each homogeneous region are expressed as a sum of mode functions, and the unknown constants are determined by matching boundary conditions. This theory has led to useful solutions for scattering from objects of simple geometry in a conductive whole-space when the characteristic dimensions of the inhomogeneity do not exceed about 25 wavelengths. In the past, the important geophysical problems of scattering from multiple conductors, conductors of arbitrary shape, and conductors in a conductive half-space have received little attention because of the intractability of their formal solution.

The possibility of a general numerical solution of antenna and scattering problems was suggested first about ten years ago by Sinclair (1959), and was based upon an integral equation approach investigated by Albert and Synge (1948) and Synge (1948). In this short paper, Sinclair pointed out that with the availability of high speed digital computers it is possible to obtain numerical solutions of electromagnetic boundary

value problems where suitable analytical solutions are often difficult to obtain. He notes that while ". . . analytical solutions may be aesthetically more pleasing than numerical solutions, . . . this is of little interest to the engineer concerned with the design of a particular electromagnetic system."

Of perhaps more importance is that he notes also that ". . . even when analytical solutions can be obtained for electromagnetic problems, it is usually found that a great amount of calculation is required to obtain numerical values, as, for example, when wave functions in a given coordinate system have to be computed. In many cases, direct numerical solution of a suitable differential or integral equation can yield the same accuracy of result with little, if any, increase in the amount of computing required." In particular, we might note that D'Yakonov (1959 a,b) has published a solution to a circular cylinder and a sphere in a conductive half-space, and we have yet to witness numerical results for either of these particular problems.

Some of the first numerical results of electromagnetic scattering problems were presented by Mei and Van Bladel (1963 a,b) and Andreasen (1964, 1965 a,b). Later published work includes significant papers by Mitzner (1967, 1968). In these papers, the electromagnetic fields exterior to the inhomogeneities are written in terms of integrals around the contour bounding each inhomogeneity and in terms of a surface impedance boundary condition. These integrals involve the two-dimensional Green's function and equivalent electric and magnetic surface current densities at the boundary of each inhomogeneity. The unknown equivalent current densities are estimated by enforcing the electromagnetic boundary conditions at a finite number of points on the boundary of each inhomogeneity. In so

doing, a number of sampled values of the unknown current distribution is determined, from which the scattered fields can be calculated at any point using the general integral representations.

In the present study, integral representations are chosen inside the scatterer as well as exterior to the scatterer. This approach removes restrictions upon the conductivity and curvature of the scatterer inherent in the above formulations, although it leads to more complicated integral equations. However, it leads also to a consideration of the problem of scattering from cylinders in a conductive half-space.

Since the coutour can be deformed into any shape desired, it is possible to formulate and solve any scattering problem within the storage and time limitations of a computer solution. Although this study will be restricted to scattering from two-dimensional inhomogeneities, it is shown that the incident field is arbitrary.

The purpose of this dissertation is to consider the theory of integral representations as applied to solving two-dimensional geophysical scattering problems. In particular, examples will be given to demonstrate the validity and generality of this approach. However, due to the length of this subject, a general numerical analysis of geophysical scattering problems must be left to a later study.

CHAPTER 2

DERIVATION OF INTEGRAL REPRESENTATIONS FOR $\vec{E}$ AND $\vec{H}$

Silver (1965, p. 201) has shown that if a two-dimensional waveguide is homogeneous in structure along the axial direction, only two independent field components, E_y and H_y, exist, and all other quantities may be derived from these. Since similar conclusions can be drawn for two-dimensional scattering problems, the first task in treatment of scattering problems is to obtain general representations of the axial field components.

Integral expressions for E_y and H_y were obtained by Papas (1950) and Borgnis and Papas (1955) in investigating scattering from circular cylinders of infinite conductivity. Andreasen (1965 b) showed that their work could be modified to general integral representations for E_y and H_y. In this paper, Andreasen assumed that the surface impedance of the inhomogeneity was very small with respect to the impedance of the exterior region so that his final integral representations are not sufficiently general for earth scattering problems.

We will follow Andreasen's development to obtain general integral representations for $\vec{E}$ and $\vec{H}$ interior and exterior to the cylinder. In section (2-5), it will be shown that the general integral representations reduce to those given by Andreasen if it is assumed that the scatterer has a low surface impedance and that the skin depth is much smaller than the radius of curvature. Although the integral representations in the exterior region are modified only slightly by making these approximations, the advantage obtained is that the solution of the resulting integral equations is much easier. However, if the problem of a cylinder in a con-

ductive half-space is to be examined, the general integral representations must be considered.

2-1 Derivation of Integral Expressions for E_y and H_y

We begin with Green's theorem (Stratton, 1941, p. 165) for any two scalar functions u and v,

$$\int_{Vol} \left\{ u \nabla^2 v - v \nabla^2 u \right\} d(vol) = \oint_{area} \left\{ u \frac{\partial v}{\partial n'} - v \frac{\partial u}{\partial n'} \right\} d(area). \quad (2\text{-}1)$$

In equation (2-1), $\partial/\partial n'$ is the derivative in the direction of the outward normal to the volume of interest, which is defined in Fig. 1 as the volume between the surfaces C_1 and C_2.

If we add and subtract $k^2 uv$ on the left-hand side of equation (2-1), we obtain

$$\int_{Vol} \left\{ u (\nabla^2 + k^2) v - v (\nabla^2 + k^2) u \right\} d(vol) = \oint_{area} \left\{ u \frac{\partial v}{\partial n'} - v \frac{\partial u}{\partial n'} \right\} d(area). \quad (2\text{-}2)$$

Assuming that the scatterer is two-dimensional, then an integral expression for $E_y(\bar{\rho})$, the total electric field intensity in the source free volume between C_1 and C_2, can be obtained by setting $u = E_y^t(\bar{\rho})$ and $v = G(\bar{\rho}, \bar{\rho}')$ where $E_y^t(\bar{\rho})$ and $G(\bar{\rho}, \bar{\rho}')$ satisfy the equations

$$\left.\begin{aligned} (\nabla^2 + k^2) E_y^t(\bar{\rho}) &= 0 \\ (\nabla^2 + k^2) G(\bar{\rho}, \bar{\rho}') &= -\delta(\bar{\rho} - \bar{\rho}') \end{aligned}\right\}. \quad (2\text{-}3)$$

The vector $\bar{\rho}'$ refers to a source point on the surface and $\bar{\rho}$ refers to a point in the volume between and on the surfaces C_1 and C_2. Applying equation (2-2)

to (2-3), we obtain

$$-\int_{Vol} E_y^t(\bar{\rho})\,\delta(\bar{\rho}-\bar{\rho}')\,d(vol) = -E_y^t(\bar{\rho}') = \int_{area}\left\{E_y^t(\bar{\rho})\frac{\partial G}{\partial n'}(\bar{\rho},\bar{\rho}') - G(\bar{\rho},\bar{\rho}')\frac{\partial E_y^t}{\partial n'}(\bar{\rho}')\right\} d(area) \quad (2\text{-}4)$$

However, equation (2-4) gives $E_y^t(\bar{\rho}')$ at a source point in terms of the total field around the boundary. To obtain $E_y^t(\bar{\rho})$, we invoke the reciprocity relation of the observation point and the source point. As a result, we may interchange $\bar{\rho}$ and $\bar{\rho}'$ in equation (2-4) and replace $G(\bar{\rho}',\bar{\rho})$ by $G(\bar{\rho},\bar{\rho}')$ provided the Green's function is symmetric.

Morse and Feshbach (1953, p. 808) show that $G(\bar{\rho},\bar{\rho}')$ is symmetric if it satisfies some homogeneous boundary conditions on the boundary surfaces in both the $\bar{\rho}$ and $\bar{\rho}'$ coordinate system. Since the choice of which function we adopt for $G(\bar{\rho},\bar{\rho}')$ is optional provided equation (2-3) is satisfied (see Jackson, 1962, p. 18), we will ensure that $G(\bar{\rho},\bar{\rho}')$ is symmetrical by choosing the whole space value of $G(\bar{\rho},\bar{\rho}')$. Thus, a homogeneous Dirichlet boundary condition exists at infinity since $G(\bar{\rho},\bar{\rho}')$ satisfies the radiation condition.

Equation (2-4) now becomes

$$E_y^t(\bar{\rho}) = -\int_{C_1}\left\{E_y^t(\bar{\rho}')\frac{\partial G}{\partial n'}(\bar{\rho},\bar{\rho}') - G(\bar{\rho},\bar{\rho}')\frac{\partial E_y^t}{\partial n'}(\bar{\rho}')\right\} ds'$$

$$-\int_{C_2}\left\{E_y^t(\bar{\rho}')\frac{\partial G}{\partial n'}(\bar{\rho},\bar{\rho}') - G(\bar{\rho},\bar{\rho}')\frac{\partial E_y^t}{\partial n'}(\bar{\rho}')\right\} ds'. \quad (2\text{-}5)$$

The total electric field intensity at any point is represented by the sum of an incident electric field $E_y^i(\bar{\rho})$ and a scattered electric field $E_y^{sc}(\bar{\rho})$.

$$E_y^t(\bar{\rho}) = E_y^i(\bar{\rho}) + E_y^{sc}(\bar{\rho}) . \tag{2-6}$$

If we let the outer surface C_2 approach infinity, then the second integral of equation (2-5) becomes

$$\int_{C_2} \left\{ E_y^t(\bar{\rho}') \frac{\partial G}{\partial n'}(\bar{\rho},\bar{\rho}') - G(\bar{\rho},\bar{\rho}') \frac{\partial E_y^i}{\partial n'}(\bar{\rho}') \right\} ds'$$

$$+ \int_{C_2} \left\{ E_y^{sc}(\bar{\rho}') \frac{\partial G}{\partial n'}(\bar{\rho},\bar{\rho}') - G(\bar{\rho},\bar{\rho}') \frac{\partial E_y^{sc}}{\partial n'}(\bar{\rho}') \right\} ds'. \tag{2-7}$$

Stratton (1941, p. 360) states that every two-dimensional electromagnetic field at great distances from the source can be represented by linear combinations of elementary wave functions of the form $\psi_{nk} = e^{in\theta} H_n^{(1)}(k\rho) e^{-i\omega t}$. Assuming that the source of this wave is on a line, then the elementary wave functions are independant of θ and only ψ_{ok} is required. Thus, as $\rho \to \infty$, these (circular) cylindrical waves will behave like $\frac{e^{ik\rho}}{\sqrt{\rho}}$ when $H_o^{(1)}(k\rho)$ is expanded for large ρ.

As C_2 approaches infinity, the scattered field $E_y^{sc}(\bar{\rho}')$ and $G(\bar{\rho},\bar{\rho}')$ will behave as cylindrical waves for each point $\bar{\rho}'$ on C_2. Consequently, both functions will behave as $\frac{e^{ik\bar{\rho}'}}{\sqrt{\bar{\rho}'}}$ except for constant factors. As a result, the second term of (2-7) becomes

$$AB \int_{C_2} \left\{ \frac{e^{ik\bar{\rho}'}}{\sqrt{\bar{\rho}'}} \frac{\partial}{\partial n'} \left(\frac{e^{ik\bar{\rho}'}}{\sqrt{\bar{\rho}'}} \right) - \frac{e^{ik\bar{\rho}'}}{\sqrt{\bar{\rho}'}} \frac{\partial}{\partial n'} \left(\frac{e^{ik\bar{\rho}'}}{\sqrt{\bar{\rho}'}} \right) \right\} ds' ,$$

and the difference of the two terms under the second integral tends to zero for each $\bar{\rho}'$, and the contribution of the second integral is zero.

This is not true for the first integral since by assumption the incoming plane waves never vanish at infinity. In fact, the first integral is equal to $-E_y^i(\bar{\rho})$, which can be seen by applying equation (2-2) to

$$\left.\begin{aligned}(\nabla^2+k^2)\,E_y^i(\bar{\rho}) &= 0\\ (\nabla^2+k^2)\,G(\bar{\rho},\bar{\rho}') &= -\delta(\bar{\rho}-\bar{\rho}')\end{aligned}\right\}. \tag{2-8}$$

Equation (2 5) now becomes

$$E_y^t(\bar{\rho}) = E_y^i(\bar{\rho}) + \int_{C_1}\left\{G(\bar{\rho},\bar{\rho}')\frac{\partial E_y^t}{\partial n'}(\bar{\rho}') - E_y^t(\bar{\rho}')\frac{\partial G}{\partial n'}(\bar{\rho},\bar{\rho}')\right\} ds'. \tag{2-9}$$

By comparing equations (2-6) and (2-9), it is evident that the scattered electric field intensity is given by

$$E_y^{sc}(\bar{\rho}) = \int_{C_1}\left\{G(\bar{\rho},\bar{\rho}')\frac{\partial E_y^t}{\partial n'}(\bar{\rho}') - E_y^t(\bar{\rho}')\frac{\partial G}{\partial n'}(\bar{\rho},\bar{\rho}')\right\} ds'. \tag{2-10}$$

Similar expressions for $H_y^t(\bar{\rho})$ and $H_y^{sc}(\bar{\rho})$ can be obtained by setting $u = H_y^t(\bar{\rho})$ and $v = G(\bar{\rho},\bar{\rho}')$ in equation (2-2), where

$$\left.\begin{aligned}(\nabla^2+k^2)\,H_y^t(\bar{\rho}) &= 0\\ (\nabla^2+k^2)\,G(\bar{\rho},\bar{\rho}') &= -\delta(\bar{\rho}-\bar{\rho}')\end{aligned}\right\}. \tag{2-11}$$

Following a development which parallels the above, we find that

$$H_y^t(\bar{\rho}) = H_y^i(\bar{\rho}) + \int_{C_1}\left\{G(\bar{\rho},\bar{\rho}')\frac{\partial H_y^t}{\partial n'}(\bar{\rho}') - H_y^t(\bar{\rho}')\frac{\partial G}{\partial n'}(\bar{\rho},\bar{\rho}')\right\} ds', \tag{2-12}$$

$$H_y^{sc}(\bar{\rho}) = \int_{C_1}\left\{G(\bar{\rho},\bar{\rho}')\frac{\partial H_y^t}{\partial n'}(\bar{\rho}') - H_y^t(\bar{\rho}')\frac{\partial G}{\partial n'}(\bar{\rho},\bar{\rho}')\right\} ds'. \tag{2-13}$$

Equations (2-9) and (2-10) and equations (2-12) and (2-13) are integral expressions for $E_y(\bar{\rho})$ and $H_y(\rho)$ respectively. However, since a normal derivative of $E_y^t(\bar{\rho}')$ and $H_y^t(\bar{\rho}')$ is required rather than a tangential derivative, these expressions are not in a particularly convenient form. Andreasen (1965 b) has shown that by manipulating Maxwell's equations, the normal derivative of E_y and H_y can be transformed into more suitable forms. Using these representations, an integral equation solution for the unknown boundary values of $\vec{E}$ and $\vec{H}$ can be formulated easily.

2-2 Suitable Expressions for the Normal Derivatives of E_y and H_y

Starting with Maxwell's first two equations and assuming a time dependence of $e^{-i\omega t}$, then

$$\vec{\nabla} \times \vec{E} = -\frac{\partial \vec{B}}{\partial t} = i\mu\omega \vec{H} \quad , \tag{2-14}$$

$$\vec{\nabla} \times \vec{H} = \frac{\partial \vec{D}}{\partial t} + \vec{J} = (\sigma - i\omega\varepsilon)\vec{E} \quad , \tag{2-15}$$

from which we may write

$$i\mu\omega H_x = ik_y E_z - \frac{\partial E_y}{\partial z} \quad , \tag{2-16a}$$

$$i\mu\omega H_y = \frac{\partial E_x}{\partial z} - \frac{\partial E_z}{\partial x} \quad , \tag{2-16b}$$

$$i\mu\omega H_z = \frac{\partial E_y}{\partial x} - ik_y E_x \quad , \tag{2-16c}$$

and

$$(\sigma - i\omega\varepsilon) E_x = ik_y H_z - \frac{\partial H_y}{\partial z} , \tag{2-17a}$$

$$(\sigma - i\omega\varepsilon) E_y = \frac{\partial H_x}{\partial z} - \frac{\partial H_z}{\partial x} , \tag{2-17b}$$

$$(\sigma - i\omega\varepsilon) E_z = \frac{\partial H_y}{\partial x} - ik_y H_x . \tag{2-17c}$$

In equations (2-16) and (2-17), we have assumed that the y dependence of all field components is of the form $e^{ik_y y}$. Such an axial dependence would arise when a primary three-dimensional current distribution and the field it radiates has been expanded over a continuous mode distribution according to

$$\psi(x,y,z) = \frac{1}{2\pi} \int_{-\infty}^{\infty} \bar{\psi}(x,k_y,z)\, e^{ik_y y}\, dk_y . \tag{2-18}$$

However, this problem will be discussed in more detail in Chapter 6, when three-dimentional source distributions are considered. It is sufficient to note here that in the special case of a plane wave obliquely incident upon cylinders in free space, k_y reduces to the axial component of the free space propagation constant. Whenever a plane wave is incident normal to cylinders in a whole-space, k_y is zero.

Substituting (2-17c) into (2-16a), then

$$i\mu\omega H_x = \frac{ik_y}{(\sigma - i\omega\varepsilon)} \left(\frac{\partial H_y}{\partial x} - ik_y H_x \right) - \frac{\partial E_y}{\partial z} . \tag{2-19}$$

Rearranging in terms of H_x, we find that

$$\gamma^2 H_x = ik_y \frac{\partial H_y}{\partial x} - (\sigma - i\omega\varepsilon) \frac{\partial E_y}{\partial z} \quad , \tag{2-20}$$

where $$\gamma^2 = k^2 - k_y^2 \quad . \tag{2-21}$$

Similarly, substituting (2-17a) into (2-16c)

$$i\mu\omega H_z = \frac{\partial E_y}{\partial x} - \frac{ik_y}{(\sigma - i\omega\varepsilon)} \left(ik_y H_z - \frac{\partial H_y}{\partial z} \right) \quad , \tag{2-22}$$

or

$$\gamma^2 H_z = (\sigma - i\omega\varepsilon) \frac{\partial E_y}{\partial x} + ik_y \frac{\partial H_y}{\partial z} \quad . \tag{2-23}$$

Defining the positive tangental direction on the contour by

$$\hat{s} = \hat{n}' \times \hat{y} \quad , \tag{2-24}$$

and adding equations (2-20) and (2-23), we find that the transverse magnetic field intensity, $\vec{H}_{tr}$, is given by

$$\gamma^2 \vec{H}_t = ik_y \vec{\nabla}_t H_y + (\sigma - i\omega\varepsilon)(\vec{\nabla}_t E_y) \times \hat{y} \quad . \tag{2-25}$$

Following an analogous argument, we can obtain an expression for the transverse electric field intensity $\vec{E}_{tr}$. Substituting (2-16c) into (2-17a)

$$(\sigma - i\omega\varepsilon) E_x = \frac{ik_y}{i\mu\omega} \left(\frac{\partial E_y}{\partial x} - ik_y E_x \right) - \frac{\partial H_y}{\partial z} \quad , \tag{2-26}$$

or

$$\gamma^2 E_x = ik_y \frac{\partial E_y}{\partial x} - i\mu\omega \frac{\partial H_y}{\partial z} , \tag{2-27}$$

and substituting (2-16a) into (2-17c)

$$(\sigma - i\omega\varepsilon) E_z = \frac{\partial H_y}{\partial x} - \frac{ik_y}{i\mu\omega} \left(ik_y E_z - \frac{\partial E_y}{\partial z} \right) , \tag{2-28}$$

or

$$\gamma^2 E_z = i\mu\omega \frac{\partial H_y}{\partial x} + ik_y \frac{\partial E_y}{\partial z} . \tag{2-29}$$

Adding equations (2-27) and (2-29)

$$\gamma^2 \vec{E}_t = i\mu\omega \left(\vec{\nabla}_t H_y \right) \times \hat{y} + ik_y \vec{\nabla}_t E_y . \tag{2-30}$$

Taking the dot product of $\hat{s}$ and equations (2-25) and (2-30),

$$\gamma^2 H_s = ik_y \frac{\partial H_y}{\partial s} + (\sigma - i\omega\varepsilon) \frac{\partial E_y}{\partial n'} , \tag{2-31}$$

and

$$\gamma^2 E_s = i\mu\omega \frac{\partial H_y}{\partial n'} + ik_y \frac{\partial E_y}{\partial s} . \tag{2-32}$$

If we multiply (2-31) by $i\mu\omega$ and rearrange, then

$$\frac{\partial E_y}{\partial n'} = \frac{i\mu\omega}{k^2} \gamma^2 H_s + \frac{\mu\omega k_y}{k^2} \frac{\partial H_y}{\partial s} , \tag{2-33}$$

or

$$\frac{\partial E_y}{\partial n'} = \frac{i Z \gamma^2}{k} H_s + \frac{Z k_y}{k} \frac{\partial H_y}{\partial s} , \tag{2-34}$$

where Z is the intrinsic impedance of the medium and is given by $\frac{\mu\omega}{k}$. Similarly, equation (2-32) becomes

$$\frac{\partial H_y}{\partial n'} = - \frac{i \gamma^2}{Z k} E_s - \frac{k_y}{Z k} \frac{\partial E_y}{\partial s} . \tag{2-35}$$

If we substitute equation (2-34) and (2-35) into equations (2-9) and (2-12), we would obtain general integrodifferential representations for $E_y^t(\bar{\rho})$ and $H_y^t(\bar{\rho})$ in terms of the axial and tangential components of $\bar{E}$ and $\bar{H}$ on the contour. By applying the appropriate boundary conditions, we could determine E_y, E_s, H_y and H_s on the boundary and, with these quantities known, be able to calculate the scattered fields at any point in space. However, to conform with some of the terminology in the literature, and to obtain a more physical interpretation in certain instances, it is desirable to introduce the concept of equivalent electric and magnetic surface current densities (see Harrington, 1961, p. 106).

In brief, the equivalence principle states that many source distributions inside (outside) a given region can produce the same field outside (inside) that region*. As a result, equivalent electric and magnetic surface currents can be introduced to generate the same field external (internal) to a region as do the original sources internal (external) to that region. For our problem, these surface currents are

---

* Note that this informs us that the inverse problem is not unique.

chosen such that the boundary conditions, continuity of tangential $\vec{E}$ and tangential $\vec{H}$, are satisfied. Thus, the equivalent electric surface current density is set equal to the tangential component of the magnetic field intensity and the equivalent magnetic surface current density is set equal to the tangential component of the electric field intensity at the boundary.

From the continuity of tangential $\vec{H}$, we obtain

$$\hat{n} \times (\vec{H}_{ext} - \vec{H}_{int}) = 0 \,, \tag{2-36}$$

or

$$\hat{n} \times \vec{H}_{ext} = \hat{n} \times \vec{H}_{int} = \vec{K} \,, \tag{2-37}$$

where $\hat{n}$ is taken to be the outward normal from the scatterer. We conclude then, that the equivalent electric curface current density components are given by,

$$\hat{n} \times H_s \hat{s} \Rightarrow H_s = K_y \,, \tag{2-38a}$$

$$\hat{n} \times H_y \hat{y} \Rightarrow H_y = -K_s \,. \tag{2-38b}$$

Similarly, the equivalent magnetic surface current density components are given by,

$$E_s = M_y \,, \tag{2-39a}$$

$$E_y = -M_s \,. \tag{2-39b}$$

Upon introducing equations (2-38) and (2-39) into equations (2-34) and (2-35), our final expressions for the normal derivative of E_y and H_y on the boundary become

$$\frac{\partial E_y}{\partial n'} = \frac{i Z \gamma^2}{k} K_y - \frac{Z k_y}{k} \frac{\partial K_s}{\partial s} \,, \tag{2-40}$$

$$\frac{\partial H_y}{\partial n'} = -\frac{i \gamma^2}{Z k} M_y + \frac{k_y}{Z k} \frac{\partial M_s}{\partial s} \,. \tag{2-41}$$

2-3 General Field Representations for the Exterior Region

Coupled integrodifferential representations for $E_y^t(p)$ and $H_y^t(p)$ are obtained when equations (2-40) and (2-41) are introduced into (2-9) and (2-12).

$$E_y^t(\bar{\rho}) = E_y^i(\bar{\rho}) + \int_{C_1} G(\bar{\rho},\bar{\rho}') \left\{ i\frac{\eta\gamma^2}{k} K_y(\bar{\rho}') - \frac{\eta k_y}{k} \frac{\partial K_s}{\partial s'}(\bar{\rho}') \right\} ds' + \int_{C_1} M_s(\bar{\rho}') \frac{\partial G}{\partial n'}(\bar{\rho},\bar{\rho}')\, ds' \,, \tag{2-42}$$

and

$$H_y^t(\bar{\rho}) = H_y^i(\bar{\rho}) - \int_{C_1} G(\bar{\rho},\bar{\rho}') \left\{ \frac{i\gamma^2}{\eta k} M_y(\bar{\rho}') - \frac{k_y}{\eta k} \frac{\partial M_s}{\partial s'}(\bar{\rho}') \right\} ds' + \int_{C_1} K_s(\bar{\rho}') \frac{\partial G}{\partial n'}(\bar{\rho},\bar{\rho}')\, ds' \,. \tag{2-43}$$

It is shown in Appendix A that the two-dimensional Green's function is

$$G(\bar{\rho},\bar{\rho}') = \frac{i}{4} H_0^{(1)}(\gamma|\bar{\rho}-\bar{\rho}'|) \,, \tag{2-44}$$

where $H_0^{(1)}$ is the Hankel function of the first kind and order zero, representing an outgoing wave, and γ is the transverse propagation constant, and is related to the propagation constant k of the medium by equation (2-21).

The derivatives of the current components in equations (2-42) and (2-43) can be eliminated analytically with integration by parts. On carrying out the partial integration, and introducing equation (2-44), we find

$$E_y^t(\bar{\rho}) = E_y^i(\bar{\rho}) - \frac{Z\gamma^2}{4k}\int_{C_1} K_y(\bar{\rho}')\, H_o^{(1)}(\gamma|\bar{\rho}-\bar{\rho}'|)\, ds'$$

$$+ \frac{iZk_y}{4k}\int_{C_1} K_s(\bar{\rho}')\frac{\partial H_o^{(1)}}{\partial s'}(\gamma|\bar{\rho}-\bar{\rho}'|)ds' + \frac{i}{4}\int_{C_1} M_s(\bar{\rho}')\frac{\partial H_o^{(1)}}{\partial n'}(\gamma|\bar{\rho}-\bar{\rho}'|)\, ds', \quad (2\text{-}45)$$

and

$$H_y^t(\bar{\rho}) = H_y^i(\bar{\rho}) + \frac{\gamma^2}{4Zk}\int_{C_1} M_y(\bar{\rho}')\, H_o^{(1)}(\gamma|\bar{\rho}-\bar{\rho}'|)\, ds'$$

$$- \frac{ik_y}{4Zk}\int_{C_1} M_s(\bar{\rho}')\frac{\partial H_o^{(1)}}{\partial s'}(\gamma|\bar{\rho}-\bar{\rho}'|)ds' + \frac{i}{4}\int_{C_1} K_s(\bar{\rho}')\frac{\partial H_o^{(1)}}{\partial n'}(\gamma|\bar{\rho}-\bar{\rho}'|)\, ds'. \quad (2\text{-}46)$$

The normal and tangential derivatives of $H_o^{(1)}(\gamma|\bar{\rho}-\bar{\rho}'|)$ are given by

$$\frac{\partial H_o^{(1)}(\gamma|\bar{\rho}-\bar{\rho}'|)}{\partial\begin{pmatrix}n'\\ s'\end{pmatrix}} = \begin{pmatrix}\hat{n}'\\ \hat{s}'\end{pmatrix}\cdot\left[\nabla'_{\text{tan}}\, H_o^{(1)}(\gamma|\bar{\rho}-\bar{\rho}'|)\right]. \quad (2\text{-}47)$$

Since

$$\frac{dZ_\nu(\zeta)}{d\zeta} = -\frac{\nu}{\zeta}Z_\nu(\zeta) + Z_{\nu-1}(\zeta), \quad (2\text{-}48)$$

where $Z_\nu(\zeta)$ is any Bessel function,

and $Z_{-n}(\zeta) = (-1)^n Z_n(\zeta)$,

then

$$\frac{dZ_\nu(\gamma\zeta)}{dx} = \frac{dZ_\nu(\gamma\zeta)}{d(\gamma\zeta)}\cdot\frac{d(\gamma\zeta)}{dx} = \gamma\left[-\frac{\nu}{\gamma\zeta}Z_\nu(\gamma\zeta) + Z_{\nu-1}(\gamma\zeta)\right]\frac{d\zeta}{dx}. \quad (2\text{-}49)$$

Thus, the transverse derivative of $H_o^{(1)}(\gamma|\bar{\rho}-\bar{\rho}'|)$ is given by

$$\nabla'_{th}\, H_o^{(1)}(\gamma|\bar{\rho}-\bar{\rho}'|) = \left[\frac{d}{dx'}\hat{x} + \frac{d}{dz'}\hat{z}\right] H_o^{(1)}\left(\gamma\sqrt{(x-x')^2+(z-z')^2}\right)$$

$$= \frac{\gamma}{|\bar{\rho}-\bar{\rho}'|}\left[(x-x')\hat{x} + (z-z')\hat{z}\right] H_1^{(1)}(\gamma|\bar{\rho}-\bar{\rho}'|)$$

$$= \gamma\left(\cos\beta\,\hat{x} + \sin\beta\,\hat{z}\right) H_1^{(1)}(\gamma|\bar{\rho}-\bar{\rho}'|) \quad , \tag{2-50}$$

where β is defined in Fig. 2 as the angle formed by the $\hat{x}$ axis and the line between the point of observation and a point on the contour.

From Fig. 2, we have

$$\hat{n}' = \cos\alpha\,\hat{x} + \sin\alpha\,\hat{z} \quad , \tag{2-51}$$

$$\hat{n} = \cos(\alpha+180°)\hat{x} + \sin(\alpha+180°)\hat{z} = -\hat{n}' \quad , \tag{2-52}$$

$$\hat{s} = \cos(\alpha+90°)\hat{x} + \sin(\alpha+90°)\hat{z} = -\sin\alpha\,\hat{x} + \cos\alpha\,\hat{z} \, . \tag{2-53}$$

Using equations (2-50), (2-51) and (2-53), the normal and tangential derivatives of $H_0^{(1)}(\gamma|\bar{\rho}-\bar{\rho}'|)$ become

$$\frac{\partial}{\partial n'} H_0^{(1)}(\gamma|\bar{\rho}-\bar{\rho}'|) = \gamma\left(\cos\beta\cos\alpha + \sin\beta\sin\alpha\right) H_1^{(1)}(\gamma|\bar{\rho}-\bar{\rho}'|)$$

$$= \gamma\cos(\beta-\alpha)\, H_1^{(1)}(\gamma|\bar{\rho}-\bar{\rho}'|) \quad , \tag{2-54}$$

and

$$\frac{\partial}{\partial s'} H_0^{(1)}(\gamma|\bar{\rho}-\bar{\rho}'|) = \gamma\sin(\beta-\alpha)\, H_1^{(1)}(\gamma|\bar{\rho}-\bar{\rho}'|) \, . \tag{2-55}$$

When equations (2-54) and (2-55) are introduced into equations (2-45) and (2-46), we find

$$E_y^t(\bar{\rho}) = E_y^i(\bar{\rho}) - \frac{Z\gamma^2}{4k}\int_{C_1} K_y(\bar{\rho}')\, H_0^{(1)}(\gamma|\bar{\rho}-\bar{\rho}'|)\, ds'$$

$$+ \frac{iZk_y\gamma}{4k}\int_{C_1} K_s(\bar{\rho}')\sin(\beta-\alpha)\, H_1^{(1)}(\gamma|\bar{\rho}-\bar{\rho}'|)\, ds' + \frac{i\gamma}{4}\int_{C_1} M_s(\bar{\rho}')\cos(\beta-\alpha)\, H_1^{(1)}(\gamma|\bar{\rho}-\bar{\rho}'|)\, ds', \tag{2-56}$$

and

$$H_y^t(\bar{\rho}) = H_y^i(\bar{\rho}) + \frac{\gamma^2}{4Zk}\int_{C_1} M_y(\bar{\rho}')\, H_0^{(1)}(\gamma|\bar{\rho}-\bar{\rho}'|)\, ds'$$

$$- \frac{ik_y\gamma}{4Zk}\int_{C_1} M_s(\bar{\rho}')\sin(\beta-\alpha)\, H_1^{(1)}(\gamma|\bar{\rho}-\bar{\rho}'|)\, ds' + \frac{i\gamma}{4}\int_{C_1} K_s(\bar{\rho}')\cos(\beta-\alpha)\, H_1^{(1)}(\gamma|\bar{\rho}-\bar{\rho}'|)\, ds'. \tag{2-57}$$

Equations (2-56) and (2-57) are the desired coupled integral representations of $E_y^t(\bar{\rho})$ and $H_y^t(\bar{\rho})$ for the exterior problem. The point of observation, $\bar{\rho}$, is exterior to the inhomogeneities present, and C_1 represents a contour integration around each scatterer present. Once the equivalent surface current densities are known, the field components are determined from equations (2-14), (2-15), (2-56) and (2-57).

From equations (2-14) and (2-56), the scattered transverse magnetic field intensity is given by

$$\vec{H}_t = \frac{1}{i\mu\omega}\,\vec{\nabla}\times\left(E_y\,\hat{y}\right) = \frac{i}{\mu\omega}\left(\frac{\partial E_y}{\partial z}\,\hat{x} - \frac{\partial E_y}{\partial x}\,\hat{z}\right). \tag{2-58}$$

It follows from equation (2-49) that

$$\left(\frac{\partial}{\partial z}\hat{x} - \frac{\partial}{\partial x}\hat{z}\right) H_0^{(1)}(\gamma|\bar{\rho}-\bar{\rho}'|) = -\frac{\gamma}{|\bar{\rho}-\bar{\rho}'|}\left[(z-z')\hat{x} - (x-x')\hat{z}\right] H_1^{(1)}(\gamma|\bar{\rho}-\bar{\rho}'|)$$

$$= -\gamma\left[\sin\beta\hat{x} - \cos\beta\hat{z}\right] H_1^{(1)}(\gamma|\bar{\rho}-\bar{\rho}'|) \,, \tag{2-59}$$

and

$$\left(\frac{\partial}{\partial z}\hat{x} - \frac{\partial}{\partial x}\hat{z}\right) H_1^{(1)}(\gamma|\bar{\rho}-\bar{\rho}'|) = -\gamma\left[\sin\beta\hat{x} - \cos\beta\hat{z}\right]\left[\frac{H_1^{(1)}(\gamma|\bar{\rho}-\bar{\rho}'|)}{\gamma|\bar{\rho}-\bar{\rho}'|} - H_0^{(1)}(\gamma|\bar{\rho}-\bar{\rho}'|)\right]. \tag{2-60}$$

On expanding $\cos(\beta-\alpha)$, we find that

$$\frac{\partial}{\partial z}\cos(\beta-\alpha) = \frac{\partial}{\partial z}\left[\cos\alpha\,\frac{(x-x')}{|\bar{\rho}-\bar{\rho}'|} + \sin\alpha\,\frac{(z-z')}{|\bar{\rho}-\bar{\rho}'|}\right]$$

$$= \frac{1}{|\bar{\rho}-\bar{\rho}'|}\left(-\cos\alpha\sin\beta\cos\beta + \sin\alpha - \sin\alpha\sin^2\beta\right)$$

$$= -\frac{\cos\beta\sin(\beta-\alpha)}{|\bar{\rho}-\bar{\rho}'|} \,, \tag{2-61}$$

and

$$\frac{\partial}{\partial x}\cos(\beta-\alpha) = \frac{\sin\beta\sin(\beta-\alpha)}{|\bar{\rho}-\bar{\rho}'|} \,. \tag{2-62}$$

Similarly,

$$\frac{\partial}{\partial z}\sin(\beta-\alpha) = \frac{\partial}{\partial z}\left[-\sin\alpha\,\frac{(x-x')}{|\bar{\rho}-\bar{\rho}'|} + \cos\alpha\,\frac{(z-z')}{|\bar{\rho}-\bar{\rho}'|}\right]$$

$$= \frac{\cos\beta\cos(\beta-\alpha)}{|\bar{\rho}-\bar{\rho}'|}\,, \tag{2-63}$$

and

$$\frac{\partial}{\partial x}\sin(\beta-\alpha) = -\frac{\sin\beta\cos(\beta-\alpha)}{|\bar{\rho}-\bar{\rho}'|}\,. \tag{2-64}$$

When equations (2-56), (2-59), (2-60), (2-61), (2-62), (2-63), and (2-64) are introduced into equation (2-58), we find that the scattered transverse magnetic field intensity is given by

$$\vec{H}_{tn}^{sc} = \frac{i\gamma^3}{4k^2}\int_{C_1} K_y(\bar{\rho}')\,H_1^{(1)}(\gamma|\bar{\rho}-\bar{\rho}'|)(\sin\beta\hat{x}-\cos\beta\hat{z})\,ds'$$

$$-\frac{k_y\gamma^2}{4k^2}\int_{C_1} K_s(\bar{\rho}')\left\{\sin(\beta-\alpha)\left[H_0^{(1)}(\gamma|\bar{\rho}-\bar{\rho}'|) - \frac{H_1^{(1)}(\gamma|\bar{\rho}-\bar{\rho}'|)}{\gamma|\bar{\rho}-\bar{\rho}'|}\right]\left[\sin\beta\hat{x}-\cos\beta\hat{z}\right]\right.$$

$$\left. + \cos(\beta-\alpha)\,\frac{H_1^{(1)}(\gamma|\bar{\rho}-\bar{\rho}'|)}{\gamma|\bar{\rho}-\bar{\rho}'|}\left[\cos\beta\hat{x}+\sin\beta\hat{z}\right]\right\}ds'$$

$$-\frac{\gamma^2}{4\mu\omega}\int_{C_1} M_s(\bar{\rho}')\left\{\cos(\beta-\alpha)\left[H_0^{(1)}(\gamma|\bar{\rho}-\bar{\rho}'|) - \frac{H_1^{(1)}(\gamma|\bar{\rho}-\bar{\rho}'|)}{\gamma|\bar{\rho}-\bar{\rho}'|}\right]\left[\sin\beta\hat{x}-\cos\beta\hat{z}\right]\right.$$

$$\left. - \sin(\beta-\alpha)\,\frac{H_1^{(1)}(\gamma|\bar{\rho}-\bar{\rho}'|)}{\gamma|\bar{\rho}-\bar{\rho}'|}\left[\cos\beta\hat{x}+\sin\beta\hat{z}\right]\right\}ds'\,, \tag{2-65}$$

or

$$\vec{H}_{tn}^{sc} = \frac{i\gamma^3}{4k^2}\int_{c_1} K_y(\bar{\rho}')\, H_1^{(1)}(\gamma|\bar{\rho}-\bar{\rho}'|)(\sin\beta\,\hat{x} - \cos\beta\,\hat{z})\, ds'$$

$$- \frac{k_y\gamma^2}{4k^2}\int_{c_1} K_s(\bar{\rho}')\Big\{\sin(\beta-\alpha)\, H_0^{(1)}(\gamma|\bar{\rho}-\bar{\rho}'|)(\sin\beta\,\hat{x} - \cos\beta\,\hat{z})$$

$$+ \frac{H_1^{(1)}(\gamma|\bar{\rho}-\bar{\rho}'|)}{\gamma|\bar{\rho}-\bar{\rho}'|}\left(\cos(2\beta-\alpha)\,\hat{x} + \sin(2\beta-\alpha)\,\hat{z}\right)\Big\} ds'$$

$$- \frac{\gamma^2}{4\mu\omega}\int_{c_1} M_s(\bar{\rho}')\Big\{\cos(\beta-\alpha)\, H_0^{(1)}(\gamma|\bar{\rho}-\bar{\rho}'|)(\sin\beta\,\hat{x} - \cos\beta\,\hat{z})$$

$$- \frac{H_1^{(1)}(\gamma|\bar{\rho}-\bar{\rho}'|)}{\gamma|\bar{\rho}-\bar{\rho}'|}\left(\sin(2\beta-\alpha)\,\hat{x} - \cos(2\beta-\alpha)\,\hat{z}\right)\Big\} ds'. \qquad (2\text{-}66)$$

Similarly, from equations (2-15) and (2-57), the scattered transverse electric field intensity is given by

$$\vec{E}_{tr}^{sc} = \frac{1}{(\sigma - i\omega\varepsilon)}\vec{\nabla}\times\left(H_y^{sc}\,\hat{y}\right) = -\frac{i\omega\mu}{k}\left(\frac{\partial H_y^{sc}}{\partial z}\,\hat{x} - \frac{\partial H_y^{sc}}{\partial x}\,\hat{z}\right). \qquad (2\text{-}67)$$

It follows from above that

$$\vec{E}_{tn}^{sc} = \frac{i\gamma^3}{4k^2}\int_{c_1} M_y(\bar{\rho}')\, H_1^{(1)}(\gamma|\bar{\rho}-\bar{\rho}'|)(\sin\beta\,\hat{x} - \cos\beta\,\hat{z})\, ds'$$

$$- \frac{k_y\gamma^2}{4k}\int_{c_1} M_s(\bar{\rho}')\Big\{\sin(\beta-\alpha)\, H_0^{(1)}(\gamma|\bar{\rho}-\bar{\rho}'|)(\sin\beta\,\hat{x} - \cos\beta\,\hat{z})$$

$$+ \frac{H_1^{(1)}(\gamma|\bar{\rho}-\bar{\rho}'|)}{\gamma|\bar{\rho}-\bar{\rho}'|}\left(\cos(2\beta-\alpha)\,\hat{x} + \sin(2\beta-\alpha)\,\hat{z}\right)\Big\} ds'$$

$$+ \frac{Z\gamma^2}{4k}\int_{C_1} K_s(\bar{\rho}')\Big\{\cos(\beta-\alpha)\,H_0^{(1)}(\gamma|\bar{\rho}-\bar{\rho}'|)\left(\sin\beta\,\hat{x} - \cos\beta\,\hat{z}\right)$$

$$- \frac{H_1^{(1)}(\gamma|\bar{\rho}-\bar{\rho}'|)}{\gamma|\bar{\rho}-\bar{\rho}'|}\left(\sin(2\beta-\alpha)\,\hat{x} - \cos(2\beta-\alpha)\,\hat{z}\right)\Big\} ds'. \qquad (2\text{-}68)$$

2-4 General Field Representations for the Interior Region

We wish to obtain general integral representations of $E_y^t(\bar{\rho})$ and $H_y^t(\bar{\rho})$ for the interior problem. As in the exterior problem, we begin with the modified form of Green's theorem, equation (2-2), and set the two scalar functions u and v equal to $E_y^t(\bar{\rho})$ and $G(\bar{\rho},\bar{\rho}')$ respectively. Since our volume of interest is bounded only by an outer surface C_1, Green's theorem yields the result that

$$E_y^t(\bar{\rho}) = -\int_{C_1}\Big\{E_y^t(\bar{\rho}')\frac{\partial G^i}{\partial n}(\bar{\rho},\bar{\rho}') - G^i(\bar{\rho},\bar{\rho}')\frac{\partial E_y^t}{\partial n}(\bar{\rho}')\Big\} ds'. \qquad (2\text{-}69)$$

In equation (2-69), $\hat{n}$ is the outward normal to the volume of interest (Fig.3) and is equal to $-\hat{n}'$ of the exterior problem. $G^i(\bar{\rho},\bar{\rho}')$ is the whole-space Green's function of the interior region, and is given by

$$G^i(\bar{\rho},\bar{\rho}') = \frac{i}{4} H_0^{(1)}(\gamma_1|\bar{\rho}-\bar{\rho}'|). \qquad (2\text{-}70)$$

Thus, our integral expression for $E_y^t(\bar{\rho})$ is

$$E_y^t(\bar{\rho}) = -\int_{C_1} \left\{ G^i(\bar{\rho},\bar{\rho}') \frac{\partial E_y^t}{\partial n'}(\bar{\rho}') - E_y^t(\bar{\rho}') \frac{\partial G^i}{\partial n'}(\bar{\rho},\bar{\rho}') \right\} ds' . \tag{2-71}$$

By comparing equations (2-71) and (2-10), it is evident that our integral expression for $E_y^t(\bar{\rho})$ for the interior problem is equal to the negative of our integral expression for $E_y^{sc}(\bar{\rho})$ for the exterior problem. Thus, we may write the integral representation of $E_y^t(\bar{\rho})$ from equation ((2-56) as

$$E_y^t(\bar{\rho}) = \frac{Z_i \gamma_i^2}{4k_i} \int_{C_1} K_y(\bar{\rho}') H_0^{(1)}(\gamma_i|\bar{\rho}-\bar{\rho}'|)\, ds' - \frac{iZ_i k_{y_i} \gamma_i}{4k_i} \int_{C_1} K_s(\bar{\rho}') \sin(\beta-\alpha) H_1^{(1)}(\gamma_i|\bar{\rho}-\bar{\rho}'|)\, ds'$$
$$- \frac{i\gamma_i}{4} \int_{C_1} M_s(\bar{\rho}') \cos(\beta-\alpha) H_1^{(1)}(\gamma_i|\bar{\rho}-\bar{\rho}'|)\, ds' . \tag{2-72}$$

Since similar conclusions can be drawn for $H_y^t(\bar{\rho})$, we have from equation (2-57),

$$H_y^t(\bar{\rho}) = -\frac{\gamma_i^2}{4Z_i k_i} \int_{C_1} M_y(\bar{\rho}') H_0^{(1)}(\gamma_i|\bar{\rho}-\bar{\rho}'|)\, ds' + \frac{ik_{y_i}\gamma_i}{4Z_i k_i} \int_{C_1} M_s(\bar{\rho}') \sin(\beta-\alpha) H_1^{(1)}(\gamma_i|\bar{\rho}-\bar{\rho}'|)\, ds'$$
$$- \frac{i\gamma_i}{4} \int_{C_1} K_s(\bar{\rho}') \cos(\beta-\alpha) H_1^{(1)}(\gamma_i|\bar{\rho}-\bar{\rho}'|)\, ds' . \tag{2-73}$$

From equations (2-66) and (2-68), the transverse field components are given by

$$\vec{H}^{t}_{t_1} = -\frac{i\gamma_i^3}{4k_i^2}\int_{C_1} K_y(\bar{\rho}')\, H_1^{(1)}(\gamma_i|\bar{\rho}-\bar{\rho}'|)(\sin\beta\,\hat{x} - \cos\beta\,\hat{z})\,ds'$$

$$+\frac{k_{y_i}\gamma_i^2}{4k_i^2}\int_{C_1} K_s(\bar{\rho}')\Big\{\sin(\beta-\alpha)\,H_0^{(1)}(\gamma_i|\bar{\rho}-\bar{\rho}'|)(\sin\beta\,\hat{x} - \cos\beta\,\hat{z})$$

$$+\frac{H_1^{(1)}(\gamma_i|\bar{\rho}-\bar{\rho}'|)}{\gamma_i|\bar{\rho}-\bar{\rho}'|}(\cos(2\beta-\alpha)\,\hat{x} + \sin(2\beta-\alpha)\,\hat{z})\Big\}\,ds'$$

$$+\frac{\gamma_i^2}{4\mu_i\omega}\int_{C_1} M_s(\bar{\rho}')\Big\{\cos(\beta-\alpha)\,H_0^{(1)}(\gamma_i|\bar{\rho}-\bar{\rho}'|)(\sin\beta\,\hat{x} - \cos\beta\,\hat{z})$$

$$-\frac{H_1^{(1)}(\gamma_i|\bar{\rho}-\bar{\rho}'|)}{\gamma_i|\bar{\rho}-\bar{\rho}'|}(\sin(2\beta-\alpha)\,\hat{x} - \cos(2\beta-\alpha)\,\hat{z})\Big\}\,ds', \qquad (2\text{-}74)$$

and

$$\vec{E}^{t}_{t_1} = \frac{-i\gamma_i^3}{4Z_i k_i^2}\int_{C_1} M_y(\bar{\rho}')\, H_1^{(1)}(\gamma_i|\bar{\rho}-\bar{\rho}'|)(\sin\beta\,\hat{x} - \cos\beta\,\hat{z})\,ds'$$

$$+\frac{k_{y_i}\gamma_i^2}{4k_i^2}\int_{C_1} M_s(\bar{\rho}')\Big\{\sin(\beta-\alpha)\,H_0^{(1)}(\gamma_i|\bar{\rho}-\bar{\rho}'|)(\sin\beta\,\hat{x} - \cos\beta\,\hat{z})$$

$$+\frac{H_1^{(1)}(\gamma_i|\bar{\rho}-\bar{\rho}'|)}{\gamma_i|\bar{\rho}-\bar{\rho}'|}(\cos(2\beta-\alpha)\,\hat{x} + \sin(2\beta-\alpha)\,\hat{z})\Big\}\,ds'$$

$$-\frac{Z_i\gamma_i^2}{4k_i}\int_{C_1} K_s(\bar{\rho}')\Big\{\cos(\beta-\alpha)\,H_0^{(1)}(\gamma_i|\bar{\rho}-\bar{\rho}'|)(\sin\beta\,\hat{x} - \cos\beta\,\hat{z})$$

$$-\frac{H_1^{(1)}(\gamma_i|\bar{\rho}-\bar{\rho}'|)}{\gamma_i|\bar{\rho}-\bar{\rho}'|}(\sin(2\beta-\alpha)\,\hat{x} - \cos(2\beta-\alpha)\,\hat{z})\Big\}\,ds'. \qquad (2\text{-}75)$$

2-5 Representations for $\vec{E}$ and $\vec{H}$ When the Scatterer Has a Low Surface Impedance

The integral representations for $\vec{E}$ and $\vec{H}$ simplify considerably when the scatterer is assumed to be highly conducting. The reason for this is that $\vec{E}$ and $\vec{H}$ take a particularly simple form just inside the scatterer, and may be assumed to be zero further from the boundary as a result of attenuation.

The angle of refraction at any local site on the contour is given by Snell's Law as

$$\cos\theta_2 = \sqrt{1 - \frac{k_e^2}{k_i^2}\sin^2\theta_1}\ . \qquad (2\text{-}76)$$

In equation (2-76), θ_1 is defined from Fig. 4 as the angle of incidence and θ_2 as the angle of refraction. It is evident that if $k_i >> k_e$, θ_2 is approximately zero even for grazing exterior angles of incidence. As a result, the total field at any point just inside the scatterer may be represented by a wave propagating normally away from the coutour. Following Stratton (1941, p. 354), we may write that the transverse electric portion of the field must satisfy the relationship

$$E_s = -Z_{is} H_y \ , \qquad (2\text{-}77a)$$

($E_y = E_n = H_s = H_n = 0$) and the transverse magnetic portion of the field must satisfy the relationship

$$E_y = Z_{iy} H_s \ , \qquad (2\text{-}77b)$$

($E_s = E_n = H_y = H_n = 0$). Z_{is} and Z_{iy} are the cylindrical surface impedances which Stratton (p.360) shows are given by

$$Z_{is} = \frac{\mu_i \omega}{\sqrt{h_i^2 - k_i^2}} \frac{\frac{\partial Z_n(\beta)}{\partial \beta}}{Z_n(\beta)} , \tag{2-78a}$$

and

$$Z_{iy} = \frac{\mu_i \omega \sqrt{h_i^2 - k_i^2}}{k_i^2} \frac{Z_n(\beta)}{\frac{\partial Z_n(\beta)}{\partial \beta}} . \tag{2-78b}$$

$Z_n(\beta)$ represents a radially outward travelling wave and is given by

$$Z_n(\beta) = H_n^{(1)}\left(\sqrt{k_i^2 - h_i^2}\,\rho\right) . \tag{2-79}$$

Since the wave is normal to the interface, h is zero in equations (2-78) and (2-79) and we find that

$$Z_{is} = \frac{\mu_i \omega}{i k_i}\left[\frac{n}{k_i \rho} - \frac{H_{n+1}^{(1)}(k_i \rho)}{H_n^{(1)}(k_i \rho)}\right] , \tag{2-80a}$$

and

$$Z_{iy} = \frac{i \mu_i \omega}{k_i} \frac{1}{\left[\frac{n}{k_i \rho} - \frac{H_{n+1}^{(1)}(k_i \rho)}{H_n^{(1)}(k_i \rho)}\right]} . \tag{2-80b}$$

When $k_i \rho$ is large, we can expand $H_n^{(1)}(k_i \rho)$ as

$$H_n^{(1)}(\beta) \sim \sqrt{\frac{2}{\pi \beta}}\, e^{i\left(\beta - \frac{2n+1}{4}\pi\right)}\left(1 + O\left(\frac{1}{|\beta|}\right)\right) , \tag{2-81}$$

so that

$$\frac{H_{m+1}^{(1)}(k_i\rho)}{H_m^{(1)}(k_i\rho)} \longrightarrow e^{-i\frac{\pi}{2}} = -i \quad , \tag{2-82}$$

where $|k_i\rho| >> 1$, $|k_i\rho| >> n^2$ and $-\frac{\pi}{2} \leq \arg(k_i\rho) \leq \pi/2$.

Equation (2-82) is a good approximation if the curvature is small compared to the attenuation per unit distance. In this case, equations (2-80) reduce to plane wave surface impedances given by

$$Z_{is} = \frac{\mu_i \omega}{k_{is}} \quad , \tag{2-83a}$$

and

$$Z_{iy} = \frac{\mu_i \omega}{k_{iy}} \quad , \tag{2-83b}$$

where the subscripts on Z are taken to agree with the subscripts on $\vec{E}$ to indicate that the plane wave impedance is calculated using the propagation constant of that component of the electric field.

As well as being a very simple representation for the internal field, equations (2-77) are important in that they relate the equivalent magnetic surface current densities to the equivalent electric surface current densities. When equations (2-38) and (2-39) are introduced into equations (2-77), we find that

$$M_y = Z_{is} K_s , \tag{2-84a}$$

$$M_s = -Z_{iy} K_y . \tag{2-84b}$$

As a result, our field representations for the exterior region, equations

(2-56), (2-57), (2-66) and (2-68), reduce to

$$E_y^t(\bar{\rho}) = E_y^i(\bar{\rho}) - \frac{z\gamma^2}{4k}\int_{C_1} K_y(\bar{\rho}')\, H_o^{(1)}(\gamma|\bar{\rho}-\bar{\rho}'|)\, ds'$$

$$+ \frac{i z k_y \gamma}{4k}\int_{C_1} K_s(\bar{\rho}')\sin(\beta-\alpha)\, H_1^{(1)}(\gamma|\bar{\rho}-\bar{\rho}'|)\, ds' - \frac{i\gamma}{4}\int_{C_1} z_{iy}(\bar{\rho}')\, K_y(\bar{\rho}')\cos(\beta-\alpha)\, H_1^{(1)}(\gamma|\bar{\rho}-\bar{\rho}'|)\, ds', \tag{2-85}$$

and

$$H_y^t(\bar{\rho}) = H_y^i(\bar{\rho}) + \frac{\gamma^2}{4zk}\int_{C_1} z_{is}(\bar{\rho}')\, K_s(\bar{\rho}')\, H_o^{(1)}(\gamma|\bar{\rho}-\bar{\rho}'|)\, ds'$$

$$+ \frac{i k_y \gamma}{4zk}\int_{C_1} z_{iy}(\bar{\rho}')\, K_y(\bar{\rho}')\sin(\beta-\alpha)\, H_1^{(1)}(\gamma|\bar{\rho}-\bar{\rho}'|)\, ds' + \frac{i\gamma}{4}\int_{C_1} K_s(\bar{\rho}')\cos(\beta-\alpha)\, H_1^{(1)}(\gamma|\bar{\rho}-\bar{\rho}'|)\, ds'. \tag{2-86}$$

The scattered transverse field quantities become

$$\vec{H}_t^{sc} = \frac{i\gamma^3}{4k^2}\int_{C_1} K_y(\bar{\rho}')\, H_1^{(1)}(\gamma|\bar{\rho}-\bar{\rho}'|)(\sin\beta\,\hat{x} - \cos\beta\,\hat{z})\, ds'$$

$$- \frac{k_y\gamma^2}{4k^2}\int_{C_1} K_s(\bar{\rho}')\left\{\sin(\beta-\alpha)\, H_o^{(1)}(\gamma|\bar{\rho}-\bar{\rho}'|)(\sin\beta\,\hat{x} - \cos\beta\,\hat{z})\right.$$

$$\left. + \frac{H_1^{(1)}(\gamma|\bar{\rho}-\bar{\rho}'|)}{\gamma|\bar{\rho}-\bar{\rho}'|}\left(\cos(2\beta-\alpha)\,\hat{x} + \sin(2\beta-\alpha)\,\hat{z}\right)\right\} ds'$$

$$+ \frac{\gamma^2}{4\mu\omega}\int_{C_1} z_{iy}(\bar{\rho}')\, K_y(\bar{\rho}')\left\{\cos(\beta-\alpha)\, H_o^{(1)}(\gamma|\bar{\rho}-\bar{\rho}'|)(\sin\beta\,\hat{x} - \cos\beta\,\hat{z})\right.$$

$$\left. - \frac{H_1^{(1)}(\gamma|\bar{\rho}-\bar{\rho}'|)}{\gamma|\bar{\rho}-\bar{\rho}'|}\left(\sin(2\beta-\alpha)\,\hat{x} - \cos(2\beta-\alpha)\,\hat{z}\right)\right\} ds', \tag{2-87}$$

and

$$\bar{E}_{t_1}^{sc} = \frac{i\gamma^3}{4k^2}\int_{C_1} Z_{is}(\bar{\rho}')\,K_s(\bar{\rho}')\,H_1^{(1)}(\gamma|\bar{\rho}-\bar{\rho}'|)(\sin\beta\hat{x}-\cos\beta\hat{z})\,ds'$$

$$+\frac{k_y\gamma^2}{4k^2}\int_{C_1} Z_{iy}(\bar{\rho}')\,K_y(\bar{\rho}')\Big\{\sin(\beta-\alpha)\,H_0^{(1)}(\gamma|\bar{\rho}-\bar{\rho}'|)(\sin\beta\hat{x}-\cos\beta\hat{z})$$

$$+\frac{H_1^{(1)}(\gamma|\bar{\rho}-\bar{\rho}'|)}{\gamma|\bar{\rho}-\bar{\rho}'|}(\cos(2\beta-\alpha)\hat{x}+\sin(2\beta-\alpha)\hat{z})\Big\}\,ds'$$

$$+\frac{z\gamma^2}{4k}\int_{C_1} K_s(\bar{\rho}')\Big\{\cos(\beta-\alpha)\,H_0^{(1)}(\gamma|\bar{\rho}-\bar{\rho}'|)(\sin\beta\hat{x}-\cos\beta\hat{z})$$

$$-\frac{H_1^{(1)}(\gamma|\bar{\rho}-\bar{\rho}'|)}{\gamma|\bar{\rho}-\bar{\rho}'|}(\sin(2\beta-\alpha)\hat{x}-\cos(2\beta-\alpha)\hat{z})\Big\}\,ds'. \quad (2\text{-}88)$$

CHAPTER 3

SCATTERING FROM PERFECTLY CONDUCTING CYLINDERS

We wish to evaluate scattering from cylinders for the limiting case, $Z_{i_s} = Z_{i_y} = 0$. Further, we will assume that the field is constant in the y direction ($k_y = 0$) as is the case, for example, when a plane wave is incident normal to the cylinder axis. By making these approximations, equations (2-85) and (2-86) uncouple and reduce to very simple integral representations. As a result, the solution of the integral equations encountered in solving for scattering from cylinders of arbitrary impedance is more easily understood, and in addition, many of the numerical problems which are met may be studied individually.

Mei and Van Bladel (1963b) and Andreasen (1964) have examined the problem of scattering from perfectly conducting cylinders. Andreasen (1965a) also has examined the problem of scattering from perfectly conducting bodies of revolution. In this chapter, the principle difference from their studies will be in the physical situation to which the solution is applied.

3-1 Basic Integral Equations

If we assume that $Z_{i_s} = Z_{i_y} = 0$ and that $k_y = 0$ in equations (2-85) and (2-86), then we find that the most basic integral representations for E_y and H_y are

$$E_y^t(\bar{\rho}) = E_y^i(\bar{\rho}) - \frac{\mu_1 \omega}{4} \int_{C_1} K_y(\bar{\rho}') H_0^{(1)}(k_1 |\bar{\rho} - \bar{\rho}'|) ds' \quad , \tag{3-1}$$

and

$$H_y^t(\bar{\rho}) = H_y^i(\bar{\rho}) + \frac{ik_1}{4}\int_{C_1} K_s(\bar{\rho}')\cos(\beta-\alpha)\,H_1^{(1)}(k_1|\bar{\rho}-\bar{\rho}'|)\,ds' \quad , \tag{3-2}$$

or

$$E_y^{sc}(\bar{\rho}) = -\frac{\mu_1\omega}{4}\int_{C_1} K_y(\bar{\rho}')\,H_0^{(1)}(k_1|\bar{\rho}-\bar{\rho}'|)\,ds' \quad , \tag{3-3}$$

and

$$H_y^{sc}(\bar{\rho}) = \frac{ik_1}{4}\int_{C_1} K_s(\bar{\rho}')\,H_1^{(1)}(k_1|\bar{\rho}-\bar{\rho}'|)\,ds' \quad , \tag{3-4}$$

where we have referred to the earth parameters by the subscript 1.

The electric field intensity radiated by a line source may be determined by setting the surface current density in equation (3-3) equal to a delta function source. With

$$K_y(\bar{\rho}') = I\,\delta(\bar{\rho}_L-\bar{\rho}') \quad , \tag{3-5}$$

where I is the current in amps on the line source, equation (3-3) becomes

$$E_y(\bar{\rho}) = -\frac{\mu_1\omega}{4} I\,H_0^{(1)}(k_1|\bar{\rho}-\bar{\rho}_L|) \, . \tag{3-6}$$

From equation (3-6) it is evident that the integral representation for the scattered field given by equation (3-3) may be interpreted as the summation of a continuous distribution of weighted line sources around the cylinder contour, radiating into the exterior region. In fact, it is shown in Appendix B that equation (3-3) may be derived from just such a physical

argument, rather than the mathematical approach used in Chapter 2. A similar use of physical reasoning could have been used to derive equation (3-4).

Before calculating the scattered fields from equations (3-3) and (3-4), we must determine first the current distribution about the cylinder. To do this, we enforce the boundary conditions on tangential $\vec{E}$ and $\vec{H}$. For perfect conductors, these boundary conditions are

$$\hat{n} \times \vec{E}^{t} = 0 \,, \tag{3-7a}$$

$$\hat{n} \times \vec{H}^{t} = \vec{K} \,. \tag{3-7b}$$

If we let the point of observation approach a boundary point given by the vector $\bar{\rho}''$ and apply equation (3-7a), then equation (3-1) reduces to

$$E_y^i(\bar{\rho}'') = \frac{\mu_1 \omega}{4} \int_{C_1} K_y(\bar{\rho}') H_o^{(1)}(k_1 |\bar{\rho}'' - \bar{\rho}'|) ds' \,. \tag{3-8}$$

Equation (3-8) is a singular Fredholm integral equation of the first kind and can be solved numerically for the unknown function $K_y(\bar{\rho}')$ once the contour C_1 has been specified. If we assume that the incident plane wave possesses only an axial component of electric field intensity (hereafter referred to as E_y-polarization), then we may write that $E_y^i(\bar{\rho}'')$ in equation (3-8) is given by

$$E_y^i(\bar{\rho}'') = Z_1 H_o e^{-ik_1(x'' \sin\phi_{in} + z'' \cos\phi_{in})} \,, \tag{3-9}$$

where H_o is the magnitude of the magnetic field intensity in air, and ϕ_{in} is the direction of propagation of the incident wave in Fig. 2.

Similarly, when the boundary condition given by equation (3-7b) is applied to equation (3-2), we find that

$$H_y^i(\bar{\rho}'') = -K_s(\bar{\rho}'') - \frac{ik_1}{4}\int_{C_1} K_s(\bar{\rho}')\cos(\beta''-\alpha)H_1^{(1)}(k_1|\bar{\rho}''-\bar{\rho}'|)\,ds'. \quad (3\text{-}10)$$

Equation (3-10) is a singular Fredholm integral equation of the second kind. If we assume this time that the incident field possesses only an axial component of magnetic field intensity (hereafter referred to as H_y-polarization), then we may write that $H_y^i(\bar{\rho}'')$ in equation (3-10) is given by

$$H_y^i(\bar{\rho}'') = H_0 e^{ik_1(x''\sin\beta_{in} + z''\cos\beta_{in})} \quad (3\text{-}11)$$

Once equations (3-8) and (3-10) have been solved for $K_y(\bar{\rho}')$ and $K_s(\bar{\rho}')$, we can calculate the scattered axial components of the field from equations (3-3) and (3-4). The scattered transverse components become, from equations (2-87) and (2-88)

$$\overline{H}_{tn}^{sc} = \frac{ik_1}{4}\int_{C_1} K_y(\bar{\rho}')H_1^{(1)}(k_1|\bar{\rho}-\bar{\rho}'|)(\sin\beta\hat{x} - \cos\beta\hat{z})\,ds', \quad (3\text{-}12)$$

and

$$\vec{E}_{tn}^{sc} = \frac{\mu_1\omega}{4}\int_{C_1} K_s(\bar{\rho}')\left\{\cos(\beta-\alpha)H_0^{(1)}(k_1|\bar{\rho}-\bar{\rho}'|)(\sin\beta\hat{x} - \cos\beta\hat{z})\right.$$

$$\left. - \frac{H_1^{(1)}(k_1|\bar{\rho}-\bar{\rho}'|)}{k_1|\bar{\rho}-\bar{\rho}'|}(\sin(2\beta-\alpha)\hat{x} - \cos(2\beta-\alpha)\hat{z})\right\}ds'. \quad (3\text{-}13)$$

312 Numerical Solution of Singular Fredholm Integral Equations

Kopal (1955, Chapter VIII) discusses several numerical methods used to solve Fredholm integral equations. However, the common approaches used in solving integral equations which occur in scattering problems

may be divided into two general philosophies. These are referred to as an expansion of the unknown

1) In functions of full range support, and
2) In functions of subrange support.

In full range support, one function is chosen to represent the unknown around the contour, whereas in subrange support the unknown is expanded in functions over small intervals. In investigating geophysical scattering problems, an expansion of the unknown in functions of subrange support is preferred to an expansion of the unknown in functions of full range support since

1) The matrix is better conditioned
2) The integration time is faster, and
3) The edges of rectangular inhomogeneities can be handled better.

Having decided on expansion of the unknown in functions of subrange support, there are a variety of methods available for interpolation in the use of these expansions. A suitable method is to expand the unknown in a set of N algebraic functions and require the integral equation to be satisfied at N points. We have not investigated another popular method, that of sinusoidal interpolation, since we do not have a good estimate for the wave number in sinusoidal interpolation.

We will discuss two sets of algebraic functions which can be used. The first set of functions has the advantage that a solution can be obtained clearly and easily, whereas the second set has the advantage of being a more accurate representation of the unknown.

3-2-1 Constant Current Density Approximation

We assume in all discussions that the contour of the cylinder has been divided into N straight intervals as is shown in Fig. 5. Then we can choose to represent our unknown current density by a set of algebraic functions consisting of a constant current density over each interval. This is represented graphically in Fig. 6, and can be written as

$$K_y(\bar{\rho}') = \sum_{j=1}^{N} K_j u_j(s') \quad , \tag{3-14}$$

where $u_j(s') = \begin{cases} 1 & , \quad (s_j - w_j) < s' \leq (s_j + w_j) \\ 0 & , \quad \text{elsewhere} \end{cases}$,

s' is the contour coordinate,

s_j is the midpoint of the jth interval,

w_j is the half-width of the jth interval

and K_j is the amplitude of the electric or magnetic surface current density in the jth interval

When equation (3-14) is introduced into (3-8), we find that

$$Z_1 H_0 e^{ik_1(x''\sin\phi_m + z''\cos\phi_m)} = \frac{\mu_1\omega}{4}\int_{C_1}\sum_{j=1}^{N} K_{y_j} u_j(s') H_0^{(1)}(k_1|\bar{\rho}'' - \bar{\rho}'|)\, ds'$$

$$= \frac{\mu_1\omega}{4}\sum_{j=1}^{N} K_{y_j}\int_{s_j - w_j}^{s_j + w_j} H_0^{(1)}(k_1|\bar{\rho}'' - \bar{\rho}'|)\, ds' . \tag{3-15}$$

The resulting integral can be computed numerically over each interval of the contour. Thus, equation (3-15) reduces to a linear equation with N unknowns.

$$A_1 = B_{11} K_{y_1} + B_{12} K_{y_2} + \cdots \quad \cdots + B_{1N} K_{y_N} . \tag{3-16}$$

If we enforce the boundary condition at the midpoint of each interval, we will obtain N linearly independent equations with N unknowns, and the problem has reduced to solving a matrix of the form

$$(\mathcal{B})(K_y) = (A) \quad . \tag{3-17}$$

Using standard matrix inversion techniques, N sampled values of the current distribution are obtained.

$$(K_y) = (\mathcal{B})^{-1}(A) \tag{3-18}$$

Equation (3-18) is an approximate solution of equation (3-8).

3-2-2 Quadratic Current Density Approximation

Unfortunately, the constant current density approximation given by equation (3-14) is not always accurate, especially over those intervals on which K(s') varies rapidly. Rather than take a smaller sampling interval in these regions, a better approximation is to choose a set of algebraic functions which consists of a quadratic function over each interval. Thus, we may write

$$K(s') = \sum_{j=1}^{N} a_j(s') \tag{3-19}$$

where

$$a_j(s') = \begin{cases} A_j + B_j(s'-s_j) + C_j(s'-s_j)^2 & , (s_j - w_j) < s' \leq (s_j + w_j) \\ 0 & , \text{elsewhere} \end{cases}$$

Equation (3-19) contains three constants per interval which are determined by invoking three boundary conditions per interval:

1) Enforce the usual E.M. boundary conditions at the midpoint of each interval,

2) Enforce continuity of the quadratic function at the edges of each interval, and

3) Enforce continuity of the first derivative of the quadratic function at the edges of each interval.

However, this would increase the matrix size by a factor of three, and hence the solution time by a factor of $27(3^3)$, although superior accuracy would be achieved.

An approximate solution which yields an N x N matrix is that which assumes that the only unknowns are the set K_j where

$K_j = K_j(s_j)$ = amplitude of the current density at the midpoint of each interval.

With this set of unknowns, we interpolate over each interval by fitting a quadratic function to the amplitude of the current density at the midpoint of the jth interval and the midpoint of the two adjacent intervals, as is shown in Fig. 7. While the accuracy of this set of quadratic functions is not as great as that for the original set chosen, it is still greater than the accuracy of the constant current density representation, and yet it requires essentially the same computer time as the constant current density representation.

If we fit equation (3-19) to the amplitude of the current density at the midpoint of the jth interval and the midpoint of the two adjacent intervals, we find that

$$K_j = A_j$$

$$K_{j-1} = A_j - B_j (w_j + w_{j-1}) + C_j (w_j + w_{j-1})^2$$

$$K_{j+1} = A_j + B_j (w_j + w_{j+1}) + C_j (w_j + w_{j+1})^2 \quad . \tag{3-20}$$

By allowing the half width of each interval to be distinct in equations (3-20), we have allowed ourselves the freedom to choose smaller intervals for those regions where the current density varies most rapidly.

Solving equations (3-20), we find that

$$A_j = K_j$$

$$B_j = \frac{K_{j+1} - (1-\lambda_j^2) K_j - \lambda_j^2 K_{j-1}}{(1+\lambda_j)(w_j + w_{j+1})}$$

$$C_j = \frac{K_{j+1} - (1+\lambda_j) K_j + \lambda_j K_{j-1}}{\tilde{\ell}_j (1+\lambda_j)} \quad , \tag{3-21}$$

where

$$\lambda_j = \frac{w_j + w_{j+1}}{w_j + w_{j-1}} \quad ,$$

and

$$\tilde{\ell}_j = (w_j + w_{j+1})(w_j + w_{j-1}) \quad .$$

Introducing these values for the coefficients into equation (3-19), equation (3-8) can be rewritten as

$$Z_1 H_0 \, e^{ik_1 (x'' \sin\phi_{in} + z'' \cos\phi_{in})} =$$

$$\sum_{j=1}^{N} \frac{\mu_1 \omega}{4} \left\{ K_{y_j} \int_{s_j - w_j}^{s_j + w_j} H_0^{(1)}(k_1 |\bar{\rho}'' - \bar{\rho}'|) \left(1 - \frac{(1-\lambda_j)(s'-s_j)}{w_j + w_{j+1}} - \frac{(s'-s_j)^2}{\tilde{\ell}_j} \right) ds' \right.$$

$$+ K_{y_{j+1}} \int_{s_j - w_j}^{s_j + w_j} H_0^{(1)}(k_1|\bar{\rho}'' - \bar{\rho}'|) \frac{(s'-s_j)}{(1+\lambda_j)} \left(\frac{1}{w_j + w_{j+1}} + \frac{s'-s_j}{\tilde{\iota}_j} \right) ds'$$

$$- K_{y_{j-1}} \int_{s_j - w_j}^{s_j + w_j} H_0^{(1)}(k_1|\bar{\rho}'' - \bar{\rho}'|) \frac{\lambda_j (s'-s_j)}{(1+\lambda_j)} \left(\frac{\lambda_j}{w_j + w_{j+1}} - \frac{s'-s_j}{\tilde{\iota}_j} \right) ds' \Bigg\} . \qquad (3\text{-}22)$$

As before, the remaining integrals in equation (3-22) can be performed numerically, and thus the integral over each interval contributes to three coefficients in each row of the coefficient matrix. It should be noted, however, that care must be taken in programming equation (3-22) to ensure that the Nth and first intervals are coupled whenever the contour C_1 is closed.

It is possible to rewrite equation (3-22) in terms of K_{y_j} alone, and we find that

$$Z_1 H_0 e^{-ik_1(x'' \sin\theta_{in} + z'' \cos\theta_{in})} =$$

$$\sum_{j=1}^{N} \frac{\mu_1 \omega}{4} K_{y_j} \Bigg\{ \int_{s_j - w_j}^{s_j + w_j} H_0^{(1)}(k_1|\bar{\rho}'' - \bar{\rho}'|) \left(1 - \frac{(1-\lambda_j)(s'-s_j)}{w_j + w_{j+1}} - \frac{(s'-s_j)^2}{\tilde{\iota}_j} \right) ds'$$

$$+ \int_{s_{j-1} - w_{j-1}}^{s_{j-1} + w_{j-1}} H_0^{(1)}(k_1|\bar{\rho}'' - \bar{\rho}'|) \frac{(s'-s_{j-1})}{(1+\lambda_{j-1})} \left(\frac{1}{w_j + w_{j-1}} + \frac{s'-s_{j-1}}{\tilde{\iota}_{j-1}} \right) ds'$$

$$- \int_{s_{j+1} - w_{j+1}}^{s_{j+1} + w_{j+1}} H_0^{(1)}(k_1|\bar{\rho}'' - \bar{\rho}'|) \frac{\lambda_{j+1}(s'-s_{j+1})}{(1+\lambda_{j+1})} \left(\frac{\lambda_{j+1}}{w_{j+1} + w_{j+2}} - \frac{s'-s_{j+1}}{\tilde{\iota}_{j+1}} \right) ds' \Bigg\} . \qquad (3\text{-}23)$$

However, equation (3-22) is preferred for its greater ease in programming.

Equation (3-22) reduces to a linear equation with N unknowns, similar to equation (3-16). By enforcing the boundary condition at the midpoint of

each interval, we obtain a modified coefficient matrix which yields an improved estimate of the N sampled values of the current distribution.

$$[K_y'] = [B']^{-1}[A] . \tag{3-24}$$

A similar interpolation procedure can be applied to equation (3-10), assuming H_y-polarization, and we would find that

$$H_o e^{ik_1(x''\sin\phi_{in} + z''\cos\phi_{in})} = -K_{s_i}$$

$$- \sum_{j=1}^{N} \frac{ik_1}{4} \left\{ K_{s_j} \int_{s_j - w_j}^{s_j + w_j} H_1^{(1)}(k_1|\bar{\rho}'' - \bar{\rho}'|) \cos(\beta'' - \alpha) \left(1 - \frac{(1-\lambda_j)(s'-s_j)}{w_j + w_{j+1}} - \frac{(s'-s_j)^2}{\tilde{\ell}_j}\right) ds' \right.$$

$$+ K_{s_{j+1}} \int_{s_j - w_j}^{s_j + w_j} H_1^{(1)}(k_1|\bar{\rho}'' - \bar{\rho}'|) \cos(\beta'' - \alpha) \frac{(s'-s_j)}{(1+\lambda_j)} \left(\frac{1}{w_j + w_{j+1}} + \frac{s'-s_j}{\tilde{\ell}_j}\right) ds'$$

$$\left. - K_{s_{j-1}} \int_{s_j - w_j}^{s_j + w_j} H_1^{(1)}(k_1|\bar{\rho}'' - \bar{\rho}'|) \cos(\beta'' - \alpha) \frac{\lambda_j (s'-s_j)}{(1+\lambda_j)} \left(\frac{\lambda_j}{w_j + w_{j+1}} - \frac{s'-s_j}{\tilde{\ell}_j}\right) ds' \right\} , \tag{3-25}$$

where K_{s_1} is the amplitude of the current density at the point $\bar{\rho}''$ where the boundary condition is being enforced.

Once equations (3-22) and (3-25) have been solved for the N sampled values of K_y and K_s, the scattered field quantities can be calculated from equations (3-3), (3-4), (3-12), and (3-13).

3-2-3 Integration Through the Point of Singularity

When the integration is carried out over the interval in which the boundary condition has been applied (the ith interval), the Hankel function possesses a singularity and the contribution of this interval must be

evaluated analytically. Fortunately, the argument of the Hankel function is small in this interval, so that we can make the following approximations:

$$H_o^{(1)}\left(k\left|\bar{\rho}-\bar{\rho}'\right|\right) = H_o^{(1)}\left(k\sqrt{\delta^2+s'^2}\right)$$

$$\sim 1 - \frac{k^2}{4}\left(\delta^2+s'^2\right) + \frac{2i}{\pi}\left\{\left(1-\frac{k^2}{4}\left(\delta^2+s'^2\right)\right)\ln\frac{\gamma k}{2}\left(\delta^2+s'^2\right)^{1/2} + \frac{k^2}{4}\left(\delta^2+s'^2\right)\right\}, \qquad (3\text{-}26)$$

and

$$H_1^{(1)}\left(k\left|\bar{\rho}-\bar{\rho}'\right|\right) \sim \frac{k\sqrt{\delta^2+s'^2}}{2}\left[1 - \frac{k^2\left(\delta^2+s'^2\right)}{8} + \frac{2i}{\pi}\left\{\left[1-\frac{k^2\left(\delta^2+s'^2\right)}{8}\right]\ln\frac{\gamma k}{2}\left(\delta^2+s'^2\right)^{1/2} - \frac{2}{k^2\left(\delta^2+s'^2\right)} - \frac{1}{2} + \frac{5k^2\left(\delta^2+s'^2\right)}{32}\right\}\right], \qquad (3\text{-}27)$$

where $\gamma' = \ln \gamma = .57722$ = Euler's constant,

s' is the contour coordinate measured from the center of the ith interval (see Fig. 8),

and δ is the distance of the point of observation above the center of the ith interval.

If $|k|\left|\bar{\rho}-\bar{\rho}'\right| \leq .5$, an error of less than 0.1% in the value of $H_o^{(1)}(k|\bar{\rho}-\rho'|)$ and $H_1^{(1)}(k|\bar{\rho}-\bar{\rho}'|)$ is obtained when using equations (3-26) and (3-27).

Approximating the Hankel functions by equations (3-26) and (3-27), the contribution of the ith interval to $\bar{E}$ and $\bar{H}$ is evaluated with the point of observation a distance δ above the contour. Having obtained these integrals, then the contribution of the singularity to the boundary condition is taken as the limit as δ approaches zero. It should be pointed

out that since the original boundary conditions on $\vec{E}$ and $\vec{H}$ (equations (3-7)) are derived by a similar limiting process, this procedure is completely rigorous.

If the point of observation is taken to be a distance δ above the center of the ith interval, then the contribution of the singular interval to equation (3-22) can be written as

$$\lim_{\delta\to 0}\left[\frac{\mu_i\omega}{4}\left\{\left[HK00-\frac{(1-\lambda_i)}{w_i+w_{i+1}}HK01-\frac{HK02}{\tau_i}\right]K_{y_i}+\frac{1}{1+\lambda_i}\left[\frac{HK01}{w_i+w_{i+1}}+\frac{HK02}{\tau_i}\right]K_{y_{i+1}}-\frac{\lambda_i}{1+\lambda_i}\left[\frac{\lambda_i HK01}{w_i+w_{i+1}}-\frac{HK02}{\tau_i}\right]K_{y_{i-1}}\right\}\right], \tag{3-28}$$

$$HK00=\int_{-w_i}^{w_i}H_0^{(1)}\left(k_1\sqrt{\delta^2+s'^2}\right)ds', \tag{3-29a}$$

$$HK01=\int_{-w_i}^{w_i}s'\,H_0^{(1)}\left(k_1\sqrt{\delta^2+s'^2}\right)ds', \tag{3-29b}$$

$$HK02=\int_{-w_i}^{w_i}s'^2\,H_0^{(1)}\left(k_1\sqrt{\delta^2+s'^2}\right)ds'. \tag{3-29c}$$

Equations (3-29) have been evaluated in Appendix D assuming that $H_0^{(1)}\left(k_1\sqrt{\delta^2+s'^2}\right)$ is given by equation (3-26). After the integrals have been obtained, we find that

$$\lim_{\delta\to 0}(HK00)=2w_i\left\{\left(1-\frac{k^2w_i^2}{12}\right)+\frac{2i}{\pi}\left[\left(1-\frac{k^2w_i^2}{12}\right)\ln\frac{\gamma k w_i}{2}-\left(1-\frac{k^2w_i^2}{9}\right)\right]\right\}, \tag{3-30a}$$

$$\lim_{\delta\to 0}(HK01)=0 \tag{3-30b}$$

$$\lim_{\delta \to 0} (HK02) = \frac{2w_i^3}{3}\left\{\left(1-\frac{3k^2w_i^2}{20}\right)+\frac{2i}{\pi}\left[\left(1-\frac{3k^2w_i^2}{20}\right)\ln\frac{\gamma k w_i}{2}-\frac{1}{3}\left(1-\frac{27k^2w_i^2}{50}\right)\right]\right\}. \quad (3\text{-}30c)$$

When equations (3-30) are introduced into equation (3-28), we find that the contribution of the singular interval to the coefficient of K_{y_i} is

$$B_i' \sim \frac{\mu_i \omega w_i}{2}\left[\left\{\left(1-\frac{k^2w_i^2}{12}\right)+\frac{2i}{\pi}\left[\left(1-\frac{k^2w_i^2}{12}\right)\ln\frac{\gamma k w_i}{2}-\left(1-\frac{k^2w_i^2}{9}\right)\right]\right\}\right.$$

$$\left.-\frac{w_i^2}{3\tau_i}\left\{\left(1-\frac{3k^2w_i^2}{20}\right)+\frac{2i}{\pi}\left[\left(1-\frac{3k^2w_i^2}{20}\right)\ln\frac{\gamma k w_i}{2}-\frac{1}{3}\left(1-\frac{27k^2w_i^2}{50}\right)\right]\right\}\right]. \quad (3\text{-}31)$$

Similarly, the contribution to the coefficient of $K_{y_{i+1}}$ is

$$B_{i+1}' \sim \frac{\mu_i \omega w_i^3}{6\tau_i(1+\lambda_i)}\left\{\left(1-\frac{3k^2w_i^2}{20}\right)+\frac{2i}{\pi}\left[\left(1-\frac{3k^2w_i^2}{20}\right)\ln\frac{\gamma k w_i}{2}-\frac{1}{3}\left(1-\frac{27k^2w_i^2}{50}\right)\right]\right\}, \quad (3\text{-}32)$$

and the contribution to the coefficient of $K_{y_{i-1}}$ is

$$B_{i-1}' = \lambda_i B_{i+1}' \quad . \quad (3\text{-}33)$$

Equations (3-31), (3-32) and (3-33) are to be substituted for the right-hand side of equation (3-22) whenever j = i.

A similar limiting process is required to evaluate the contribution of the singular interval in equation (3-25). We have from Fig. 8 that

$$\cos(\beta-\alpha) = -\cos\left(180^\circ-(\beta-\alpha)\right) = \frac{-\delta}{\sqrt{\delta^2+s'^2}} \quad . \quad (3\text{-}34)$$

It follows from above that the contribution of the ith interval to equation (3-25) can be written as

$$\lim_{\delta \to 0} \left[\frac{i k_1 \delta}{4} \left\{ \left[I_1 - \frac{(1-\lambda_i)}{W_i + W_{i+1}} I_2 - \frac{I_3}{\tilde{\ell}_i} \right] K_{s_i} \right.\right.$$

$$\left.\left. + \frac{1}{1+\lambda_i} \left[\frac{I_2}{W_i + W_{i+1}} + \frac{I_3}{\tilde{\ell}_i} \right] K_{s_{i+1}} - \frac{\lambda_i}{1+\lambda_i} \left[\frac{\lambda_i I_2}{W_i + W_{i+1}} - \frac{I_3}{\tilde{\ell}_i} \right] K_{s_{i-1}} \right\} \right], \qquad (3\text{-}35)$$

where

$$I_1 = \int_{-W_i}^{W_i} \frac{H_1^{(1)}\left(k_1 \sqrt{\delta^2 + s'^2}\right)}{\sqrt{\delta^2 + s'^2}} ds' \quad , \qquad (3\text{-}36a)$$

$$I_2 = \int_{-W_i}^{W_i} \frac{s' H_1^{(1)}\left(k_1 \sqrt{\delta^2 + s'^2}\right)}{\sqrt{\delta^2 + s'^2}} ds' \quad , \qquad (3\text{-}36b)$$

$$I_3 = \int_{-W_i}^{W_i} \frac{s'^2 H_1^{(1)}\left(k_1 \sqrt{\delta^2 + s'^2}\right)}{\sqrt{\delta^2 + s'^2}} ds' \quad . \qquad (3\text{-}36c)$$

Equations (3-36) have been evaluated in Appendix D assuming that $H_1^{(1)}\left(k_1 \sqrt{\delta^2 + s'^2}\right)$ is given by equation (3-27). After the integrals have been obtained, we find that

$$\lim_{\delta \to 0} (\delta I_1) = \frac{-4i}{\pi k_1} \lim_{\delta \to 0} \left(\tan^{-1} \frac{W_i}{\delta} \right) = \frac{-2i}{k_1} \quad , \qquad (3\text{-}37a)$$

$$\lim_{\delta \to 0} (\delta I_2) = 0 \quad , \qquad (3\text{-}37b)$$

$$\lim_{\delta \to 0} (\delta I_3) = 0 \quad . \qquad (3\text{-}37c)$$

When equations (3-37) have been introduced into equation (3-35), then the contribution of the singular interval reduces to

$$\frac{K_{s_i}}{2} \quad , \tag{3-38}$$

which must be added to $-K_{s_i}$ in equation (3-35). Thus, we may rewrite the integral equation for H_y-polarization as

$$H_o e^{ik_1(x''\sin\phi_m + z''\cos\phi_m)} = -\frac{K_{s_i}}{2} \quad , \quad j = i \quad ,$$

$$= -\sum_{j=1}^{N} \frac{ik_1}{4} \left\{ K_{s_j} \int_{s_j - w_j}^{s_j + w_j} H_1^{(1)}(k_1|\bar{\rho}'' - \bar{\rho}'|)\cos(\beta'' - \alpha)\left(1 - \frac{(1-\lambda_j)(s'-s_j)}{w_j + w_{j+1}} - \frac{(s'-s_j)^2}{\tilde{\Sigma}_j}\right) ds' \right.$$

$$+ K_{s_{j+1}} \int_{s_j - w_j}^{s_j + w_j} H_1^{(1)}(k_1|\bar{\rho}'' - \bar{\rho}'|)\cos(\beta'' - \alpha)\frac{(s'-s_j)}{(1+\lambda_j)}\left(\frac{1}{w_j + w_{j+1}} + \frac{s'-s_j}{\tilde{\Sigma}_j}\right) ds'$$

$$\left. - K_{s_{j-1}} \int_{s_j - w_j}^{s_j + w_j} H_1^{(1)}(k_1|\bar{\rho}'' - \bar{\rho}'|)\cos(\beta'' - \alpha)\frac{\lambda_j(s'-s_j)}{(1+\lambda_j)}\left(\frac{\lambda_j}{w_j + w_{j+1}} - \frac{s'-s_j}{\tilde{\Sigma}_j}\right) ds' \right\}, \quad j \neq i \, . \tag{3-39}$$

3-3 Symmetry Considerations

Andreasen (1964) has pointed out that a considerable amount of computer time can be saved whenever the cross section of the scatterer is symmetric with respect to the z axis. In this case, it is possible to expand the incident field into a sum of an even mode of x and an odd mode of x and solve separately the matrix equations for the even and odd modes of the equivalent current density.

For example, assume Ey-polarization and expand the incident field as

$$E_y^i = E_{ye}^i + E_{yo}^i \quad , \tag{3-40}$$

and the propagation constant as

$$k_1 = k_{1r} + i k_{1i} \quad . \tag{3-41}$$

Then it is evident from equation (3-9) that

$$E_{ye}^i = Z_1 H_o e^{ik_1 z'' \cos\phi_{in}} \left[\cos(k_{1r} x'' \sin\phi_{in}) \cosh(k_{1i} x'' \sin\phi_{in}) \right.$$
$$\left. - i \sin(k_{1r} x'' \sin\phi_{in}) \sinh(k_{1i} x'' \sin\phi_{in}) \right] , \tag{3-42a}$$

$$E_{yo}^i = - Z_1 H_o e^{ik_1 z'' \cos\phi_{in}} \left[\cos(k_{1r} x'' \sin\phi_{in}) \sinh(k_{1i} x'' \sin\phi_{in}) \right.$$
$$\left. - i \sin(k_{1r} x'' \sin\phi_{in}) \cosh(k_{1i} x'' \sin\phi_{in}) \right] . \tag{3-42b}$$

When the even and odd mode of the equivalent current density are separated, the coefficient matrix for each mode is given by

$$\left(B'_{i,j}\right)_e = \sum_{j=1}^{N/2} \left(B'_{i,j} + B'_{i,N+1-j} \right) \quad , \quad i = 1, N/2 \, , \tag{3-43a}$$

$$\left(B'_{i,j}\right)_o = \sum_{j=1}^{N/2} \left(B'_{i,j} - B'_{i,N+1-j} \right) \quad , \quad i = 1, N/2 \, , \tag{3-43b}$$

where we have assumed that the first interval is the mirror image of the Nth interval with respect to the z axis.

The even and odd modes of the equivalent current density are determined by solving separately the matrix equation obtained when equation (3-43a) is equated to equation (3-42a) and equation (3-43b) is equated to equation (3-42b). Thus, the total equivalent current distribution is given by

$$K_i = K_{ie} + K_{io} \quad , \qquad i = 1, N/2 \quad ,$$

$$K_{N+1-i} = K_{ie} - K_{io} \quad , \quad i = 1, N/2 \quad . \tag{3-44}$$

Since matrix inversion routines are proportional to N^3, it has been four times faster to invert two matrices of order N/2 than it would have been to invert just one matrix of order N.

Whenever the scatterer is symmetric with respect to the direction of propagation, only an even mode of the equivalent current exists, and assuming vertical incidence, it is given by

$$E^i_{ye} = Z_1 H_o e^{ik_1 z} \quad . \tag{3-45}$$

The even coefficient matrix is given still by equation (3-43a) and, having solved the matrix equation obtained by equating equation (3-43a) and (3-45), the total equivalent current distribution is given by

$$K_i = K_{ie} \quad , \qquad i = 1, N/2 \quad ,$$

$$K_{N+1-i} = K_{ie} \quad , \qquad i = 1, N/2 \quad . \tag{3-46}$$

3-4 Numerical Examples

If the integrands of equations (3-3), (3-4), (3-8) and (3-10) are smoothly varying functions along each interval, then it is sufficient to approximate the integrand in this interval by a parabola. Thus, we may use Simpson's rule with n = 2 to integrate numerically across the interval. For example, the approximate value of the integral across the jth interval

of equation (3-22) is

$$E_{y_j}(\bar{\rho}) = \frac{\mu_1 \omega w_j}{12}\left\{ K_{y_j}\left[H_0^{(1)}(k_1|\bar{\rho}-\bar{\rho}_1'|)\left(1 + \frac{(1-\lambda_j)w_j}{w_j + w_{j+1}} - \frac{w_j^2}{\tilde{\tau}_j}\right)\right.\right.$$

$$\left. + 4\, H_0^{(1)}(k_1|\bar{\rho}-\bar{\rho}_2'|) + H_0^{(1)}(k_1|\bar{\rho}-\bar{\rho}_3'|)\left(1 - \frac{(1-\lambda_j)w_j}{w_j + w_{j+1}} - \frac{w_j^2}{\tilde{\tau}_j}\right)\right]$$

$$- \frac{w_j K_{y_{j+1}}}{(1+\lambda_j)}\left[H_0^{(1)}(k_1|\bar{\rho}-\bar{\rho}_1'|)\left(\frac{1}{w_j + w_{j+1}} - \frac{w_j}{\tilde{\tau}_j}\right) - H_0^{(1)}(k_1|\bar{\rho}-\bar{\rho}_3'|)\left(\frac{1}{w_j + w_{j+1}} + \frac{w_j}{\tilde{\tau}_j}\right)\right]$$

$$\left. + \frac{w_j \lambda_j K_{y_{j-1}}}{(1+\lambda_j)}\left[H_0^{(1)}(k_1|\bar{\rho}-\bar{\rho}_1'|)\left(\frac{\lambda_j}{w_j + w_{j+1}} + \frac{w_j}{\tilde{\tau}_j}\right) - H_0^{(1)}(k_1|\bar{\rho}-\bar{\rho}_3'|)\left(\frac{\lambda_j}{w_j + w_{j+1}} - \frac{w_j}{\tilde{\tau}_j}\right)\right]\right\}, \qquad (3\text{-}47)$$

where the position vectors $\bar{\rho}_1$, $\bar{\rho}_2$ and $\bar{\rho}_3$ have been defined in Fig. 9.

To demonstrate the validity of the integral representations and their numerical solution, we will compare the numerical results with the analytical results obtained for the case of scattering from circular cylinders. It is shown in Appendix C that the transverse magnetic field intensity which is scattered by a perfectly conducting circular cylinder in the presence of an Ey-polarized plane wave is

$$H_\rho^{sc}(\rho,\phi) = -\frac{2iH_0}{k_1\rho} e^{ik_1 h} \sum_{n=1}^{\infty} n i^{-n} \frac{J_n(k_1 R)}{H_n^{(1)}(k_1 R)} H_n^{(1)}(k_1\rho) \sin n\phi \quad , \qquad (3\text{-}48a)$$

and

$$H_\phi^{sc}(\rho,\phi) = -iH_0 e^{ik_1 h} \sum_{n=0}^{\infty} i^{-n} \varepsilon_n \frac{J_n(k_1 R)}{H_n^{(1)}(k_1 R)}\left\{\frac{n}{k_1\rho} H_n^{(1)}(k_1\rho) - H_{n+1}^{(1)}(k_1\rho)\right\} \cos n\phi \quad , \qquad (3\text{-}48b)$$

where $$\varepsilon_n = \begin{cases} 1 & , \quad n = 0 \\ 2 & , \quad n \geq 1 \end{cases} ,$$

and R is the radius of the cylinder.

The induced surface current density around the cylinder is

$$K_y(\varphi) = \frac{2H_o}{\pi k_1 R} e^{ik_1 h} \sum_{n=0}^{\infty} i^{-n} \varepsilon_n \frac{\cos n\varphi}{H_n^{(1)}(k_1 R)} , \qquad (3\text{-}49a)$$

and

$$M_s(\varphi) = 0. \qquad (3\text{-}49b)$$

The distance h in equations (3-48) and (3-49) is the depth from the earth-air interface to the center of the cylinder. Since some point must be adopted as origin for a phase and attenuation reference, the earth-air interface has been chosen to facilitate comparison of these results with those of the half-space problem considered in Chapter 7. In addition, we will chose our incident field to be the transmitted field of a plane wave incident upon a conductive half-space. This choice of incident field also will facilitate our discussion in Chapter 7 when we wish to estimate the significance of coupling between the conductor and the earth-air interface. It should be noted, however, that this still is a "ficticious" model in that reflections from the earth-air interface are ignored when computing the currents induced on the surface of the conductor and also, the earth-air interface is ignored when computing the scattered fields at this boundary.

We have from Stratton (1941, p. 493) that the transmitted electric field intensity of an Ey-polarized plane wave incident upon a conductive half-space is

$$E_y^{trans} = \frac{2\mu_1 k_0 \cos\varphi_{in}}{\mu_1 k_0 \cos\varphi_{in} - \mu_0 \sqrt{k_1^2 - k_0^2 \sin^2\varphi_{in}}} Z_0 H_0 e^{ik_1(x'' \sin\varphi_{th} - z'' \cos\varphi_{th})} \tag{3-50}$$

where φ_{th} is given from Snell's Law, equation (2-76) as

$$\cos\varphi_{th} = \sqrt{1 - \frac{k_0^2}{k_1^2} \sin^2\varphi_{in}} \quad .$$

We will consider only the special case of normal incidence since in most problems of geophysical interest the transmitted field propagates normally away from the interface even for grazing angles of incidence. In addition, this approximation yields the greatest saving in computer time as a result of the symmetry. Thus, equation (3-50) reduces to

$$E_y^{trans} = \frac{2Z_1}{1 + Z_1/Z_0} H_0 e^{-ik_1 z''} \quad . \tag{3-51}$$

From equation (3-51), it is evident that the desired incident field for Ey-polarization is obtained by setting φ_{in} equal to 180° and replacing $Z_1 H_0$ by

$$\frac{2Z_1}{1 + Z_1/Z_0} H_0 \tag{3-52}$$

in the pertinent equations.

The unknown equivalent electric surface current density around the cylinder was determined from equations (3-22) after $Z_1 H_0$ had been replaced by (3-52). The cylinder coutour was approximated by inscribing 10, 20 and 40 intervals as is shown in Fig. 10 for N = 20. By increasing the number N of sampled values, we estimate more accurately the cylinder contour,

the integration around the contour, and the current density distribution.

Figs. 11 through 16 demonstrate that the integral representations derived for Ey scattering from perfect conductors are valid, and that the numerical solution rapidly converges as N increases. We have assumed normal incidence in this example and that: the depth z_1 to the top of the cylinder is 20 m, the cylinder radius is 100 m, the incident field frequency is 1000 hz, and the conductivity of the whole space is 10^{-3} mhos/m.

Since the induced current density is symmetric with respect to the z-axis, only part of the results have been plotted in Figs. 11 and 12. It is seen that the maximum current amplitude occurs on the shadow side of the cylinder, as discussed by King and Wu (1959) for the case of scattering from circular cylinders in air. However, since the cylinder is situated in a conducting medium, the minimum current amplitude is due also to attenuation of the incident field as it propagates through the ground. The maximum errors occur at the points of maximum and minimum illumination, although the errors rapidly decrease to less than 1% as N is increased.

In Figs. 13 through 16, the scattered magnetic field intensity obtained from these N sampled values of the current density has been plotted for points of observation near the cylinder on the plane 20 m above it. It is seen that a slight instability in the field occurs close to the cylinder, especially for N = 10, but disappears as N increases. This problem, which will be discussed below, is caused by the inaccuracy of a parabolic approximation to the integration along that part of the contour in close proximity to the observer. However, it is sufficient to observe here that the instability obviously decreases as the sampling

width decreases. We see that for N = 40, the maximum error is less than 0.5%.

It can be shown by following a development similar to that of Harrington (1961, p. 235) or Appencix C. that the axial magnetic field intensity which is scattered by a perfectly conducting circular cylinder in the presence of an Hy-polarized plane wave is

$$H_y^{sc}(\rho,\varphi) = H_0 e^{ik_1 h} \sum_{n=0}^{\infty} i^{-n} \varepsilon_n a_n H_n^{(1)}(k_1\rho)\cos n\varphi \quad , \tag{3-53}$$

where

$$a_n = - \frac{n J_n(k_1 R) - k_1 R J_{n+1}(k_1 R)}{n H_n^{(1)}(k_1 R) - k_1 R H_{n+1}^{(1)}(k_1 R)} \quad ,$$

and

$$\varepsilon_n = \begin{cases} 1 & , \quad n = 0 \\ 2 & , \quad n \geq 1 \end{cases} \quad .$$

As in equations (3-48) and (3-49), we have chosen our origin to be at the earth-air interface.

It follows from equation (3-51) that the transmitted magnetic field intensity of an Hy-polarized plane wave incident normal to a conductive half-space is

$$H_y^{trans} = \frac{2 H_0}{1 + z_1/z_0} e^{ik_1 z''} \quad . \tag{3-54}$$

Thus, the desired incident field for Hy-polarization is obtained by setting φ_{in} equal to zero and replacing H_0 by

$$\frac{2 H_0}{1 + z_1/z_0} \quad , \tag{3-55}$$

in the pertinent equations.

10, 20 and 40 sampled values of the equivalent electric surface current density were determined from equation (3-39) after H_o had been replaced by (3-55), considering the same cylinder studied for Ey-polarization. Figs. 17 and 18 show the axial (y) magnetic field intensity obtained from these sampled values for points near the cylinder. Again, an instability is observed, and although the amplitude of the oscillations is larger than for Ey-polarization, it also obviously decreases as the sampling width decreases. Since these oscillations are meaningless with respect to the actual problem, no attempt has been made to define them properly. We see, however, that good convergence of the Hy-polarization integral representations is obtained for N = 40, with the maximum error being less than 1.0%.

We have already pointed out that the instabilities arise from the inaccuracy of a parabolic approximation to the integration along that part of the coutour in close proximity to the observer. This can be seen in the following way: Assume that the equivalent surface current density across the jth interval is approximately constant. Then the contribuiton of the integral along the jth interval to the scattered field in equations (3-3) and (3-4) can be written as

$$E_{yj}^{sc} \sim -\frac{\mu_1 \omega}{4} K_{yj} \int_{s_j - w_j}^{s_j + w_j} H_o^{(1)}(k_1 |\bar{\rho} - \bar{\rho}'|)\, ds' \quad , \tag{3-56}$$

and

$$H_{yj}^{sc} \sim \frac{i k_1}{4} K_{sj} \int_{s_j - w_j}^{s_j + w_j} \cos(\beta - \alpha)\, H_1^{(1)}(k_1 |\bar{\rho} - \bar{\rho}'|)\, ds' . \tag{3-57}$$

Since the Hankel function is singular when both the real and imaginary parts of the argument are zero, it is evident that the value of the argument of equations (3-56) and (3-57) will pass through a pseudo-

singularity for points of observation close to the contour. Fig. 19 represents a hypothetical plot of the integrand of equation (3-56) or (3-57) for a point close to the contour, and the "best" parabola which would be interpreted for this curve. It is seen that the area under the parabola is not a good approximation to the true area.

If the point of observation is to one side of the interval, as in Fig. 20, then a parabolic approximation to the integration of equations (3-56) or (3-57) is much better. Although the parabola still does not represent a good approximation to the integrand, it is seen that the area under the parabola could constitute a fair estimate of the area under the hypothetical curve since the positive and negative errors tend to compensate one another.

Inasmuch as this problem arises when the argument of the Hankel function is small, it can be overcome by making a small argument expansion and integrating analytically across these intervals as was done in section (3-2-3). For the best accuracy, this should be done for points of observation just to one side of the interval, as in Fig. 20, as well as for points of observation over the interval. Thus, small argument expansions will be used for intervals near where the boundary condition is being enforced, as well as when calculating the scattered fields.

Before the small argument expansion is made, it is convenient to rewrite the integral representation in a more suitable form involving as few analytical integrations as possible. It is shown in Appendix D that, in general, the contribution of the jth interval to the boundary electric field intensity (equation (3-22)) can be written as

$$E_{y_j} = \frac{\mu_1 \omega}{4}\left\{\left[HK00 - \frac{(1-\lambda_j)}{A_j}(HK01 - c_j HK00) - \frac{(HK02 - 2c_j HK01 + c_j^2 HK00)}{\tilde{\tau}_j}\right] K_{y_j}\right.$$

$$+ \frac{K_{y_{j+1}}}{1+\lambda_j}\left[\frac{HK01 - c_j HK00}{A_j} + \frac{(HK02 - 2c_j HK01 + c_j^2 HK00)}{\tilde{\tau}_j}\right]$$

$$\left. - \frac{\lambda_j K_{y_{j-1}}}{1+\lambda_j}\left[\frac{\lambda_j (HK01 - c_j HK00)}{A_j} - \frac{(HK02 - 2c_j HK01 + c_j^2 HK00)}{\tilde{\tau}_j}\right]\right\}, \qquad (3\text{-}58)$$

where

$$\left.\begin{aligned} \Delta_j &= w_j + w_{j+1} \\ \lambda_j &= \frac{w_j + w_{j+1}}{w_j + w_{j-1}} \\ \tilde{\tau}_j &= (w_j + w_{j+1})(w_j + w_{j-1}) \\ a &= (x - x_1')\sin\alpha_j - (z - z_1')\cos\alpha_j \\ b &= (x - x_3')\sin\alpha_j - (z - z_3')\cos\alpha_j = a + 2w_j \\ c_j &= a + w_j \\ \delta &= -[(x - x_1')\cos\alpha_j + (z - z_1')\sin\alpha_j] \end{aligned}\right\}, \qquad (3\text{-}59)$$

and

$$HK00 = \int_a^b H_0^{(1)}\left(k_1\sqrt{\delta^2 + s'^2}\right) ds', \qquad (3\text{-}60a)$$

$$HK01 = \int_a^b s' H_0^{(1)}\left(k_1\sqrt{\delta^2 + s'^2}\right) ds', \qquad (3\text{-}60b)$$

$$HK02 = \int_a^b s'^2 H_0^{(1)}\left(k_1\sqrt{\delta^2 + s'^2}\right) ds'. \qquad (3\text{-}60c)$$

The geometrical symbols in equation (3-58) are defined in Fig. 21. Using the small argument approximation for $H_o(k_1\sqrt{\delta^2 + s'^2})$ given by equation (3-26), equations (3-60) have been evaluated in Appendix D.

Similarly, it is shown in Appendix D that in general the contribution of the jth interval to the scattered magnetic field intensity (equation (3-12) can be written as

$$\vec{H}^{sc}_{t_j} = -\frac{ik_1}{4}\left[(A\cos\alpha_j + B\delta\sin\alpha_j)\hat{x} + (A\sin\alpha_j - B\delta\cos\alpha_j)\hat{z}\right], \tag{3-61}$$

where

$$A = \left[I_2 - \frac{(1-\lambda_j)}{\Delta_j}(I_3 - c_j I_2) - \frac{I_4 - 2c_j I_3 + c_j^2 I_2}{\tilde{L}_j}\right] K_{y_j}$$

$$+ \frac{K_{y_{j+1}}}{1+\lambda_j}\left[\frac{I_3 - c_j I_2}{\Delta_j} + \frac{I_4 - 2c_j I_3 + c_j^2 I_2}{\tilde{L}_j}\right]$$

$$- \frac{\lambda_j K_{y_{j-1}}}{1+\lambda_j}\left[\frac{\lambda_j (I_3 - c_j I_2)}{\Delta_j} - \frac{I_4 - 2c_j I_3 + c_j^2 I_2}{\tilde{L}_j}\right], \tag{3-62a}$$

$$B = \left[I_1 - \frac{(1-\lambda_j)}{\Delta_j}(I_2 - c_j I_1) - \frac{I_3 - 2c_j I_2 + c_j^2 I_1}{\tilde{L}_j}\right] K_{y_j}$$

$$+ \frac{K_{y_{j+1}}}{1+\lambda_j}\left[\frac{I_2 - c_j I_1}{\Delta_j} + \frac{I_3 - 2c I_2 + c^2 I_1}{\tilde{L}_j}\right]$$

$$- \frac{\lambda_j K_{y_{j-1}}}{1+\lambda_j}\left[\frac{\lambda_j (I_2 - c_j I_1)}{\Delta_j} - \frac{I_3 - 2c_j I_2 + c_j^2 I_1}{\tilde{L}_j}\right], \tag{3-62b}$$

$$I_1 = \int_a^b \frac{H_1^{(1)}\left(k_1\sqrt{\delta^2 + s'^2}\right)}{(\delta^2 + s'^2)^{1/2}}\, ds', \tag{3-63a}$$

$$I_2 = \int_a^b s' \frac{H_1^{(1)}\left(k_1\sqrt{\delta^2 + s'^2}\right)}{(\delta^2 + s'^2)^{1/2}}\, ds', \tag{3-63b}$$

$$I_3 = \int_a^b s'^2 \frac{H_1^{(1)}\left(k_1\sqrt{\delta^2+s'^2}\right)}{(\delta^2+s'^2)^{1/2}}\,ds' \,, \tag{3-63c}$$

$$I_4 = \int_a^b s'^3 \frac{H_1^{(1)}\left(k_1\sqrt{\delta^2+s'^2}\right)}{(\delta^2+s'^2)^{1/2}}\,ds' \,, \tag{3-63d}$$

Equations (3-63) have been evaluated in Appendix D after approximating $H_1(k_1\sqrt{\delta^2+s'^2})$ by equation (3-27). If equations (3-58) through (3-63) are used to calculate the contribution of the jth interval when both $|k_1||\bar{\rho}-\bar{\rho}_1'|$ and $|k_1||\bar{\rho}-\bar{\rho}_3'|$ are less than 0.3, then the observed instabilities disappear and an accuracy comparable to that obtained on the flanks of the scattered field results for points of observation near the scatterer contour.

A similar analysis must be carried out for H_y-polarization. Again, it is shown in Appendix D that in general the contribution of the jth interval to the boundary axial magnetic field intensity (equation 3-39) can be written as

$$H_{y_j} = \frac{ik_1\delta}{4}\cdot B \,, \tag{3-64}$$

where B is given by equation (3-62b). The approximate contribution of the jth interval to the scattered axial magnetic field intensity is given by equation (3-64), but with opposite sign.

To demonstrate that equations (3-58) through (3-64) are necessary to predict accurately the scattered field for points of observation close to the scatterer without taking an excessive number of sampled values of the surface current density, we have chosen a particularly good example. The real and the imaginary parts of the axial magnetic field intensity

have been plotted in Figs. 22 and 23 assuming an Hy-polarized plane wave incident normal to a conductive half-space. The depth z_1 to the top of the cylinder is 3 m, the cylinder radius is 100 m, the incident field frequency is 1000 hz, the conductivity of the whole-space is 10^{-3} mhos/m, and the cylinder contour has been approximated by 20 intervals. It is seen that the undesirable oscillations have been eliminated completely by using the small argument approximation given by equations (3-64), with a maximum error of about 1% being obtained through 20 sampled values of the current density.

The important conclusion to be drawn from Figs. 11 through 18 is that if the numerical integration is inaccurate, a significant change in all the sampling widths brings about a significant change in the predicted scattered field. We are led to believe that if the predicted fields then converge, the numerical integration and sampling have been performed correctly. In future discussions, a small argument approximation will be used whenever $(|k_1||\tilde{\rho} - \tilde{\rho}'|)_{max} \leq .3$ for any interval.

To illustrate the generality of the program, we will examine the field scattered by a vertical slab which is 30 m wide and 300 m deep, assuming an Ey-polarized incident plane wave. The general cross section has been drawn in Fig. 24 (a) and a detail of the contour at one corner has been drawn in Fig. 24 b. A sharper corner for the slab could have been chosen, but this would require a tighter sampling interval to define properly both the contour and the current density. We have assumed that the depth z_1 to the top of the slab is 20 m, the incident field frequency is 1000 hz and the conductivity of the whole-space is 10^{-3} mhos/m.

The variation in the magnitude of the equivalent electric surface

current density from the top (s' = 0 m) to the bottom (s' = 312 m) of the slab is shown in Fig. 25. The variation of the phase of the equivalent electric surface current density around this part of the contour is shown in Fig. 26. Since only slight differences are obtained in the current density distribution for 30 and 42 sampled values, we have assumed that a convergent solution has been found.

A very interesting variation in the magnitude of the surface current density is seen to occur around the bottom limit of the slab. We see that the current density increases around the bend in the contour and then is constant on the bottom flat portion. (Actually, there is a very slight decrease in the amplitude of the current density at s' = 312 m). Van Bladel (1964, p. 388) points out that although the total current in the neighborhood of a corner remains finite, the current density becomes infinite at the corners. Thus, we may expect an increase in the magnitude of the current density wherever the radius of curvature becomes small. For this reason, a small sampling interval is required in these regions so that the current density is defined properly.

If we wish to study scattering from a rectangular slab, we should not attempt to place a sampling point at a corner. Instead, Andreasen (1964) recommends that the current density should be sampled evenly to each side of the corner.

The scattered magnetic field intensity calculated from these sampled values of the current density has been plotted in Figs. 27 and 28. It is important to note that the phase of $\vec{H}$ is dependent upon the position of the observer in space. This result will be true for any cylinder when the electrical parameters of the earth are similar to those of this

example.

In Figs. 29 through 32, analytical results are given for the horizontal magnetic field intensity scattered by a perfectly conducting circular cylinder in a whole-space having various conductivities. We have assumed normal incidence of an Ey-polarized plane wave in this example and that: the depth z_1 to the top of the cylinder is 20 m, the cylinder radius is 100 m, and the incident field frequency is 1000 hz.

It is seen that for extremely low conductivities of the whole-space, the magnetic field intensity has a large amplitude and is predominantly out-of-phase with the incident field. As the conductivity of the whole-space increases, we observe that the amplitude of the magnetic field intensity decreases, the in-phase component becomes larger than the out-of-phase component and then becomes smaller again, and the peaks of the vertical field shift closer to the crossover.

The decrease in amplitude and change in phase of the scattered field are caused by both the decrease in wavelength with respect to the radius of the cylinder and by an increase in the attenuation of the fields as the conductivity of the whole-space increases. This can be seen intuitively from equations (3-49a). When the wavelength in the whole-space is very much greater than the radius of the cylinder, $|k_1 R| << 1$ and the order zero of the Hankel function becomes dominant. Thus, using the small argument expansion for $H_0^{(1)}(k_1 R)$, the surface current density is given by

$$K_y(\phi) \sim \frac{-i H_0 e^{ik_1 h}}{k_1 R \ln(k_1 R)} , \qquad (3\text{-}65)$$

and we see that it is independent of ϕ and 90° out-of-phase with the incident field if k_1 is real (which is true when the whole-space has a

low conductivity) and h is small with respect to the wavelength. As a result, the magnetic field intensity near the cylinder will be large, 90° out of phase with the incident field, and the field will be that of a line of current.

In Figs. 29 and 30, the wavelength of the incident field is always very much greater than the radius of the cylinder and, as a result, the magnitude of the scattered field is large for the three cases. However, a decrease in the amplitude of the out-of-phase component and an increase in the in-phase component is observed since higher order terms become important in equation (3-49a) as the conductivity of the whole-space increases and since k_1 becomes larger in equation (3-65). In addition, there is some phase shift as both the incident and scattered fields propagate through the earth.

In Figs. 31 and 32, we see that the amplitude of the scattered fields becomes significantly smaller as the wavelength of the incident field approaches the radius of the cylinder and as the skin depth (δ') decreases. We see also that the peak of the vertical field component in Fig. 32 shifts towards the crossover as the conductivity of the whole space increases. The reason for this is that the surface current density shifts to being predominantly on the illuminated side of the cylinder as the wavelength decreases. When the wavelength is very much greater than the cylinder radius, the current density is constant around the cylinder and this current radiates like a line source located at the center of the cylinder. However, as the wavelength decreases, there is an increased tendency for the current density to be zero on the shadow side of the cylinder, as is seen in Fig. 11, so that the location of an effective

line source is above the center of the cylinder (i.e. nearer the observer). Thus, the peak in the vertical field component will be closer to the cross-over. In addition, we observe in Figs. 31 and 32 that the spacial wavelength of the fields becomes apparent in the data for high conductivities of the whole-space.

Since the wavelength (λ) and the skin depth (δ') in the whole-space determine the behavior of scattering from perfectly conducting cylinders, a similar trend will occur as the frequency of the incident field increases. In Figs. 33 and 34, we have assumed normal incidence of an Ey-polarized plane wave and that: the depth z_1 to the top of the cylinder is 20 m, the cylinder radius is 100 m, and the conductivity of the whole-space is 10^{-3} mhos/m. It is seen that as the frequency increases, the amplitude of the magnetic field intensity decreases and the peaks of the vertical field shift closer to the cross over, as was observed in Figs. 29 through 32. Note, however, that the in-phase component is larger than the out-of-phase component at low frequencies since the ratio wavelength/skin depth is as large as in Fig. 31 for $\sigma_1 = 10^{-5}$ mhos/m. Nonetheless, a large amplitude is observed at low frequencies since the wavelength is very much greater than the radius of the cylinder.

In Fig. 35, the conductivity of the whole-space has been set equal to zero so that the effect of the wavelength alone in determining the magnitude and phase of the scattered magnetic field can be studied. It is seen that as the wavelength decreases, the amplitude of the scattered magnetic field decreases. However, unlike scattering from perfectly conducting cylinders in a conductive whole-space, the out-of-phase component is always larger than the in-phase component.

The results of Figs. 29 through 35 have been summarized in Figs. 36 and 37 by plotting the peak value of $|H_x|$ against log (λ/R) and the phase of the peak value of $|H_x|$ against log (λ/R) for two ratios of wavelength to skin depth. Note, however, that these results assume that the conductivity of the cylinder is infinite. If finitely conducting circular cylinders are to be examined, the wavelength inside the cylinder must be considered also. Thus, a third axis of log (λ_{cyl}/R_{cyl}) could be plotted out of the page and the area between $\lambda/\delta = 0$ and $\lambda/\delta = 6.28$ in Figs. 36 and 37 would become a volume distribution.

Fig. 36 illustrates that the general effect of wavelength upon the magnitude of the scattered field is to increase $|H_x|$ as λ/R increases for a fixed point of observation. Consequently, as the frequency of the incident field is increased, the magnitude of the scattered field will decrease. However, Fig. 36 points out also that if $\lambda \geq 5R$, the magnitude of the scattered magnetic field intensity is larger in a conductive earth than if the same wavelength had been used in free space.

This interesting result is due to the fact that the magnetic field intensity transmitted at the fictitious earth-air interface increases in magnitude as the conductivity of the earth increases. Inasmuch as the transmitted electromagnetic field is considered to be the incident field in these examples, this indicates that the equivalent electric surface current density will increase with conductivity. whenever attenuation is not important since $K_y = H_s^t$ at the surface of a perfectly conducting cylinder.

This effect can be understood best by studying the transmitted magnetic field intensity. If we assume that k is equal to k_o in air, then it is evident from equation (3-51) that the magnitude of the trans-

mitted horizontal magnetic field intensity will be given by

$$\left| H_x^i \right| = \left| \frac{2}{1 + z_1/z_o} H_o e^{-ik_o z} \right| = \left| H_o e^{-ik_o z} \right| . \qquad (3\text{-}66)$$

However, in a conductive medium where $\lambda/\delta' = 6.28$ and $\lambda = \lambda_{air}$ of equation (3-66), k will be given by $k_o + ik_o$ and the magnitude of the transmitted magnetic field intensity will become

$$\left| H_x^i \right| = \left| \frac{2}{1 + \frac{\mu_o \omega}{k_o + ik_o}} H_o e^{+k_o z - ik_o z} \right| > \left| H_o e^{-ik_o z} \right| , \qquad (3\text{-}67)$$

if attenuation is not significant. Thus, it is evident from equation (3-67) that for a given wavelength, $|H_x^i|$ is larger in a conductive half-space than in air whenever attenuation is not too important.

Intuitively, it is expected that attenuation will not be important for $z_1 \sim R$ and $|kR| << 1$. Consequently, it follows that the curve of $|H_x|$ versus log (λ/R) will be displaced downwards with increasing λ/δ' for $\lambda \leq 5R$ and displaced upwards with increasing λ/δ' for $\lambda \geq 5R$.

Fig. 37 illustrates the variation of the phase of H_x with increasing λ/R. It is seen that there is a minimum in the plase of H_x for $\lambda \sim 30R$ and that the effect of the conductive half-space is to reduce the phase of H_x.

Figs. 38 and 39 compare the analytical solution with an approximate solution given by Meyer (1963) which sometimes has been used to predict plane wave scattering by conducting cylinders in a whole-space of low conductivity. For comparison, we have assumed normal incidence of an Ey-polarized plane wave and that: the depth z_1 to the top of the cylinder is 20 m, the cylinder radius is 100 m, and the frequency of the incident

field is 10^{-3} mhos/m. It is evident that for perfectly conducting cylinders, Meyer's solution fails to predict the amplitude and phase of the scattered field even for free space exterior to the cylinder. The reason for this discrepancy is that his solution has not accounted for the contribution of the incident electric field intensity, which is of paramount importance in a whole space of low conductivity.

3-5 Accuracy and Limitations

The validity of the integral representations for scattering from perfectly conducting cylinders has been demonstrated by comparing the numerical results with the analytical results for the case of scattering from circular cylinders. In general, however, the accuracy of the numerical results can be demonstrated only by observing the solution convergence as the number of sampled values is increased. Mei and Van Bladel (1963b) and Andreasen (1964) have suggested that about 10 subdivisions per wavelength are sufficient to give a convergent result. As a general rule, however, this seems to be applicable only to scatterers in free space.

In Figs. 40 and 41, numerical results are compared with analytical results for the horizontal magnetic field intensity predicted when a cylinder has been sampled 14 times and 36 times per wavelength. It is seen that only when the cylinder has been sampled 36 times per wavelength do we obtain a maximum error of less than 1%. Thus, we stress that only by checking the convergence can we ensure accuracy of the numerical results. A general rule on the sampling interval could lead to an unrecognized error since the skin depth and the wavelength interact to influence

what sampling interval is required.

In Fig. 42, numerical results are compared with analytical results when the cylinder of Figs. 40 and 41 has been sampled 14 times and the order n of Simpson's rule across each interval is 2 and 4. It is seen that increasing the order n from 2 to 4 increases the maximum error in the predicted results. However, since no significant change is observed when n is increased to 6, this remaining error must represent the inaccuracy of the current density representation.

It should be noted that increasing the number of sampled values of the current density is not always the most economical way to increase solution accuracy. The reason for this is that it is more desirable to obtain solution convergence by increasing the order n in Simpson's rule rather than to increase the number of sampling points whenever the parabolic approximation to the current density is accurate and the scatterer contour is described accurately. This procedure is more economical since the computer time required to solve a set of N linear equations is proportional to N^3, whereas the computer time required to set up the coefficient matrix is proportional to the product of N^2 and the order of Simpson's rule.

In Figs 40 and 41, it is seen that a small error is obtained in the predicted result when the cylinder is sampled 36 times per wavelength and that an n of 2 is sufficient. Although this sampling interval improved the current density representation, it also increased the integration accuracy to greater than that of Fig. 42 with n equal to 4. Thus, it is evident in this example that once the current density is sampled accurately, the order 2 in Simpson's rule is sufficient for integration

accuracy. We note thereby that increasing the number of sampled values of the current density is the best general test since it checks both the integration accuracy and the accuracy of the current density representation.

CHAPTER 4

SCATTERING FROM CYLINDERS WITH LOW SURFACE IMPEDANCE

In Chapter 3, the problem of scattering from perfectly conducting cylinders was examined assuming both Ey and Hy polarizations. In addition, the representation of the unknown surface current densities and the solution of the resulting singular Fredholm integral equations was discussed. In this chapter, we wish to consider the more general case of scattering from cylinders which have both a low surface impedance and a small curvature compared to the attenuation per unit distance.

Andreasen (1965b) has considered this problem, but it should be noted that although he states that the field must not penetrate deeply into the scattering body, his solution also requires that the contour curvature is small compared to the attenuation per unit distance. Mitzner (1967, 1968) has extended this work somewhat by introducing curvature dependent boundary conditions. However, as in Chapter 2, the analysis of this section closely follows that of Andreasen, with the principle difference being the physical situation to which the solution is applied.

4-1 Derivation of the Integral Equations

It was shown in Section 2-5 that if the surface impedance of the scatterer is low with respect to the surrounding whole space, and if the curvature of the scatterer is small compared to the attenuation per unit distance, then the axial field components in the conductive whole-space can be written as

$$E_y^t(\bar{\rho}) = E_y^i(\bar{\rho}) - \frac{Z_1 \gamma_1^2}{4k_1}\int_{C_1} K_y(\bar{\rho}')\, H_o^{(1)}(\gamma_1|\bar{\rho}-\bar{\rho}'|)\, ds'$$

$$+ \frac{iZ_1 k_{y_1}\gamma_1}{4k_1}\int_{C_1} K_s(\bar{\rho}')\sin(\beta-\alpha)\, H_1^{(1)}(\gamma_1|\bar{\rho}-\bar{\rho}'|)\, ds'$$

$$- \frac{i\gamma_1}{4}\int_{C_1} Z_{2y}(\bar{\rho}')\, K_y(\bar{\rho}')\cos(\beta-\alpha)\, H_1^{(1)}(\gamma_1|\bar{\rho}-\bar{\rho}'|)\, ds' , \qquad (4\text{-}1)$$

and

$$H_y^t(\bar{\rho}) = H_y^i(\bar{\rho}) + \frac{\gamma_1^2}{4Z_1 k_1}\int_{C_1} Z_{2s}(\bar{\rho}')\, K_s(\bar{\rho}')\, H_o^{(1)}(\gamma_1|\bar{\rho}-\bar{\rho}'|)\, ds'$$

$$+ \frac{ik_{y_1}\gamma_1}{4Z_1 k_1}\int_{C_1} Z_{2y}(\bar{\rho}')\, K_y(\bar{\rho}')\sin(\beta-\alpha)\, H_1^{(1)}(\gamma_1|\bar{\rho}-\bar{\rho}'|)\, ds'$$

$$+ \frac{i\gamma_1}{4}\int_{C_1} K_s(\bar{\rho}')\cos(\beta-\alpha)\, H_1^{(1)}(\gamma_1|\bar{\rho}-\bar{\rho}'|)\, ds' , \qquad (4\text{-}2)$$

where the earth parameters have been referred to by the subscript 1 and the cylinder parameters have been referred to by the subscript 2.

As in Chapter 3, the unknown current densities, Ky and Ks, are determined by enforcing the boundary conditions on tangential $\vec{E}$ and $\vec{H}$ and solving the resulting integral equations. For finitely conducting bodies, these boundary conditions are

$$\hat{n} \times (\vec{E}_1^t - \vec{E}_2^t) = 0 , \qquad (4\text{-}3a)$$

and

$$\hat{n} \times \left(\bar{H}_1^t - \bar{H}_2^t \right) = 0. \tag{4-3b}$$

Since we assume that the surface impedance of the scatterer is low with respect to the surrounding whole-space and that the curvature of the scatterer is small compared to the attenuation per unit distance, the representation of the fields inside the conductor is particularly simple. Thus, we can write from section (2-5) that just inside the contour boundary

$$E_{y_2}^t = Z_{2y} H_{s_2}^t = Z_{2y} K_y , \tag{4-4a}$$

$$H_{y_2}^t = - K_s . \tag{4-4b}$$

If we let the point of observation approach a boundary point given by the position vector $\bar{\rho}''$ and enforce (4-3), then equations (4-1) and (4-2) reduce to the desired coupled integral equations

$$E_y^i(\bar{\rho}'') = Z_{2y}(\bar{\rho}'') K_y(\bar{\rho}'') + \frac{Z_1 \gamma_1^2}{4k_1} \int_{C_1} K_y(\bar{\rho}') H_0^{(1)}(\gamma_1 |\bar{\rho}'' - \bar{\rho}'|) ds'$$

$$- \frac{i Z_1 k_{y_1} \gamma_1}{4k_1} \int_{C_1} K_s(\bar{\rho}') \sin(\beta'' - \alpha) H_1^{(1)}(\gamma_1 |\bar{\rho}'' - \bar{\rho}'|) ds'$$

$$+ \frac{i\gamma_1}{4} \int_{C_1} Z_{2y}(\bar{\rho}') K_y(\bar{\rho}') \cos(\beta'' - \alpha) H_1^{(1)}(\gamma_1 |\bar{\rho}'' - \bar{\rho}'|) ds' , \tag{4-5}$$

and

$$H_y^i(\bar{\rho}'') = -K_s(\bar{\rho}'') - \frac{\gamma_1^2}{4Z_1 k_1}\int_{C_1} Z_{2s}(\bar{\rho}')\,K_s(\bar{\rho}')\,H_0^{(2)}(\gamma_1|\bar{\rho}''-\bar{\rho}'|)\,ds'$$

$$- \frac{ik_{y_1}\gamma_1}{4Z_1 k_1}\int_{C_1} Z_{2y}(\bar{\rho}')\,K_y(\bar{\rho}')\sin(\beta''-\alpha)\,H_1^{(2)}(\gamma_1|\bar{\rho}''-\bar{\rho}'|)\,ds'$$

$$- \frac{i\gamma_1}{4}\int_{C_1} K_s(\bar{\rho}')\cos(\beta''-\alpha)\,H_1^{(2)}(\gamma_1|\bar{\rho}''-\bar{\rho}'|)\,ds' . \qquad (4\text{-}6)$$

The integral equations can be solved by dividing the contour into N intervals and expressing each integral as a weighted sum of N sampled values of $K_y(\bar{\rho})$ and $K_s(\bar{\rho})$. A system of 2N linear equations will result and these can be solved for the unknown sampled values of $K_y(\bar{\rho})$ and $K_s(\bar{\rho})$. However, the solution of coupled integral equations will be discussed in Chapter 5, since in this chapter we will discuss only E_y-polarized fields which are incident normal to the conductor. In this case, equations (4-5) and (4-6) uncouple.

If we assume that $k_{y_1} = 0$ in equations (4-5) and (4-6), then the integral equations uncouple and can be solved separately for each axial component. We find that

$$E_y^i(\bar{\rho}'') = Z_{2y}(\bar{\rho}'')K_y(\bar{\rho}'') + \frac{\mu_1\omega}{4}\int_{C_1} K_y(\bar{\rho}')\,H_0^{(2)}(k_1|\bar{\rho}''-\bar{\rho}'|)\,ds'$$

$$+ \frac{ik_1}{4}\int_{C_1} Z_{2y}(\bar{\rho}')\,K_y(\bar{\rho}')\cos(\beta''-\alpha)\,H_1^{(2)}(k_1|\bar{\rho}''-\bar{\rho}'|)\,ds' , \qquad (4\text{-}7)$$

and

$$H_y^i(\bar{\rho}'') = -K_s(\bar{\rho}'') - \frac{k_1}{4Z_1}\int_{C_1} Z_{2s}(\bar{\rho}')\,K_s(\bar{\rho}')\,H_o^{(2)}(k_1|\bar{\rho}''-\bar{\rho}'|)\,ds'$$

$$- \frac{ik_1}{4}\int_{C_1} K_s(\rho')\cos(\beta''-\alpha)\,H_1^{(2)}(k_1|\bar{\rho}''-\bar{\rho}'|)\,ds'. \qquad (4\text{-}8)$$

For simplicity, we will confine our study on this chapter to E_y-polarized incident fields (equation (4-7)). It should be noted, however, that the numerical solution of equation (4-8) is the same as the numerical solution of equation (4-7). Its solution would not present any numerical complications.

It is interesting to note that the first integral of equation (4-7) is the field scattered by a perfectly conducting cylinder and that the additional terms account for the finite conductivity of the scatterer. It was seen in Chapter 3 that on the basis of physical reasoning, the first integral could be thought of as the electric field due to axial currents at the surface of the conductor. These axial currents are equal to the transverse tangential magnetic field intensity and are present even at the surface of perfectly conducting scatterers.

In a similar manner, the additional terms can be thought of as the electric field due to transverse magnetic currents at the surface of the conductor. These transverse currents are equal to the axial electric field intensity and are present only at the surface of finitely conducting scatterers. As a result of the approximations made in deriving equation (4-7), we have been able to set the transverse magnetic currents equal to $-Z_{2y}(\bar{\rho})\,K_y(\bar{\rho})$.

Thus, we could have derived equation (4-7) on the basis of physical reasoning alone. The portion of the scattered electric field due to an axial electric current would yield a term given by equation (3-8). Similarly, the portion of the scattered electric field due to a transverse magnetic current would yield terms given by equation (3-10) with $H_y^i(\bar{\rho}'')$ replaced by $E_y^i(\bar{\rho}'')$ and K_s replaced by M_s.

The numerical solution of equation (4-7) is the same as that of equation (3-8) or equation (3-10). Thus, the contour C_1 is divided into N sampled values of $K_y(\bar{\rho})$ and each integral is expressed as a weighted sum of N sampled values of $K_y(\bar{\rho})$. By forcing the boundary condition to hold at the midpoint of each interval, a system of N linear equations will result and these can be solved for the unknown sampled values of $K_y(\bar{\rho})$.

Integration through the point of singularity in equation (4-7) also presents no problem since the contribution of each integral in the singular interval has been examined in section (3-2-3). Thus, we can rewrite equation (4-7) as

$$E_y^i(\bar{\rho}'') = \frac{Z_{2y}(\bar{\rho}'')K_y(\bar{\rho}'')}{2} + \frac{\mu_1\omega}{4}\int_{C_1} K_y(\bar{\rho}')\,H_0^{(2)}(k_1|\bar{\rho}''-\bar{\rho}'|)\,ds'$$

$$+ \frac{ik_1}{4}\int_{C_1} Z_{2y}(\bar{\rho}')\,K_y(\bar{\rho}')\cos(\beta''-\alpha)\,H_1^{(2)}(k_1|\bar{\rho}-\bar{\rho}'|)\,ds', \qquad (4\text{-}9)$$

where it is assumed that the contribution of the first integral in the singular interval is given by equations (3-31), (3-32) and (3-33) and that of the second integral is zero.

Once equation (4-9) has been solved for N sampled values of $K_y(\bar{\rho})$, the scattered magnetic field intensity is given by equation (2-87) with $k_y = 0$. We find that

$$\bar{H}_{t_1}^{sc} = \frac{ik_1}{4}\int_{C_1} K_y(\bar{\rho}')\, H_1^{(1)}(k_1|\bar{\rho}-\bar{\rho}'|)\,(\sin\beta\,\hat{x} - \cos\beta\,\hat{z})\,ds'$$

$$+ \frac{k_1^2}{4\mu_1\omega}\int_{C_1} Z_{2y}(\bar{\rho}')\,K_y(\bar{\rho}')\left\{\cos(\beta-\alpha)\,H_0^{(1)}(k_1|\bar{\rho}-\bar{\rho}'|)\,(\sin\beta\,\hat{x} - \cos\beta\,\hat{z})\right.$$

$$\left. - \frac{H_1^{(1)}(k_1|\bar{\rho}-\bar{\rho}'|)}{k_1|\bar{\rho}-\bar{\rho}'|}\,(\sin(2\beta-\alpha)\,\hat{x} - \cos(2\beta-\alpha)\,\hat{z})\right\} ds'. \qquad (4\text{-}10)$$

As in Chapter 3, it is necessary to make a small argument expansion to the Hankel function and integrate analytically whenever the point of observation is close ($|k_1|\,|\bar{\rho} - \bar{\rho}'| \leq .3$) to the interval over which the integration is being performed. Both integrals of equation (4-9) have been examined under these conditions in a similar analysis in section (3-4). Thus, the first integral is replaced by equation (3-58) and the second integral is replaced by ($-Z_{2y}$) times equation (3-64).

The first integral of equation (4-10) was examined also in section (3-4) and should be replaced by equation (3-61) whenever the point of observation is close to the contour. However, the second integral has not been examined and it is shown in Appendix D that in general the contribution of its jth interval to the scattered magnetic field intensity can be written as

$$\bar{H}_{t_j} = \frac{k_1^2}{4\mu_1\omega} Z_{2y}(\bar{\rho}')\left\{\left[\delta\left(C\cos\alpha_j + \delta D\sin\alpha_j\right) - \frac{1}{k_1}\left((\delta^2 E - F)\sin\alpha_j + 2\delta G\cos\alpha_j\right)\right]\hat{x}\right.$$

$$+\left[\delta\left(C\sin\alpha_j-\delta D\cos\alpha_j\right)+\frac{1}{k_1}\left(\left(\delta^2E-F\right)\cos\alpha_j-2\delta G\sin\alpha_j\right)\right]\frac{\hat{z}}{z}\Bigg\}, \qquad (4\text{-}11)$$

where

$$C=\left[I_6-\frac{(1-\lambda_j)}{\Delta_j}\left(I_7-c_jI_6\right)-\frac{\left(I_8-2c_jI_7+c_j^2I_6\right)}{\tilde{\zeta}_j}\right]K_{y_j}$$

$$+\frac{K_{y_{j+1}}}{1+\lambda_j}\left[\frac{I_7-c_jI_6}{\Delta_j}+\frac{I_8-2c_jI_7+c_j^2I_6}{\tilde{\zeta}_j}\right]-\frac{\lambda_jK_{y_{j-1}}}{1+\lambda_j}\left[\frac{\lambda_j(I_7-c_jI_6)}{\Delta_j}-\frac{I_8-2c_jI_7+c_j^2I_6}{\tilde{\zeta}_j}\right], \qquad (4\text{-}12a)$$

$$D=\left[I_5-\frac{(1-\lambda_j)}{\Delta_j}\left(I_6-c_jI_5\right)-\frac{\left(I_7-2c_jI_6+c_j^2I_5\right)}{\tilde{\zeta}_j}\right]K_{y_j}$$

$$+\frac{K_{y_{j+1}}}{1+\lambda_j}\left[\frac{I_6-c_jI_5}{\Delta_j}+\frac{I_7-2c_jI_6+c_j^2I_5}{\tilde{\zeta}_j}\right]-\frac{\lambda_jK_{y_{j-1}}}{1+\lambda_j}\left[\frac{\lambda_j(I_6-c_jI_5)}{\Delta_j}-\frac{I_7-2c_jI_6+c_j^2I_5}{\tilde{\zeta}_j}\right], \qquad (4\text{-}12b)$$

$$E=\left[I_9-\frac{(1-\lambda_j)}{\Delta_j}\left(I_{10}-c_jI_9\right)-\frac{\left(I_{11}-2c_jI_{10}+c_j^2I_9\right)}{\tilde{\zeta}_j}\right]K_{y_j}$$

$$+\frac{K_{y_{j+1}}}{1+\lambda_j}\left[\frac{I_{10}-c_jI_9}{\Delta_j}+\frac{I_{11}-2c_jI_{10}+c_j^2I_9}{\tilde{\zeta}_j}\right]-\frac{\lambda_jK_{y_{j-1}}}{1+\lambda_j}\left[\frac{\lambda_j(I_{10}-c_jI_9)}{\Delta_j}-\frac{I_{11}-2c_jI_{10}+c_j^2I_9}{\tilde{\zeta}_j}\right], \qquad (4\text{-}12c)$$

$$F=\left[I_{11}-\frac{(1-\lambda_j)}{\Delta_j}\left(I_{12}-c_jI_{11}\right)-\frac{I_{13}-2c_jI_{12}+c_j^2I_{11}}{\tilde{\zeta}_j}\right]K_{y_j}$$

$$+\frac{K_{y_{j+1}}}{1+\lambda_j}\left[\frac{I_{12}-c_jI_{11}}{\Delta_j}+\frac{I_{13}-2c_jI_{12}+c_j^2I_{11}}{\tilde{\zeta}_j}\right]-\frac{\lambda_jK_{y_{j-1}}}{1+\lambda_j}\left[\frac{\lambda_j(I_{12}-c_jI_{11})}{\Delta_j}-\frac{I_{13}-2c_jI_{12}+c_j^2I_{11}}{\tilde{\zeta}_j}\right], \qquad (4\text{-}12d)$$

$$G=\left[I_{10}-\frac{(1-\lambda_j)}{\Delta_j}\left(I_{11}-c_jI_{10}\right)-\frac{\left(I_{12}-2c_jI_{11}+c_j^2I_{10}\right)}{\tilde{\zeta}_j}\right]K_{y_j}$$

$$+\frac{K_{y_{j+1}}}{1+\lambda_j}\left[\frac{I_{11}-c_jI_{10}}{\Delta_j}+\frac{I_{12}-2c_jI_{11}+c_j^2I_{10}}{\tilde{\zeta}_j}\right]-\frac{\lambda_jK_{y_{j-1}}}{1+\lambda_j}\left[\frac{\lambda_j(I_{11}-c_jI_{10})}{\Delta_j}-\frac{I_{12}-2c_jI_{11}+c_j^2I_{10}}{\tilde{\zeta}_j}\right], \qquad (4\text{-}12e)$$

and

$$I_5 = \int_a^b \frac{H_0^{(1)}\left(k_1\sqrt{\delta^2+s'^2}\right)}{\delta^2+s'^2}\,ds', \tag{4-13a}$$

$$I_6 = \int_a^b \frac{s'\,H_0^{(1)}\left(k_1\sqrt{\delta^2+s'^2}\right)}{\delta^2+s'^2}\,ds', \tag{4-13b}$$

$$I_7 = \int_a^b \frac{s'^2\,H_0^{(1)}\left(k_1\sqrt{\delta^2+s'^2}\right)}{\delta^2+s'^2}\,ds', \tag{4-13c}$$

$$I_8 = \int_a^b \frac{s'^3\,H_0^{(1)}\left(k_1\sqrt{\delta^2+s'^2}\right)}{\delta^2+s'^2}\,ds', \tag{4-13d}$$

$$I_9 = \int_a^b \frac{H_1^{(1)}\left(k_1\sqrt{\delta^2+s'^2}\right)}{(\delta^2+s'^2)^{3/2}}\,ds', \tag{4-14a}$$

$$I_{10} = \int_a^b \frac{s'\,H_1^{(1)}\left(k_1\sqrt{\delta^2+s'^2}\right)}{(\delta^2+s'^2)^{3/2}}\,ds', \tag{4-14b}$$

$$I_{11} = \int_a^b \frac{s'^2\,H_1^{(1)}\left(k_1\sqrt{\delta^2+s'^2}\right)}{(\delta^2+s'^2)^{3/2}}\,ds', \tag{4-14c}$$

$$I_{12} = \int_a^b \frac{s'^3\,H_1^{(1)}\left(k_1\sqrt{\delta^2+s'^2}\right)}{(\delta^2+s'^2)^{3/2}}\,ds', \tag{4-14d}$$

$$I_{13} = \int_a^b \frac{s'^4\,H_1^{(1)}\left(k_1\sqrt{\delta^2+s'^2}\right)}{(\delta^2+s'^2)^{3/2}}\,ds'. \tag{4-14e}$$

The undefined parameters are given by equations (3-59) and are defined in Fig. 21.

Using the small argument approximation for $H_o(k_1\sqrt{\delta^2 + s^2})$ and $H_1(k_1\sqrt{\delta^2 + s^2})$ given by equations (3-26) and (3-27), equations (4-13) and (4-14) have been evaluated in Appendix D.

4-2 Numerical Examples: Cylinders in a Conductive Whole-Space

Equations (4-9) and (4-10) were programmed assuming that the incident field is the transmitted field of a plane wave incident normal to a conductive half-space (equation (3-51)). Their validity can be demonstrated by comparing the numerical results with the analytical results obtained for the case of scattering from circular cylinders.

It is shown in Appendix C that the transverse magnetic field intensity which is scattered by a finitely conducting circular cylinder in the presence of an E_y-polarized plane wave is

$$H_\rho^{sc}(\rho,\phi) = \frac{2iH_o}{k_1\rho} e^{ik_1 h} \sum_{n=1}^{\infty} n\, i^{-n} a_n H_n^{(1)'}(k_1\rho) \sin n\phi \quad , \tag{4-15a}$$

and

$$H_\phi^{sc}(\rho,\phi) = iH_o e^{ik_1 h} \sum_{n=0}^{\infty} i^{-n} \varepsilon_n a_n \left\{ \frac{n}{k_1\rho} H_n^{(1)}(k_1\rho) - H_{n+1}^{(1)}(k_1\rho) \right\} \cos n\phi \quad , \tag{4-15b}$$

where

$$a_n = - \frac{J_n(k_1 R) - c_n J_n'(k_1 R)}{H_n^{(1)}(k_1 R) - c_n H_n^{(1)'}(k_1 R)} \quad , \tag{4-16a}$$

$$c_n = \frac{Z_2 J_n(k_2 R)}{Z_1 J_n'(k_2 R)} \quad , \tag{4-16b}$$

$$\varepsilon_n = \begin{cases} 1, & n = 0 \\ 2, & n \geq 1 \end{cases},$$

R is the radius of the cylinder

and the derivatives in (4-16a) and (4-16b) are with respect to the argument kR.

The equivalent surface current densities around the surface of the cylinder are

$$K_y(\phi) = i H_0 e^{ik_1 h} \sum_{n=0}^{\infty} i^{-n} \varepsilon_n \left(J_n'(k_1 R) + a_n H_n^{(1)\prime}(k_1 R) \right) \cos n\phi, \qquad (4\text{-}17a)$$

and

$$M_s(\phi) = -Z_1 H_0 e^{ik_1 h} \sum_{n=0}^{\infty} i^{-n} \varepsilon_n \left(J_n(k_1 R) + a_n H_n^{(1)}(k_1 R) \right) \cos n\phi, \qquad (4\text{-}17b)$$

where a_n is given by equations (4-16), and the derivatives in equation (4-17a) are with respect to the argument $k_1 R$.

In the case of scattering from conductors which have a low surface impedance and which have a small curvature compared to the attenuation per unit distance, it is expected that

$$M_s(\phi) \sim -Z_{2y} K_y(\phi). \qquad (4\text{-}18)$$

The distance h in equations (4-15) and (4-17) is the depth from the earth-air interface to the center of the cylinder.

Figs. 43 and 44 demonstrate that the integral representations derived for E_y scattering from highly conducting scatterers are valid. We have assumed normal incidence in this example and that: the depth z_1 to the top of the cylinder is 20 m, the cylinder radius is 100 m, the incident field frequency is 1000 hz, the conductivity of the whole space is 10^{-3} mhos/m.

and the conductivity of the cylinder is 10 mhos/m. The equivalent electric surface current density has been sampled 40 times and, for this example, a maximum error of less than .3% has been obtained.

In Figs. 45 and 46, it is shown that the curvature must be small compared to the attenuation per unit distance if equations (4-9) and (4-10) are to predict the correct results. In this example, we have assumed normal incidence of an E_y-polarized plane wave and that: the depth z_1 to the top of the cylinder is 20 m, the cylinder radius is 100 m, the incident field frequency is 1000 hz, the conductivity of the whole space is 0. mhos/m, and that the conductivity of the cylinder is 10^{-3} mhos/m. Since the impedance contrast is large, it is valid to assume that the total field at any point just inside the scatterer may be represented by a wave propagating normally away from the contour. However, since the curvature is 0.01/m and the attenuation per unit distance is 0.002/m, the small curvature approximation has been violated. As a result, the convergent numerical results predict a field whose in-phase components are in error by 20% and whose out-of-phase components are in error by 1000%. The numerical results are like those of a scatterer which is more highly conducting than the actual inhomogeneity.

4-3 Numerical Examples: Topographic Scattering

The integral representations derived in Chapter 2 can be used also to investigate topographic scattering problems by considering the contour C_1 to be very large with respect to the wavelength of the incident field and the topographic region of interest. As C_1 becomes large, the fields

will be determined only by the interface on the upper part of the cylinder and, as a result, they will become independent of the contour chosen outside of this central region of interest. Thus, the contour integral can be replaced by an integral over $(-\infty,\infty)$ and, assuming $k_y = 0$, equation (4-1) becomes

$$E_y^t(\bar{\rho}) = E_y^i(\bar{\rho}) - \frac{\mu_0\omega}{4}\int_{-\infty}^{\infty} K_y(\bar{\rho}')\, H_0^{(1)}(k_0|\bar{\rho}-\bar{\rho}'|)\, ds'$$

$$- \frac{ik_0}{4}\int_{-\infty}^{\infty} Z_{1y}(\bar{\rho}')\, K_y(\bar{\rho}')\cos(\beta-\alpha)\, H_1^{(1)}(k_0|\bar{\rho}-\bar{\rho}'|)\, ds', \qquad (4\text{-}19)$$

where parameters of the air are referred to by the subscript o, and parameters of the earth by the subscript 1.

The equivalent surface current density in equation (4-19) can be thought of as being made up of two parts:

1) a portion due to fields scattered by the topography, plus
2) a portion due to fields reflected by the half-space.

Since the topography will be confined to a central section of the contour in all examples that will be discussed, it follows that outside a region bounded by (-a,a), the equivalent electric surface current density arises from fields reflected by the half-space alone. Thus, outside of the region (-a,a), the equivalent surface current density is known and is obtained from the analytical solution to the incident field impinging upon a flat half-space. Consequently, equation (4-19) can be rewritten as

$$E_y^t(\bar{\rho}) = E_y^i(\bar{\rho}) - \frac{\mu_0\omega}{4}\left[\int_{-\infty}^{-a-s_i} K_y^i(\bar{\rho}')\,H_0^{(1)}(k_0|\bar{\rho}-\bar{\rho}'|)\,ds' + \int_{a-s_i}^{\infty} K_y^i(\bar{\rho}')\,H_0^{(1)}(k_0|\bar{\rho}-\bar{\rho}'|)\,ds'\right.$$

$$- \frac{ik_0}{4}\left[\int_{-\infty}^{-a-s_i} Z_{1y}(\bar{\rho}')\,K_y^i(\bar{\rho}')\cos(\beta-\alpha)\,H_1^{(1)}(k_0|\bar{\rho}-\bar{\rho}'|)\,ds'\right.$$

$$\left.\left. + \int_{a-s_i}^{\infty} Z_{1y}(\bar{\rho}')\,K_y^i(\bar{\rho}')\cos(\beta-\alpha)\,H_1^{(1)}(k_0|\bar{\rho}-\bar{\rho}'|)\,ds'\right]\right.$$

$$- \frac{\mu_0\omega}{4}\int_{-a-s_i}^{a-s_i} K_y(\bar{\rho}')\,H_0^{(1)}(k_0|\bar{\rho}-\bar{\rho}'|)\,ds' - \frac{ik_0}{4}\int_{-a-s_i}^{a-s_i} Z_{1y}(\bar{\rho}')K_y(\bar{\rho}')\cos(\beta-\alpha)H_1^{(1)}(k_0|\bar{\rho}-\bar{\rho}'|)\,ds', \qquad (4\text{-}20)$$

where s_i is the x coordinate of the position vector $\bar{\rho}$, and K_y^i is the equivalent current density which arises from the incident field alone.

In this way, an infinite integral equation has been transformed into a finite integral equation plus several infinite integrals. It should be noted, however, that no approximations were made in going from (4-19) to (4-20) since the interval (-a,a) always is taken large enough to obtain a convergent solution in the region of interest. It does assume, nonetheless, that the half-space contour is flat outside of (-a,a).

It is possible also to transform the infinite integrals to integrals that can be evaluated numerically over a finite interval. By rewriting the infinite integrals as

$$- \frac{\mu_0\omega}{4}\int_{-\infty}^{\infty} K_y^i(\bar{\rho}')\,H_0^{(1)}(k_0|\bar{\rho}-\bar{\rho}'|)\,ds' - \frac{ik_0}{4}\int_{-\infty}^{\infty} Z_{1y}(\bar{\rho}')\,K_y^i(\bar{\rho}')\cos(\beta-\alpha)\,H_1^{(1)}(k_0|\bar{\rho}-\bar{\rho}'|)\,ds'$$

$$+ \frac{\mu_0\omega}{4}\int_{-a-s_i}^{a-s_i} K_y^i(\bar{\rho}')\,H_0^{(1)}(k_0|\bar{\rho}-\bar{\rho}'|)\,ds' + \frac{ik_0}{4}\int_{-a-s_i}^{a-s_i} Z_{1y}(\bar{\rho}')\,K_y^i(\bar{\rho}')\cos(\beta-\alpha)\,H_1^{(1)}(k_0|\bar{\rho}-\bar{\rho}'|)\,ds', \qquad (4\text{-}21)$$

it follows from (4-19) that for $\bar{\rho}$ above the half-space, the integrals over $(-\infty, \infty)$ must equal the electric field intensity reflected by a flat half-space. Thus, equation (4-20) reduces to

$$E_y^t(\bar{\rho}) = E_y^i(\bar{\rho}) + E_y^{reflec}(\bar{\rho}) + \frac{\mu_0\omega}{4}\int_{-a-s_i}^{a-s_i} K_y^i(\bar{\rho}')\, H_0^{(1)}(k_0|\bar{\rho}-\bar{\rho}'|)\,ds'$$

$$+ \frac{ik_0}{4}\int_{-a-s_i}^{a-s_i} z_{1y}(\bar{\rho}')\, K_y^i(\bar{\rho}')\cos(\beta-\alpha)\, H_1^{(1)}(k_0|\bar{\rho}-\bar{\rho}'|)\,ds'$$

$$- \frac{\mu_0\omega}{4}\int_{-a-s_i}^{a-s_i} K_y(\bar{\rho}')\, H_0^{(1)}(k_0|\bar{\rho}-\bar{\rho}'|)\,ds'$$

$$- \frac{ik_0}{4}\int_{-a-s_i}^{a-s_i} z_{1y}(\bar{\rho}')\, K_y(\bar{\rho}')\cos(\beta-\alpha)\, H_1^{(1)}(k_0|\bar{\rho}-\bar{\rho}'|)\,ds'. \qquad (4\text{-}22)$$

It is important to remember, however, that in equation (4-22) the contour integrals involving K_y^i are along a flat half-space while the contour integrals involving K_y are along the topographic profile. In addition, (4-22) assumes that $\bar{\rho}$ is above the half-space.

By following an analysis similar to section (4-1), it is found that the desired integral equation is

$$E_y^i(\bar{\rho}'') = \frac{z_{1y}(\bar{\rho}'')\,K_y(\bar{\rho}'')}{2} - E_y^{reflec}(\bar{\rho}'') - \frac{\mu_0\omega}{4}\int_{-a-s_i}^{a-s_i} K_y^i(\bar{\rho}')\, H_0^{(1)}(k_0|\bar{\rho}''-\bar{\rho}'|)\,ds'$$

$$- \frac{ik_0}{4}\int_{-a-s_i}^{a-s_i} z_{1y}(\bar{\rho}')\, K_y^i(\bar{\rho}')\cos(\beta''-\alpha)\, H_1^{(1)}(k_0|\bar{\rho}''-\bar{\rho}'|)\,ds'$$

$$+ \frac{\mu_0\omega}{4}\int_{-a-s_i}^{a-s_i} K_y(\bar{\rho}')\, H_0^{(1)}(k_0|\bar{\rho}''-\bar{\rho}'|)\,ds'$$

$$+ \frac{ik_0}{4}\int_{-a-s_i}^{a-s_i} z_{1y}(\bar{\rho}')\, K_y(\bar{\rho}')\cos(\beta-\alpha)\, H_1^{(1)}(k_0|\bar{\rho}''-\bar{\rho}'|)\,ds'. \qquad (4\text{-}23)$$

As in earlier examples, we will confine our study to normal incidence of an E_y-polarized plane wave. Thus, it follows from equation (2-38a) and Stratton (1941, p. 493) that

$$K_y^i = H_x^{inc} + H_x^{reflec} = H_x^{inc} + \frac{Z_0 - Z_1}{Z_0 + Z_1} H_0$$

$$= \frac{2Z_0}{Z_0 + Z_1} H_0 \quad , \tag{4-24}$$

and

$$E_y^{reflec} = -Z_0 \frac{Z_0 - Z_1}{Z_0 + Z_1} H_0 e^{ik_0 z} \quad . \tag{4-25}$$

It is interesting to note that equations (4-24) and (4-25) can be obtained analytically from equations (4-19) and (4-23) if we assume that an E_y-polarized plane wave is incident normal to a flat half-space. In this case, the equivalent electric surface current density is constant and equation (4-19) becomes

$$E_y^{reflec} = -\frac{\mu_0 \omega}{4} K_y^i \int_{-\infty}^{\infty} H_0^{(1)}\left(k_0\sqrt{\delta^2 + s'^2}\right) ds' + \frac{ik_0\delta}{4} Z_{1,y} K_y^i \int_{-\infty}^{\infty} \frac{H_1^{(1)}\left(k_0\sqrt{\delta^2 + s'^2}\right)}{(\delta^2 + s'^2)^{1/2}} ds' \tag{4-26}$$

It is shown in Appendix E that

$$\int_0^{\infty} \frac{H_\nu^{(1)}\left(k\sqrt{s'^2 + \delta^2}\right) s'^{2\mu+1}}{(s'^2 + \delta^2)^{\nu/2}} ds' = \frac{2^\mu \Gamma(\mu+1)}{k^{\mu+1} \delta^{\nu-\mu-1}} H_{\nu-\mu-1}^{(1)}(k\delta), \tag{4-27}$$

provided Re(k), Im(k) $\geq$ 0, Re(δ) > 0, and Re(μ) > -1.

Setting ν = 0 and μ = -1/2 in (4-27), we find that

$$\int_0^\infty H_0^{(1)}\left(k_0\sqrt{s'^2+\delta^2}\right)ds' = \frac{i}{k_0}\left(\sin k_0|\delta| - i\cos k_0|\delta|\right), \tag{4-28}$$

and setting ν = 1 and μ = -1/2,

$$\int_0^\infty \frac{H_1^{(1)}\left(k_0\sqrt{s'^2+\delta^2}\right)}{\left(s'^2+\delta^2\right)^{1/2}}ds' = \frac{1}{k_0|\delta|}\left(\sin k_0|\delta| - i\cos k_0|\delta|\right). \tag{4-29}$$

Thus, equation (4-26) becomes

$$E_y^{\text{reflec}} = -\frac{(Z_0 - Z_1)}{2}K_y^i\, e^{ik_0|\delta|}. \tag{4-30}$$

Taking the limit of (4-30) as δ approaches zero and introducing the result into (4-23), it is found that with (-a, a) equal to (0, 0), then

$$E_y^i(\bar{\rho}'') = \frac{Z_0 + Z_1}{2}K_y^i. \tag{4-31}$$

Note, however that to obtain (4-31), $\frac{Z_{1y}(\bar{\rho}'')\,K_y(\bar{\rho}'')}{2}$ in equation (4-23) has been replaced by $Z_{1y}(\bar{\rho}'')\,K_y(\bar{\rho}'')$. This has been done since the singular contribution of the last term of (4-23) had been added to (4-23) in deriving the integral equation and now must be subtracted before the last term can be ignored.

Thus, it follows from (4-31) that

$$K_y^i = \frac{2Z_0}{Z_0 + Z_1}H_0, \tag{4-32}$$

which agrees with (4-24). Introducing (4-32) into (4-30), we find that

$$E_y^{reflec} = -Z_o \frac{Z_o - Z_1}{Z_o + Z_1} e^{ik_o|\delta|}, \tag{4-33}$$

which agrees with (4-25).

In deriving (4-22) and the subsequent results, it was assumed that the point of observation was above or level with the flat half-space. However, if the topographic profile includes a valley which extends below the half-space, it is not valid to replace the integrals over $(-\infty,\infty)$ in equation (4-21) by E_y^{reflec} whenever $\bar{\rho}$ is below the half-space.

To establish what value the integrals do yield, it is necessary to remember that in applying the equivalence principle in section (2-2), the same fields were obtained only within the volume of interest. For a point of observation outside the volume of interest, the predicted fields will be zero since the boundary conditions have been satisfied by the equivalent surface current densities (see Harrington, 1961, p. 106). Thus, the total field will be zero when the point of observation is below the half-space, and it follows from (4-19) that the integrals over $(-\infty,\infty)$ must be equal to the negative of the incident electric field intensity.

This result can be obtained analytically if it is assumed that the incident field is an E_y-polarized plane wave incident normal to a flat half-space. In this case, the equivalent electric surface current density is constant and for a point of observation below the half-space, the infinite integrals of (4-21) become

$$-\frac{\mu_o \omega}{4} K_y^i \int_{-\infty}^{\infty} H_o^{(1)}(k_o\sqrt{\delta^2+s'^2})\,ds' - \frac{ik_o\delta}{4} Z_{iy} K_y^i \int_{-\infty}^{\infty} \frac{H_1^{(1)}(k_o\sqrt{\delta^2+s'^2})}{\sqrt{\delta^2+s'^2}}\,ds' . \tag{4-34}$$

Using the results of (4-28) and (4-29), equation (4-34) yields

$$- \frac{Z_o + Z_1}{2} K_y^i e^{ik_o|\delta|} . \tag{4-35}$$

Introducing the analytical values for K_y^i from equation (4-24), the contribution of the infinite integrals is found to be

$$- Z_o H_o^i e^{ik_o|\delta|}) \tag{4-36}$$

which is the negative of the incident field.

We can summarize these results by rewriting the integral equation (4-23) as

$$E_y^i(\bar{\rho}'') = \frac{Z_{iy}(\bar{\rho}'') K_y(\bar{\rho}'')}{2} + \left\{ \begin{matrix} -E_y^{reflec}(\bar{\rho}''^{o,+}) \\ E_y^i(\bar{\rho}''^{-}) \end{matrix} \right\} - I_E(k_o, \bar{\rho}'', \bar{\rho}')$$

$$+ \frac{\mu_o \omega}{4} \int_{-a-s_i}^{a-s_i} K_y(\bar{\rho}') H_o^{(1)}(k_o|\bar{\rho}'' - \bar{\rho}'|) ds' + \frac{ik_o}{4} \int_{-a-s_i}^{a-s_i} Z_{iy}(\bar{\rho}') K_y(\bar{\rho}') \cos(\beta - \alpha) H_1^{(1)}(k_o|\bar{\rho}'' - \bar{\rho}'|) ds', \tag{4-37}$$

where $-E_y^{reflec}(\bar{\rho}''^{o,+})$ is the electric field intensity reflected by a flat conductive half-space and is to be used when the point of observation is above or on the flat half-space,

$E_y^i(\bar{\rho}''^{-})$ is the incident electric field intensity and is to be used when the point of observation is below the flat half-space,

and

$$I_E(k_o, \bar{\rho}'', \bar{\rho}') = \frac{\mu_o \omega}{4} \int_{-a-s_i}^{a-s_i} K_y^i(\bar{\rho}') H_o^{(1)}(k_o|\bar{\rho} - \bar{\rho}'|) ds' + \frac{ik_o}{4} \int_{-a-s_i}^{a-s_i} Z_{iy}(\bar{\rho}') K_y^i(\bar{\rho}') \cos(\beta - \alpha) H_1^{(1)}(k_o|\bar{\rho}'' - \bar{\rho}'|) ds' . \tag{4-38}$$

It should be remembered that the contour integrals in (4-38) are along a flat half-space while the contour integrals in (4-37) are along the topographic profile.

If we assume that an E_y-polarized plane wave is incident normal to a flat half-space, then K_y^i is constant and equation (4-38) can be rewritten as

$$I_E(k_o,\bar{\rho}'',\bar{\rho}') = \frac{\mu_o\omega}{4} K_y^i \int_{-a-s_i}^{a-s_i} H_o^{(1)}(k_o\sqrt{\delta^2+s'^2})\,ds' - \frac{ik_o\delta Z_{iy} K_y^i}{4}\int_{-a-s_i}^{a-s_i} \frac{H_1^{(1)}(k_o\sqrt{\delta^2+s'^2})}{\sqrt{\delta^2+s'^2}}\,ds' . \tag{4-39}$$

Special care must be taken at the edges of the interval in which K_y is assumed to be unknown to ensure that the unknown parabolic current distribution is continuous with the known current distribution. This is accomplished by assuming that the 0th and Nth + 1 intervals lie outside (-a,a), that W_o and W_{N+1} should be approximately equal to W_1 and W_N to ensure that the parabolic fit to the current density is not violated.

If, however, the incident field is an E_y-polarized plane wave incident normal to a half-space, then it is valid to assume that W_o and W_{N+1} are infinite since the parabolic fit to the current density is not violated. In this case, consider the general integral

$$A\int_{s_j-w_j}^{s_j+w_j} K_y(\bar{\rho}')F(\bar{\rho}'',\bar{\rho}')\,ds' , \tag{4-40}$$

where A is a constant and $F(\bar{\rho}'',\bar{\rho}')$ is the kernal of the integral, to represent each integral along the topographic profile in equation (4-37). Then the contribution of the first interval to (4-40) is (compare with equation (3-22) as $W_{N-1} = W_o \to \infty$)

$$A\left\{ K_{y_1} \int_{s_1-W_1}^{s_1+W_1} F(\bar{\rho}'', \bar{\rho}') \left(1 - \frac{s'-s_1}{W_1+W_2}\right) ds' \right.$$

$$\left. + K_{y_2} \int_{s_1-W_1}^{s_1+W_1} F(\bar{\rho}'', \bar{\rho}') \frac{s'-s_1}{W_1+W_2} ds' \right\}. \tag{4-41}$$

Similarly, the contribution of the last interval to (4-40) is

$$A\left\{ K_{y_N} \int_{s_N-W_N}^{s_N+W_N} F(\bar{\rho}'', \bar{\rho}') \left(1 + \frac{s'-s_N}{W_N+W_{N-1}}\right) ds' \right.$$

$$\left. - K_{y_{N-1}} \int_{s_N-W_N}^{s_N+W_N} F(\bar{\rho}'', \bar{\rho}') \frac{s'-s_N}{W_N+W_{N-1}} ds' \right\}. \tag{4-42}$$

In particular, when the boundary condition is applied in the first interval, (4-41) reduces to

$$A K_{y_1} \int_{s_1-W_1}^{s_1+W_1} F(\bar{\rho}'', \bar{\rho}') ds', \tag{4-43}$$

and when the boundary condition is applied in the last interval, (4-42) reduces to

$$A K_{y_N} \int_{s_N-W_N}^{s_N+W_N} F(\bar{\rho}'', \bar{\rho}') ds'. \tag{4-44}$$

An expression for the scattered magnetic field intensity is obtained by following a similar analysis for equation (4-10). Assuming that the contour is flat outside the interval (-a,a) and that the equivalent surface current density arises from the incident field, then it would be found that

$$\vec{H}_{tn}^{sc}(\bar{\rho}) = \left\{ \begin{array}{l} \vec{H}_{tn}^{reflec}(\bar{\rho}^{0,+}) \\ -\vec{H}_{tn}^{i}(\bar{\rho}^{-}) \end{array} \right\} - \vec{I}_H(k_0, \bar{\rho}, \bar{\rho}')$$

$$+ \frac{ik_0}{4} \int_{-a-s_c}^{a-s_c} K_y(\bar{\rho}') H_1^{(1)}(k_0 |\bar{\rho} - \bar{\rho}'|)(\sin\beta\,\hat{x} - \cos\beta\,\hat{z})\, ds'$$

$$+\frac{k_0}{4z_0}\int_{-a-s_i}^{a-s_i} Z_{1y}(\bar{\rho}')\,K_y(\bar{\rho}')\cos(\beta-\alpha)\,H_0^{(1)}(k_0|\bar{\rho}-\bar{\rho}'|)(\sin\beta\hat{x}-\cos\beta\hat{z})\,ds'$$

$$-\frac{k_0}{4z_0}\int_{-a-s_i}^{a-s_i} Z_{1y}(\bar{\rho}')\,K_y(\bar{\rho}')\,\frac{H_1^{(1)}(k_0|\bar{\rho}-\bar{\rho}'|)}{k_0|\bar{\rho}-\bar{\rho}'|}\left(\sin(2\beta-\alpha)\hat{x}-\cos(2\beta-\alpha)\hat{z}\right)ds', \tag{4-45}$$

where s_i is the x coordinate of the point of observation,

$H_{tr}^{reflec}(\bar{\rho}^{0,+})$ is the magnetic field intensity reflected by a flat conductive half-space and is to be used when the point of observation is above or on the flat half-space,

$-H_{tr}^{1}(\bar{\rho})$ is the incident magnetic field intensity and is to be used when the point of observation is below the flat half-space,

and

$$\bar{\bar{I}}_H(k_0,\bar{\rho},\bar{\rho}') = \frac{ik_0}{4}\int_{-a-s_i}^{a-s_i} K_y^i(\bar{\rho}')\,H_1^{(1)}(k_0|\bar{\rho}-\bar{\rho}'|)\left(\sin\beta\hat{x}-\cos\beta\hat{z}\right)ds'$$

$$+\frac{k_0}{4z_0}\int_{-a-s_i}^{a-s_i} Z_{1y}(\bar{\rho}')\,K_y^i(\bar{\rho}')\cos(\beta-\alpha)\,H_0^{(1)}(k_0|\bar{\rho}-\bar{\rho}'|)(\sin\beta\hat{x}-\cos\beta\hat{z})\,ds'$$

$$-\frac{k_0}{4z_0}\int_{-a-s_i}^{a-s_i} Z_{1y}(\bar{\rho}')\,K_y^i(\bar{\rho}')\,\frac{H_1^{(1)}(k_0|\bar{\rho}-\bar{\rho}'|)}{k_0|\bar{\rho}-\bar{\rho}'|}\left(\sin(2\beta-\alpha)\hat{x}-\cos(2\beta-\alpha)\hat{z}\right)ds', \tag{4-46}$$

As in equations (4-37) and (4-38), the contour integrals involving K_y^1 are along a flat half-space while the contour integrals involving K_y are along the topographic profile.

It is shown in Appendix D that the trigonometric expressions can be written as

$$\sin\beta = -\frac{(s'\cos\alpha + \delta\sin\alpha)}{(\delta^2+s'^2)^{1/2}} \quad , \tag{4-47a}$$

$$\cos\beta = \frac{s'\sin\alpha - \delta\cos\alpha}{(\delta^2+s'^2)^{1/2}} \quad , \tag{4-47b}$$

$$\cos(\beta-\alpha) = \frac{-\delta}{(\delta^2+s'^2)^{1/2}} \quad , \tag{4-47c}$$

$$\sin(2\beta-\alpha) = \frac{(\delta^2-s'^2)\sin\alpha + 2s'\delta\cos\alpha}{(\delta^2+s'^2)} \quad , \tag{4-47d}$$

and

$$\cos(2\beta-\alpha) = \frac{(\delta^2-s'^2)\cos\alpha - 2s'\delta\sin\alpha}{(\delta^2+s'^2)} \quad , \tag{4-47e}$$

where the parameters are defined in Fig. 21.

Thus, expanding the trigonometric expressions according to equations (4-47), noting that the half-space is parallel to the x-axis ($\alpha = -90°$), and assuming that the incident field is an Ey-polarized plane wave incident normal to the half-space, then equation (4-47) can be rewritten as

$$\overline{\overline{I}}_H(k_0,\bar{\rho},\bar{\rho}') = \frac{ik_0}{4}k_y^i\left(\delta I_1\hat{x} + I_2\hat{z}\right) - \frac{k_0^2 Z_{1y}k_y^i}{4\mu_0\omega}\left[\left(\delta^2 I_5 - \frac{\delta^2 I_9 - I_{11}}{k_0}\right)\hat{x} + \delta\left(I_6 - \frac{2I_{10}}{k_0}\right)\hat{z}\right] \quad , \tag{4-48}$$

where I_1, I_2, I_5, I_6, I_9, I_{10} and I_{11} are given by equations (3-63a), (3-63b), (4-13a), (4-13b), (4-14a), (4-14b) and (4-14c) respectively, with $a = -a-s_t$ and $b = a-s_t$.

It should be noted that equations (4-40) through (4-44) must be considered at the edges of the interval (-a,a) to ensure continuity of the known and unknown current distributions in equation (4-45).

Equations (4-37) and (4-45) were programmed assuming that the incident field is an E_y-polarized plane wave incident normal to a conductive half-space. Their validity can be demonstrated by comparing the numerical results with the analytical results obtained for the case of reflection from a conductive half-space, equation (4-24).

It should be noted, however, that it is not necessary to sample the contour at least ten times per wavelength to describe adequately the equivalent surface current density while testing the validity of the integral representations. The reason for this is that with normal incidence the equivalent surface current density is constant. As a result, the contour can be described by any number of intervals if integration accuracy is maintained.

To take advantage of this fact, the integrals over the contour section (-a,a) in equation (4-37) were replaced by equations (3-58) and $(-Z_{2_y})$ times equation (3-64), and those in equation (4-45) were replaced by equation (4-11). In this form, all independent integrals in equations (3-58), (3-64) and (4-11) were integrated numerically with the integration tolerance being specified by an integration sampling rate per wavelength.

The concept of an integration sampling rate per wavelength was chosen to correspond to the integration accuracy that would be obtained if the contour had been sampled evenly at this same rate. For example, if a contour section one wavelength long had been sampled previously by 10 intervals of equal width, then the same accuracy can be achieved by one

interval with an integration sampling rate of 10. This is equal to an n of 20 in Simpson's rule for this interval width, but in general n will be different for each interval, although the integration sampling rate will be the same.

Table 1 demonstrates that the integral representations are valid for topographic scattering problems and summarizes the accuracy and convergence of the solution as the numerical variables are changed. It should be remembered that since the incident field is normal to the interface at all points and that since the curvature is zero, equations (4-37) and (4-45) represent an exact formulation of this particular problem. Thus, Table 1 is a good indication of solution accuracy and convergence under various numerical conditions.

In this example, we have assumed that an E_y-polarized plane wave is normally incident to a horizontal interface and that: the height z_o of the observation point is 100 m above the interface, the incident field frequency is 1000 hz, the conductivity of the upper region is 0, and the conductivity of the lower region is 10^{-3} mhos/m. In particular, Table 1 assumes that the point of observation is at x = -400 m. This point was chosen over x = 0 (the center of the half-space contour) since H_z always is given by a computer round-off error of about 10^{-14} at the center of any contour symmetric with respect to the z-axis. Thus, by choosing x = -400 m, H_z is proportional to the accuracy of the solution rather than the computer round-off.

In Table 1, "a" is the half-width of the contour section (-a,a) within which the surface current density is assumed to be unknown, N is the number of sampling points of the equivalent surface current density

± a	Real(H_x)	Imag. (H_x)	Real(H_z)	Imag (H_z)	N	Int. rate	Re
	Analytical Results						
	.9894	.01251	0.	0.			
	Numerical Results						
600,000	1.0127	.00511	8×10^{-3}	2×10^{-3}	14	10	.3
	.9944	.01104	2×10^{-3}	5×10^{-4}	14	20	.3
	.9897	.01266	7×10^{-5}	2×10^{-5}	14	20	.5
300,000	1.0124	.00528	9×10^{-3}	3×10^{-3}	12	10	.3
	.9944	.01105	1×10^{-3}	5×10^{-4}	12	20	.3
	.9942	.01103	1×10^{-3}	5×10^{-4}	12	30	.3
	.9917	.01280	5×10^{-5}	4×10^{-7}	22	10	.3
	.9897	.01268	1×10^{-5}	3×10^{-6}	22	20	.3
	.9896	.01267	7×10^{-5}	1×10^{-5}	12	20	.5
	.9895	.01267	8×10^{-5}	2×10^{-5}	12	30	.5
50,000	1.0129	.00520	8×10^{-3}	3×10^{-3}	8	10	.3
	.9943	.01093	2×10^{-3}	5×10^{-4}	8	20	.3
	.9908	.01275	1×10^{-4}	3×10^{-5}	8	10	.5
	.9896	.01264	8×10^{-5}	1×10^{-5}	8	20	.5
20,000	1.0131	.00546	9×10^{-3}	3×10^{-2}	6	10	.3
	.9946	.01103	2×10^{-3}	5×10^{-4}	6	20	.3
	.9897	.01269	9×10^{-6}	5×10^{-6}	6	10	.5
	.9896	.01268	8×10^{-6}	3×10^{-6}	6	20	.5
5,000	.9894	.01251	1×10^{-14}	1×10^{-14}	4	10	.3
	.9894	.01251	1×10^{-14}	1×10^{-14}	4	20	.3
	.9894	.01251	1×10^{-14}	1×10^{-14}	4	20	.5

Table 1. Magnetic field intensity reflected by a horizontal interface between air and a conductive earth: E_y-polarization, x = -400 m, z_o = 100 m, f = 1000 hz, σ_1 = 0 mhos/m, and $\sigma_{earth} = 10^{-3}$ mhos/m.

within (-a,a), int. rate is the integration sampling rate per wavelength and Re is that value for which the small argument solution to equations (4-37) and (4-45) is used if $|k_o r| \leq$ Re over the entire width of a sampling interval.

It is evident from the data of Table 1 for a = 5000 that equations (4-37) and (4-45) are an accurate formulation of the problem whenever $|k_o a| << \text{Re}/2$. This is not surprising since the small argument approximations are very accurate for these small arguments and they are used to evaluate all integrals when the contour section (-a,a) is so short. However, when $|k_o a| > \text{Re}/2$, both Simpson's rule and the small argument approximations are used to evaluate equations (4-37) and (4-45), in which case the usual solution accuracy of 1% or better is achieved.

It is evident from the data of Table 1 for a = 300,000 that the solution accuracy can be increased by raising the number of sampling points within the interval (-a,a) or by increasing Re, as well as by increasing the integration sampling rate. This result is actually more a function of the manner in which the program has been written than the numerical nature of the solution. The reason for this is that the small argument approximation is used only when $|kr| \leq$ Re for all points on an interval.

As an example of why this is a programming effect, it should be noted that the small argument approximation would not be used to calculate the contribution of an interval to the fields if $|kr_a| \sim .01$ and $|kr_b| \sim .4$ (where r_a and r_b are the radial distances to each edge of the interval) and Re were .3. Instead, Simpson's rule would be used and significant integration errors would be incurred unless a large integration sampling rate had been specified. However, by choosing an Re of .5, the more

accurate small argument approximation would be used for this interval and solution accuracy would be improved substantially. Alternatively, the contour could have been sampled more frequently and the interval of this example might now be sampled twice such that $|kr_a| \sim .01$, $|kr_c| \sim .09$ and $|kr_b| \sim .4$. Thus, even with an Re of .3, a more accurate solution would be obtained since the small argument approximation would be used for the interval (r_a, r_c) whereas numerical integration would be used for the interval (r_c, r_b).

It is apparent that the above situation can arise in equation (4-37) whenever small interval widths are adjacent to large interval widths and/or in equation (4-45) whenever the point of observation is close to the contour ($|kr| << \lambda$). As a result, it is necessary to choose small contour sampling widths near the points of observation and gradually increase the contour sampling widths on each side away from the points of observation. In this way it is possible to sample accurately the equivalent surface current density with the smallest possible matrix size and still be assured of obtaining a solution accuracy of about 10^{-5}.

To illustrate the application of the method to topographic scattering problems which cannot be handled analytically, the field scattered by the hill of Fig. 47 has been considered in Figs. 48 through 51. In this problem, the contour has been computed in meters according to the Gaussian distribution

$$\text{Height} = 100\, e^{-\frac{1}{2}\left(\frac{x}{100}\right)^2} . \qquad (4\text{-}49)$$

In Figs. 48 through 51, it is assumed that an Ey-polarized plane wave is incident normal to the topography and that: the point of

observation Z_o is 150 m above the half-space, the incident field frequency is 1000 hz, the conductivity of the upper medium is 0, and the conductivity of the lower medium is 10^{-3} mhos/m.

The vertical magnetic field intensity has been examined in Figs. 48 through 50 to establish solution convergence. This field was chosen over the horizontal magnetic field intensity since it is more sensitive to both the inhomogeneity and round-off errors.

It is evident from Fig. 48 that for this example, a contour section bounded by (-10,000, + 10,000) [ie $(-\lambda_{air}/30, +\lambda_{air}/30)$], is sufficient to describe the unknown surface current density. In Figs. 49 and 50, the sampling density required within the horizontal region (-10,000, + 10,000) has been tested for solution convergence. On the basis of Figs. 48 through 50, it was decided that an accuracy to better than 1% (at the peak value of H_z) could be obtained if the contour was sampled 44 times within the contour section bounded by (-10,000, + 10,000).

In Fig. 51, the horizontal magnetic field intensity scattered by the hill has been plotted assuming a constant flight level of 150 m above the half-space and also, assuming a contour flight level which is 150 m above the interface. It is seen that by contour flying, the peak electromagnetic response of the hill has been reduced by a factor of two. In addition, the electromagnetic response has been held to a constant over the central portion of the hill. However, even by contour flying, there has been an approximate increase in the peak value of real (H_x) of 12% as a result of topography.

It should be noted from Fig. 47, however, that since the curvature approximations have been violated in this example, real $(\vec{H})$ will be about

20% too large whereas imaginary $(\vec{H})$ may be meaningless. Nonetheless, it has been feasible to estimate these errors since the curvature violation and electrical parameters are approximately the same in each problem. As a result, it is possible to estimate that for the contour flight example of Fig. 51, there should be an actual increase in the peak value of real (H_x) of about 10% as a result of topography.

CHAPTER 5

SCATTERING FROM CYLINDERS WITH ARBITRARY IMPEDANCE

In Chapters 3 and 4, an integral equation solution to scattering from perfectly conducting and highly conducting cylinders was discussed. In this analysis, the general integral representations were investigated under simplifying assumptions so that each numerical difficulty could be studied individually.

Having examined some particular problems encountered in formulating an integral equation solution to geophysical scattering problems, we are prepared now to examine electromagnetic scattering from cylinders with arbitrary impedance. Once this analysis has been completed, any two-dimensional problem can be formulated and solved (within the time and storage limitations of the computer), including the very important problem of scattering from cylinders in a conductive half-space.

5-1 Derivation of the Integral Equations

The general coupled integral representations of $E_y^t(\bar{\rho})$ and $H_y^t(\bar{\rho})$ in the exterior medium were given in Chapter 2 (equations (2-56) and (2-57) as

$$E_y^t(\bar{\rho}) = E_y^i(\bar{\rho}) - \frac{Z_1\gamma_1^2}{4k_1}\int_{C_1} K_y(\bar{\rho}')\, H_0^{(1)}(\gamma_1|\bar{\rho}-\bar{\rho}'|)\, ds'$$

$$+ \frac{iZ_1 k_{y_1}\gamma_1}{4k_1}\int_{C_1} K_s(\bar{\rho}')\sin(\beta-\alpha)\, H_1^{(1)}(\gamma_1|\bar{\rho}-\bar{\rho}'|)\, ds' \qquad (5\text{-}1)$$

$$+ \frac{i\gamma_1}{4}\int_{C_1} M_s(\bar{\rho}')\cos(\beta-\alpha)\, H_1^{(1)}(\gamma_1|\bar{\rho}-\bar{\rho}'|)\, ds' \,,$$

and

$$H_y^t(\bar{\rho}) = H_y^i(\bar{\rho}) + \frac{\gamma_1^2}{4z_1k_1}\int_{c_1} M_y(\bar{\rho}')\,H_0^{(1)}(\gamma_1|\bar{\rho}-\bar{\rho}'|)\,ds'$$

$$- \frac{ik_{y_1}\gamma_1}{4z_1k_1}\int_{c_1} M_s(\bar{\rho}')\sin(\beta-\alpha)\,H_1^{(1)}(\gamma_1|\bar{\rho}-\bar{\rho}'|)\,ds'$$

$$+ \frac{i\gamma_1}{4}\int_{c_1} K_s(\bar{\rho}')\cos(\beta-\alpha)\,H_1^{(1)}(\gamma_1|\bar{\rho}-\bar{\rho}'|)\,ds' \quad , \tag{5-2}$$

where the earth parameters have been referred to by the subscript 1.

The transverse field intensities are obtained by adding the incident transverse magnetic field intensity and transverse electric field intensity to the scattered transverse field quantities (equations (2-66) and (2-68)), and we find that

$$\vec{H}_{th}^{t}(\bar{\rho}) = \vec{H}_{th}^{i}(\bar{\rho}) + \frac{i\gamma_1^3}{4k_1^2}\int_{c_1} K_y(\bar{\rho}')\vec{F}_1(\gamma_1,\bar{\rho},\bar{\rho}')\,ds'$$

$$- \frac{k_{y_1}\gamma_1^2}{4k_1^2}\int_{c_1} K_s(\bar{\rho}')\vec{F}_2(\gamma_1,\bar{\rho},\bar{\rho}')\,ds' - \frac{\gamma_1^2}{4\mu_1\omega}\int_{c_1} M_s(\bar{\rho}')\vec{F}_3(\gamma_1,\bar{\rho},\bar{\rho}')\,ds', \tag{5-3}$$

and

$$\vec{E}_y^t(\bar{\rho}) = \vec{E}_y^i(\bar{\rho}) + \frac{i\gamma_1^3}{4k_1^2}\int_{c_1} M_y(\bar{\rho}')\vec{F}_1(\gamma_1,\bar{\rho},\bar{\rho}')\,ds'$$

$$- \frac{k_{y_1}\gamma_1^2}{4k_1^2}\int_{c_1} M_s(\bar{\rho}')\vec{F}_2(\gamma_1,\bar{\rho},\bar{\rho}')\,ds' + \frac{z_1\gamma_1^2}{4k_1}\int_{c_1} K_s(\bar{\rho}')\vec{F}_3(\gamma_1,\bar{\rho},\bar{\rho}')\,ds', \tag{5-4}$$

where

$$\vec{F}_1(\gamma,\bar{\rho},\bar{\rho}') = H_1^{(1)}(\gamma|\bar{\rho}-\bar{\rho}'|)(\sin\beta\,\hat{x} - \cos\beta\,\hat{z}), \tag{5-5a}$$

$$\vec{F}_2(\gamma,\bar{\rho},\bar{\rho}') = \sin(\beta-\alpha)\,H_0^{(1)}(\gamma|\bar{\rho}-\bar{\rho}'|)(\sin\beta\,\hat{x} - \cos\beta\,\hat{z})$$

$$- \frac{H_1^{(1)}(\gamma|\bar{\rho}-\bar{\rho}'|)}{\gamma|\bar{\rho}-\bar{\rho}'|}(\cos(2\beta-\alpha)\,\hat{x} + \sin(2\beta-\alpha)\,\hat{z}), \tag{5-5b}$$

and

$$\overline{\overline{F}}_3(\gamma,\bar{\rho},\bar{\rho}') = \cos(\beta-\alpha)\,H_0^{(1)}(\gamma|\bar{\rho}-\bar{\rho}'|)(\sin\beta\hat{x}-\cos\beta\hat{z})$$

$$-\frac{H_1^{(1)}(\gamma|\bar{\rho}-\bar{\rho}'|)}{\gamma|\bar{\rho}-\bar{\rho}'|}(\sin(2\beta-\alpha)\hat{x}-\cos(2\beta-\alpha)\hat{z}). \tag{5-5c}$$

Similarly, the integral representations of the fields inside the scatterer are obtained from equations (2-72), (2-73), (2-74) and (2-75). It is found that

$$\begin{aligned}
E_y^t(\bar{\rho}) &= \frac{Z_2\gamma_2^2}{4k_2}\int_{C_1} K_y(\bar{\rho}')H_0^{(1)}(\gamma_2|\bar{\rho}-\bar{\rho}'|)ds' \\
&\quad - \frac{iZ_2k_{y_2}\gamma_2}{4k_2}\int_{C_1} K_s(\bar{\rho}')\sin(\beta-\alpha)H_1^{(1)}(\gamma_2|\bar{\rho}-\bar{\rho}'|)ds' \\
&\quad - \frac{i\gamma_2}{4}\int_{C_1} M_s(\bar{\rho}')\cos(\beta-\alpha)H_1^{(1)}(\gamma_2|\bar{\rho}-\bar{\rho}'|)\,ds',
\end{aligned} \tag{5-6}$$

$$\begin{aligned}
H_y^t(\bar{\rho}) &= -\frac{\gamma_2^2}{4Z_2k_2}\int_{C_1} M_y(\bar{\rho}')H_0^{(1)}(\gamma_2|\bar{\rho}-\bar{\rho}'|)ds' \\
&\quad + \frac{ik_{y_2}\gamma_2}{4Z_2k_2}\int_{C_1} M_s(\bar{\rho}')\sin|\beta-\alpha)H_1^{(1)}(\gamma_2|\bar{\rho}-\bar{\rho}'|)ds' \\
&\quad - \frac{i\gamma_2}{4}\int_{C_1} K_s(\bar{\rho}')\cos(\beta-\alpha)H_1^{(1)}(\gamma_2|\bar{\rho}-\bar{\rho}'|)ds',
\end{aligned} \tag{5-7}$$

$$\begin{aligned}
\overline{\overline{H}}_{tn}^t(\bar{\rho}) &= -\frac{i\gamma_2^3}{4k_2^2}\int_{C_1} K_y(\bar{\rho}')\overline{\overline{F}}_1(\gamma_2,\bar{\rho},\bar{\rho}')ds' \\
&\quad + \frac{k_{y_2}\gamma_2^2}{4k_2^2}\int_{C_1} K_s(\bar{\rho}')\overline{\overline{F}}_2(\gamma_2,\bar{\rho},\bar{\rho}')ds' + \frac{\gamma_2^2}{4\mu_2\omega}\int_{C_1} M_s(\bar{\rho}')\overline{\overline{F}}_3(\gamma_2,\bar{\rho},\bar{\rho}')ds',
\end{aligned} \tag{5-8}$$

and

$$\vec{E}^{t}_{th}(\bar{\rho}) = -\frac{i\gamma_2^3}{4k_2^2}\int_{C_1} M_y(\bar{\rho}')\,\vec{F}_1(\gamma_2,\bar{\rho},\bar{\rho}')\,ds';$$

$$+\frac{k_{y_2}\gamma_2^2}{4k_2^2}\int_{C_1} M_s(\bar{\rho}')\,\vec{F}_2(\gamma_2,\bar{\rho},\bar{\rho}')\,ds' - \frac{z_2\gamma_2^2}{4k_2}\int_{C} K_s(\bar{\rho}')\,\vec{F}_3(\gamma_2,\bar{\rho},\bar{\rho}')\,ds', \tag{5-9}$$

where the cylinder parameters have been referred to by the subscript 2, and $\vec{F}_1(\gamma_2,\bar{\rho},\bar{\rho}')$, $\vec{F}_2(\gamma_2,\bar{\rho},\bar{\rho}')$ and $\vec{F}_3(\gamma_2,\bar{\rho},\bar{\rho}')$ are given by equations (5-5).

The unknown current components $K_y(\bar{\rho})$, $K_s(\bar{\rho})$, $M_y(\bar{\rho})$ and $M_s(\bar{\rho})$ are obtained by enforcing the boundary conditions on tangential $\vec{E}$ and $\vec{H}$ and solving the resulting integral equations. We have from equation (2-53) that the tangential unit vector $\hat{s}$, is given by

$$\hat{s} = -\sin\alpha_i\,\hat{x} + \cos\alpha_i\,\hat{z}, \tag{5-10}$$

where α_i is the normal into the cylinder at the boundary point. Thus, the tangential components of $\vec{E}$ and $\vec{H}$ in the transverse plane are found by taking the dot product of (5-10) with equations (5-3), (5-4), (5-8) and (5-9). We find that exterior to the cylinder,

$$H^{t}_{s}(\bar{\rho}) = \hat{s}\cdot\vec{H}^{i}_{th}(\bar{\rho}) + \frac{i\gamma_1^3}{4k_1^2}\int_{C_1} K_y(\bar{\rho}')\,G_1(\gamma_1,\bar{\rho},\bar{\rho}')\,ds'$$

$$-\frac{k_{y_1}\gamma_1^2}{4k_1^2}\int_{C_1} K_s(\bar{\rho}')\,G_2(\gamma_1,\bar{\rho},\bar{\rho}')\,ds' - \frac{\gamma_1^2}{4\mu_1\omega}\int_{C_1} M_s(\bar{\rho}')\,G_3(\gamma_1,\bar{\rho},\bar{\rho}')\,ds', \tag{5-11}$$

and

$$E^{t}_{s}(\bar{\rho}) = \hat{s}\cdot\vec{E}^{i}_{th}(\bar{\rho}) + \frac{i\gamma_1^3}{4k_1^2}\int_{C_1} M_y(\bar{\rho}')\,G_1(\gamma_1,\bar{\rho},\bar{\rho}')\,ds'$$

$$-\frac{k_{y_1}\gamma_1^2}{4k_1^2}\int_{C_1} M_s(\bar{\rho}')\,G_2(\gamma_1,\bar{\rho},\bar{\rho}')\,ds' + \frac{z_1\gamma_1^2}{4k_1}\int_{C_1} K_s(\bar{\rho}')\,G_3(\gamma_1,\bar{\rho},\bar{\rho}')\,ds'. \tag{5-12}$$

Interior to the cylinder,

$$H_s^t(\bar{\rho}) = -\frac{i\gamma_2^3}{4k_2^2}\int_{C_1} K_y(\bar{\rho}')\, G_1(\gamma_2,\bar{\rho},\bar{\rho}')ds'$$

$$+\frac{k_{y_2}\gamma_2^2}{4k_2^2}\int_{C_1} K_s(\bar{\rho}')\, G_2(\gamma_2,\bar{\rho},\bar{\rho}')ds' + \frac{\gamma_2^2}{4\mu_2\omega}\int_{C_1} M_s(\bar{\rho}')\, G_3(\gamma_2,\bar{\rho},\bar{\rho}')ds' \,, \tag{5-13}$$

and

$$E_s^t(\bar{\rho}) = -\frac{i\gamma_2^3}{4k_2^2}\int_{C_1} M_y(\bar{\rho}')\, G_1(\gamma_2,\bar{\rho},\bar{\rho}')ds'$$

$$+\frac{k_{y_2}\gamma_2^2}{4k_2^2}\int_{C_1} M_s(\bar{\rho}')\, G_2(\gamma_2,\bar{\rho},\bar{\rho}')ds' - \frac{z_2\gamma_2^2}{4k_2}\int_{C_1} K_s(\bar{\rho}')\, G_3(\gamma_2,\bar{\rho},\bar{\rho}')ds' \,, \tag{5-14}$$

where

$$G(\gamma,\bar{\rho},\bar{\rho}') = \hat{s}\cdot\vec{F}(\gamma,\bar{\rho},\bar{\rho}') \,, \tag{5-15a}$$

$$G_1(\gamma,\bar{\rho},\bar{\rho}') = -H_1^{(1)}(\gamma|\bar{\rho}-\bar{\rho}'|)\cos(\beta-\alpha_i) \tag{5-15b}$$

$$G_2(\gamma,\bar{\rho},\bar{\rho}') = -\sin(\beta-\alpha)\cos(\beta-\alpha_i)\,H_0^{(1)}(\gamma|\bar{\rho}-\bar{\rho}'|) + \frac{H_1^{(1)}(\gamma|\bar{\rho}-\bar{\rho}'|)}{\gamma|\bar{\rho}-\bar{\rho}'|}\sin(2\beta-\alpha-\alpha_i) \,, \tag{5-15c}$$

$$G_3(\gamma,\bar{\rho},\bar{\rho}') = -\cos(\beta-\alpha)\cos(\beta-\alpha_i)\,H_0^{(1)}(\gamma|\bar{\rho}-\bar{\rho}'|) + \frac{H_1^{(1)}(\gamma|\bar{\rho}-\bar{\rho}'|)}{\gamma|\bar{\rho}-\bar{\rho}'|}\cos(2\beta-\alpha-\alpha_i) \,. \tag{5-15d}$$

If we let the point of observation approach a boundary point given by the position vector $\bar{\rho}''$ and equate tangential components of $\vec{E}$ and $\vec{H}$, we obtain the desired coupled integral equations:

$$E_y^i(\bar{\rho}'') = \frac{1}{4}\int_{C_1} K_y(\bar{\rho}')\left[\frac{Z_1\gamma_1^2}{k_1} H_0^{(1)}(\gamma_1|\bar{\rho}''-\bar{\rho}'|) + \frac{Z_2\gamma_2^2}{k_2} H_0^{(1)}(\gamma_2|\bar{\rho}''-\bar{\rho}'|)\right] ds'$$

$$- \frac{i}{4}\int_{C_1} K_s(\bar{\rho}')\sin(\beta-\alpha)\left[\frac{Z_1 k_{y_1}\gamma_1}{k_1} H_1^{(1)}(\gamma_1|\bar{\rho}-\bar{\rho}'|) + \frac{Z_2 k_{y_2}\gamma_2}{k_2} H_1^{(1)}(\gamma_2|\bar{\rho}''-\bar{\rho}'|)\right] ds'$$

$$- \frac{i}{4}\int_{C_1} M_s(\bar{\rho}')\cos(\beta-\alpha)\left[\gamma_1 H_1^{(1)}(\gamma_1|\bar{\rho}''-\bar{\rho}'|) + \gamma_2 H_1^{(1)}(\gamma_2|\bar{\rho}''-\bar{\rho}'|)\right] ds', \tag{5-16}$$

$$H_y^i(\bar{\rho}'') = -\frac{1}{4}\int_{C_1} M_y(\bar{\rho}')\left[\frac{\gamma_1^2}{Z_1 k_1} H_0^{(1)}(\gamma_1|\bar{\rho}''-\bar{\rho}'|) + \frac{\gamma_2^2}{Z_2 k_2} H_0^{(1)}(\gamma_2|\bar{\rho}''-\bar{\rho}'|)\right] ds'$$

$$+ \frac{i}{4}\int_{C_1} M_s(\bar{\rho}')\sin(\beta-\alpha)\left[\frac{k_{y_1}\gamma_1}{Z_1 k_1} H_1^{(1)}(\gamma_1|\bar{\rho}''-\bar{\rho}'|) + \frac{k_{y_2}\gamma_2}{Z_2 k_2} H_1^{(1)}(\gamma_2|\bar{\rho}''-\bar{\rho}'|)\right] ds'$$

$$- \frac{i}{4}\int_{C_1} K_s(\bar{\rho}')\cos(\beta-\alpha)\left[\gamma_1 H_1^{(1)}(\gamma_1|\bar{\rho}''-\bar{\rho}'|) + \gamma_2 H_1^{(1)}(\gamma_2|\bar{\rho}''-\bar{\rho}'|)\right] ds', \tag{5-17}$$

$$\hat{s}\cdot\bar{H}_{th}^i(\bar{\rho}'') = -\frac{i}{4}\int_{C_1} K_y(\bar{\rho}')\left[\frac{\gamma_1^3}{k_1^2} G_1(\gamma_1,\bar{\rho}'',\bar{\rho}') + \frac{\gamma_2^3}{k_2^2} G_1(\gamma_2,\bar{\rho}'',\bar{\rho}')\right] ds'$$

$$+ \frac{1}{4}\int_{C_1} K_s(\bar{\rho}')\left[\frac{k_{y_1}\gamma_1^2}{k_1^2} G_2(\gamma_1,\bar{\rho}'',\bar{\rho}') + \frac{k_{y_2}\gamma_2^2}{k_2^2} G_2(\gamma_2,\bar{\rho}'',\bar{\rho}')\right] ds'$$

$$+ \frac{1}{4}\int_{C_1} M_s(\bar{\rho}')\left[\frac{\gamma_1^2}{\mu_1\omega} G_3(\gamma_1,\bar{\rho}'',\bar{\rho}') + \frac{\gamma_2^2}{\mu_2\omega} G_3(\gamma_2,\bar{\rho}'',\bar{\rho}')\right] ds', \tag{5-18}$$

and

$$\hat{s}\cdot\bar{E}_{th}^i(\bar{\rho}'') = -\frac{i}{4}\int_{C_1} M_y(\bar{\rho}')\left[\frac{\gamma_1^3}{k_1^2} G_1(\gamma_1,\bar{\rho}'',\bar{\rho}') + \frac{\gamma_2^3}{k_2^2} G_1(\gamma_2,\bar{\rho}'',\bar{\rho}')\right] ds'$$

$$+ \frac{1}{4}\int_{C_1} M_s(\bar{\rho}')\left[\frac{k_{y_1}\gamma_1^2}{k_1^2} G_2(\gamma_1,\bar{\rho}'',\bar{\rho}') + \frac{k_{y_2}\gamma_2^2}{k_2^2} G_2(\gamma_2,\bar{\rho}'',\bar{\rho}')\right] ds'$$

$$- \frac{1}{4}\int_{C_1} K_s(\bar{\rho}')\left[\frac{Z_1\gamma_1^2}{k_1} G_3(\gamma_1,\bar{\rho}'',\bar{\rho}') + \frac{Z_2\gamma_2^2}{k_2} G_3(\gamma_2,\bar{\rho}'',\bar{\rho}')\right] ds'. \tag{5-19}$$

Equations (5-16), (5-17), (5-18) and (5-19) are four coupled integral equations with four unknown current components $K_y(\bar{\rho})$, $K_s(\bar{\rho})$, $M_y(\bar{\rho})$ and $M_s(\bar{\rho})$. They are solved by dividing the contour into N sampled values of each unknown current components and solving the resulting system of 4N linear equations for the unknown sampled values of $K_y(\bar{\rho})$, $K_s(\bar{\rho})$, $M_y(\bar{\rho})$, and $M_s(\bar{\rho})$. The solution of four coupled integral equations is similar to the solution of two coupled integral equations, which is discussed in section (5-3).

If we assume that $k_y = 0$, then equations (5-16) and (5-18) uncouple from equations (5-17) and (5-19) and can be solved separately for each axial component of the total field. However, we will confine our study to E_y-polarized incident fields, in which case it is sufficient to consider equations (5-16) and (5-18) alone. It should be noted, however, that the numerical solution of equations (5-17) and (5-19) is the same as the numerical solution of equations (5-16) and (5-18). In fact, the calculation of the scattering matrix would not be much more difficult even if k_y were not assumed to be zero. The only differences would be that a larger storage would be required for the matrix and its inversion would be more time consuming.

Assuming that $k_y = 0$ and confining our study to E_y-polarized incident fields, we find that the integral equations reduce to

$$E_y^i(\bar{\rho}'') = \frac{\mu_1 \omega}{4} \int_{C_1} K_y(\bar{\rho}') \left[H_o^{(1)}(k_1|\bar{\rho}''-\bar{\rho}'|) + \frac{\mu_2}{\mu_1} H_o^{(1)}(k_2|\bar{\rho}''-\bar{\rho}'|) \right] ds'$$

$$- \frac{i}{4} \int_{C_1} M_s(\bar{\rho}') \cos(\beta''-\alpha) \left[k_1 H_o^{(1)}(k_1|\bar{\rho}''-\bar{\rho}'|) + k_2 H_1^{(1)}(k_2|\bar{\rho}''-\bar{\rho}'|) \right] ds' , \qquad (5\text{-}20)$$

and

$$\hat{s}\cdot\vec{H}^{i}_{tan}(\bar{\rho}'') = \frac{i}{4}\int_{C_1} K_y(\bar{\rho}')\cos(\beta''-\alpha_i)\left[k_1 H_1^{(1)}(k_1|\bar{\rho}''-\bar{\rho}'|)+k_2 H_1^{(1)}(k_2|\bar{\rho}''-\bar{\rho}'|)\right]ds'$$

$$-\frac{1}{4}\int_{C_1} M_s(\bar{\rho}')\cos(\beta''-\alpha)\cos(\beta''-\alpha_i)\left[\frac{k_1}{Z_1}H_0^{(1)}(k_1|\bar{\rho}''-\bar{\rho}'|)+\frac{k_2}{Z_2}H_0^{(1)}(k_2|\bar{\rho}''-\bar{\rho}'|)\right]ds'$$

$$+\frac{1}{4}\int_{C_1} M_s(\bar{\rho}')\cos(2\beta''-\alpha-\alpha_i)\left[\frac{H_1^{(1)}(k_1|\bar{\rho}''-\bar{\rho}'|)}{Z_1|\bar{\rho}''-\bar{\rho}'|}+\frac{H_1^{(1)}(k_2|\bar{\rho}''-\bar{\rho}'|)}{Z_2|\bar{\rho}''-\bar{\rho}'|}\right]ds'. \qquad (5\text{-}21)$$

Assuming that the incident field is the transmitted field of a E_y-polarized plane wave incident normal to a conductive half-space, then

$$E_y^i(\bar{\rho}'') = \frac{2Z_1}{1+Z_1/Z_0}H_0\, e^{-ik_1 z''}, \qquad (5\text{-}22)$$

and

$$\hat{s}\cdot\vec{H}^{i}_{tan}(\bar{\rho}'') = \frac{-2\sin\alpha_i}{1+Z_1/Z_0}H_0\, e^{-ik_1 z''}. \qquad (5\text{-}23)$$

Once $K_y(\bar{\rho})$ and $M_s(\bar{\rho})$ have been estimated from equations (5-20) and (5-21), the total or scattered magnetic field intensity is calculated from equation (5-3) or (5-8) by setting $k_y = 0$. Depending upon which region the fields are desired, it is found that

$$\vec{H}^{sc}_{tan}(\bar{\rho}) = \frac{ik_1}{4}\int_{C_1} K_y(\bar{\rho}')H_1^{(1)}(k_1|\bar{\rho}-\bar{\rho}'|)(\sin\beta\,\hat{x}-\cos\beta\,\hat{z})ds'$$

$$-\frac{k_1}{4Z_1}\int_{C_1} M_s(\bar{\rho}')\cos(\beta-\alpha)H_0^{(1)}(k_1|\bar{\rho}-\bar{\rho}'|)(\sin\beta\,\hat{x}-\cos\beta\,\hat{z})ds'$$

$$+\frac{k_1}{4Z_1}\int_{C_1} M_s(\bar{\rho}')\frac{H_1^{(1)}(k_1|\bar{\rho}-\bar{\rho}'|)}{k_1|\bar{\rho}-\bar{\rho}'|}(\sin(2\beta-\alpha)\hat{x}-\cos(2\beta-\alpha)\hat{z})ds', \qquad (5\text{-}24)$$

exterior to the cylinder, and

$$\vec{H}_h^t(\bar{\rho}) = -\frac{ik_2}{4}\int_{C_1} K_y(\bar{\rho}')\, H_1^{(1)}(k_2|\bar{\rho}-\bar{\rho}'|)(\sin\beta\,\hat{x} - \cos\beta\,\hat{z})\,ds'$$

$$+ \frac{k_2}{4Z_2}\int_{C_1} M_s(\bar{\rho}')\cos(\beta-\alpha)\,H_0^{(1)}(k_2|\bar{\rho}-\bar{\rho}'|)(\sin\beta\,\hat{x} - \cos\beta\,\hat{z})\,ds'$$

$$+ \frac{k_2}{4Z_2}\int_{C_1} M_s(\bar{\rho}')\,\frac{H_1^{(1)}(k_2|\bar{\rho}-\bar{\rho}'|)}{k_2|\bar{\rho}-\bar{\rho}'|}\left(\sin(2\beta-\alpha)\hat{x} - \cos(2\beta-\alpha)\hat{z}\right)ds', \tag{5-25}$$

interior to the cylinder.

It is interesting to note that the general integral equation (5-20) can be reduced to the integral equation for cylinders with low surface impedance (equation (4-7)) by a different derivation than discussed in sections (2-5) and (4-1). If it is assumed that k_2 becomes very large with respect to k_1 and that the curvature of the cylinder is small, then only that part of the contour in the immediate vicinity of the point at which the boundary condition is being enforced contributes to the contour integral of the interior field representations. Under these conditions, the contour integral can be replaced by an integral over the interval $(-\infty, \infty)$ since the fields will be independent of the contour chosen outside of this region of interest. Consequently, equation (5-20) can be rewritten as

$$E_y^i(\bar{\rho}'') = \frac{\mu_1\omega}{4}\int_{C_1} K_y(\bar{\rho}')\,H_0^{(1)}(k_1|\bar{\rho}''-\bar{\rho}'|)\,ds' - \frac{ik_1}{4}\int_{C_1} M_s(\bar{\rho}')\cos(\beta''-\alpha)\,H_1^{(1)}(k_1|\bar{\rho}''-\bar{\rho}'|)\,ds'$$

$$+ \lim_{\delta\to 0}\left[\frac{\mu_2\omega\,K_y(\bar{\rho}'')}{4}\int_{-\infty}^{\infty} H_0^{(1)}(k_2\sqrt{s'^2+\delta^2})\,ds'\right.$$

$$\left. - \frac{ik_2\,M_s(\bar{\rho}'')}{4}\int_{-\infty}^{\infty}\cos(\beta''-\alpha)\,H_1^{(1)}(k_2\sqrt{s'^2+\delta^2})\,ds'\right]. \tag{5-26}$$

Noting that

$$\cos(\beta''-\alpha) = \frac{\delta}{\sqrt{\delta^2+s'^2}} \tag{5-27}$$

for a point of observation just inside the cylinder, then the last two integrals of equation (5-26) can be evaluated analytically from equations (4-28) and (4-29). Thus, equation (5-26) reduces to

$$E_y^i(\bar{\rho}'') = \frac{Z_{2y}(\bar{\rho}'')K_y(\bar{\rho}'')}{2} - \frac{M_s(\bar{\rho}'')}{2} + \frac{\mu_1\omega}{4}\int_{C_1} K_y(\bar{\rho}')H_0^{(1)}(k_1|\bar{\rho}''-\bar{\rho}'|)ds'$$

$$- \frac{ik_1}{4}\int_{C_1} M_s(\bar{\rho}')\cos(\beta''-\alpha)H_1^{(1)}(k_1|\bar{\rho}''-\bar{\rho}'|)ds'. \tag{5-28}$$

On replacing $M_s(\bar{\rho})$ by $-Z_{2y}K_y$ as discussed in section (2-5), we find that

$$E_y^i(\bar{\rho}'') = Z_{2y}(\bar{\rho}'')K_y(\bar{\rho}'') + \frac{\mu_1\omega}{4}\int_{C_1} K_y(\bar{\rho}')H_0^{(1)}(k_1|\bar{\rho}''-\bar{\rho}'|)ds'$$

$$+ \frac{ik_1}{4}\int_{C_1} Z_{2y}(\bar{\rho}')K_y(\bar{\rho}')\cos(\beta''-\alpha)H_1^{(1)}(k_1|\bar{\rho}''-\bar{\rho}'|)ds'. \tag{5-29}$$

Equation (5-29) agrees with equation (4-7).

As in Chapters 3 and 4, it is necessary for integration accuracy to make a small argument approximation to the Hankel functions whenever $|k||\bar{\rho}-\bar{\rho}'|$ is less than 0.3 and integrate the resulting expressions analytically. Fortunately, the necessary integrals have been studied already in Chapters 3 and 4. From equations (3-8) and (3-10), we can write that the small argument contribution of the jth interval to equation (5-20) is

$$E_y^i(\bar{\rho}'') = E_{y_j}(k_1, \bar{\rho}'', \bar{\rho}') + E_{y_j}(k_2, \bar{\rho}'', \bar{\rho}')$$

$$+ \frac{ik_1\delta}{4} B_j(k_1, \bar{\rho}'', \bar{\rho}') + \frac{ik_2\delta}{4} B_j(k_2, \bar{\rho}'', \bar{\rho}'), \tag{5-30}$$

where $E_{y_j}(k, \bar{\rho}'', \bar{\rho}')$ is given by equations (3-58), (3-59) and (3-60) with current component $K_y(\bar{\rho})$,

and $B_j(k, \bar{\rho}'', \bar{\rho}')$ is given by equations (3-62b) and (3-63) with current component $M_s(\bar{\rho})$.

Similarly, the contribution of the jth interval to the scattered magnetic field intensity (equation (5-24)) can be written from equation (4-10) as

$$\vec{H}_{h_j}(\bar{\rho}) = -\frac{ik_1}{4}\Big[(A\cos\alpha_j + B\delta\sin\alpha_j)\hat{x} + (A\sin\alpha_j - B\delta\cos\alpha_j)\hat{z}\Big]$$

$$-\frac{k_1}{4z_1}\Big\{\Big[\delta(C\cos\alpha_j + \delta D\sin\alpha_j) - \frac{1}{k_1}\big((\delta^2 E - F)\sin\alpha_j + 2\delta G\cos\alpha_j\big)\Big]\hat{x}$$

$$+\Big[\delta(C\sin\alpha_j - \delta D\cos\alpha_j) + \frac{1}{k_1}\big((\delta^2 E - F)\cos\alpha_j - 2\delta G\sin\alpha_j\big)\Big]\hat{z}\Big\}, \tag{5-31}$$

where A and B are given by equations (3-62) and (3-63) with current component $K_y(\bar{\rho})$,

and C, D, E, F, and G are given by equations (4-12), (4-13) (4-14) with current component $M_s(\bar{\rho})$.

The small argument approximation to equation (5-21) is obtained by taking the dot product of $\hat{s}$ and equation (5-31) with opposite sign. Thus, from equations (5-10) and (5-31), the small argument contribution of the jth interval to equation (5-21) is found to be

$$\hat{s} \cdot \vec{H}^{i}_{t_j}(\bar{\rho}'') = H_{tang_j}(k_1, \bar{\rho}'', \bar{\rho}') + H_{tang_j}(k_2, \bar{\rho}'', \bar{\rho}') \quad , \tag{5-32}$$

where

$$H_{tang_j}(k, \bar{\rho}'', \bar{\rho}') = -\frac{ik}{4}\Big[A \sin(\alpha_i - \alpha_j) + B\delta \cos(\alpha_i - \alpha_j)\Big]$$

$$-\frac{k}{4z}\Bigg\{ \delta\Big[C \sin(\alpha_i - \alpha_j) + D\delta \cos(\alpha_i - \alpha_j)\Big]$$

$$-\frac{1}{k}\Big[(\delta^2 E - F)\cos(\alpha_i - \alpha_j) + 2\delta G \sin(\alpha_i - \alpha_j)\Big]\Bigg\} , \tag{5-33}$$

where A and B are given by equations (3-62) and (3-63) with current component $K_y(\bar{\rho})$,

and C, D, E, F, and G are given by equations (4-12), (4-13), and (4-14) with current component $M_s(\bar{\rho})$.

5-2 Integration Through the Point of Singularity

Integration through the point of singularity in equation (5-20) presents no problem if it is noted that the limit taken when applying the boundary conditions is from both sides of the interface. Thus, we find that

$$\cos(\beta-\alpha) = \frac{-\delta}{\sqrt{\delta^2+s'^2}} \tag{5-34}$$

for a point of observation just outside the cylinder, and

$$\cos(\beta-\alpha) = \frac{\delta}{\sqrt{\delta^2+s'^2}} \quad , \tag{5-35}$$

for a point of observation just inside the cylinder. Since

$$\lim_{\delta\to 0}\left(\frac{ik\delta}{4}\int_{-W_i}^{W_i} M_s(\bar{\rho}')\,\frac{H_1^{(1)}(k_1\sqrt{\delta^2+s'^2})}{(\delta^2+s'^2)^{1/2}}\,ds' = \frac{M_s(\bar{\rho}'')}{2}\right) \quad , \tag{5-36}$$

the contribution of each term in the second integral of equation (5-20) adds to zero. The contribution of the first integral of equation (5-20) in the singular interval is found by applying equations (3-31), (3-32) and (3-33) to each of the Hankel functions and summing the results.

It should be remembered, however, that equations (3-31), (3-32) and (3-33) are accurate only if the small argument approximation to the Hankel function is valid. When examining scattering from highly conducting cylinders, it is quite possible that although $|k_1| W_i \leq .3$, $|k_2| W_i > .3$ where W_i is the half width of the singular interval. This problem can be overcome by going back to equation (3-28) and rewriting HK00 and HK02 as

$$HK00 = \lim_{\delta \to 0} \int_{-\varepsilon}^{\varepsilon} H_0^{(1)}(k\sqrt{\delta^2+s'^2})\,ds' + 2\int_{\varepsilon}^{W_i} H_0^{(1)}(ks')\,ds', \tag{5-37a}$$

and

$$HK02 = \lim_{\delta \to 0} \int_{-\varepsilon}^{\varepsilon} s'^2 H_0^{(1)}(k\sqrt{\delta^2+s'^2})\,ds' + 2\int_{\varepsilon}^{W_i} s'^2 H_0^{(1)}(ks')\,ds', \tag{5-37b}$$

where

$$\varepsilon = \frac{.3}{|k_1|}. \tag{5-37c}$$

Thus, the integrals are approximated analytically over the interval $(-\varepsilon,\varepsilon)$ from equations (3-30a) and (3-30c) and numerically over the intervals $(-w_i,\varepsilon)$ and (ε,w_i). These results are then inserted into equation (3-28) to obtain the contribution to the singular interval.

In the singular interval, $\alpha_i=\alpha$, so that equation (5-21) can be rewritten as

$$\begin{aligned}
\hat{s}\cdot\bar{H}_{th}^{i}(\bar{\rho}'') = {} & \frac{i}{4}\int_{C_1} K_y(\bar{\rho}')\cos(\beta''-\alpha)\left[k_1 H_1^{(1)}(k_1|\bar{\rho}''-\bar{\rho}'|)+k_2 H_1^{(1)}(k_2|\bar{\rho}''-\bar{\rho}'|)\right]ds' \\
& - \frac{1}{4}\int_{C_1} M_s(\bar{\rho}')\cos^2(\beta''-\alpha)\left[\frac{k_1}{Z_1}H_0^{(1)}(k_1|\bar{\rho}''-\bar{\rho}'|)+\frac{k_2}{Z_2}H_0^{(1)}(k_2|\bar{\rho}''-\bar{\rho}'|)\right]ds' \\
& + \frac{1}{4}\int_{C_1} M_s(\bar{\rho}')\cos 2(\beta-\alpha)\left[\frac{H_1^{(1)}(k_1|\bar{\rho}''-\bar{\rho}'|)}{Z_1|\bar{\rho}''-\bar{\rho}'|}+\frac{H_1^{(1)}(k_2|\bar{\rho}''-\bar{\rho}'|)}{Z_2|\bar{\rho}''-\bar{\rho}'|}\right]ds'.
\end{aligned} \tag{5-38}$$

It is evident that the contribution of the first integral of equation (5-38) is zero by comparing it with the second integral of equation (5-20). The contribution of the second integral of equation (5-38) also is zero and this can be shown by examining the term involving $H_o^{(1)}(k_1|\bar{\rho}''-\bar{\rho}'|)$. On expanding $M_s(\bar{\rho}')$ the contribution of the terms involving $H_o^{(1)}(k_1|\bar{\rho}''-\bar{\rho}'|)$ can be written as

$$-\frac{k_1}{4z_1}\left\{\left[I_5-\frac{(1-\lambda_i)}{w_i+w_{i+1}}I_6-\frac{I_7}{\tilde{\ell}_i}\right]M_{s_i}\right.$$

$$\left.+\frac{1}{1+\lambda_i}\left[\frac{I_6}{w_i+w_{i+1}}+\frac{I_7}{\tilde{\ell}_i}\right]M_{s_{i+1}}-\frac{\lambda_i}{1+\lambda_i}\left[\frac{\lambda_i I_6}{w_i+w_{i+1}}-\frac{I_7}{\tilde{\ell}_i}\right]M_{s_{i-1}}\right\}, \tag{5-39}$$

where

$$I_5=\lim_{\delta\to 0}\left(\delta^2\int_{-w_i}^{w_i}\frac{H_o^{(1)}(k_1\sqrt{\delta^2+s'^2})}{\delta^2+s'^2}ds'\right), \tag{5-40a}$$

$$I_6=\lim_{\delta\to 0}\left(\delta^2\int_{-w_i}^{w_i}s'\frac{H_o^{(1)}(k_1\sqrt{\delta^2+s'^2})}{\delta^2+s'^2}ds'\right), \tag{5-40b}$$

and

$$I_7=\lim_{\delta\to 0}\left(\delta^2\int_{-w_i}^{w_i}s'^2\frac{H_o^{(1)}(k_1\sqrt{\delta^2+s'^2})}{\delta^2+s'^2}ds'\right). \tag{5-40c}$$

Equations (5-40) have been evaluated in Appendix D assuming that $H_o^{(1)}(k_1\sqrt{\delta^2+s^2})$ is given by equation (3-26). It is found that on taking the limit

$$I_5=\lim_{\delta\to 0}\left[\frac{\delta^2}{2}\int_{-w_i}^{w_i}\frac{\ln(s'^2+\delta^2)}{s'^2+\delta^2}ds'\right], \tag{5-41a}$$

$$I_6 = 0 \,, \tag{5-41b}$$

and

$$I_7 = 0. \tag{5-41c}$$

Rewriting (5-41c) as

$$\lim_{\delta \to 0} \left\{ \delta^2 \left[\int_0^{\delta/30} \frac{\ln (s'^2+\delta^2)}{s'^2+\delta^2}\, ds' + \int_{\delta/30}^{30\delta} \frac{\ln (s'^2+\delta^2)}{s'^2+\delta^2}\, ds' + \int_{30\delta}^{W_i} \frac{\ln (s'^2+\delta^2)}{s'^2+\delta^2}\, ds' \right] \right\}$$

$$\sim \lim_{\delta \to 0} \left\{ \frac{\delta \ln \delta}{15} + \delta^2 \int_{\delta/30}^{30\delta} \frac{\ln (s'^2+\delta^2)}{s'^2+\delta^2}\, ds' - \frac{2\delta^2 \ln W_i}{W_i} + \frac{\delta \ln 30\delta}{15} \right\}, \tag{5-42}$$

then it is apparent that on taking the limit as

$$I_5 = 0 \,. \tag{5-43}$$

Since a similar analysis involving $H_0(k_2|\bar{\rho}'' - \bar{\rho}'|)$ would yield an analogous result, the contribution of the second integral of equation (5-38) is zero.

Noting that

$$\cos 2(\beta-\alpha) = 2\cos^2(\beta-\alpha) - 1 = \frac{2\delta^2}{(\delta^2+s'^2)} - 1 \,, \tag{5-44}$$

then the contribution of each term in the third integral of equation (5-38) can be written as

$$\lim_{\delta \to 0} \left[\frac{1}{4\pi} \left\{ \left[(2\delta^2 I_9 - I_1) - \frac{(1-\lambda_i)}{W_i + W_{i+1}} (2\delta^2 I_{10} - I_2) - \frac{(2\delta^2 I_{11} - I_3)}{\tau_i} \right] M_{s_i} \right.\right.$$

$$\left.\left. \frac{M_{s_{i+1}}}{1+\lambda_i} \left[\frac{2\delta^2 I_{10} - I_2}{W_i + W_{i+1}} + \frac{2\delta^2 I_{11} - I_3}{\tau_i} \right] - \frac{\lambda_i M_{s_{i-1}}}{1+\lambda_i} \left[\frac{\lambda_i (2\delta^2 I_{10} - I_2)}{W_i + W_{i+1}} - \frac{2\delta^2 I_{11} - I_3}{\tau_i} \right] \right\} \right], \tag{5-45}$$

where I_1, I_2, I_3, I_9, I_{10}, and I_{11} are given by equations (3-36) and (4-14).

These integrals have been evaluated in Appendix D assuming that $H_0^{(1)}(k\sqrt{\delta^2+s'^2})$ and $H_1^{(1)}(k\sqrt{\delta^2+s'^2})$ are given by equations (3-26) and (3-27). Thus, if the integration is performed over two intervals as in equations (5-37), then it is found that

$$\lim_{\delta\to 0}\left(2\delta^2 I_9 - I_1\right) = -\frac{4i}{\pi k\varepsilon} - k\varepsilon\left[\left(1-\frac{k^2\varepsilon^2}{24}\right)+\frac{2i}{\pi}\left\{\left(1-\frac{k^2\varepsilon^2}{24}\right)\ln\frac{\gamma k\varepsilon}{2}\right.\right.$$

$$\left.\left.-\left(\frac{3}{2}-\frac{19k^2\varepsilon^2}{288}\right)\right\}\right] - 2\int_{\varepsilon}^{W_i}\frac{H_1^{(1)}(ks')}{s'}\,ds' \,, \qquad (5\text{-}46a)$$

$$\lim_{\delta\to 0}\left(2\delta^2 I_{10} - I_2\right) = 0 \,, \qquad (5\text{-}46b)$$

and

$$\lim_{\delta\to 0}\left(2\delta^2 I_{11} - I_3\right) = \frac{1}{k}\left(2W_i H_0^{(1)}(kW_i) - HK00\right) \qquad (5\text{-}46c)$$

where HK00 is given by equation (5-37a)

and $\mathcal{E}$ is given by equation (5-37c).

The contribution of the third integral in the singular interval is thus found by applying equations (5-45) and (5-46) to each of the Hankel functions in the third integral of equation (5-38) and summing the results.

5-3 Numerical Solution of Coupled Integral Equations

The coupled integral equations (5-20) and (5-21) can be solved in essentially the same manner as when solving the Fredholm integral equations of Chapters 3 and 4. The integrals in each equation are approximated by a weighted sum of N sampled values of $K_y(\bar{\rho}')$ and $M_s(\bar{\rho}')$. When this is done, the integral equations reduce to a system of 2N linear equations of the form

$$(E_y^i) = (C_{11})(K_y) + (C_{12})(M_s) \quad , \tag{5-47a}$$

$$(H_{tr}^i) = (C_{21})(K_y) + (C_{22})(M_s) \quad , \tag{5-47b}$$

where (C_{11}), (C_{12}), (C_{21}) and (C_{22}) represent square matrices of order N and (E_y^i), (H_{tr}^i), (K_y) and (M_s) represent column matrices of length N.

Being cognizant of the matrix nature of equations (5-47), (K_y) and (M_s) can be obtained by treating (5-47) as two linear equations with two unknowns. On solving these equations, it is found that the best form of the solution is

$$(M_s) = \left\{\left[(C_{21})(C_{11})^{-1}\right](C_{12}) - (C_{22})\right\}^{-1}\left\{\left[(C_{21})(C_{11})^{-1}\right](E_y^i) - (H_{tr}^i)\right\} \quad , \tag{5-48a}$$

and

$$(K_y) = (C_{11})^{-1}(E_y^i) - (C_{11})^{-1}(C_{12})(M_s) \quad , \tag{5-48b}$$

where the superscript -1 denotes the matrix inverse.

Equations (5-48) are preferred to other forms since the solution is well behaved even when studying reflection from a flat half-space. In this case, $C_{12} = C_{21} = 0$ and equations (5-47) uncouple, but equations (5-48) still give the correct solution.

5-4 Numerical Examples

Equations (5-20), (5-21) and (5-24) were programmed assuming that the incident field is the transmitted field of an E_y-polarized plane

wave incident normal to a conductive half-space (equations (5-22) and (5-23)). As in Chapter 4, their validity is demonstrated by comparing the numerical results with the analytical results obtained for the case of scattering from finitely,conducting circular cylinders (equations (4-15), (4-16) and (4-17)).

In Chapters 3 and 4, it was seen that an n of 2 in Simpson's rule was sufficient in general for integration accuracy across each interval. Although this will still be true in equations (5-20), (5-21) and (5-24) for those integrals involving the exterior Green's function, it may not be sufficient for those integrals involving the interior Green's function. The reason for this is that with large values for the conductivity of the scatterer, the modulation of the integrands of the interior integral representations by the Hankel functions becomes sufficient to affect integration accuracy.

To overcome this problem, equations (5-20), (5-21), and (5-24) were rewritten in the form of equations (5-30), (5-32), and (5-31) respectively. In this form the order n in Simpson's rule is specified separately for each region and all independent integrals in equations (5-30),(5-31) and (5-32) are performed numerically.

Figs. 52 through 55 demonstrate that the general integral representations are valid, although the accuracy and convergence obtained is not as good as that realized in Chapters 3 and 4 for more highly conducting scatterers. In this example, we have assumed normal incidence of an E_y-polarized plane wave and that: the depth z_1 to the top of the cylinder is 20 m, the cylinder radius is 100 m, the incident field frequency is 1000 hz, the conductivity of the whole-space is 10^{-3} mhos/m and the conductivity of the cylinder is 10^{-2} mhos/m.

It is seen in Figs. 52 and 53 that except for imaginary (M_s), an accuracy to about 1% has been obtained with 40 sampled values of the equivalent current densities. However, an accuracy to only about 5% has been obtained for imaginary (M_s) and, as a result, the fields calculated from these currents have an accuracy to about 3% with 40 sampled values.

Fig. 56 indicates that much better convergence is obtained if the conductivity of the cylinder is increased from 10^{-2} mhos/m to 10^{-1} mhos/m. For comparison, this example has been calculated also using the integral representations derived for conductors with a low surface impedance and a small curvature. It is evident that in this example the general integral representations are required to predict imaginary (H_x) accurately.

As the conductivity of the cylinder is decreased below 10^{-2} mhos/m (assuming that all other parameters of Figs. 52 through 55 remain fixed), the accuracy and convergence of the solution become increasingly unsatisfactory. In Fig. 57, the horizontal component of the magnetic field intensity scattered by a cylinder with a conductivity of 0 has been plotted for 20, 30 and 40 sampled values of the equivalent surface current densities. Although an accuracy to less than 3% is attained in estimating the equivalent surface current densities, a surprisingly large error of 14% to 30% results for real (H_x).

Consequently, the scattered magnetic field intensity was calculated using analytical values of the equivalent current densities on the surface of a circular cylinder with a conductivity of 0. Since an accuracy to better than 3% was attained, this indicated that no programming errors existed which had not been detected in earlier tests.

However, the possibility existed also that these large errors might be due to the fact that the numerical cylinder was a polygon rather than a circular cylinder. To test this likelihood, a twenty-sided polygon with a conductivity of 0 was sampled 42 times. It is evident in Fig. 57 that the results closely duplicate the data for a forty-sided polygon, suggesting that the errors are not dependent upon curvature.

Nonetheless, Neureuther (1969) believes that this test still does not exclude the possibility that the solution is curvature dependent. The reason for this is that by sampling a twenty-sided polygon 42 times, the sampling points have been shifted closer to each corner of the polygon where the influence of the polygon curvature will be more important. As a result, it will be necessary to solve the integral equations assuming that a circular cylinder has been sampled 20 times rather than assuming that a twenty-sided polygon has been sampled 20 times before the importance of curvature can be resolved.

However, it would appear that the accuracy could be limited also by requiring a very accurate knowledge of the equivalent surface current densities whenever the reflection coefficient is small. The reason for this can be understood best by examining Figs. 58 through 60 in which the problem of a cylinder having the same electrical parameters as the surrounding whole-space has been considered. Since no field is scattered, the tangential surface current densities are equal to the tangential components of the incident field, $K_y = H_s^i$, $M_s = -E_y^i$, and equation (5-24) reduces to

$$\vec{H}_{th}^{sc}(\bar{\rho}) = \frac{i k_1}{4} \int_{C_1} H_s^i(\bar{\rho}') H_1^{(1)}(k_1|\bar{\rho}-\bar{\rho}'|)(\sin\beta\,\hat{x} - \cos\beta\,\hat{z})\,ds'$$

$$+ \frac{k_1}{4Z_1} \int_{C_1} E_y^i(\bar{\rho}') \cos(\beta-\alpha) H_0^{(1)}(k_1|\bar{\rho}-\bar{\rho}'|)(\sin\beta\,\hat{x} - \cos\beta\,\hat{z})\,ds'$$

$$- \frac{k_1}{4Z_1} \int_{C_1} E_y^i(\bar{\rho}') \frac{H_1^{(1)}(k_1|\bar{\rho}-\bar{\rho}'|)}{k_1|\bar{\rho}-\bar{\rho}'|} (\sin(2\beta-\alpha)\,\hat{x} - \cos(2\beta-\alpha)\,\hat{z})\,ds',$$

$$= 0. \qquad (5\text{-}49)$$

This result, which always must be true for any point of observation exterior to the cylinder, is deduced mathematically in section (6-1). As a result, it is evident that the accuracy obtained in predicting the scattered fields is directly dependent upon an accurate knowledge of the scattered fields around the boundary of the inhomogeneity, since in general

$$\vec{H}_h^{sc}(\bar{\rho}) = \frac{i k_1}{4} \int_{C_1} H_s^{sc}(\bar{\rho}') H_1^{(1)}(k_1|\bar{\rho}-\bar{\rho}'|)(\sin\beta\,\hat{x} - \cos\beta\,\hat{z})\,ds'$$

$$+ \frac{k_1}{4Z_1} \int_{C_1} E_y^{sc}(\bar{\rho}') \cos(\beta-\alpha) H_0^{(1)}(k_1|\bar{\rho}-\bar{\rho}'|)(\sin\beta\,\hat{x} - \cos\beta\,\hat{z})\,ds'$$

$$- \frac{k_1}{4Z_1} \int_{C_1} E_y^{sc}(\bar{\rho}') \frac{H_1^{(1)}(k_1|\bar{\rho}-\bar{\rho}'|)}{k_1|\bar{\rho}-\bar{\rho}'|} (\sin(2\beta-\alpha)\,\hat{x} - \cos(2\beta-\alpha)\,\hat{z})\,ds'. \qquad (5\text{-}50)$$

Thus, it is expected that the accuracy and convergence of the general integral representations will be poor for those problems in which the reflection coefficient is small.

In Figs. 58 through 60, a maximum error of 8×10^{-2} Amps/m (2.2%) in imaginary (M_s) yields a maximum error in real (H_x) of 3.5×10^{-2} Amps/m. Similarly, for N = 30 in Fig. 57, a maximum error of 7×10^{-2} Amps/m (1.8%) in imaginary (M_s) yields a maximum error of 3.0×10^{-2} Amps/m (19%) in real (H_x). Since the scattered field is small with respect to the incident field at the contour ($|E^{sc}|/|E^{i}| \sim .043$ and $|H^{sc}|/|H^{i}| \sim .12$ for $\theta = 0$ and, $|E^{sc}|/|E^{i}| \sim .089$ and $|H^{sc}|/|H^{i}| \sim .16$ for $\theta = \pi$), a significant percentage error is obtained in calculating the scattered fields even though the equivalent surface current densities are known to an accuracy of 2%

This conclusion is substantiated by the results of Fig. 61. In this example, we have assumed normal incidence of an E_y-polarized plane wave and that: the depth z_t to the top of the cylinder is 20 m, the cylinder radius is 100 m, the incident field frequency is 1000 hz, the conductivity of the whole space is 0, and the conductivity of the cylinder is 10^{-3} mhos/m. It is seen that an accuracy to about 2.5% in $|H_x|$ is achieved since the scattered magnetic field (which is more important than E_y in this example) now is much larger than the incident field ($|E_y^{sc}|/|E_y^{i}| \sim .24$ and $|H_s^{sc}|/|H_s^{i}| \sim 17.5$ for $\theta = 0.$). It should be noted, also, that the general integral representations are required to compute this example since the curvature approximation would have been violated had the solutions of Chapter 4 been used (compare Figs. 45 and 61).

To illustrate the application of the method to problems which cannot be handled analytically, the field scattered by the vertical slab of

Fig. 24 has been plotted in Figs. 62 and 63. It is assumed that an E_y-polarized plane wave is incident normal to the slab and that: the depth z_1 to the top of the slab is 20 m, the incident field frequency is 1000 hz, the conductivity of the whole-space is 10^{-3} mhos/m, and the conductivity of the slab is 10^{-1} mhos/m.

Since only a 1% change is obtained in the scattered magnetic field intensities as the number of sampled values of the equivalent current densities is increased from 30 to 62, we have assumed that a convergent solution has been found. This fact is suggested also by Fig. 56 in which a cylinder having the same electrical parameters and about the same contour length as the slab of Figs. 62 and 63 has an accuracy to about 1% for 30 sampled values.

It is interesting to note that at this frequency and with these electrical parameters, the inflexions of imaginary $(\hat{H})$ are indicative of cylinder width. It is evident from Fig. 62 that the slab brings about a significant decrease in imaginary (H_x) between $x = \pm 50$ m whereas the circular cylinder of Fig. 56 has a flat response between $x = \pm 50$ m. (Actually, there is a very slight decrease in imaginary (H_x) over the circular cylinder.) The reason for this behaviour is that we are observing each corner of the slab (where the radius of curvature is small) respond to the incident field. This will be discussed more thoroughly in section (7-3) where it will be seen that the corners mainly affect imaginary (K_y). As a result, the effects of corners are apparent in imaginary $(\hat{H})$.

CHAPTER 6

TWO-DIMENSIONAL AND THREE-DIMENSIONAL INCIDENT FIELDS

In Chapters 3, 4 and 5, an integral equation solution to scattering from cylinders in a conductive whole-space was examined. In the derivation of these integral equations, however, it was assumed implicitly that the incident field was that of a plane wave.

We will show now that this assumption is unnecessarily restrictive and that the integral representations are valid for any two-dimensional source configuration. In fact, any three-dimensional source configuration can be considered by expanding the primary current distribution and the field it radiates into a Fourier integral over a continuous mode distribution and solving this two-dimensional problem.

6-1 Derivation of the Integral Representations Assuming Any Two-Dimensional Source Configuration

If the incident field is other than that of a plane wave, it is invalid to write that the axial components of the total electric and magnetic field intensities satisfy the homogeneous Helmholtz equation in the exterior region (assuming that this is the region which contains the sources). However, since the scattered field intensities always satisfy the homogeneous Helmholtz equation, it is valid to write that in the exterior region

$$(\nabla^2 + k^2) E_y^{sc}(\bar{\rho}) = 0 \quad , \tag{6-1}$$

and

$$(\nabla^2+k^2)\, H_y^{sc}(\bar{\rho}) = 0. \tag{6-2}$$

The exterior Green's function remains unchanged and must satisfy an inhomogeneous Helmholtz equation given by

$$(\nabla^2+k^2)\, G^e(\bar{\rho},\bar{\rho}') = -\delta(\bar{\rho}-\bar{\rho}'). \tag{6-3}$$

Thus, it follows from section (2-1) that if equations (6-1) and (6-3) and equations (6-2) and (6-3) are introduced separately into equation (2-2), then

$$E_y^{sc}(\bar{\rho}) = \int_{c_1} \left\{ G^e(\bar{\rho},\bar{\rho}') \frac{\partial E_y^{sc}}{\partial n'}(\bar{\rho}') - E_y^{sc}(\bar{\rho}') \frac{\partial G^e}{\partial n'}(\bar{\rho},\bar{\rho}') \right\} ds', \tag{6-4}$$

and

$$H_y^{sc}(\bar{\rho}) = \int_{c_1} \left\{ G^e(\bar{\rho},\bar{\rho}') \frac{\partial H_y^{sc}}{\partial n'}(\bar{\rho}') - H_y^{sc}(\bar{\rho}') \frac{\partial G^e}{\partial n'}(\bar{\rho},\bar{\rho}') \right\} ds', \tag{6-5}$$

since the contribution from the outer contour C_2 tends to zero as C_2 approaches infinity.

However, the incident field does satisfy the homogeneous Helmholtz equation in the interior region since by assumption this domain is source free. Thus,

$$(\nabla^2+k^2)\, E_y^i(\bar{\rho}) = 0 \tag{6-6}$$

and

$$(\nabla^2+k^2)\, H_y^i(\bar{\rho}) = 0 \tag{6-7}$$

in the interior region. In addition, the exterior Green's function is defined in the interior region by equation (6-3).

As above, it follows from section (2-1) that if equations (6-6) and (6-3) and equations (6-7) and (6-3) are introduced separately into equation (2-2) for the interior region, then

$$0 = \int_{C_1} \left\{ G^e(\bar{\rho},\bar{\rho}') \frac{\partial E_y^i}{\partial n'}(\bar{\rho}') - E_y^i(\bar{\rho}') \frac{\partial G^e}{\partial n'}(\bar{\rho},\bar{\rho}') \right\} ds' \tag{6-8}$$

and

$$0 = \int_{C_1} \left\{ G^e(\bar{\rho},\bar{\rho}') \frac{\partial H_y^i}{\partial n'}(\bar{\rho}') - H_y^i(\bar{\rho}') \frac{\partial G^e}{\partial n'}(\bar{\rho},\bar{\rho}') \right\} ds' \tag{6-9}$$

since the Green's function possesses no singularities in the volume integral inasmuch as $\bar{\rho}$ refers to any point in the exterior region.

Adding equations (6-8) to (6-4) and (6-9) to (6-5), it is found that

$$E_y^{sc}(\bar{\rho}) = \int_{C_1} \left\{ G^e(\bar{\rho},\bar{\rho}') \frac{\partial E_y^t}{\partial n'}(\bar{\rho}') - E_y^t(\bar{\rho}') \frac{\partial G^e}{\partial n'}(\bar{\rho},\bar{\rho}') \right\} ds' \tag{6-10}$$

and

$$H_y^{sc}(\bar{\rho}) = \int_{C_1} \left\{ G^e(\bar{\rho},\bar{\rho}') \frac{\partial H_y^t}{\partial n'}(\bar{\rho}') - H_y^t(\bar{\rho}') \frac{\partial G^e}{\partial n'}(\bar{\rho},\bar{\rho}') \right\} ds' \,. \tag{6-11}$$

Upon adding the incident field intensities to equation (6-10) and (6-11), the desired integral expressions are obtained:

$$E_y^t(\bar{\rho}) = E_y^i(\bar{\rho}) + \int_{C_1} \left\{ G^e(\bar{\rho},\bar{\rho}') \frac{\partial E_y^t}{\partial n'}(\bar{\rho}') - E_y^t(\bar{\rho}') \frac{\partial G^e}{\partial n'}(\bar{\rho},\bar{\rho}') \right\} ds' \tag{6-12}$$

and

$$H_y^t(\bar{\rho}) = H_y^t(\bar{\rho}) + \int_{C_1} \left\{ G^e(\bar{\rho},\bar{\rho}') \frac{\partial H_y^t}{\partial n'}(\bar{\rho}') - H_y^t(\bar{\rho}') \frac{\partial G^e}{\partial n'}(\bar{\rho},\bar{\rho}') \right\} ds' . \tag{6-13}$$

It is evident on comparing equations (6-12) and (6-10) with equations (2-9) and (2-10), and equations (6-13) and (6-11) with equations (2-12) and (2-13), that the integral expressions for $E_y^t(\bar{\rho})$ and $H_y^t(\bar{\rho})$ are unchanged. Since the integral representations of the fields in the interior region remain unaltered for two-dimensional sources, it follows that the general field representations given in sections (2-3) and (2-4) are valid for any two-dimensional source distribution.

6-2 Numerical Examples: Electric Line Source

The electric field intensity at a point of observation $\bar{\rho}$ radiated by an electric line source located at $\bar{\rho}_L$ is given by equation (3-6) as

$$E_y(\bar{\rho}) = -\frac{\mu_1 \omega}{4} I H_0^{(1)}(k_1|\bar{\rho}-\bar{\rho}_L|) \quad , \tag{6-14}$$

where I is the electric current flowing in the source.

For simplicity, we will confine our examples to scattering from perfectly conducting cylinders, in which case the desired integral equation is found to be (from equation (3-8))

$$I H_0^{(1)}(k_1|\bar{\rho}-\bar{\rho}_L|) = -\int_{C_1} K_y(\bar{\rho}') H_0^{(1)}(k_1|\bar{\rho}-\bar{\rho}'|)\,ds' . \tag{6-15}$$

Once equation (6-15) has been solved for $K_y(\bar{\rho}')$, the scattered transverse magnetic field intensity is given by equation (3-12) as

$$\vec{H}_t^{sc}(\bar{\rho}) = \frac{ik_1}{4}\int_{C_1} K_y(\bar{\rho}') H_1^{(1)}(k_1|\bar{\rho}-\bar{\rho}'|)(\sin\beta\,\hat{x} - \cos\beta\,\hat{z})\,ds' . \tag{6-16}$$

To demonstrate that the integral representations are valid for two-dimensional source configurations, we will compare the numerical results

with the analytical results for the case of scattering from circular cylinders. It can be shown by following a development similar to that of Harrington (1961, p. 236) that the field scattered by a perfectly conducting circular cylinder in the presence of an electric line source which is parallel to the cylinder is given by

$$E_y^{sc}(\rho,\phi) = -\frac{\mu_1 \omega}{4} I \sum_{n=0}^{\infty} \varepsilon_n a_n H_n^{(1)}(k_1 \rho_L) H_n^{(1)}(k_1 \rho) \cos n(\phi-\phi'), \quad (6\text{-}17)$$

$$H_\phi^{sc}(\rho,\phi) = \frac{i k_1}{4} I \sum_{n=0}^{\infty} \varepsilon_n a_n H_n^{(1)}(k_1 \rho_L)\left[\frac{n}{k_1 \rho} H_n^{(1)}(k_1 \rho) - H_{n+1}^{(1)}(k_1 \rho)\right] \cos n(\phi-\phi'), \quad (6\text{-}18a)$$

and

$$H_\rho^{sc}(\rho,\phi) = \frac{i I}{2\rho} \sum_{n=1}^{\infty} n a_n H_n^{(1)}(k_1 \rho_L) H_n^{(1)}(k_1 \rho) \sin n(\phi-\phi'), \quad (6\text{-}18b)$$

where

$$a_n = -\frac{J_n(k_1 R)}{H_n^{(1)}(k_1 R)}, \quad (6\text{-}19a)$$

and

$$\varepsilon_n = \begin{cases} 1, & n = 0 \\ 2, & n \geq 1 \end{cases}. \quad (6\text{-}19b)$$

The coordinate system is defined in Fig. 64.

It is interesting to note that the "reflection coefficient" a_n is the same as that obtained for the case of an E_y-polarized plane wave (equation (3-48)) scattered by a perfectly conducting circular cylinder. Harrington (1961, p. 237) notes that in general the "reflection coefficient" is independent of the incident field. Thus, we can write immediately from equations (4-15) and (4-16) that the field scattered by a finitely conducting circular cylinder in the presence of an electric line source which is

parallel to the cylinder axis is given by equations (6-17) and (6-18) with

$$a_n = - \frac{J_n(k_1 R) - c_n J_n'(k_1 R)}{H_n^{(1)}(k_1 R) - c_n H_n^{(1)\prime}(k_1 R)} \tag{6-20a}$$

and

$$c_n = \frac{Z_2 J_n(k_2 R)}{Z_1 J_n'(k_2 R)} \tag{6-20b}$$

where the derivatives in (6-20) are with respect to the argument (kR).

This solution is similar to that given by Wait (1952).

Figs. 65 through 67 demonstrate that the integral representations are valid for two-dimensional source configurations and that the solution converges as the number of sampled values of the current density is increased. We have assumed in this example that an E_y-polarized electric line source is located 20 m above the top of a perfectly conducting cylinder and that: the cylinder radius is 100 m, the incident field frequency is 1000 hz, and the conductivity of the whole-space is 10^{-3} mhos/m.

It is seen that a larger number of sampled values of the current density is required to obtain a 1% error than when the incident field is a plane wave (compare Figs. 65 through 67 with Figs. 11 through 16). The reason for this is that the field of a line source falls off much more rapidly than that of a plane wave. As a result, a small sampling interval is required for line source scattering problems to describe accurately the rapid current variation around the cylinder.

However, it is evident from Fig. 65 that a small sampling interval is required only on the upper portion of the cylinder since this is where the largest current densities are located. At an angular distance of $\pi/4$ from

the top of the cylinder, the surface current density is 1/20 of the maximum value whereas at an angular distance of $\pi/2$, the surface current density is 1/100 of the maximum value. Thus, a small sampling interval is required only between $\theta = \pm \pi/4$.

With this fact in mind, the cylinder was sampled 26 times using the sampling distribution of Fig. 68. Intervals 1 through 8 and their mirror image about the z-axis have the same sampling distribution as used in Figs. 65 through 67 for N equal to 50. Then, the cylinder was sampled 3 times to a θ of $\pi/2$ and the lower half of the cylinder was sampled only 5 times.

A maximum change of 0.1% from the results of Figs. 66 and 67 was obtained in the horizontal interval (-100,100). The changes were largest at x = ±100, since the point of observation is closer to the less accurate sampling here than at x = 0. However, the fields close to x = 0 are of most interest to the field geophysicist since this is the region of maximum field intensities. Here, the changes are less than 0.01% from the results of Figs. 66 and 67. Thus, by an appropriate choice of interval distribution, it seems possible to obtain about the same numerical accuracy independent of the incident field using the same number of sampled values of the surface current density.

To illustrate the application of the method to problems which cannot be handled analytically, the field scattered by a perfectly conducting vertical slab (Fig. 24) has been plotted in Figs. 69 and 70. In this example, it is assumed that an E_y-polarized line source is located 20 m above the top of the slab, the incident field frequency is 1000 hz and the conductivity of the whole-space is 10^{-3} mhos/m.

The slab was sampled 30 and 42 times using the general sampling distribution of Fig. 24. Then, choosing a sampling distribution with a line source in mind, the slab was sampled twice as often as for N = 42 to a depth of 125 m on the slab (the depth at which the current was 1% of the peak value), and only 9 times on the rest of the contour. Since a change of less than 1% in the predicted field occurred when the contour was sampled twice as frequently (effectively), we can assume that a convergent solution has been found. In addition, Figs. 66 and 67 suggest that in a similar problem, an accuracy of greater than 1% can be obtained if a smooth contour is sampled 500 times per wavelength. Since this sampling rate is true for N = 50 on the slab contour above a depth of 125 m, this result suggests also that a convergent result has been obtained for N = 50.

6-3 Integral Representations Assuming Any Three-Dimensional Source Configuration

Harrington (1961, p. 292) notes that "a three-dimensional problem having cylindrical boundaries can be reduced to a two-dimensional problem by applying a Fourier transformation with respect to y (the cylinder axis)." For three-dimensional source configurations, we seek a solution to the three dimensional Helmholtz equation

$$\left(\frac{\partial^2}{\partial x^2} + \frac{\partial^2}{\partial y^2} + \frac{\partial^2}{\partial z^2} + k^2 \right) E_y^{sc}(x,y,z) = 0 . \tag{6-21}$$

Thus

$$E_y^{sc}(x,k_y,z) = \int_{-\infty}^{\infty} E_y^{sc}(x,y,z)\, e^{-ik_y y}\, dy \tag{6-22}$$

will be a solution to the two-dimensional Helmholtz equation

$$\left(\frac{\partial^2}{\partial x^2} + \frac{\partial^2}{\partial z^2} + \gamma^2 \right) E_y^{sc}(\bar{\rho},k_y) = 0 , \tag{6-23}$$

where $\gamma^2 = k^2 - k_y^2$.

We can write immediately the solution to equation (6-23) from equation (6-10) as

$$\mathcal{E}_y^{sc}(\bar{\rho}, k_y) = \int_{C_1} \left\{ \mathcal{G}^e(\bar{\rho},\bar{\rho}') \frac{\partial \mathcal{E}_y^t}{\partial n'}(\bar{\rho}', k_y) - \mathcal{E}_y^t(\bar{\rho}', k_y) \frac{\partial \mathcal{G}^e}{\partial n'}(\bar{\rho},\bar{\rho}') \right\} ds' \tag{6-24}$$

where $\mathcal{G}^e(\bar{\rho},\bar{\rho}') = \frac{i}{4} H_0^{(1)}(\gamma|\bar{\rho}-\bar{\rho}'|)$,

or, on applying a Fourier transformation to the incident field with respect to y

$$\mathcal{E}_y^t(\bar{\rho}, k_y) = \mathcal{E}_y^i(\bar{\rho}, k_y) + \int_{C_1} \left\{ \mathcal{G}^e(\bar{\rho},\bar{\rho}') \frac{\partial \mathcal{E}_y^t}{\partial n'}(\bar{\rho}', k_y) - \mathcal{E}_y^t(\bar{\rho}', k_y) \frac{\partial \mathcal{G}^e}{\partial n'}(\bar{\rho},\bar{\rho}') \right\} ds' \tag{6-25}$$

Once equation (6-25) has been solved for $E_y^t(\bar{\rho}, k_y)$, the three-dimensional solution is obtained from the inversion

$$E_y^{sc}(x, y, z) = \frac{1}{2\pi} \int_{-\infty}^{\infty} \mathcal{E}_y^{sc}(x, k_y, z)\, e^{ik_y y}\, dk_y \, . \tag{6-26}$$

Equation (6-26) asserts that the y dependence of E_y (x,y,z) (and all other transformed quantities) is of the form $e^{i k_y y}$. Since the integral representations derived in sections (2-3) and (2-4) are for just such an axial dependence, equation (6-25) can be solved once k_y is specified.

Thus, it is evident that a three-dimensional problem having cylindrical boundaries can be solved by expanding the three-dimensional incident fields into a Fourier integral over a continuous mode distribution and solving equation (6-25) for a number of discrete values of k_y. Consequently, the three-dimensional solution is obtained by fitting a curve to a weighted sum of sampled values of $\mathcal{E}_y^{sc}(\bar{\rho}, k_y)$ and performing (6-26)

numerically.

If the incident field is a plane wave in free space incident obliquely to the cylinder axis, then we can write that

$$E_y^i(x,y,z) = Z_o H_o e^{ik_o(x\cos\theta\sin\phi_{in} + y\sin\theta + z\cos\theta\cos\phi_{in})}, \qquad (6\text{-}27)$$

where ϕ_{in} is defined in Fig. 2,

and θ is the angle in an axial plane between the direction of propagation and the plane normal to the axis of the cylinder.

The transformed incident field is obtained from equation (6-22) and is found to be

$$\mathcal{E}_y^i(x,k_y,z) = 2\pi Z_o H_o e^{i\gamma_o(x\sin\phi_{in} + z\cos\phi_{in})}\,\delta(k_o\sin\theta - k_y) \qquad (6\text{-}28)$$

where

$$\gamma_o = k_o\cos\theta = \sqrt{k_o^2 - k_y^2}\,.$$

Equation (6-28) indicates that whenever the incident field varies harmonically as $e^{i k_y}$ along the cylinder axis, equation (6-26) need be solved for one value of k_y only. In the case of a plane wave in free space incident obliquely to the cylinder axis, k_y is given by

$$k_y = k_o\sin\theta\,. \qquad (6\text{-}29)$$

It should be noted, however, that this value of k_y is to be used solely in the exterior integral representations. For interior integral representations, k_y is determined in each region from Snell's Law.

If the incident field is a plane wave in a conductive whole-space incident obliquely to the cylinder axis, then equation (6-28) is invalid and instead, equation (6-25) must be solved for a number of discrete values

of k_y. Unfortunately, it is seen from the physics of this situation that the problem does not possess a solution since the plane wave amplifies in the negative y direction.

Nevertheless, it is not surprising that a solution does not exist since the problem is unrealistic in that it requires a source with an infinite power supply at infinity. This complication has been ignored in earlier chapters by assuming that a plane wave incident normal to a conductive half-space exists at the earth-air interface and attenuates from this point as it propagates into the earth. Essentially, it was sufficient to assume that a plane wave generator existed at the earth-air interface since this closely approximated the actual situation.

If oblique incidence is required, it will be necessary to assume that a plane wave generator exists at (x,o,z) and that the wave attenuates in the positive and negative y directions from this "source". However, obliquely incident plane waves propagating in a conductive whole-space are not important in most problems of geophysical interest. The reason for this is that the transmitted field at the earth-air interface propagates normally away from the boundary even for grazing angles of incidence. Thus, when discussing plane wave scattering by cylinders in a conductive whole-space, it is adequate to consider normal incidence.

These problems do not arise when a plane wave is incident obliquely to a cylinder in a conductive half-space. In this case, the plane wave is harmonic in the exterior region (air) and the problem need be solved for one value of k_y only.

CHAPTER 7

SCATTERING FROM CYLINDERS IN A CONDUCTIVE HALF-SPACE

In Chapters 3, 4 and 5, integral equation solutions to scattering from cylinders and from topography were examined. It was seen that any problem could be formulated by choosing an appropriate integral representation in each region present and a solution obtained by solving the resulting integral equations.

Having established the validity of the integral representations and the subroutines written to effect their solution, it is possible now to combine the cylinder and topographic results to study scattering from cylinders of arbitrary cross section in a conductive half-space with an arbitrary earth-air profile. Although this chapter will be concerned with normal incidence of an E_y-polarized plane wave, the results of Chapter 6 can be used to extend the analysis to sources of arbitrary configuration and polarization.

7-1 Derivation of the Integral Equations

If it is assumed that the primary field is a normally incident E_y-polarized wave ($k_y = 0$), then it follows from equations (2-56) and (2-66) that the integral representations for $\bar{E}$ and $\bar{H}$ in the region exterior to the half-space are

$$E_{y_o}^t(\bar{\rho}) = E_y^i(\bar{\rho}) - \frac{\mu_o \omega}{4} \int_{C_1} K_y'(\bar{\rho}') H_o^{(2)}(k_o|\bar{\rho}-\bar{\rho}'|)\, ds' + \frac{ik_o}{4} \int_{C_1} M_s'(\bar{\rho}') \cos(\beta-\alpha)\, H_1^{(2)}(k_o|\bar{\rho}-\bar{\rho}'|)\, ds' , \tag{7-1}$$

and

$$\vec{H}^{t}_{t_0}(\bar{\rho}) = \vec{H}^{i}_{t}(\bar{\rho}) + \frac{i k_0}{4}\int_{C_1} K'_y(\bar{\rho}')\,\vec{F}_1(k_0,\bar{\rho},\bar{\rho}')\,ds' - \frac{k_0}{4z_0}\int_{C_1} M'_s(\bar{\rho}')\,\vec{F}_3(k_0,\bar{\rho},\bar{\rho}')\,ds' \quad (7\text{-}2)$$

where

$$\vec{F}_1(k,\bar{\rho},\bar{\rho}') = H_1^{(1)}(k|\bar{\rho}-\bar{\rho}'|)(\sin\beta\,\hat{x} - \cos\beta\,\hat{z}), \quad (7\text{-}3a)$$

and

$$\vec{F}_3(k,\bar{\rho},\bar{\rho}') = \cos(\beta-\alpha)\,H_0^{(1)}(k|\bar{\rho}-\bar{\rho}'|)(\sin\beta\,\hat{x} - \cos\beta\,\hat{z}) \quad (7\text{-}3b)$$

$$- \frac{H_1^{(1)}(k|\bar{\rho}-\bar{\rho}'|)}{k|\bar{\rho}-\bar{\rho}'|}(\sin(2\beta-\alpha)\,\hat{x} - \cos(2\beta-\alpha)\,\hat{z}).$$

The parameters of the exterior region have been referred to by the subscript 0 and the equivalent surface current densities on contour 1 have been superscripted 1. The nomenclature for the contours and regions present is shown in Fig. 71.

As in Chapter 4, it is assumed that the half-space contour is flat outside an interval bounded by (-a, a) and that outside (-a, a) the equivalent surface current densities arise from fields reflected by the half-space alone. Thus, equations (7-1) can be rewritten from equations (4-22) and (4-37) as

$$E^{t}_{y_0}(\bar{\rho}) = E^{i}_{y}(\bar{\rho}) + \left\{ \begin{array}{l} E_y^{reflec}(\bar{\rho}^{\,0,+}) \\ -E^{i}_{y}(\bar{\rho}^{-}) \end{array} \right\} + I_E(k_0,\bar{\rho},\bar{\rho}')$$

$$- \frac{\mu_0\omega}{4}\int_{-a-s_i}^{a-s_i} K'_y(\bar{\rho}')\,H_0^{(1)}(k_0|\bar{\rho}-\bar{\rho}'|)\,ds' + \frac{i k_0}{4}\int_{-a-s_i}^{a-s_i} M'_s(\bar{\rho}')\cos(\beta-\alpha)\,H_1^{(1)}(k_0|\bar{\rho}-\bar{\rho}'|)\,ds', \quad (7\text{-}4)$$

and equation (7-2) can be rewritten from equation (4-45) as

$$\vec{H}^{t}_{tr_0}(\bar{\rho}) = \vec{H}^{i}_{tr}(\bar{\rho}) + \left\{ \vec{H}^{reflec}_{tr}(\bar{\rho}^{0,+}) - \vec{H}^{i}_{tr}(\bar{\rho}^{-}) \right\} - \vec{I}_{H}(k_0,\bar{\rho},\bar{\rho}')$$

$$+ \frac{ik_0}{4}\int_{-a-s_i}^{a-s_i} k'_y(\bar{\rho}')\vec{F}_1(k_0,\bar{\rho},\bar{\rho}')ds' - \frac{k_0}{4z_0}\int_{-a-s_i}^{a-s_i} M'_s(\bar{\rho}')\vec{F}_3(k_0,\bar{\rho},\bar{\rho}')ds', \tag{7-5}$$

where s_1 is the x coordinate of the point of observation,

$E_y^{reflec}(\bar{\rho}^{0,+})$ is the electric field intensity reflected by a flat conductive half-space and is to be used when the point of observation is above or on the flat half-space,

$-E_y^{i}(\bar{\rho}^{-})$ is the incident electric field intensity and is to be used when the point of observation is below the flat half-space,

$\vec{H}_{tr}^{reflec}(\bar{\rho}^{0,+})$ is the magnetic field intensity reflected by a flat conductive half-space and is to be used when the point of observation is above or on the flat half-space,

$-\vec{H}_{tr}^{1}(\bar{\rho}^{-})$ is the incident magnetic field intensity and is to be used when the point of observation is below the flat half-space,

$\vec{F}_1(k_0,\bar{\rho},\bar{\rho}')$ and $\vec{F}_3(k_0,\bar{\rho},\bar{\rho}')$ are given by equations (7-3)

$$I_E(k,\bar{\rho},\bar{\rho}') = \frac{\mu\omega}{4}\int_{-a-s_i}^{a-s_i} K_y^{i}(\bar{\rho}')H_0^{(1)}(k|\bar{\rho}-\bar{\rho}'|)$$

$$- \frac{ik}{4}\int_{-a-s_i}^{a-s_i} M_s^{i}(\bar{\rho}')\cos(\beta-\alpha)H_1^{(1)}(k|\bar{\rho}-\bar{\rho}'|)ds', \tag{7-6}$$

and

$$\vec{I}_H(k,\bar{\rho},\bar{\rho}') = \frac{ik}{4}\int_{-a-s_i}^{a-s_i} K_y^i(\bar{\rho}')H_1^{(1)}(k|\bar{\rho}-\bar{\rho}'|)(\sin\beta\,\hat{x}-\cos\beta\,\hat{z})ds'$$
$$-\frac{k}{4z}\int_{-a-s_i}^{a-s_i} M_s^i(\bar{\rho}')\cos(\beta-\alpha)H_0^{(1)}(k|\bar{\rho}-\bar{\rho}'|)(\sin\beta\,\hat{x}-\cos\beta\,\hat{z})ds' \qquad (7\text{-}7)$$
$$+\frac{k}{4z}\int_{-a-s_i}^{a-s_i} M_s^i(\bar{\rho}')\frac{H_1^{(1)}(k|\bar{\rho}-\bar{\rho}'|)}{k|\bar{\rho}-\bar{\rho}'|}(\sin(2\beta-\alpha)\hat{x}-\cos(2\beta-\alpha)\hat{z})ds'.$$

It should be noted that, as in Chapter 4, the contour integrals involving (K_y^1, M_s^i) are along a flat half-space while the contour integrals involving (K_y^1, M_s^1) are along the topographic profile.

The integral representations for $\vec{E}$ and $\vec{H}$ in region 1 do not follow directly from Chapter 4 since it is not evident what result the infinite integrals involving (K_y^i, M_s^i) will yield. To establish the value of these integrals, we will examine the electric field intensity transmitted into a homogeneous earth assuming normal incidence of an E_y-polarized wave $(k_y = 0)$. In this case, we can write from equation (2-72) that

$$E_{y_1}^t(\bar{\rho}) = \frac{\mu_1\omega}{4}\int_{-\infty}^{\infty} K_y^1(\bar{\rho}')H_0^{(1)}(k_1|\bar{\rho}-\bar{\rho}'|)ds' - \frac{ik_1}{4}\int_{-\infty}^{\infty} M_s^1(\bar{\rho}')\cos(\beta-\alpha)H_1^{(1)}(k_1|\bar{\rho}-\bar{\rho}'|)ds'. \qquad (7\text{-}8)$$

As in the exterior region, it is assumed that the half-space contour is flat outside an interval bounded by (-a, a) and that outside (-a, a) the equivalent surface current densities arise from fields reflected by the half-space alone. Thus, equation (7-8) can be rewritten as

$$E_{y_1}^t(\bar{\rho}) = \frac{\mu_1\omega}{4}\left[\int_{-\infty}^{-a-s_i} K_y^i(\bar{\rho}')H_0^{(1)}(k_1|\bar{\rho}-\bar{\rho}'|)ds' + \int_{a-s_i}^{\infty} K_y^i(\bar{\rho}')H_0^{(1)}(k_1|\bar{\rho}-\bar{\rho}'|)ds'\right]$$

$$-\frac{ik_1}{4}\left[\int_{-\infty}^{-a-s_i} M_S^i(\bar{\rho}')\cos(\beta-\alpha)\,H_1^{(1)}(k_1|\bar{\rho}-\bar{\rho}'|)\,ds' + \int_{a-s_i}^{\infty} M_S^i(\bar{\rho}')\cos(\beta-\alpha)\,H_1^{(1)}(k_1|\bar{\rho}-\bar{\rho}'|)\,ds'\right]$$

$$+\frac{\mu_1\omega}{4}\int_{-a-s_i}^{a-s_i} K_y^i(\bar{\rho}')\,H_0^{(1)}(k_1|\bar{\rho}-\bar{\rho}'|)\,ds' - \frac{ik_1}{4}\int_{-a-s_i}^{a-s_i} M_S^i(\bar{\rho}')\cos(\beta-\alpha)\,H_1^{(1)}(k_1|\bar{\rho}-\bar{\rho}'|)\,ds'. \tag{7-9}$$

By rewriting the infinite integrals of (7-9) as

$$\frac{\mu_1\omega}{4}\int_{-\infty}^{\infty} K_y^i(\bar{\rho}')\,H_0^{(1)}(k_1|\bar{\rho}-\bar{\rho}'|)\,ds' - \frac{ik_1}{4}\int_{-\infty}^{\infty} M_S^i(\bar{\rho}')\cos(\beta-\alpha)\,H_1^{(1)}(k_1|\bar{\rho}-\bar{\rho}'|)\,ds'$$

$$-\frac{\mu_1\omega}{4}\int_{-a-s_i}^{a-s_i} K_y^i(\bar{\rho}')\,H_0^{(1)}(k_1|\bar{\rho}-\bar{\rho}'|)\,ds' + \frac{ik_1}{4}\int_{-a-s_i}^{a-s_i} M_S^i(\bar{\rho}')\cos(\beta-\alpha)\,H_1^{(1)}(k_1|\bar{\rho}-\bar{\rho}'|)\,ds', \tag{7-10}$$

it follows from (7-8) that for $\bar{\rho}$ below the half-space, the integrals over $(-\infty, \infty)$ must equal the total electric field intensity transmitted into a homogeneous earth by the flat half-space. Consequently, equation (7-9) reduces to

$$E_{y_1}^t(\bar{\rho}) = E_y^{trans}(\bar{\rho}^{0,-}) - I_E(k_1, \bar{\rho}, \bar{\rho}')$$

$$+\frac{\mu_1\omega}{4}\int_{-a-s_i}^{a-s_i} K_y^i(\bar{\rho}')\,H_0^{(1)}(k_1|\bar{\rho}-\bar{\rho}'|)\,ds' - \frac{ik_1}{4}\int_{-a-s_i}^{a-s_i} M_S^i(\bar{\rho}')\cos(\beta-\alpha)\,H_1^{(1)}(k_1|\bar{\rho}-\bar{\rho}'|)\,ds'. \tag{7-11}$$

If $\bar{\rho}$ is above the half-space, the integrals over $(-\infty, \infty)$ must equal zero. The reason for this is that the integral representations predict a null field for points of observation outside the volume of interest since the boundary conditions have been satisfied by the equivalent surface current densities (see Harrington, 1961, p. 106).

Thus, in general the fields inside a conductive half-space can be written as

$$E_{y_1}^t(\bar{\rho}) = \begin{Bmatrix} 0(\bar{\rho}^+) \\ E_y^{trans}(\bar{\rho}^{0,-}) \end{Bmatrix} - I_E(k_1, \bar{\rho}, \bar{\rho}')$$

$$+\frac{\mu_1\omega}{4}\int_{-a-s_i}^{a-s_i} K_y^i(\bar{\rho}')H_o^{(1)}(k_1|\bar{\rho}-\bar{\rho}'|)\,ds' - \frac{ik_1}{4}\int_{-a-s_i}^{a-s_i} M_s^i(\bar{\rho}')\cos(\beta-\alpha)H_1^{(1)}(k_1|\bar{\rho}-\bar{\rho}'|)\,ds', \tag{7-12}$$

where $0(\bar{\rho}^+)$ designates that this term is to be set equal to zero when the point of observation is above the flat half-space,

and $E_y^{trans}(\bar{\rho}^{0,-})$ is the electric field intensity transmitted by a flat half-space and is to be used when the point of observation is below or on the flat half-space.

It can be shown analytically that the infinite integrals of equation (7-10) yield the transmitted electric field intensity for $\bar{\rho}$ below the half-space and zero for $\bar{\rho}$ above the half-space if it is assumed that the incident field is an E_y-polarized plane wave impinging normal to a flat half-space. In this case, K_y^i is constant and is given from equation (4-21) as

$$K_y^i = \frac{2Z_o}{Z_1+Z_o}H_o\,. \tag{7-13a}$$

Similarly, M_s^i is constant and is found from (2-39b) and (4-25) to be

$$M_s^i = -\left(E_y^{inc}+E_y^{reflec}\right) = -\frac{2Z_oZ_1}{Z_o+Z_1}H_o\,. \tag{7-13b}$$

Introducing equations (7-13) into (7-8) and assuming that $\bar{\rho}$ is below the half-space, then equation (7-8) becomes

$$E_{y_1}^t(\bar{\rho}^-) = \frac{Z_oZ_1H_ok_1}{2(Z_o+Z_1)}\left[\int_{-\infty}^{\infty}H_o^{(1)}\left(k_1\sqrt{\delta^2+s'^2}\right)ds' + i\delta\int_{-\infty}^{\infty}\frac{H_1^{(1)}\left(k_1\sqrt{\delta^2+s'^2}\right)}{\sqrt{\delta^2+s'^2}}ds'\right]. \tag{7-14}$$

Using the results of equations (4-28) and (4-29), then (7-14) becomes

$$E_{y_1}^{t}(\bar{\rho}^{-}) = \frac{2Z_0 Z_1}{Z_0+Z_1} H_0 e^{ik_1|\delta|} . \tag{7-15}$$

On comparing equation (7-15) with (5-22), it is evident that the infinite integrals of equation (7-10) yield the transmitted electric field intensity when $\bar{\rho}$ is below the half-space. If $\bar{\rho}$ is above the half-space, (7-14) becomes

$$E_{y_1}^{t}(\bar{\rho}^{+}) = \frac{Z_0 Z_1 H_0 k_1}{2(Z_0+Z_1)}\left[\int_{-\infty}^{\infty} H_0^{(1)}(k_1\sqrt{\delta^2+s'^2})\,ds' - i\delta\int_{-\infty}^{\infty}\frac{H_1^{(1)}(k_1\sqrt{\delta^2+s'^2})}{\sqrt{\delta^2+s'^2}}\,ds'\right] . \tag{7-16}$$

Introducing the results of equations (4-28) and (4-29) into (7-16), it is found that $E_{y1}^{t}(\bar{\rho}^{+})$ is zero.

A similar analysis can be followed for $\vec{H}_{tr}^{t}(\bar{\rho})$ in region 1 beginning with equation (2-74), or by computing $\vec{H}$ from (7-12) using Maxwell's equations. It would be found that

$$\vec{H}_{t_1}^{t}(\bar{\rho}) = \left\{ \begin{matrix} 0(\bar{\rho}^{+}) \\ \vec{H}_{t}^{trans}(\bar{\rho}^{0,-}) \end{matrix} \right\} + \vec{I}_H(k_1,\bar{\rho},\bar{\rho}') - \frac{ik_1}{4}\int_{-a-s_i}^{a-s_i} K_y'(\bar{\rho}')\vec{F}_1(k_1,\bar{\rho},\bar{\rho}')\,ds' + \frac{k_1}{4Z_1}\int_{-a-s_i}^{a-s_i} M_s'(\bar{\rho}')\vec{F}_3(k_1,\bar{\rho},\bar{\rho}')\,ds' , \tag{7-17}$$

where $0(\bar{\rho}^{+})$ designates that this term is to be set equal to zero when the point of observation is above the half-space, $H_{tr}^{trans}(\bar{\rho}^{0,-})$ is the transverse magnetic field intensity transmitted by a flat half-space and is to be used when the point

of observation is below or on the half-space, $\vec{\bar{F}}_1(k_1, \bar{\rho}, \bar{\rho}')$ and $\vec{\bar{F}}_3(k_1, \bar{\rho}, \bar{\rho}')$ are given by equations (7-3), and $\vec{\bar{I}}_H(k_1, \bar{\rho}, \bar{\rho}')$ is given by equation (7-7).

When a cylinder is present in the ground, equations (7-12) and (7-17) must include a contour integral around the cylinder boundary. Thus, in the present problem, (7-12) and (7-17) can be rewritten as

$$E_{y_1}^{t}(\bar{\rho}) = \begin{Bmatrix} 0(\bar{\rho}^{+}) \\ E_y^{trans}(\bar{\rho}^{0,-}) \end{Bmatrix} - \bar{I}_E(k_1, \bar{\rho}, \bar{\rho}')$$

$$+ \frac{\mu_1 \omega}{4} \int_{-a-s_i}^{a-s_i} K_y^1(\bar{\rho}') H_0^{(1)}(k_1|\bar{\rho}-\bar{\rho}'|)\, ds' - \frac{ik_1}{4} \int_{-a-s_i}^{a-s_i} M_s^1(\bar{\rho}') \cos(\beta-\alpha) H_1^{(1)}(k_1|\bar{\rho}-\bar{\rho}'|)\, ds' \tag{7-18}$$

$$- \frac{\mu_1 \omega}{4} \int_{C_2} K_y^2(\bar{\rho}') H_0^{(1)}(k_1|\bar{\rho}-\bar{\rho}'|)\, ds' + \frac{ik_1}{4} \int_{C_2} M_s^2(\bar{\rho}') \cos(\beta-\alpha) H_1^{(1)}(k_1|\bar{\rho}-\bar{\rho}'|)\, ds',$$

and

$$\vec{\bar{H}}_{tan_1}^{t}(\bar{\rho}) = \begin{Bmatrix} 0(\bar{\rho}^{+}) \\ \vec{\bar{H}}_{tan}^{trans}(\bar{\rho}^{0,-}) \end{Bmatrix} + \vec{\bar{I}}_H(k_1, \bar{\rho}, \bar{\rho}')$$

$$- \frac{ik_1}{4} \int_{-a-s_i}^{a-s_i} K_y^1(\bar{\rho}') \vec{\bar{F}}_1(k_1, \bar{\rho}, \bar{\rho}')\, ds' + \frac{k_1}{4Z_1} \int_{-a-s_i}^{a-s_i} M_s^1(\bar{\rho}') \vec{\bar{F}}_3(k_1, \bar{\rho}, \bar{\rho}')\, ds' \tag{7-19}$$

$$+ \frac{ik_1}{4} \int_{C_2} K_y^2(\bar{\rho}') \vec{\bar{F}}_1(k_1, \bar{\rho}, \bar{\rho}')\, ds' - \frac{k_1}{4Z_1} \int_{C_2} M_s^2(\bar{\rho}') \vec{\bar{F}}_3(k_1, \bar{\rho}, \bar{\rho}')\, ds'.$$

The parameters of the half-space have been referred to by the subscript 1 and the equivalent surface current densities on contour 2 have been superscripted 2 (see Fig. 71).

It should be noted that the integral representations for an interior region, equations (2-72) through (2-75), were derived assuming that the normals on the contour are into the interior region. Since the normal

on C_2 has been chosen as into the inhomogeneity in Fig. 71, the opposite sign to that of equations (2-72) and (2-74) has been taken for all integrals in region 1 around C_2.

Finally, the integral representations for $\vec{E}$ and $\vec{H}$ in region 2 follow directly from equations (2-72) and (2-74). Assuming normal incidence of an E_y-polarized field, it is found that

$$E_{y_2}^{+}(\bar{\rho}) = \frac{\mu_2 \omega}{4}\int_{C_2} K_y^2(\bar{\rho}')\, H_0^{(1)}(k_2|\bar{\rho}-\bar{\rho}'|)\, ds' + \frac{ik_2}{4}\int_{C_2} M_s^2(\bar{\rho}')\cos(\beta-\alpha)\, H_1^{(1)}(k_2|\bar{\rho}-\bar{\rho}'|)\, ds', \quad (7\text{-}20)$$

and

$$\vec{H}_{t_2}^{+}(\bar{\rho}) = -\frac{ik_2}{4}\int_{C_2} K_y^2(\bar{\rho}')\,\vec{F}_1(k_2,\bar{\rho},\bar{\rho}')\, ds' + \frac{k_2}{4Z_2}\int_{C_2} M_s^2(\bar{\rho}')\,\vec{F}_3(k_2,\bar{\rho},\bar{\rho}')\, ds', \quad (7\text{-}21)$$

where $\vec{F}_1(k_2,\bar{\rho},\bar{\rho}')$ and $\vec{F}_3(k_2,\bar{\rho},\bar{\rho}')$ are given by equation (7-3), and the parameters of the inhomogeneity have been referred to by the subscript 2.

The unknown current components $K_y(\bar{\rho})$ and $M_s(\bar{\rho})$ on contours 1 and 2 are obtained by enforcing the boundary conditions on tangential $\vec{E}$ and $\vec{H}$ and solving the resulting integral equations. We have from equations (2-53) that the tangential unit vector $\hat{s}$ is given by

$$\hat{s} = -\sin\alpha_i\,\hat{x} + \cos\alpha_i\,\hat{z}, \quad (7\text{-}22)$$

where α_i is the normal at the boundary point.

Thus, the tangential component of $\vec{H}_{tr}^{t}$ in each region is found by taking the dot product of (7-10) with equations (7-5), (7-17) and (7-19). It is found that

$$\bar{H}^{t}_{s_0}(\bar{\rho}) = \hat{s}\cdot\bar{H}^{i}_{t_0}(\bar{\rho}) + \begin{Bmatrix} \hat{s}\cdot\bar{H}^{reflec}_{t_0}(\bar{\rho}^{\,0,+}) \\ -\hat{s}\cdot\bar{H}^{i}_{t_0}(\bar{\rho}^{\,-}) \end{Bmatrix} - \hat{s}\cdot\bar{\bar{I}}_{H}(k_0,\bar{\rho},\bar{\rho}')$$

$$+ \frac{ik_0}{4}\int_{-a-s_i}^{a-s_i} K^{i}_{y}(\bar{\rho}')\,G_1(k_0,\bar{\rho},\bar{\rho}')\,ds' - \frac{k_0}{4Z_0}\int_{-a-s_i}^{a-s_i} M^{i}_{s}(\bar{\rho}')\,G_3(k_0,\bar{\rho},\bar{\rho}')\,ds' , \tag{7-23}$$

$$\bar{H}^{t}_{s_1}(\bar{\rho}) = \begin{Bmatrix} 0(\bar{\rho}^{+}) \\ \hat{s}\cdot\bar{H}^{trans}_{t_1}(\bar{\rho}^{\,0,-}) \end{Bmatrix} + \hat{s}\cdot\bar{\bar{I}}_{H}(k_1,\bar{\rho},\bar{\rho}')$$

$$- \frac{ik_1}{4}\int_{-a-s_i}^{a-s_i} K^{i}_{y}(\bar{\rho}')\,G_1(k_1,\bar{\rho},\bar{\rho}')\,ds' + \frac{k_1}{4Z_1}\int_{-a-s_i}^{a-s_i} M^{i}_{s}(\bar{\rho}')\,G_3(k_1,\bar{\rho},\bar{\rho}')\,ds' \tag{7-24}$$

$$+ \frac{ik_1}{4}\int_{C_2} K^{2}_{y}(\bar{\rho}')\,G_1(k_1,\bar{\rho},\bar{\rho}')\,ds' - \frac{k_1}{4Z_1}\int_{C_2} M^{2}_{s}(\bar{\rho}')\,G_3(k_1,\bar{\rho},\bar{\rho}')\,ds' ,$$

and

$$\bar{H}^{t}_{s_2}(\bar{\rho}) = -\frac{ik_2}{4}\int_{C_2} K^{2}_{y}(\bar{\rho}')\,G_1(k_2,\bar{\rho},\bar{\rho}')\,ds' + \frac{k_2}{4Z_2}\int_{C_2} M^{2}_{s}(\bar{\rho}')\,G_3(k_2,\bar{\rho},\bar{\rho}')\,ds' , \tag{7-25}$$

where

$$G(k,\bar{\rho},\bar{\rho}') = \hat{s}\cdot\bar{\bar{F}}(k,\bar{\rho},\bar{\rho}') \tag{7-26a}$$

$$G_1(k,\bar{\rho},\bar{\rho}') = -H_1^{(1)}(k|\bar{\rho}-\bar{\rho}'|)\cos(\beta-\alpha_i) \tag{7-26b}$$

$$G_3(k,\bar{\rho},\bar{\rho}') = -\cos(\beta-\alpha)\cos(\beta-\alpha_i)\,H_0^{(1)}(k|\bar{\rho}-\bar{\rho}'|) \tag{7-26c}$$

$$+ \frac{H_1^{(1)}(k|\bar{\rho}-\bar{\rho}'|)}{k|\bar{\rho}-\bar{\rho}'|}\cos(2\beta-\alpha-\alpha_i) ,$$

and

$$\hat{s}\cdot\bar{\bar{I}}_{H}(k,\bar{\rho},\bar{\rho}') = \frac{ik}{4}\int_{-a-s_i}^{a-s_i} K^{i}_{y}(\bar{\rho}')\,G_1(k,\bar{\rho},\bar{\rho}')\,ds' - \frac{k}{4Z}\int_{-a-s_i}^{a-s_i} M^{i}_{s}(\bar{\rho}')\,G_3(k,\bar{\rho},\bar{\rho}')\,ds' . \tag{7-27}$$

If we let the point of observation approach a boundary point on C_1 given by the position vector $\bar{\rho}''$ and equate tangential components of $\vec{E}$ and $\vec{H}$, it is found that

$$E_y^i(\bar{\rho}'') = \begin{Bmatrix} -E_y^{\text{reflec}}(\bar{\rho}''^{0,+}) \\ E_y^i(\bar{\rho}''^{-}) \end{Bmatrix} + \begin{Bmatrix} 0(\bar{\rho}''^{+}) \\ E_y^{\text{trans}}(\bar{\rho}''^{0,-}) \end{Bmatrix} - I_E(k_0,\bar{\rho}'',\bar{\rho}') - I_E(k_1,\bar{\rho}'',\bar{\rho}')$$

$$+ \frac{\mu_0\omega}{4}\int_{-a-s_i}^{a-s_i} K_y'(\bar{\rho}')\left[H_0^{(1)}(k_0|\bar{\rho}''-\bar{\rho}'|) + \frac{\mu_1}{\mu_0}H_0^{(1)}(k_1|\bar{\rho}''-\bar{\rho}'|)\right]ds' \qquad (7\text{-}28)$$

$$- \frac{i}{4}\int_{-a-s_i}^{a-s_i} M_s'(\bar{\rho}')\cos(\beta''-\alpha)\left[k_0 H_1^{(1)}(k_0|\bar{\rho}''-\bar{\rho}'|) + k_1 H_1^{(1)}(k_1|\bar{\rho}''-\bar{\rho}'|)\right]ds'$$

$$- \frac{\mu_1\omega}{4}\int_{C_2} K_y^2(\bar{\rho}')H_0^{(1)}(k_1|\bar{\rho}''-\bar{\rho}'|)ds' + \frac{ik_1}{4}\int_{C_2} M_s^2(\bar{\rho}')\cos(\beta''-\alpha)H_1^{(1)}(k_1|\bar{\rho}''-\bar{\rho}'|)ds',$$

and

$$\hat{s}\cdot\vec{H}_{t_1}^{\,i}(\bar{\rho}'') = \begin{Bmatrix} -\hat{s}\cdot\vec{H}_{t_1}^{\,\text{reflec}}(\bar{\rho}''^{0,+}) \\ \hat{s}\cdot\vec{H}_{t_1}^{\,i}(\bar{\rho}''^{+}) \end{Bmatrix} + \begin{Bmatrix} 0(\bar{\rho}''^{+}) \\ \hat{s}\cdot\vec{H}_{t_1}^{\,\text{trans}}(\bar{\rho}''^{0,-}) \end{Bmatrix} + \hat{s}\cdot\vec{I}_H(k_0,\bar{\rho}'',\bar{\rho}')$$

$$+ \hat{s}\cdot\vec{I}_H(k_1,\bar{\rho}'',\bar{\rho}') + \frac{i}{4}\int_{-a-s_i}^{a-s_i} K_y'(\bar{\rho}')\cos(\beta''-\alpha_i)\left[k_0 H_1^{(1)}(k_0|\bar{\rho}-\bar{\rho}'|) + k_1 H_1^{(1)}(k_1|\bar{\rho}''-\bar{\rho}'|)\right]ds'$$

$$- \frac{1}{4}\int_{-a-s_i}^{a-s_i} M_s'(\bar{\rho}')\cos(\beta''-\alpha)\cos(\beta''-\alpha_i)\left[\frac{k_0}{Z_0}H_0^{(1)}(k_0|\bar{\rho}''-\bar{\rho}'|) + \frac{k_1}{Z_1}H_0^{(1)}(k_1|\bar{\rho}''-\bar{\rho}'|)\right]ds' \qquad (7\text{-}29)$$

$$+ \frac{1}{4}\int_{-a-s_i}^{a-s_i} M_s'(\bar{\rho}')\cos(2\beta''-\alpha-\alpha_i)\left[\frac{H_1^{(1)}(k_0|\bar{\rho}''-\bar{\rho}'|)}{Z_0|\bar{\rho}''-\bar{\rho}'|} + \frac{H_1^{(1)}(k_1|\bar{\rho}''-\bar{\rho}'|)}{Z_1|\bar{\rho}''-\bar{\rho}'|}\right]ds'$$

$$- \frac{ik_1}{4}\int_{C_1} K_y^2(\bar{\rho}')\cos(\beta''-\alpha_i)H_1^{(1)}(k_1|\bar{\rho}''-\bar{\rho}'|)ds' + \frac{k_1}{4Z_1}\int_{C_2} M_s^2(\bar{\rho}')\cos(\beta''-\alpha)\cos(\beta''-\alpha_i)H_0^{(1)}(k_1|\bar{\rho}''-\bar{\rho}'|)ds'$$

$$- \frac{k_1}{4Z_1}\int_{C_1} M_s^2(\bar{\rho}')\cos(2\beta''-\alpha-\alpha_i)\frac{H_1^{(1)}(k_1|\bar{\rho}''-\bar{\rho}'|)}{k_1|\bar{\rho}''-\bar{\rho}'|}ds'.$$

Similarly, if we let the point of observation approach a boundary point on C_2 given by the position vector $\bar{\rho}'''$ and equate tangential components of $\vec{E}$ and $\vec{H}$, it is found that

$$0 = \begin{Bmatrix} 0(\bar{\rho}''' +) \\ -E_y^{trans}(\bar{\rho}''' 0,-) \end{Bmatrix} + I_E(k_1, \bar{\rho}''', \bar{\rho}') - \frac{\mu_1 \omega}{4} \int_{-a-s_i}^{a-s_i} K_y^1(\bar{\rho}') H_0^{(1)}(k_1|\bar{\rho}''' - \bar{\rho}'|) ds'$$

$$+ \frac{ik_1}{4} \int_{-a-s_i}^{a-s_i} M_S^1(\bar{\rho}') \cos(\beta''' - \alpha) H_1^{(1)}(k_1|\bar{\rho}''' - \bar{\rho}'|) ds'$$

$$+ \frac{\mu_1 \omega}{4} \int_{C_2} K_y^2(\bar{\rho}') \left[H_0^{(1)}(k_1|\bar{\rho}''' - \bar{\rho}'|) + \frac{\mu_2}{\mu_1} H_0^{(1)}(k_2|\bar{\rho}''' - \bar{\rho}'|) \right] ds' \qquad (7\text{-}30)$$

$$- \frac{i}{4} \int_{C_2} M_S^2(\bar{\rho}') \cos(\beta''' - \alpha) \left[k_1 H_1^{(1)}(k_1|\bar{\rho}''' - \bar{\rho}'|) + k_2 H_1^{(1)}(k_2|\bar{\rho}''' - \bar{\rho}'|) \right] ds' ,$$

and

$$0 = \begin{Bmatrix} 0(\bar{\rho}''' +) \\ -\hat{s} \cdot \vec{H}_{th}^{trans}(\bar{\rho}''' 0,-) \end{Bmatrix} - \hat{s} \cdot \vec{I}_H(k_1, \bar{\rho}''', \bar{\rho}') - \frac{ik_1}{4} \int_{-a-s_i}^{a-s_i} K_y^1(\bar{\rho}') \cos(\beta''' - \alpha_i) H_1^{(1)}(k_1|\bar{\rho}''' - \bar{\rho}'|) ds'$$

$$+ \frac{k_1}{4Z_1} \int_{-a-s_i}^{a-s_i} M_S^1(\bar{\rho}') \cos(\beta''' - \alpha) \cos(\beta''' - \alpha_i) H_0^{(1)}(k_1|\bar{\rho}''' - \bar{\rho}'|) ds'$$

$$- \frac{k_1}{4Z_1} \int_{-a-s_i}^{a-s_i} M_S^1(\bar{\rho}') \cos(2\beta''' - \alpha - \alpha_i) \frac{H_1^{(1)}(k_1|\bar{\rho}''' - \bar{\rho}'|)}{k_1|\bar{\rho}''' - \bar{\rho}'|} ds' \qquad (7\text{-}31)$$

$$+ \frac{i}{4} \int_{C_2} K_y^2(\bar{\rho}') \cos(\beta''' - \alpha_i) \left[k_1 H_1^{(1)}(k_1|\bar{\rho}''' - \bar{\rho}'|) + k_2 H_1^{(1)}(k_2|\bar{\rho}''' - \bar{\rho}'|) \right] ds'$$

$$- \frac{1}{4} \int_{C_2} M_S^2(\bar{\rho}') \cos(\beta''' - \alpha) \cos(\beta''' - \alpha_i) \left[\frac{k_1}{Z_1} H_0^{(1)}(k_1|\bar{\rho}''' - \bar{\rho}'|) + \frac{k_2}{Z_2} H_0^{(1)}(k_2|\bar{\rho}''' - \bar{\rho}'|) \right] ds'$$

$$+ \frac{1}{4} \int_{C_2} M_S^2(\bar{\rho}') \cos(2\beta''' - \alpha - \alpha_i) \left[\frac{H_1^{(1)}(k_1|\bar{\rho}''' - \bar{\rho}'|)}{Z_1|\bar{\rho}''' - \bar{\rho}'|} + \frac{H_1^{(1)}(k_2|\bar{\rho}''' - \bar{\rho}'|)}{Z_2|\bar{\rho}''' - \bar{\rho}'|} \right] ds' .$$

Equations (7-28) through (7-31) are the desired coupled integral equations with two unknown current components $K_y(\tilde{\rho})$ and $M_s(\tilde{\rho})$. They are solved as in Chapter 5 by dividing (-a, a) and C_2 into a total of N sampled values of each unknown current component. When this is done, the integral equations reduce to a system of linear equations of the form

$$\begin{aligned}
(E_y)' &= (A_{11}^1)(K_y^1) + (B_{11}^1)(K_y^2) + (A_{12}^1)(M_s^1) + (B_{12}^1)(M_s^2), \\
(H_s)' &= (A_{21}^1)(K_y^1) + (B_{21}^1)(K_y^2) + (A_{22}^1)(M_s^1) + (B_{22}^1)(M_s^2), \\
(0)' &= (A_{11}^2)(K_y^1) + (B_{11}^2)(K_y^2) + (A_{12}^2)(M_s^1) + (B_{12}^2)(M_s^2), \\
(0)' &= (A_{21}^2)(K_y^1) + (B_{21}^2)(K_y^2) + (A_{22}^2)(M_s^1) + (B_{22}^2)(M_s^2).
\end{aligned} \tag{7-32}$$

The superscript on A_{ij}, B_{ij} refers to the boundary upon which the boundary condition is being enforced when each matrix is determined. The primes on (E_y), (H_s) and (0) indicate that these column matrices are modified due to the contour integrals involving (K_s^i, M_s^1) on contour C_1.

Equations (7-32) can be rearranged into a system of 2N linear equations of the form of equations (5-47). It is found that

$$\begin{pmatrix} E_y \\ 0 \end{pmatrix}' = \begin{pmatrix} A_{11}^1 & B_{11}^1 \\ A_{11}^2 & B_{11}^2 \end{pmatrix} \begin{pmatrix} K_y^1 \\ K_y^2 \end{pmatrix} + \begin{pmatrix} A_{12}^1 & B_{12}^1 \\ A_{12}^2 & B_{12}^2 \end{pmatrix} \begin{pmatrix} M_s^1 \\ M_s^2 \end{pmatrix}, \tag{7-33a}$$

$$\begin{pmatrix} H_s \\ 0 \end{pmatrix}' = \begin{pmatrix} A_{21}^1 & B_{21}^1 \\ A_{21}^2 & B_{21}^2 \end{pmatrix} \begin{pmatrix} K_y^1 \\ K_y^2 \end{pmatrix} + \begin{pmatrix} A_{22}^1 & B_{22}^1 \\ A_{22}^2 & B_{22}^2 \end{pmatrix} \begin{pmatrix} M_s^1 \\ M_s^2 \end{pmatrix}. \tag{7-33b}$$

Equations (7-33) are solved in exactly the same manner as equations (5-47). Their solution is given by equations (5-48) by treating each partitioned matrix (A_{ij}, B_{ij}) as C_{ij}.

Once $K_y(\tilde{\rho})$ and $M_s(\tilde{\rho})$ have been estimated from equations (7-28)

through (7-31), the total or scattered magnetic field intensity is calculated from equation (7-5), (7-17) or (7-19), depending upon which region the field is desired. Exterior to the half-space, the scattered magnetic field is given by

$$\vec{H}^{sc}_{t_0}(\bar{\rho}) = \left\{ \begin{array}{l} \vec{H}^{reflec}_{t}(\bar{\rho}\,0,+) \\ -\vec{H}^{i}_{t}(\bar{\rho}^{-}) \end{array} \right\} - \vec{I}_H(k_0,\bar{\rho},\bar{\rho}')$$

$$- \frac{ik_0}{4}\int_{-a-s_i}^{a-s_i} K_y'(\bar{\rho}')\,H_1^{(1)}(k_0|\bar{\rho}-\bar{\rho}'|)(\sin\beta\,\hat{x} - \cos\beta\,\hat{z})\,ds' \qquad (7\text{-}34)$$

$$- \frac{k_0}{4Z_0}\int_{-a-s_i}^{a-s_i} M_s'(\bar{\rho}')\cos(\beta-\alpha)\,H_0^{(1)}(k_0|\bar{\rho}-\bar{\rho}'|)(\sin\beta\,\hat{x} - \cos\beta\,\hat{z})\,ds'$$

$$+ \frac{k_0}{4Z_0}\int_{-a-s_i}^{a-s_i} M_s'(\bar{\rho}')\,\frac{H_1^{(1)}(k_0|\bar{\rho}-\bar{\rho}'|)}{k_0|\bar{\rho}-\bar{\rho}'|}(\sin(2\beta-\alpha)\hat{x} - \cos(2\beta-\alpha)\hat{z})\,ds'$$

where $\vec{I}_H(k_0,\bar{\rho},\bar{\rho}')$ is given by equation (7-7).

It should be noted that as in Chapters 3, 4 and 5, it is necessary for integration accuracy to make a small argument approximation to the Hankel functions whenever $|k||\bar{\rho}-\bar{\rho}'|<.5$ and integrate the resulting expressions analytically. However, since the integral representations of this chapter are the same as those of Chapter 5, this problem has been discussed previously in section (5-1) (equations (5-30) through (5-33)). Similarly, integration through the point of singularity has been examined in section (5-2).

It is interesting to note that equations (7-30) and (7-31) reduce to (5-20) and (5-21), the integral equations for scattering from cylinders in a conductive whole-space, if we assume that the earth-air interface is horizontal and ignore coupling* between the cylinder and the interface.

* The term coupling will be used to describe the electromagnetic interaction between the cylinder and half-space contours which modifies the equivalent surface current densities on the cylinder surface from their whole-space value.

In this case, $K'_y(\bar{\rho})$ and $M'_s(\bar{\rho})$ arise from the incident field alone and, as a result, (-a, a) can be set equal to (-0., 0.). Thus, equations (7-30) and (7-31) reduce to

$$\begin{Bmatrix} 0(\bar{\rho}^+) \\ E_y^{trans}(\bar{\rho}^-, 0) \end{Bmatrix} = \frac{\mu_1 \omega}{4} \int_{C_2} K_y^2(\bar{\rho}') \left[H_0^{(1)}(k_1|\bar{\rho}''' - \bar{\rho}'|) + \frac{\mu_2}{\mu_1} H_0^{(1)}(k_2|\bar{\rho}''' - \bar{\rho}'|) \right] ds' \tag{7-35}$$

$$- \frac{i}{4} \int_{C_2} M_s^2(\bar{\rho}') \cos(\beta''' - \alpha) \left[k_1 H_1^{(1)}(k_1|\bar{\rho}''' - \bar{\rho}'|) + k_2 H_1^{(1)}(k_2|\bar{\rho}''' - \bar{\rho}'|) \right] ds',$$

and

$$\begin{Bmatrix} 0(\bar{\rho}^+) \\ \hat{z} \cdot H_{trans}(\bar{\rho}^-, 0) \end{Bmatrix} = \frac{i}{4} \int_{C_2} K_y^2(\bar{\rho}') \cos(\beta''' - \alpha_i) \left[k_1 H_1^{(1)}(k_1|\bar{\rho}''' - \bar{\rho}'|) + k_2 H_1^{(1)}(k_2|\bar{\rho}''' - \bar{\rho}'|) \right] ds'$$

$$- \frac{1}{4} \int_{C_2} M_s^2(\bar{\rho}') \cos(\beta''' - \alpha) \cos(\beta''' - \alpha_i) \left[\frac{k_1}{Z_1} H_0^{(1)}(k_1|\bar{\rho}''' - \bar{\rho}'|) + \frac{k_2}{Z_2} H_0^{(1)}(k_2|\bar{\rho}''' - \bar{\rho}'|) \right] ds' \tag{7-36}$$

$$+ \frac{1}{4} \int_{C_2} M_s^2(\bar{\rho}') \cos(2\beta''' - \alpha - \alpha_i) \left[\frac{H_1^{(1)}(k_1|\bar{\rho}''' - \bar{\rho}'|)}{Z_1|\bar{\rho}''' - \bar{\rho}'|} + \frac{H_1^{(1)}(k_2|\bar{\rho}''' - \bar{\rho}'|)}{Z_2|\bar{\rho}''' - \bar{\rho}'|} \right] ds'.$$

Assuming that the cylinder is below the half-space, it is evident on comparing equations (7-35) and (7-36) with (5-20) and (5-21) that these are the same integral equations as derived to examine scattering from cylinders in a conductive whole space. In (7-35) and (7-36), the incident field is the field transmitted into a flat, homogeneous half-space.

7-2 Numerical Examples

(7-31)

Equations (7-28), (7-29), (7-30), and (7-34) were programmed assuming that the incident field is an E_y-polarized plane wave incident normal to

a conductive half-space. In this case, K_y^i and M_s^i are constant and given by (7-13). Furthermore, the integrals I_E and $\overline{\overline{I}}_H$ reduce to expressions which are similar to equations (4-39) and (4-48). Thus, we can rewrite (7-4) and (7-5) as

$$I_E(k,\bar{\rho},\bar{\rho}') = \frac{\mu\omega}{4} K_y^i \int_{-a-s_i}^{a-s_i} H_0^{(1)}\left(k\sqrt{\delta^2+s'^2}\right) ds' + \frac{ik\delta}{4} M_s^i \int_{-a-s_i}^{a-s_i} \frac{H_1^{(1)}\left(k\sqrt{\delta^2+s'^2}\right)}{\sqrt{\delta^2+s'^2}} ds', \quad (7\text{-}37)$$

and

$$\overline{\overline{I}}_H(k,\bar{\rho},\bar{\rho}') = \frac{ik}{4} K_y^i \left(\delta I_1 \hat{x} + I_2 \hat{z}\right) + \frac{kM_s^i}{4z}\left[\left(\delta^2 I_5 - \frac{\delta^2 I_9 - I_{11}}{k}\right)\hat{x} + \delta\left(I_6 - \frac{2I_{10}}{k}\right)\hat{z}\right], \quad (7\text{-}38)$$

where I_1, I_2, I_5, I_6, I_{10} and I_{11} are given by equations (3-63a), (3-63b), (4-13a), (4-13b), (4-14a), (4-14b) and (4-14c) respectively, with $a = -a-s_i$ and $b = a-s_i$.

When the point of observation ($\bar{\rho}$) is on the half-space, a limiting process similar to integrating through the singular interval (section 5-2) must be taken before (7-37) and (7-38) can be evaluated. Noting that this limit is taken from opposite sides of the interface in each region, it is found that for points of observation in air, equations (7-37) and (7-38) reduce to

$$I_E(k_0,\bar{\rho},\bar{\rho}') = \frac{\mu_0\omega}{4} K_y^i \lim_{\delta\to 0}\left\{HK_{00}\right\} + \frac{M_s^i}{2}, \quad (7\text{-}39a)$$

and

$$\vec{I}_H(k_0,\bar{\rho},\bar{\rho}') = K_y^i\left(\frac{1}{2}\hat{x} + \frac{ik_0}{4}\left\{\lim_{\delta\to 0} I_2\right\}\hat{z}\right) - \frac{M_s^i}{4z_0}\lim_{\delta\to 0}\left\{\delta^2 I_q - I_{11}\right\}\hat{x} \qquad (7\text{-}39b)$$

Similarly, for points of observation in the ground,

$$\vec{I}_E(k_1,\bar{\rho},\bar{\rho}') = \frac{\mu_1\omega}{4} K_y^i \lim_{\delta\to 0}\left\{HK00\right\} - \frac{M_s^i}{2}, \qquad (7\text{-}40a)$$

and

$$\vec{I}_H(k_1,\bar{\rho},\bar{\rho}') = K_y^i\left(-\frac{1}{2}\hat{x} + \frac{ik_1}{4}\left\{\lim_{\delta\to 0} I_2\right\}\hat{z}\right) - \frac{M_s^i}{4z_1}\lim_{\delta\to 0}\left\{\delta^2 I_q - I_{11}\right\}\hat{x}. \qquad (7\text{-}40b)$$

If follows from section (5-2) and Appendix D that

$$\lim_{\delta\to 0}\left\{HK00\right\} = \lim_{\delta\to 0}\int_{-\varepsilon_\ell}^{\varepsilon_u} H_0^{(1)}\left(k\sqrt{\delta^2+s'^2}\right)ds' + \int_{-a-s_i}^{-\varepsilon_\ell} H_0^{(1)}(k|s'|)ds' + \int_{\varepsilon_u}^{a-s_i} H_0^{(1)}(ks')ds',$$

$$= (\varepsilon_u-\varepsilon_\ell) - \frac{k^2}{12}(\varepsilon_u^3-\varepsilon_\ell^3) + \frac{ik^2}{6\pi}(\varepsilon_u^3-\varepsilon_\ell^3) + \frac{2i}{\pi}\left\{\varepsilon_u\left(1-\frac{k^2\varepsilon_u^2}{12}\right)\ln\frac{\gamma k\varepsilon_u}{2}\right.$$

$$\left. - \varepsilon_\ell\left(1-\frac{k^2\varepsilon_\ell^2}{12}\right)\ln\frac{\gamma k|\varepsilon_\ell|}{2} + \frac{k^2}{36}(\varepsilon_u^3-\varepsilon_\ell^3) - (\varepsilon_u-\varepsilon_\ell)\right\} \qquad (7\text{-}41)$$

$$+ \int_{-a-s_i}^{-\varepsilon_\ell} H_0^{(1)}(k|s'|)ds' + \int_{\varepsilon_u}^{a-s_i} H_0^{(1)}(ks')ds',$$

where

$$\left\{\begin{matrix}\varepsilon_u\\ \varepsilon_\ell\end{matrix}\right\} = \pm\frac{.5}{|k|}.$$

Equation (7-41) states that HK00 is approximated analytically over $(-\varepsilon_\ell,\varepsilon_u)$ by taking the limit as $\delta\longrightarrow 0$ of the small argument solution given

in Appendix D, and numerically over the intervals $(-a-s_i\ ,\ -\varepsilon_\ell\ )$ and $(\varepsilon_u\ ,\ a-s_i)$. The subscripts on ε imply that if $\varepsilon_\ell > |-a-s_i|$ or $\varepsilon_u > (a-s_i)$, $-\varepsilon_\ell$ or ε_u is to be replaced by $-a-s_i$ or $a-s_i$ respectively, and the first or second integral of (7-41) ignored.

It is shown in Appendix D that I_2 can be evaluated analytically, and it is found that

$$\lim_{\delta\to 0}\ (I_2) = \lim_{\delta\to 0}\int_{-a-s_i}^{a-s_i} \frac{s' H_1^{(1)}\left(k\sqrt{\delta^2+s'^2}\right)}{\sqrt{\delta^2+s'^2}}\,ds'$$

$$= \frac{1}{k}\left[H_0^{(1)}(k|-a-s_i|) - H_0^{(1)}(k|a-s_i|)\right]. \tag{7-42}$$

Finally, it follows from section (5-2) and Appendix D that

$$\lim_{\delta\to 0}\ \left(\delta^2 I_9 - I_{11}\right) = \lim_{\delta\to 0}\left\{\delta^2\int_{-a-s_i}^{a-s_i}\frac{H_1^{(1)}\left(k\sqrt{\delta^2+s'^2}\right)ds'}{(\delta^2+s'^2)^{3/2}} - \int_{-a-s_i}^{a-s_i}\frac{s'^2 H_1^{(1)}\left(k\sqrt{\delta^2+s'^2}\right)ds'}{(\delta^2+s'^2)^{3/2}}\right\},$$

$$= -\frac{2i}{\pi k}\left(\frac{1}{\varepsilon_u} - \frac{1}{\varepsilon_\ell}\right) - \frac{k}{2}\left\{(\varepsilon_u-\varepsilon_\ell) - \frac{k^2}{24}\left(\varepsilon_u^3-\varepsilon_\ell^3\right)\right\}$$

$$-\frac{2i}{\pi}\left[\frac{1}{2}(\varepsilon_u-\varepsilon_\ell) - \frac{5k^2}{96}\left(\varepsilon_u^3-\varepsilon_\ell^3\right)\right] + \frac{2i}{\pi}\left[\varepsilon_u\left(1-\frac{k^2\varepsilon_u^2}{24}\right)\ln\frac{\gamma k}{2}|\varepsilon_u| \right. \tag{7-43}$$

$$\left. - \varepsilon_\ell\left(1-\frac{k^2\varepsilon_\ell^2}{24}\right)\ln\frac{\gamma k}{2}|\varepsilon_\ell| + \frac{k^2}{72}\left(\varepsilon_u^3-\varepsilon_\ell^3\right) - (\varepsilon_u-\varepsilon_\ell)\right]$$

$$- \int_{-a-s_i}^{-\varepsilon_\ell}\frac{H_1^{(1)}(k|s'|)}{|s'|}\,ds' - \int_{\varepsilon_u}^{a-s_i}\frac{H_1^{(1)}(ks')}{s'}\,ds'.$$

As in equation (7-41), $-\varepsilon_\ell$ or ε_u is to be replaced by $-a-s_i$ or $a-s_1$ respectively, if $\varepsilon_\ell > |-a-s_i|$ or $\varepsilon_u > (a-s_i)$ and the first or second integral of (7-43) ignored.

Assuming that the incident field is an E_y-polarized plane wave impinging normal to a conductive half-space, then

$$E_y^i(\bar{\rho}'') = Z_0 H_0 e^{-ik_0 z''} , \tag{7-44a}$$

and

$$\hat{s} \cdot \vec{H}_{tq}^{\,i}(\bar{\rho}'') = -\sin\alpha_i \, H_0 e^{-ik_0 z''} . \tag{7-44b}$$

The reflected field intensities are given by equations (4-24) and (4-25) as

$$E_y^{reflec}(\bar{\rho}'') = -Z_0 \frac{Z_0 - Z_1}{Z_0 + Z_1} H_0 e^{ik_0 z''} , \tag{7-45a}$$

and

$$\hat{s} \cdot \vec{H}_{tq}^{\,reflec}(\bar{\rho}'') = -\sin\alpha_i \frac{Z_0 - Z_1}{Z_0 + Z_1} H_0 e^{ik_0 z''} . \tag{7-45b}$$

Finally, the transmitted field intensities are given from equations (5-22) and (5-23) as

$$E_y^{trans}(\bar{\rho}''') = \frac{2 Z_1 Z_0}{Z_0 + Z_1} H_0 e^{-ik_1 z''} , \tag{7-46a}$$

and

$$\hat{s} \cdot \vec{H}_{tq}^{\,trans}(\bar{\rho}''') = -\frac{2\sin\alpha_i}{Z_0 + Z_1} Z_0 H_0 e^{-ik_1 z''} . \tag{7-46b}$$

It should be remembered, that equations (4-40) through (4-44) must be considered at the edges of the interval (-a, a) to ensure continuity of the unknown current distributions with K_y^i and M_s^i.

Figs. 72 through 79 demonstrate that the integral representations derived for scattering from cylinders in a conductive half-space are valid and that the solution converges rapidly for these electrical parameters as the sampling rate is increased. In Figs. 72 through 78, we have assumed that the conductivity of the air is equal to the conductivity of the half-space (10^{-3} mhos/m), so that the solution must reduce to the solution for scattering from circular cylinders in a conductive whole-space. It should be noted, however, that since the entire integral equation must be solved (i.e., no expressions in equations (7-28) through (7-31) reduce to zero when this assumption is made), such a test forms an accurate check on the formulation of the problem for scattering from cylinders in a conductive half-space.

In addition, we have assumed normal incidence of an E_y-polarized plane wave in Figs. 72 through 78 and that: the height Z_o of the point of observation above the half-space is 1 m, the depth Z_1, from the half-space to the top of the cylinder is 19 m, the cylinder radius is 100 m, the incident field frequency is 1000 hz, the conductivity σ_0 of air is 10^{-3} mhos/m, the conductivity σ_1 of the half-space is 10^{-3} mhos/m, and the conductivity σ_2 of the cylinder is 10^{-1} mhos/m.

Fig. 72 indicates that with these electrical parameters a contour section bounded by (-1000, + 1000) is sufficient to describe the unknown surface current densities. Fig. 73 shows that an error of less than 2% in the peak value of real (H_x) is achieved if the half-space profile is

sampled 20 times. It is seen also that a slight instability arises in the field, although the amplitude of the oscillations decreases as the sampling width on the topographic profile decreases.

As in the examples in Chapter 3, these oscillations arise from the inaccuracy of the numerical integration across intervals of the contour in close proximity to the point of observation. It was noted in section (4-3) that the integration inaccuracy is a result of the manner in which the program has been written since the small argument approximation is used only when $|kr| \leq Re$ for all points on an interval. As a result, it was found that the numerical integration was inaccurate across any interval in which part of the contour is greater than R_e while most of the contour is much less than R_e.

It was seen from Table 1 that for such an interval, solution accuracy could be increased by raising the number of sampling points within the interval (-a, a) or by increasing R_e. Note, however, that R_e cannot exceed the validity of the small argument expansion for the Hankel functions. Figs. 73 and 74 indicate that these oscillations are a result of integration inaccuracies since their magnitude is quite dependent upon the sampling rate (Fig. 73) and the value of R_e (Fig. 74).

To overcome this problem, the program should be rewritten so that both the small argument approximation and Simpson's rule can be used in integrating whenever R_e falls within an interval. Since these oscillations amount to less that 1% of the total field with an R_e of .5 and careful sampling, the present program has not been changed. However, before a general analysis of scattering problems is undertaken, this change should be made to avoid an unrecognized error.

Fig. 75 shows that by sampling the topographic contour 29 times and the cylinder contour 30 times, an overall error less than 2% of the peak value of H_x has been achieved for the horizontal magnetic field intensity. Similarly, Fig. 76 shows that with the exception of several discrete points, an error of less than 2% of the peak value of H_z has been achieved for the vertical magnetic field intensity as well.

The discontinuities in H_z are observed only when the point of observation is near the contour and directly over the edge of two intervals. In this case, the contribution to the fields comes mainly from that part of the contour in the immediate vicinity of the point of observation. As a result, the discontinuity in the parabolic fit to the current density (see Fig. 7) predominates and a poor estimate of the scattered field is obtained.

Further observations which point to the break in the current density as the origin of these discontinuities in H_z are:

1) The magnitude of the error in H_z decreases (Fig. 76) as the parabolic fit to the surface current density improves (i.e., as the number of sampled values on the topographic contour increases).
2) The magnitude of the error is larger for points of observations near the cylinder (i.e., the parabolic fit is least satisfactory in those regions of the contour where the field intensities vary most rapidly).

Thus, the discontinuities in H_z are predictable and can be excluded from the smooth profile of H_z whenever they occur.

Figs. 77 and 78 show that when the topographic profile has been

sampled 29 times and the cylinder contour 30 times, an error of less than 1% has been obtained in estimating K_y while an error of less than 6% has been obtained in estimating M_s. However, since the peak value of M_s is about 1/3 the peak value of K_y, this decreased accuracy in estimating M_s is not surprising.

Figs. 72 through 78 have demonstrated that the formulation of the problem of scattering from cylinders in a conductive half-space reduces to that for scattering from cylinders in a conductive whole-space if the conductivity of the air is set equal to the conductivity of the ground. A second check on the formulation of the problem and the program is to set the conductivity of the cylinder equal to the conductivity of the ground. In this case, the solution must reduce to the solution for plane wave reflection from a homogeneous half-space.

Fig. 79 shows that the solution does reduce to that for reflection from a homogeneous half-space. In this example, we have assumed normal incidence of an E_y-polarized plane wave and that: the height Z_0 of the point of observation above the half-space is 1 m, the depth Z_1 from the half-space to the top of the cylinder is 20 m, the cylinder radius is 100 m, the incident field frequency is 1000 hz, the conductivity σ_0 of air is 0., the conductivity σ_1 of the half-space is 10^{-3} mhos/m and the conductivity σ_2 of the cylinder is 10^{-3} mhos/m.

It is seen that an error of about 3% has been obtained with 20 sampled values on the half-space contour and 40 sampled values on the cylinder contour. This accuracy is not surprising since it was observed in section (5-3) that solution accuracy was poorest when the reflection coefficient was small. (In this case, the reflection coefficient is

zero.) However, it does indicate that when the reflection coefficient on the cylinder is small, the numerical results will have an error of less than 3% of the half-space value.

Figs. 80 through 84 give the convergent numerical solution for scattering from a circular cylinder in a conductive half-space. We have assumed normal incidence of an E_y-polarized plane wave and that: the height Z_0 of the point of observation above the half-space is 1 m, the depth Z_1 from the half-space to the cylinder is 20 m, the cylinder radius is 100 m, the incident field frequency is 1000 hz, the conductivity σ_0 of air is 0., the conductivity σ_1 of the half-space is 10^{-3} mhos/m, and the conductivity σ_2 of the cylinder is 10^{-1} mhos/m. The topographic profile has been sampled 41 times between (-2100, + 2100) and the cylinder contour has been sampled 30 times. It is estimated that with these parameters an error of less than 2% of the peak value of $\vec{H}$ has been obtained.

Fig. 80 shows that the peak value of real (H_x) for a circular cylinder in a conductive half-space is about 10% greater than that obtained for scattering from a circular cylinder in a conductive whole-space when the field transmitted into the half-space is taken as the field incident upon the cylinder. It should be remembered that this whole-space solution ignores coupling between the cylinder and the earth-air interface, and the boundary condition which must be met by the scattered field at the earth-air interface. The large response of real (H_x) observed on the flanks of the anomaly is due mainly to the magnetic field intensity reflected from a homogeneous half-space.

Fig. 81 shows that the peak value of real (H_z) is about 10% less

than that obtained for scattering from a circular cylinder in a conductive whole-space when the field transmitted into the half-space is taken as the field incident upon the cylinder. As above, the whole-space solution ignores coupling between the cylinder and the earth-air interface, and the boundary condition which must be met by the scattered field at the earth-air interface. The reason that the peak value of (H_x) is greater than the whole-space solution while the peak value of (H_z) is less is that the horizontal magnetic field intensity reflected from the half-space has not been added to the whole-space scattering solution. This has been done in Fig. 82 and it is seen that now the peak value of (H_x) is about 20% less than that obtained for a cylinder in a conductive whole-space.

Figs. 83 and 84 show that the effect of coupling between the cylinder and the earth-air interface on the induced surface current densities is to reduce the electrical surface current densities by about 10% and the magnetic surface current density by 20% in this example. Note from Fig. 78, however, that the same accuracy cannot be attached to M_s as to K_y.

It is easy to argue that the effect of coupling between the cylinder and the earth-air interface is to decrease the equivalent surface current densities. This is seen by examining the polarization of the fields as they are modified by each boundary:

1) When the incident field is transmitted into the conductive ground, the polarization of the wave remains unchanged at ($+E_y$, $+H_x$).
2) The field scattered by the more highly conducting cylinder will possess an E_y-polarization 180° out of phase with the

incident electric polarization. Directly above the top of the cylinder, the polarization of the scattered field will be $(-E_y , +H_x)$.

3) The field reflected by a dielectric medium back into a conductive medium will have the same electric polarization as the original wave, but the magnetic field intensity will undergo a 180° phase shift. As a result, the polarization of the field reflected back into the ground directly above the cylinder will be $(-E_y , -H_x)$.

The "effective" incident field that is scattered by the cylinder is the sum of fields 1) and 3). Consequently, it is apparent that coupling between the cylinder and the earth-air interface will decrease the equivalent surface current densities.

The surprisingly small coupling effect can be reconciled by noting that the half-space contour in the immediate vicinity of the cylinder is in the static region ($kR << 1$) of the fields scattered by the cylinder. In this region, it appears that the reflection at the half-space interface is small. By analogy, we can examine the response of a sphere in a conductive half-space to a static uniform electric field. The solution to the sphere problem has been investigated by Grant and West (1965, p. 425), and they note that interaction between the sphere and the earth-air interface is less than 10% if $(Z_1 + R) \geq 1.3\ R$, where Z_1 is the depth from the earth-air interface to the top of a sphere of radius R. In Figs. 84 and 85, $(Z_1 + R) = 1.2\ R$ and it is seen that the half-space solution differs from the whole-space solution by 10% for K_y and about 20% for M_s.

To illustrate the convergence of the method for VLF scattering

problems, the field scattered by a circular cylinder has been examined in Fig. 85 assuming that the incident field frequency is 30,000 hz. Further, we have assumed normal incidence of an E_y-polarized plane wave and that: the height Z_o of the point of observation above the half-space is 1 m, the depth Z_1 from the half-space to the top of the cylinder is 19 m, the cylinder radius is 100 m, the incident field frequency is 1000 hz, the conductivity σ_0 of air is 10^{-3} mhos/m, the conductivity σ_1 of the half-space is 10^{-3} mhos/m, and the conductivity σ_2 of the cylinder is 10^{-1} mhos/m.

Since the conductivity of the air and ground are taken to be the same, the numerical solution must reduce to the analytical solution for scattering from a circular cylinder in a conductive whole-space. It is seen that an error of less than 2% of the peak value of real (H_x) has been achieved with 39 sampled values of the topographic contour between (-285, +285) and 30 sampled values of the cylinder contour.

The field scattered when the vertical slab of Fig. 24 is placed in a conductive half-space has been plotted in Figs. 86 through 90. In addition, the vertical field scattered by this slab in a conductive whole-space (Fig. 62) has been plotted in Fig. 87 for comparison of the half-space and the whole-space solutions. We have assumed normal incidence of an E_y-polarized plane wave in this example and that: the height Z_o of the point of observation above the half-space is 1 m, the depth Z_1 from the half-space to the top of the cylinder is 20 m, the incident field frequency is 1000 hz, the conductivity σ_0 of air is 0., the conductivity σ_1 of the half-space is 10^{-3} mhos/m, and the conductivity σ_2 of the cylinder is 10^{-1} mhos/m.

It is evident that the main effect of the half-space is to reduce the amplitude and phase of the scattered field, as was the case for the circular cylinder of Figs. 80. In particular, it is seen that the inflextions of imaginary $\vec{(H)}$ which were observed for scattering from finitely conducting slabs in a conductive whole-space are still present.

It was noted in section (5-4) that these inflextions in imaginary $\vec{(H)}$ were caused by each corner of the slab responding to the incident field. This is seen most clearly in Fig. 89 where the equivalent electric surface current density on the right half of the slab has been plotted. It is evident that the upper right hand corner of the slab, even though it has been smoothed, brings about a negative peak in imaginary (K_y) at a distance of 25 m around the contour from the top of the slab. The upper left hand corner of the slab will bring about a similar response.

Thus, the observed inflexions in imaginary $\vec{(H)}$ can be explained by treating the peak in imaginary (K_y) at each corner as a line source. Whenever the radius of curvature is small, the current density will remain finite but exhibit an increase in magnitude. It should be noted, however, that the work of Mei and Van Bladel (1963b) in studying scattering from perfectly conducting rectangular cylinders indicates that this behaviour does not occur for H_y-polarized incident fields (or at least it will not be as marked).

The field scattered by the topographic profile of Fig. 47 has been considered in Figs. 91 through 95. In this example, we have assumed normal incidence of an E_y-polarized plane wave and that: the height Z_o of the point of observation above the half-space is 150 m, the

incident field frequency is 1000 hz, the conductivity σ_o of air is 0., and the conductivity σ_1 of the half-space is 10^{-3} mhos/m.

In Figs. 91 through 93, imaginary (H_x) has been examined to establish solution convergence. Since imaginary (H_x) is less than 10% of real (H_x), a solution convergence of 1% in Figs. 91 through 93 establishes convergence accurately for other components also. It is evident from Figs. 91 and 92 that an error of about 3% (at the peak value of imaginary (H_x) can be obtained if the contour is sampled 33 times within the contour section (-1100, +1100).

The decrease in accuracy obtained when the contour is sampled 43 times is a result of integration inaccuracies as was discussed for Figs. 72 through 74. This is seen even more clearly in Fig. 92 where the solution has been obtained for an Re of .3 and .55 when the contour has been sampled 57 times between (-1100, +1100). Note that the largest departure from the convergent solution occurs in both Fig. 91 and 92 at x = -900 m, since the integration inaccuracies occur at the edges of the interval (-1100, +1100) where large interval widths have been taken. As in earlier examples, it can be demonstrated also that this is an integration accuracy problem by increasing the sampling density. Consequently, the contour has been sampled twice as frequently between $300 \leq |x| \leq 1100$ as for N = 57, and an Re of .3 was retained. It is evident from Fig. 92 that an accurate solution has been obtained in this manner.

Fig. 93 indicates that a contour section bounded by (-5000, +5000) is sufficient to describe accurately the unknown surface current density. On the basis of Figs. 91 through 93 it is seen that an error of about 3%

(at the peak value of imaginary (H_x), or about .2% at the peak value of real (H_x)) can be achieved if the contour is sampled 43 times within the contour section bounded by (-5000, +5000).

In Figs. 93 and 94, the magnetic field intensity scattered by the hill has been plotted assuming a constant flight level of 150 m above the half-space and a contour flight level of 150 m above the topographic profile. It is seen that as in Fig. 51, the peak electromagnetic response of H_x is reduced by a factor of two by contour flying. However, even by contour flying, there has been an approximate increase in the peak value of real (H_x) of about 6% as a result of topography. It should be noted, however, that this value is approximately one half the response predicted in Chapter 4 when the low surface impedance solution was applied to this problem. (It is interesting to note that in a similar problem, Ward (1967b, p. 271) deduced a topographic response of 10% on the basis of physical reasoning alone.)

It is evident from Fig. 95 that by contour flying the peak response of H_z is reduced by about 10% and the position of the peak value (H_z) shifts away from the cross over. The shift in peak H_z away from the cross over is in accordance with the fact that the point of observation is further from the current sources than when the fields are observed on a constant flight level.

To illustrate the application of the method to the most general problem of scattering from cylinders in a conductive half-space, the field scattered by a vertical slab within a hill has been plotted in Figs. 97 through 102. The geometry of the problem is shown in Fig. 96. In Figs. 97 and 98, we have assumed normal incidence of an E_y-polarized

plane wave and that: the height Z_0 of the point of observation above the half-space is 150 m, the height Z_1 from the half-space to the top of the cylinder is 50 m, the incident field frequency is 1000 hz, the conductivity σ_0 of air is 0., the conductivity σ_1 of the half-space is 10^{-3} mhos/m, and the conductivity σ_2 of the cylinder is 10^{-1} mhos/m.

The field scattered by the hill alone has been plotted for comparison, and it is evident that with these electrical parameters the fields scattered by the slab predominate over those scattered by the hill. It is not evident from a study of imaginary (H_x), however, that the cylinder is a slab. The reason for this is that it could be argued that the inflexion of the peak value of imaginary (H_x) arises from the contribution of the fields scattered by the hill. Nonetheless, it would be possible to identify the scatterer as a slab since the hill does not give rise to the observed inflexion in scattered H_z.

In Figs. 99 and 100, the conductivity of the slab has been increased from 10^{-1} mhos/m to 10. mhos/m. All other parameters of Figs. 97 and 98 remain unchanged. It is seen that the amplitude of the scattered fields has increased and the inflexions in imaginary $\vec{(H)}$ are absent. It is not surprising, however, that these inflexions will disappear as the slab conductivity is increased since we observed in Figs. 25 through 28 that they are not present when the slab is assumed to be perfectly conducting.

In Figs. 101 and 102, the conductivity of the half-space has been decreased from 10^{-3} mhos/m to 10^{-4} mhos/m, but all other parameters of Figs. 97 and 98 remain the same. It is evident again that the amplitude of the scattered fields has increased and the inflexions in imaginary $\vec{(H)}$ are absent. In addition, it is seen that the fields scattered by

the hill are only about 2% different from the half-space value. Note, however, that topography still is important since if modifies the field transmitted into the half-space from a plane wave to a wave propagating normally away from the hill profile.

The increased amplitude observed when the ground conductivity has been decreased is expected from Fig. 36 since λ/A , where A is the largest dimension of the body, has increased by a factor of 3. The disappearance of the inflexions in imaginary $(\vec{H})$, however, was not anticipated. A study of imaginary (K_y) around the slab contour indicates that there is a slight increase in the magnitude of imaginary (K_y) at the corners, but not as marked as in Figs. 97 and 98 and not sufficient to be observed on a plane of observation 150 m above the half-space.

Mei and Van Bladel (1963b) have shown that the current density is singular at the corners of a perfectly conducting rectangular slab when the incident field is an E_y-polarized plane wave. Figs. 25 and 26 indicate that the current density on a perfectly conducting slab is well behaved if the corners are rounded as much as in Figs. 24.

Figs. 99 through 102 show that for a large reflection coefficient, no inflexions in imaginary $(\vec{H})$ are observed. However, Figs. 97 and 98 indicate that inflexions are observed with a smaller reflection coefficient. Thus, we conclude that the inflexions observed in imaginary $(\vec{H})$ over wide slabs are dependent upon the reflection coefficient and the radius of curvature at the slab corners.

CHAPTER 8

CONCLUSIONS

8-1 Summary

The purpose of this dissertation has been to consider the theory of integral representations as applied to the solution of two-dimensional geophysical scattering problems. The examples given have demonstrated that for two-dimensional source problems, equations (2-56), (2-57), (2-66), and (2-67) are the most general integral representations of the fields in the exterior (source) region. Similarly, equations (2-72), (2-73), (2-74), and (2-75) are the most general integral representations of the fields in each homogeneous interior (source free) region. In addition, it was shown in section (6-3) that these two-dimensional integral representations can be used to solve for scattering from cylinders assuming three-dimensional source configurations by expanding the primary current distribution and the field it radiates into a Fourier integral over a continuous mode distribution.

Using these integral representations, it was shown that the solution to any two-dimensional scattering problem could be obtained by choosing an appropriate integral representation in each homogeneous region present and solving the resulting integral equation. It was found that for plane wave scattering problems, an error of less than 5% can be obtained without difficulty if $\sigma_{cyl} \geq 10^{-2}$ mhos/m or $\sigma_{cyl}/\sigma_{ground} \geq 10$ for frequencies up to 30,000 hz. Since these cylinders constitute a large proportion of the scatterers encountered in electromagnetic prospecting, this solution

accuracy is considered satisfactory. In those cases where $\sigma_{cyl} < 10^{-2}$ mhos/m or $\sigma_{cyl}/\sigma_{ground} < 10$, the reflection coefficient of the cylinder is small and solution accuracy decreases.

Solution convergence generally was established in several steps:

1) The numerical problem was examined first for the case of scattering from a circular cylinder assuming that the cylinder was about the same size and had the same electrical parameters as the general problem. The conductivity of the air was set equal to the conductivity of the ground and the numerical solution was compared with the analytical solution for scattering from circular cylinders in a conductive whole-space. In this way, a general impression of solution accuracy and convergence was obtained.

2) The width (-a, a) of the contour section required to describe the unknown surface current densities on the half-space was determined for the general problem.

3) The integration accuracy on both the topographic and cylinder contours was decided.

4) The distribution of sampling points necessary on each contour was found by increasing N. Although general rules cannot be given to suggest the sampling densities that might be required, several observations can be made:

   a) The magnitude of the equivalent surface current densities will be large and vary rapidly on those parts of the contour having a small radius of curvature (see Figs. 25, 26, 88 and 89). Conse-

quently, a small sampling interval is required in these regions to represent accurately the surface current densities.

b) The equivalent current densities are equal to the tangential components of the total electromagnetic field quantities on the boundary. Thus, in those problems where attenuation is significant or the incident field strength falls off rapidly, the scattered field is determined primarily by that portion of the scatterer contour closest to the source and point of observation. Consequently, small sampling intervals are required in these regions only. (For example, see the fields scattered by a circular cylinder in the presence of an electric line source, Figs. 65 through 68.)

5) Although not always investigated, an estimate of the size of numerical round-off with the above numerical parameters can be obtained by setting all conductivities equal to that of the half-space (see Fig. 60).

It is important to note that in those examples where integration accuracy was not maintained (see Figs. 13 through 18, 72, 73, and 88), the result was apparent as an oscillatory behaviour in scattered $\vec{H}$ when none was anticipated.

It would be misleading to state that the program accompanying this thesis solves the problem of scattering from a vertical slab buried under a hill (Figs. 95-97) in 2 minutes on a CDC 6600, or equivalently, about

10 minutes on a CDC 6400. The reason for this is that the convergence tests listed above require a considerable amount of computer time before the desired equivalent surface current densities can be computed. However, it should be remembered that once an accurate estimate of K and M has been obtained, the fields can be studied in detail using a small amount of computer time since it is only necessary to solve the integral equations once for each scattering problem.

It would appear that solution accuracy can be improved and/or solution time reduced in several ways:

1) The work of Zaki (1969) can be followed to account for contour curvature.
2) The work of Green (1965) in studying finite difference problems indicates that it might be possible to extrapolate the results obtained at several sampling densities to a more accurate solution.

8-2 Conclusions

As a result of applying integral representations to investigate geophysical scattering problems (assuming normal incidence of an E_y-polarized plane wave in most cases), the following important observations and conclusions have been reached.

1) The phase of $\vec{H}$ is dependent upon the position of the observer in space, even for perfectly conducting scatterers (see Figs. 27 and 28).
2) The phase of $\vec{H}$ normally is not zero, even for perfectly con-

ducting scatterers because of the importance of the axial electric field intensity (see Fig. 37).

3) Coupling reduces the induced surface current densities approximately 10% to 20% assuming a standard ground conductivity of 10^{-3} mhos/m, a cylinder conductivity of 10^{-1} mhos/m, a frequency of 1000 hz, and a separation of 20 m between the top of the conductor and the half-space (see Figs. 83 and 84).

4) Inflexions in imaginary $(\tilde{H})$ can occur in the field scattered by a single conductor if the radius of curvature on the upper portion of a finitely conducting scatterer is small at several sites (see Figs. 86 through 90). These inflexions are dependent upon the radius of curvature and the reflection coefficient on the slab contour (see Figs. 97 through 102). Note, however, that these results probably are applicable to E_y-polarized incident fields only.

5) A smooth hill 600 m wide and 100 m high with a maximum slope of 31° increases real (H_x) approximately 11% over that field reflected by a flat half-space assuming a standard ground conductivity of 10^{-3} mhos/m and a constant flight level of 150 m. The result of contour flying over this hill at 150 m is to reduce the peak horizontal response of the hill by a factor of two and yield a constant field intensity over the central position of the hill. The peak response of H_z is reduced about 10% and shifted away from the cross

over (see Figs. 94 and 95). When the conductivity of the ground is reduced to 10^{-4} mhos/m, the fields scattered by the hill are less than 2% different from the half-space values (see Figs. 101 and 102).

8-3 Extensions and Applications

The above observations and conclusions were reached in demonstrating the validity and utility of the integral representations. It is clear that many important questions will be answered when a general numerical analysis of scattering from cylinders in a conductive half-space is undertaken. Furthermore, the work can be extended to study some of the most basic scattering problems encountered in geophysical exploration. Some of the general problems which now can be investigated include the following:

1) The effects of overburden on the scattered field can be studied like the half-space solution by choosing a fourth integral representation in the homogeneous overburden layer. Outside (-a, a) we assume that the layer is flat and the equivalent surface current densities arise from the primary field incident upon a flat layer overlying a conductive half-space. Alternatively, a finite overburden layer can be considered by treating the overburden as having a catenary-like cross section.
2) The fields scattered by cylinders in a conductive half-space assuming H_y-polarized incident fields can be examined

by programming the H_y-polarization solutions given in this dissertation.

3) Scattering from multiple conductors can be considered by choosing an integral representation in each additional scatterer present.

4) The magnitude, phase, and geometry of the fields scattered by cylinders in a conductive half-space assuming finite sources can be studied by following the methods outlined in Chapter 6. When the finite dimensions of the dipole become important and/or coupling between the ground and source is important, the techniques of Chapter 6 may not be satisfactory. Instead, the problem should be considered as an antenna scattering problem and the current distribution on the antenna included as an unknown. Work in this direction for dipoles over a lossy earth has been reported in an abstract by Arens and Embry (1968).

5) An analysis of scattering from finitely conducting bodies of revolution can be undertaken by extending the work of Andreasen (1965 a) to include interior integral representations and applying the results to geophysical scattering problems. Note, however, that this solution requires that the incident field be expandable into a set of orthogonal TE and TM modes propagating along the symmetry axis of the body considered.

6) The time response of fields scattered from cylinders of arbitrary cross section can be studied by transforming frequency domain results into the time domain. Although this may not be the most economical manner in which the problem can be solved,

it is straight-forward in principle.

7) Since elastic waves obey the same Helmholtz equation as electromagnetic waves, the analysis of this dissertation can be repeated to investigate seismic scattering problems. Acoustical scattering problems have been investigated in some detail in the literature (for example, see Mitzner (1967b), Copley (1968), and Schenck (1968)), but the results were not applied to seismic exploration problems.

In each of the above cases, an analysis should be undertaken to determine where approximate solutions that have been developed are valid and more expedient. In those situations where approximate solutions are not available, it is important to determine when approximations can be made to the numerical scattering solution. For example:

a) The much simpler solution discussed in Chapter 4 can be used to describe scattering from the cylinder (but not the half-space) whenever the cylinder can be treated accurately as having a low surface impedance.

b) If coupling between the cylinder and the half-space can be ignored, the scattering problem can be considered in several parts and a solution can be obtained more accurately and quickly than if the entire problem were solved once.

The application of the results of this thesis to plane wave scattering by cylinders encountered in geophysical exploration leads to the following important conclusions:

1) In AFMAG surveys, the ratio of real $(\vec{H})$ to imaginary $(\vec{H})$ is a function of traverse position x and ground conductivity σ_1, as well as the cylinder conductivity σ_2. In addition, the magnitude of the scattered field is highly dependent upon the contribution of the electric field intensity $\vec{E}$, so that it cannot be ignored. As a result, investigations such as that by Ward and Fraser (1966) in which the contribution of the electric field intensity and host rock conductivity have been ignored are likely to have a limited application to AFMAG interpretation for cylinders.

2) Topography can give rise to a tilt angle of about 5° at an operating frequency of 1000 hz., ground conductivity of 10^{-3} mhos/m. and normal incidence of an Ey-polarized plane wave according to the analysis presented in Chapter 7. However, before these results can be applied directly to AFMAG interpretation, an investigation must be undertaken in which the incident plane wave can assume an arbitrary polarization and angle of incidence. The reason for this is that in air, the incident AFMAG fields are propagating at grazing angles to the earth-air interface with a vertical electric and horizontal magnetic polarization. This direction of propagation will not affect the conclusions reached in 1) since the field transmitted into the half-space will be propagating normally away from the earth-air interface even for grazing angles of incidence. Thus, both Ey and Hy polarizations are possible.

3) In no case has a zero phase been observed. Even perfectly conducting scatters buried in a conductive half-space will produce an out-of-phase response for plane wave incident fields. This result is particularly significant since early work such as that by Ward and Fraser (1966) had indicated that AFMAG fields scattered by a perfectly conducting cylinder would yield no quadrature response.
4) Conclusions 1) through 3) are equally important for V.L.F.-E.M. studies. The conductivity of the bedrock and the electric field vector must be included in any analysis, and the incident field should possess an arbitrary polarization and angle of incidence.

The above extensions and applications indicate that integral equation formulations represent a powerful technique for solving many of the complicated electromagnetic scattering problems encountered in geophysical exploration. By verifying approximate solutions which have been developed and continuing the analysis of this dissertation where none exist, electromagnetic interpretation in mining geophysics can be based on sound theoretical investigations.

APPENDIX A

DERIVATION OF THE TWO-DIMENSIONAL GREEN'S FUNCTION

The two dimensional Green's function in an infinite region is given in many texts (see Noble, 1962, p. 239), but the proof is generally left to the reader. For this reason and for the sake of completeness, a general derivation of the two-dimensional Green's function is given. It follows a development similar to Fuller (1968) in obtaining the three-dimensional Green's function.

We wish to obtain a particular solution to the inhomogeneous scalar Helmholtz equation.

$$(\nabla^2 + k^2)\, G(x,y,z;x',y',z') = -\delta(x-x')\,\delta(y-y')\,\delta(z-z') \,. \tag{A-1}$$

Assume that both $G(x,y,z;\, x',y',z')$ and $\delta(x-x')\,\delta(y-y')\,\delta(z-z')$ have a Fourier Transform given by

$$\left.\begin{matrix} G(x,y,z;\,x',y',z') \\ \delta(x-x')\,\delta(y-y')\,\delta(z-z') \end{matrix}\right\} = \frac{1}{(2\pi)^3} \int_{-\infty}^{\infty}\!\!\int\!\!\int \left.\begin{matrix} g(k_x,k_y,k_z) \\ 1 \end{matrix}\right\} e^{i[k_x(x-x')+k_y(y-y')+k_z(z-z')]}\, dk_x\, dk_y\, dk_z \,. \tag{A-2}$$

Substituting equations (A-2) into (A-1) and carrying out the operations, we find that a sufficient condition for a solution is

$$g(k_x,k_y,k_z) = \frac{1}{(k_x^2+k_y^2+k_z^2-k^2)} \,. \tag{A-3}$$

Thus,

$$G(x,y,z;x',y',z') = \frac{1}{(2\pi)^3} \int_{-\infty}^{\infty}\!\!\int\!\!\int \frac{e^{i[k_x(x-x')+k_y(y-y')+k_z(z-z')]}}{(k_x^2+k_y^2+k_z^2-k^2)}\, dk_x\, dk_y\, dk_z \,. \tag{A-4}$$

Transforming to polar coordinates such that the position vector $\bar{\lambda}$ is $x\hat{i} + y\hat{j} + z\hat{k}$, then

$$\begin{aligned} &k_x(x-x') + k_y(y-y') + k_z(z-z') = \bar{k}_1 \cdot (\bar{\lambda} - \bar{\lambda}') = k_1 |\bar{\lambda} - \bar{\lambda}'| \cos\theta \\ &k_x^2 + k_y^2 + k_z^2 = k_1^2 \\ &dk_x\, dk_y\, dk_z = k_1^2 \sin\theta\, dk_1\, d\theta\, d\varphi \end{aligned} \qquad \text{(A-5)}$$

Equation (A-4) becomes

$$G(\bar{\lambda}, \bar{\lambda}') = \frac{1}{(2\pi)^3} \int_0^\infty \int_0^\pi \int_0^{2\pi} \frac{e^{ik_1|\bar{\lambda}-\bar{\lambda}'|\cos\theta}}{(k_1^2 - k^2)} k_1^2 \sin\theta\, dk_1\, d\theta\, d\varphi$$

$$= \frac{1}{(2\pi)^2} \int_0^\infty \int_0^\pi \frac{e^{ik_1|\bar{\lambda}-\bar{\lambda}'|\cos\theta}}{(k_1^2 - k^2)} k_1^2 \sin\theta\, dk_1\, d\theta$$

$$= \frac{-i}{4\pi^2 |\bar{\lambda}-\bar{\lambda}'|} \int_0^\infty \frac{k_1}{k_1^2 - k^2} \left(e^{ik_1|\bar{\lambda}-\bar{\lambda}'|} - e^{-ik_1|\bar{\lambda}-\bar{\lambda}'|} \right) dk_1$$

$$= \frac{-i}{4\pi^2 |\bar{\lambda}-\bar{\lambda}'|} \left[\int_0^\infty \frac{k_1 e^{ik_1|\bar{\lambda}-\bar{\lambda}'|}}{(k_1^2 - k^2)} dk_1 + \int_{-\infty}^{0} \frac{\alpha e^{i\alpha|\bar{\lambda}-\bar{\lambda}'|}}{(\alpha^2 - k^2)} d\alpha \right]$$

$$= \frac{-i}{4\pi^2 |\bar{\lambda}-\bar{\lambda}'|} \int_{-\infty}^\infty \frac{k_1 e^{ik_1|\bar{\lambda}-\bar{\lambda}'|}}{(k_1^2 - k^2)} dk_1 \quad . \qquad \text{(A-6)}$$

The integrand of equation (A-6) has poles at $\pm k$ where k is a complex number given by $\alpha + i\beta$. In the complex plane, $k_1 = |k_1| e^{i\theta_1} = |k_1|(\cos\theta_1 + i \sin\theta_1)$. For $0 \leq \theta_1 \leq \pi$, $\sin\theta_1$ is positive, so that

$$e^{ik_1|\bar{\lambda}-\bar{\lambda}'|} = e^{i|\bar{\lambda}-\bar{\lambda}'||k_1|\cos\theta_1} \cdot e^{-|\bar{\lambda}-\bar{\lambda}'||k_1|\sin\theta_1} \quad . \qquad \text{(A-7)}$$

Thus, the integrand of equation (A-6) approaches zero as $k_1 \to \infty$, and we can add the dashed contour shown without changing the value of the integral.

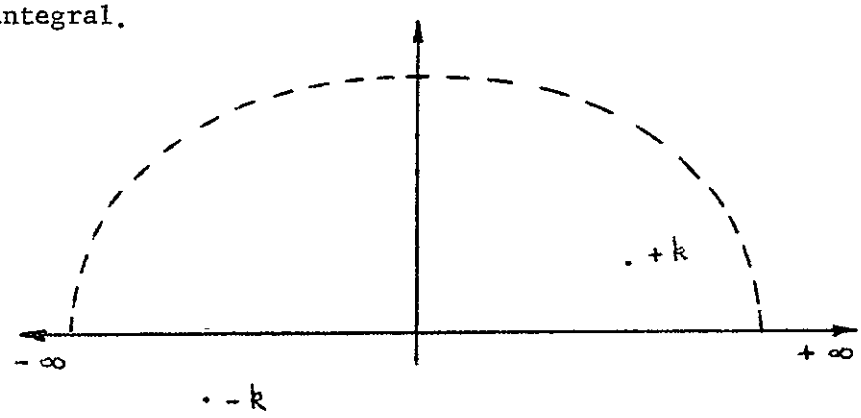

Thus, by Cauchy's Residue Theorem, equation (A-6) becomes

$$G(\bar{x}, \bar{x}') = \frac{e^{ik|\bar{x}-\bar{x}'|}}{4\pi|\bar{x}-\bar{x}'|} \tag{A-8}$$

Equation (A-8) gives the three-dimensional Green's function in an infinite region. The two-dimensional Green's function is obtained by integrating out the axial dependence of equation (A-8). Thus, in two dimensions

$$G(\bar{\rho}, \bar{\rho}') = \frac{1}{4\pi} \int_{-\infty}^{\infty} \frac{e^{ik\sqrt{(x-x')^2 + t^2 + (z-z')^2}}}{\sqrt{(x-x')^2 + t^2 + (z-z')^2}} dt \tag{A-9}$$

where $t = y - y'$.

Ward (1967, p. 131) shows that

$$\frac{1}{4\pi} \int_{-\infty}^{\infty} \frac{e^{ikR}}{R} dy = \frac{1}{2\pi} K_0\left(-ik\sqrt{x^2+y^2}\right) \tag{A-10}$$

where $R = \sqrt{x^2 + y^2 + z^2}$ and K_0 is a modified Bessel function of the second kind of order zero.

We have the relationship from Watson (1966, p. 78) that

$$K_0(t) = \frac{1}{2}\pi i\, e^{\frac{1}{2}0\pi i} H_0^{(1)}(it) \quad , -\pi < \arg t \leq \pi/2 \quad . \tag{A-11}$$

Thus,

$$G(\bar{\rho},\bar{\rho}') = \frac{i}{4} H_0^{(1)}\left(k\sqrt{(x-x')^2+(z-z')^2}\right) = \frac{i}{4} H_0^{(1)}\left(k|\bar{\rho}-\bar{\rho}'|\right). \tag{A-12}$$

APPENDIX B

ALTERNATE DERIVATION OF THE FIELD SCATTERED FROM PERFECTLY CONDUCTING CYLINDERS

We wish to solve for the field scattered from perfectly conducting cylinders in a conductive whole-space, assuming an incident electric field polarization which is parallel to the axial direction of the cylinders. To support this scattered field, we postulate the existence of electric currents which are induced such that the boundary condions on $\vec{E}$ and $\vec{H}$ are satisfied.

We have assumed that E^i possesses an axial component only. Furthermore, we will assume that the incident field is constant in this direction. As a result, the induced currents will possess an axial component only and, from this, the scattered electric field must be axial also.

This scattered electric field must satisfy an inhomogeneous Helmholtz equation given by

$$(\nabla^2 + k^2) E_y^{sc}(\bar{x}) = -i\mu\omega K_y(\bar{x}) \tag{B-1}$$

To solve equation (B-1), assume that both $E_y^{sc}(x,y,z)$ and $K_y(x,y,z)$ have a Fourier Transform given by

$$\left.\begin{matrix} E_y^{sc}(x,y,z) \\ K_y(x,y,z) \end{matrix}\right\} = \frac{1}{(2\pi)^3} \iiint_{-\infty}^{\infty} \left.\begin{matrix} \mathcal{E}(k_x,k_y,k_z) \\ K(k_x,k_y,k_z) \end{matrix}\right\} e^{i(k_x x + k_y y + k_z z)} dk_x\, dk_y\, dk_z \tag{B-2}$$

When equations (B-2) are introduced into equations (B-1) and the operations carried out, we find that a sufficient condition for a solution is

$$\mathcal{E}(k_x, k_y, k_z) = i\mu\omega\, g(k_x, k_y, k_z) \cdot K(k_x, k_y, k_z) , \tag{B-3}$$

where

$$g(k_x, k_y, k_z) = \frac{1}{k_x^2 + k_y^2 + k_z^2 - k^2}$$

Then, by the convolution theorem, we can write the solution in (x,y,z) space as

$$E_y^{sc}(x, y, z) = i\mu\omega\, G(x, y, z) \bigstar K_y(x, y, z) \tag{B-4}$$

where G(x,y,z) is the three-dimensional Green's function and

is the inverse Fourier Transform of $g(k_x, k_y, k_z)$.

Thus,

$$G(x, y, z) = \frac{1}{(2\pi)^3} \iiint_{-\infty}^{\infty} \frac{e^{i(k_x x + k_y y + k_z z)}}{(k_x^2 + k_y^2 + k_z^2 - k^2)} dk_x dk_y dk_z . \tag{B-5}$$

We have evaluated equation (B-5) in Appendix A so that we may write

$$G(x, y, z) = \frac{e^{ikr}}{4\pi r} . \tag{B-6}$$

When equation (B-6) is introduced into equation (B-4), we find that the scattered electric field intensity is given by

$$E_y^{sc}(x, y, z) = \frac{i\mu\omega}{4\pi} \iiint_{-\infty}^{\infty} \frac{K_y(\bar{x}')\, e^{ik|\bar{x} - \bar{x}'|}}{|\bar{x} - \bar{x}'|} dx' dy' dz' \tag{B-7}$$

where

$$|\bar{x} - \bar{x}'| = \sqrt{(x - x')^2 + (y - y')^2 + (z - z')^2} .$$

However, since $K_y(x',y',z')$ is constant along the axial direction, equation (B-7) reduces to

$$E_y^{sc}(x,z) = \frac{j\mu\omega}{4\pi}\int_{-\infty}^{\infty}\int K_y(x',z')\int_{-\infty}^{\infty}\frac{e^{-jk\sqrt{(x-x')^2+(y-y')^2+(z-z')^2}}}{\sqrt{(x-x')^2+(y-y')^2+(z-z')^2}}\,dy'\,dx'\,dz' \qquad \text{(B-8)}$$

This integral has been evaluated also in Appendix A, from which we may write

$$E_y^{sc}(x,z) = -\frac{\mu\omega}{4}\int_{-\infty}^{\infty}\int K_y(x',z')\,H_0^{(1)}\left(k\sqrt{(x-x')^2+(z-z')^2}\right)dx'\,dz'. \qquad \text{(B-9)}$$

Since the cylinders are assumed to be perfectly conducting, $K_y(x',z')$ is a surface current density. Thus, equation (B-9) reduces to a contour integral representation for the scattered electric field intensity.

$$E_y^{sc}(\bar{\rho}) = -\frac{\mu\omega}{4}\int_C K_y(\bar{\rho}')\,H_0^{(1)}\left(k|\bar{\rho}-\bar{\rho}'|\right)ds', \qquad \text{(B-10)}$$

where $|\bar{\rho}-\bar{\rho}'| = \sqrt{(x-x')^2+(z-z')^2}$.

APPENDIX C

SCATTERING FROM A FINITELY CONDUCTING CIRCULAR CYLINDER

The solution for plane wave scattering from a finitely conducting circular cylinder in a conductive whole-space is very important for testing the validity of the integral equation scattering programs which we have developed. A solution which can be compared with that given by Wait (1959) is given below.

If we assume that the incident plane wave is E_y-polarized, then we can write, referring to Fig. 103

$$E_y^i = E_o e^{-ik_1 z'} = E_o e^{ik_1 h} e^{-ik_1 \rho \cos\phi} . \tag{C-1}$$

Using the cylindrical wave transformation given by Harrington (1961, p. 231), equation (C-1) can be rewritten as

$$E_y^i = E_o e^{ik_1 h} \sum_{n=-\infty}^{\infty} i^{-n} J_n(k_1\rho) e^{in\phi} = E_o e^{ik_1 h} \sum_{n=0}^{\infty} i^{-n} \varepsilon_n J_n(k_1\rho) \cos n\phi , \tag{C-2}$$

where $$\varepsilon_n = \begin{cases} 1, & n = 0, \\ 2, & n \geq 1. \end{cases}$$

The total electric field intensity at any point in space is represented by the sum of an incident electric field E_y^i and a scattered electric field E_y^{sc}

$$E_y^t = E_y^i + E_y^{sc} . \tag{C-3}$$

To represent outward-travelling waves external to the cylinder, the scattered field must be of the form

$$E_y^{sc} = E_0 e^{ik_1 h} \sum_{n=0}^{\infty} i^{-n} \varepsilon_n a_n H_n^{(1)}(k_1\rho) \cos n\varphi . \tag{C-4}$$

Inside the cylinder, we expect standing waves which are finite at the origin. Thus, we seek solutions of the form

$$E_y^{int} = E_0 e^{ik_1 h} \sum_{n=0}^{\infty} i^{-n} \varepsilon_n b_n J_n(k_2\rho) \cos n\varphi . \tag{C-5}$$

At the cylinder boundary, the condition that tangential $\vec{E}$ is continuous must be met. Since we equate each coefficient of $\cos n\varphi$, this implies that

$$J_n(k_1 R) + a_n H_n^{(1)}(k_1 R) = b_n J_n(k_2 R) . \tag{C-6}$$

To obtain a second equation between a_n and b_n, we will enforce continuity of tangential $\vec{H}$, that is H_φ. We have from Maxwell's first equation that

$$\vec{H}_n = \frac{-i}{\mu\omega} (\vec{\nabla} \times \vec{E}) = \frac{-i}{\mu\omega} \left(\frac{1}{\rho} \frac{\partial E_y}{\partial \varphi} \hat{a}_\rho - \frac{\partial E_y}{\partial \rho} \hat{a}_\varphi \right) . \tag{C-7}$$

Thus, from equations (C-2), (C-4) and (C-5), we have that

$$H_\varphi^i = \frac{i E_0}{\mu_1 \omega} e^{ik_1 h} \sum_{n=0}^{\infty} i^{-n} \varepsilon_n J_n'(k_1\rho) \cos n\varphi , \tag{C-8a}$$

$$H_\varphi^{sc} = \frac{i E_0}{\mu_1 \omega} e^{ik_1 h} \sum_{n=0}^{\infty} i^{-n} \varepsilon_n a_n H_n^{(1)\prime}(k_1\rho) \cos n\varphi , \tag{C-8b}$$

$$H_\varphi^{int} = \frac{i E_0}{\mu_2 \omega} e^{ik_1 h} \sum_{n=0}^{\infty} i^{-n} \varepsilon_n b_n J_n'(k_2\rho) \cos n\varphi \,. \qquad \text{(C-8c)}$$

In equations (C-8), differentiation is with respect to ρ. Continuity of tangential $\vec{H}$ implies that

$$Z_2 \left[J_n'(k_1 R) + a_n H_n^{(1)\prime}(k_1 R) \right] = Z_1 b_n J_n'(k_2 R) \,, \qquad \text{(C-9)}$$

where we have equated each coefficient of $\cos n\varphi$, and now differentiation is with respect to the argument (kR) of equation (C-9).

Solving equations (C-6) and (C-9) for a_n, we find that

$$a_n = - \frac{J_n(k_1 R) - c_n J_n'(k_1 R)}{H_n^{(1)}(k_1 R) - c_n H_n^{(1)\prime}(k_1 R)} \,, \qquad \text{(C-10)}$$

where $$c_n = \frac{Z_2 J_n(k_2 R)}{Z_1 J_n'(k_2 R)} \,,$$

$$J_n'(k_1 R) = \frac{n}{k_1 R} J_n(k_1 R) - J_{n+1}(k_1 R) \,,$$

$$J_n'(k_2 R) = \frac{n}{k_2 R} J_n(k_2 R) - J_{n+1}(k_2 R) \,,$$

and

$$H_n^{(1)\prime}(k_1 R) = \frac{n}{k_1 R} H_n^{(1)}(k_1 R) - H_{n+1}^{(1)}(k_1 R) \,.$$

If we set

$$E_0 = Z_1 H_0 \,, \qquad \text{(C-11)}$$

then the scattered electric field intensity is given from equation (C-4) as

$$E_y^{sc}(\rho,\varphi) = Z_1 H_0 e^{ik_1 h} \sum_{n=0}^{\infty} i^{-n} \varepsilon_n a_n H_n^{(1)}(k_1\rho) \cos n\varphi \quad , \tag{C-12}$$

where a_n is given by equation (C-10).

From equations (C-7) and (C-12), the transverse magnetic field intensity is given as

$$H_\rho^{sc}(\rho,\varphi) = \frac{2iH_0}{k_1\rho} e^{ik_1 h} \sum_{n=1}^{\infty} n i^{-n} a_n H_n^{(1)}(k_1\rho) \sin n\varphi \quad , \tag{C-13}$$

and

$$H_\varphi^{sc}(\rho,\varphi) = iH_0 e^{ik_1 h} \sum_{n=0}^{\infty} i^{-n} \varepsilon_n a_n \left\{ \frac{n}{k_1\rho} H_n^{(1)}(k_1\rho) - H_{n+1}^{(1)}(k_1\rho) \right\} \cos n\varphi, \tag{C-14}$$

where a_n is given by equation (C-10).

The equivalent electric and magnetic current densities on the surface of the cylinder, assuming E_y-polarization, are given from equations (2-38a) and (2-39b) as

$$K_y = H_s^t = H_\varphi^t \quad , \tag{C-15}$$

$$M_s = -E_y^t \quad . \tag{C-16}$$

Thus, from equations (C-8a) and (C-8b), the equivalent electric current density is

$$K_y(\varphi) = iH_0 e^{ik_1 h} \sum_{n=0}^{\infty} i^{-n} \varepsilon_n \left(J_n'(k_1 R) + a_n H_n^{(1)\prime}(k_1 R) \right) \cos n\varphi \quad , \tag{C-17}$$

and from equations (C-2) and (C-12), the equivalent magnetic current density is

$$M_s(\theta) = -E_1 H_0 e^{ik_1 h} \sum_{n=0}^{\infty} \varepsilon^{-n} \varepsilon_n \left(J_n(k_1 R) + a_n H_n^{(1)}(k_1 R) \right) \cos n\theta , \tag{C-18}$$

where a_n is given by equation (C-10).

The derivatives in equation (C-17) are with respect to the argument $(k_1 R)$, and are given in equation (C-10).

A useful approximation and check on our solution is to study the asymptotic results as $\sigma_2 \to \infty$. In this case

$$\lim_{\sigma_2 \to \infty} |k_2| = \sqrt{\mu_2 \omega \sigma_2} = \infty . \tag{C-19}$$

Since

$$\lim_{k_2 \to \infty} J_n(k_2 R) = \sqrt{\frac{2}{\pi k_2 R}} \cos\left(k_1 R - \frac{\pi}{4} - \frac{n\pi}{2} \right) , \tag{C-20}$$

(Watson, 1966, p. 195),

then

$$\lim_{k_2 \to \infty} J_n'(k_2 R) = \frac{n}{(k_2 R)^{3/2}} \sqrt{\frac{2}{\pi}} \cos\left(k_1 R - \frac{\pi}{4} - \frac{n\pi}{2} \right) - \sqrt{\frac{2}{\pi k_2 R}} \cos\left(k_1 R - \frac{\pi}{4} - (n+1)\frac{\pi}{2} \right) , \tag{C-21}$$

and

$$\lim_{k_2 \to \infty} \frac{J_n(k_2 R)}{J_n'(k_2 R)} \longrightarrow \frac{\cos\left(k_1 R - \pi/4 - n\pi/2 \right)}{\cos\left(k_1 R - \pi/4 - (n+1)\pi/2 \right)} . \tag{C-22}$$

Thus,

$$\lim_{k_2 \to \infty} C_n = -\lim_{k_2 \to \infty} \frac{\mu_2 k_1 \cos\left(k_1 R - \pi/4 - n\pi/2 \right)}{\mu_1 k_2 \cos\left(k_1 R - \pi/4 - (n+1)\pi/2 \right)} = 0 , \tag{C-23}$$

and hence the reflection coefficient reduces to

$$a_n = - \frac{J_n(k_1 R)}{H_n^{(1)}(k_1 R)} \quad . \tag{C-24}$$

Except for a different time dependency, this is the same reflection coefficient as obtained by Harrington (1961, p.233) for scattering from perfectly conducting cylinders.

Introducing equation (C-24) into equations (C-12), (C-13), and (C-14), the scattered field quantities become

$$E_y^{sc}(\bar{\rho}, \phi) = -Z_1 H_0 e^{ik_1 h} \sum_{n=0}^{\infty} i^{-n} \varepsilon_n \frac{J_n(k_1 R)}{H_n^{(1)}(k_1 R)} H_n^{(1)}(k_1 \rho) \cos n\phi \,, \tag{C-25}$$

$$H_\rho^{sc}(\rho, \phi) = \frac{-2i H_0}{k_1 \rho} e^{ik_1 h} \sum_{n=1}^{\infty} n i^{-n} \frac{J_n(k_1 R)}{H_n^{(1)}(k_1 R)} H_n^{(1)}(k_1 \rho) \sin n\phi \,, \tag{C-26}$$

and

$$H_\phi^{sc}(\bar{\rho}, \phi) = -i H_0 e^{ik_1 h} \sum_{n=0}^{\infty} i^{-n} \varepsilon_n \frac{J_n(k_1 R)}{H_n^{(1)}(k_1 R)} \left\{ \frac{n}{k_1 \rho} H_n^{(1)}(k_1 \rho) - H_{n+1}^{(1)}(k_1 \rho) \right\} \cos n\phi \,. \tag{C-27}$$

The equivalent electric and magnetic current densities reduce to

$$K_y(\phi) = i H_0 e^{ik_1 h} \sum_{n=0}^{\infty} i^{-n} \varepsilon_n \left(J_n'(k_1 R) - \frac{J_n(k_1 R)}{H_n^{(1)}(k_1 R)} H_n^{(1)\prime}(k_1 R) \right) \cos n\phi \,, \tag{C-28}$$

and

$$M_s(\phi) = 0 \,. \tag{C-29}$$

If we introduce the Wronskian relationship (modified from Watson, 1966, p. 77)

$$J_m(k_1R)H^{(1)}_{m+1}(k_1R) - J_{m+1}(k_1R)H^{(1)}_m(k_1R) = -\frac{2i}{\pi k_1 R} \quad , \tag{C-30}$$

then

$$J'_m(k_1R)H^{(1)}_m(k_1R) - J_m(k_1R)H^{(1)\prime}_m(k_1R) = J_m(k_1R)H^{(1)}_{m+1}(k_1R) - J_{m+1}(k_1R)H^{(1)}_m(k_1R)$$

$$= -\frac{2i}{\pi k_1 R} \quad . \tag{C-31}$$

Thus, equation (C-28) reduces to

$$K_y(\varphi) = \frac{2H_o}{\pi k_1 R} e^{ik_1 h} \sum_{m=0}^{\infty} i^{-n} \varepsilon_n \frac{\cos m\varphi}{H^{(1)}_m(k_1R)} \quad . \tag{C-32}$$

APPENDIX D

SOLUTION FOR POINTS OF OBSERVATION CLOSE TO THE SCATTERER CONTOUR

When investigating the scattered fields close to the scatterer contour ($|k||\bar{\rho} - \bar{\rho}'| << 1$), we found that a parabolic approximation to the integrand of each integral was inaccurate across those intervals near the point of observation. This was due to the pseudo-singular behaviour of the Hankel function, and we stated that this problem could be overcome by making a small argument approximation to the Hankel function in this region of the contour integration and integrating the resulting expression analytically.

To integrate analytically, it is convenient to translate the $(x - x', z - z')$ coordinate system to one which has its $\hat{s}'$ axis parallel to the contour interval and its $\hat{\delta}$ axis normal to the interval and through the point of observation. Thus, it is evident from Fig. 104 that this yields

$$\left.\begin{aligned} s' &= -(\bar{\rho} - \bar{\rho}') \cdot \hat{s}' \\ \delta &= (\bar{\rho} - \bar{\rho}') \cdot \hat{\delta} \end{aligned}\right\}, \tag{D-1}$$

Since

$$\left.\begin{aligned} \hat{s}' &= \cos(\alpha + 90^\circ)\hat{x} + \sin(\alpha + 90^\circ)\hat{z} = -\sin\alpha\,\hat{x} + \cos\alpha\,\hat{z} \\ \hat{\delta} &= -\sin(\alpha + 90^\circ)\hat{x} + \cos(\alpha + 90^\circ)\hat{z} = -\cos\alpha\,\hat{x} - \sin\alpha\,\hat{z} \end{aligned}\right\}, \tag{D-2}$$

we find that

$$s' = (x - x')\sin\alpha - (z - z')\cos\alpha \,, \tag{D-3a}$$

$$\delta = -\left[(x - x')\cos\alpha + (z - z')\sin\alpha\right] . \tag{D-3b}$$

Similarly,

$$(x-x') = s'\sin\alpha - \delta\cos\alpha \,, \tag{D-4a}$$

$$(z-z') = -(s'\cos\alpha + \delta\sin\alpha) \,. \tag{D-4b}$$

D-1 Perfectly Conducting Scatterers: E_y-Polarization

The problem of the pseudo-singular behavior of the Hankel function first arises when estimating the surface current density on a perfectly conducting scatterer assuming E_y-polarization. Thus, we must evaluate

$$E_y^i(\bar{\rho}'') = \frac{-k}{4}\int_a^b K_y(\bar{\rho}')\, H_o^{(1)}(k|\bar{\rho}''-\bar{\rho}'|)\, ds' \,, \tag{D-5}$$

for $|k||\bar{\rho}''-\bar{\rho}'| \ll 1$. The surface current density $K_y(\bar{\rho}')$ over this interval is given from equations (3-19) and (3-21) as

$$K_y(s') = \left[1 - \frac{(1-\lambda_j)(s'-c_j)}{\Delta_j} - \frac{(s'-c_j)^2}{\hat{\tau}_j}\right] K_{y_j}$$

$$+\left[\frac{s'-c_j}{\Delta_j(1+\lambda_j)} + \frac{(s'-c_j)^2}{\hat{\tau}_j(1+\lambda_j)}\right] K_{y_{j+1}} - \left[\frac{\lambda_j^2(s'-c_j)}{\Delta_j(1+\lambda_j)} - \frac{\lambda_j(s'-c_j)^2}{\hat{\tau}_j(1+\lambda_j)}\right] K_{y_{j-1}} \,, \tag{D-6}$$

where

$$\Delta_j = w_j + w_{j+1} \,,$$

$$\lambda_j = \frac{w_j + w_{j+1}}{w_j + w_{j-1}} \,,$$

$$\hat{\tau}_j = (w_j + w_{j+1})(w_j + w_{j-1}) \,,$$

$$c_j = (x-x_j)\sin\alpha_j - (z-z_j)\cos\alpha_j \,.$$

When equation (D-6) is introduced into equation (D-5), we find the following solution to our problem:

$$E_j^i(\bar{\rho}'') = \frac{\mu\omega}{4}\left\{\left[HK00 - \frac{(1-\lambda_j)}{\Delta_j}(HK01 - c_j HK00) - \frac{(HK02 - 2c_j HK01 + c_j^2 HK00)}{\tau_j}\right]K_{y_j}\right.$$

$$+ \frac{K_{y_{j+1}}}{1+\lambda_j}\left[\frac{HK01 - c_j HK00}{\Delta_j} + \frac{HK02 - 2c_j HK01 + c_j^2 HK00}{\tau_j}\right]$$

$$\left. - \frac{\lambda_j K_{y_{j-1}}}{1+\lambda_j}\left[\frac{\lambda_j(HK01 - c_j HK00)}{\Delta_j} - \frac{HK02 - 2c_j HK01 + c_j^2 HK00}{\tau_j}\right]\right\}, \quad \text{(D-7)}$$

where
$$HK00 = \int_a^b H_o^{(1)}\left(k\sqrt{\delta^2+s'^2}\right)ds', \quad \text{(D-8a)}$$

$$HK01 = \int_a^b s' H_o^{(1)}\left(k\sqrt{\delta^2+s'^2}\right)ds', \quad \text{(D-8b)}$$

$$HK02 = \int_a^b s'^2 H_o^{(1)}\left(k\sqrt{\delta^2+s'^2}\right)ds'. \quad \text{(D-8c)}$$

Equations (D-8) can be evaluated analytically after $H_o^{(1)}\left(k\sqrt{\delta^2+s'^2}\right)$ has been approximated by equation (3-26). However, the following integrals will be required to carry out this integration:

$$\int \ln\frac{\gamma k}{2}\left(\delta^2+s'^2\right)^{1/2}ds' = s'\ln\frac{\gamma k}{2}\left(s'^2+\delta^2\right)^{1/2} - \left(s' - \delta\tan^{-1}\frac{s'}{\delta}\right) + C, \quad \text{(D-9a)}$$

$$\int s'\ln\frac{\gamma k}{2}\left(\delta^2+s'^2\right)^{1/2}ds' = \frac{1}{2}\left[s'^2\ln\frac{\gamma k}{2}\left(s'^2+\delta^2\right)^{1/2} - \frac{1}{2}\left(s'^2 - \delta^2\ln\left(s'^2+\delta^2\right)\right)\right] + C, \quad \text{(D-9b)}$$

$$\int s'^2\ln\frac{\gamma k}{2}\left(\delta^2+s'^2\right)^{1/2}ds' = \frac{1}{3}\left[s'^3\ln\frac{\gamma k}{2}\left(s'^2+\delta^2\right)^{1/2} - \left(\frac{s'^3}{3} - \delta^2 s' + \delta^3\tan^{-1}\frac{s'}{\delta}\right)\right] + C, \quad \text{(D-9c)}$$

$$\int s'^3\ln\frac{\gamma k}{2}\left(\delta^2+s'^2\right)^{1/2}ds' = \frac{1}{4}\left[s'^4\ln\frac{\gamma k}{2}\left(s'^2+\delta^2\right)^{1/2} - \frac{1}{2}\left(\frac{s'^4}{2} - \delta^2 s'^2 + \delta^4\ln\left(s'^2+\delta^2\right)\right)\right] + C, \quad \text{(D-9d)}$$

$$\int s'^4 \ln \frac{\gamma k}{2} (\delta^2+s'^2)^{1/2} ds' = \frac{1}{5}\left[s'^5 \ln \frac{\gamma k}{2} (s'^2+\delta^2)^{1/2} - \left(\frac{s'^5}{5} - \frac{\delta^2 s'^3}{3} + \delta^4 s' - \delta^5 \tan^{-1}\frac{s'}{\delta}\right)\right] + C , \quad \text{(D-9e)}$$

$$\int s'^5 \ln \frac{\gamma k}{2} (\delta^2+s'^2)^{1/2} ds' = \frac{1}{6}\left[s'^6 \ln \frac{\gamma k}{2} (s'^2+\delta^2)^{1/2} - \frac{1}{2}\left(\frac{s'^6}{3} - \frac{\delta^2 s'^4}{2} + \delta^4 s'^2 - \delta^6 \ln (s'^2+\delta^2)\right)\right] + C , \quad \text{(D-9f)}$$

where we have used the facts that

$$\int f(s') \ln \frac{\gamma k}{2} (\delta^2+s'^2)^{1/2} ds' = \ln \frac{\gamma k}{2} \int f(s') ds' + \frac{1}{2} \int f(s') \ln (s'^2+\delta^2) ds' , \quad \text{(D-10)}$$

$$\int \ln g(s') ds' = s' \ln g(s') - \int \frac{s' g'(s')}{g(s')} ds' , \quad \text{(D-11)}$$

$$\int f(s') \ln g(s') ds' = F(s') \ln g(s') - \int \frac{F(s') g'(s')}{g(s')} ds' , \quad \text{(D-12)}$$

with $$F(s') = \int f(s') ds' ,$$

and g(s') and f(s') are assumed to be rational functions.

Introducing equation (3-26) into equation (D-8a) and carrying out the integration, we find that

$$H_{KOO} \sim \left(1 - \frac{k^2\delta^2}{4}\right)(b-a) - \frac{k^2}{12}(b^3-a^3) + \frac{i}{2\pi}\left\{ k^2\delta^2 (b-a) + \frac{k^2}{3}(b^3-a^3) \right\}$$

$$+ \frac{2i}{\pi}\left\{ b\left(1 - \frac{k^2\delta^2}{4} - \frac{k^2 b^2}{12}\right) \ln \frac{\gamma k}{2} (b^2+\delta^2)^{1/2} - a\left(1 - \frac{k^2\delta^2}{4} - \frac{k^2 a^2}{12}\right) \ln \frac{\gamma k}{2} (a^2+\delta^2)^{1/2} \right.$$

$$\left. + \frac{k^2}{36}(b^3-a^3) - \left(1 - \frac{k^2\delta^2}{6}\right)\left(b-a-\delta\left(\tan^{-1}\frac{b}{\delta} - \tan^{-1}\frac{a}{\delta}\right)\right) \right\} . \quad \text{(D-13)}$$

Similarly, introducing equation (3-26) into equation (D-8b), we find that

$$H_{K01} \sim \frac{1}{2}\left(1-\frac{k^2\delta^2}{4}\right)\left(b^2-a^2\right)-\frac{k^2}{16}\left(b^4-a^4\right)+\frac{i}{4\pi}\left\{k^2\delta^2\left(b^2-a^2\right)+\frac{k^2}{2}\left(b^4-a^4\right)\right\}$$

$$+\frac{i}{\pi}\left\{b^2\left(1-\frac{k^2\delta^2}{4}-\frac{k^2b^2}{8}\right)\ln\frac{\gamma k}{2}\left(b^2+\delta^2\right)^{1/2}-a^2\left(1-\frac{k^2\delta^2}{4}-\frac{k^2a^2}{8}\right)\ln\frac{\gamma k}{2}\left(a^2+\delta^2\right)^{1/2}\right.$$

$$\left.+\frac{k^2}{32}\left(b^4-a^4\right)-\frac{1}{2}\left(1-\frac{k^2\delta^2}{8}\right)\left(b^2-a^2-\delta^2\ln\frac{b^2+\delta^2}{a^2+\delta^2}\right)\right\}. \qquad \text{(D-14)}$$

Finally, introducing equation (3-26) into equation (D-8c), we find that

$$H_{K02} \sim \frac{1}{3}\left(1-\frac{k^2\delta^2}{4}\right)\left(b^3-a^3\right)-\frac{k^2}{20}\left(b^5-a^5\right)+\frac{i}{2\pi}\left\{\frac{k^2\delta^2}{3}\left(b^3-a^3\right)+\frac{k^2}{5}\left(b^5-a^5\right)\right\}$$

$$+\frac{2i}{3\pi}\left\{b^3\left(1-\frac{k^2\delta^2}{4}-\frac{3k^2b^2}{20}\right)\ln\frac{\gamma k}{2}\left(b^2+\delta^2\right)^{1/2}-a^3\left(1-\frac{k^2\delta^2}{4}-\frac{3k^2a^2}{20}\right)\ln\frac{\gamma k}{2}\left(a^2+\delta^2\right)^{1/2}\right.$$

$$\left.+\frac{3k^2}{100}\left(b^5-a^5\right)-\left(1-\frac{k^2\delta^2}{10}\right)\left(\frac{b^3-a^3}{3}-\delta^2\left(b-a-\delta\left(\tan^{-1}\frac{b}{\delta}-\tan^{-1}\frac{a}{\delta}\right)\right)\right)\right\}. \qquad \text{(D-15)}$$

Having estimated the current density on a perfectly conducting scatterer, we now wish to calculate the magnetic field intensity close to the scatterer. Thus,

$$\bar{H}(\bar{\rho}) = \frac{ik}{4}\int_a^b K_y(\bar{\rho}')\,H_1^{(2)}\left(k|\bar{\rho}-\bar{\rho}'|\right)\left[\sin\beta\,\hat{x}-\cos\beta\,\hat{z}\right]ds', \qquad \text{(D-16)}$$

must be evaluated for $|k||\bar{\rho}-\bar{\rho}'|<<1$. Translating our coordinate system via equations (D-4), then

$$\sin\beta = \frac{z-z'}{|\bar{\rho}-\bar{\rho}'|} = -\frac{(s'\cos\alpha+\delta\sin\alpha)}{(\delta^2+s'^2)^{1/2}}, \qquad \text{(D-17a)}$$

and

$$\cos\beta = \frac{x-x'}{|\bar{\rho}-\bar{\rho}'|} = \frac{s'\sin\alpha - \delta\cos\alpha}{(\delta^2+s'^2)^{1/2}} \quad . \tag{D-17b}$$

Thus, after approximating the current density by equation (D-6), the following form of equation (D-16) is obtained:

$$\bar{H} = -\frac{ik}{4}\left[(A\cos\alpha + \delta B\sin\alpha)\hat{x} + (A\sin\alpha - \delta B\cos\alpha)\hat{z}\right] , \tag{D-18}$$

where

$$A = \left[I_2 - \frac{(1-\lambda_j)}{\Delta_j}(I_3 - c_j I_2) - \frac{I_4 - 2c_j I_3 - c_j^2 I_2}{\tilde{\Sigma}_j}\right] K_{y_j}$$

$$+ \frac{K_{y_{j+1}}}{1+\lambda_j}\left[\frac{I_3 - c_j I_2}{\Delta_j} + \frac{I_4 - 2c_j I_3 + c_j^2 I_2}{\tilde{\Sigma}_j}\right]$$

$$- \frac{\lambda_j K_{y_{j-1}}}{1+\lambda_j}\left[\frac{\lambda_j (I_3 - c_j I_2)}{\Delta_j} - \frac{I_4 - 2c_j I_3 + c_j^2 I_2}{\tilde{\Sigma}_j}\right] , \tag{D-19a}$$

$$B = \left[I_1 - \frac{(1-\lambda_j)}{\Delta_j}(I_2 - c_j I_1) - \frac{I_3 - 2c_j I_2 + c_j^2 I_1}{\tilde{\Sigma}_j}\right] K_{y_j}$$

$$+ \frac{K_{y_{j+1}}}{1+\lambda_j}\left[\frac{I_2 - c_j I_1}{\Delta_j} + \frac{I_3 - 2c_j I_2 + c_j^2 I_1}{\tilde{\Sigma}_j}\right]$$

$$- \frac{\lambda_j K_{y_{j-1}}}{1+\lambda_j}\left[\frac{\lambda_j (I_2 - c_j I_1)}{\Delta_j} - \frac{I_3 - 2c_j I_2 + c_j^2 I_1}{\tilde{\Sigma}_j}\right] , \tag{D-19b}$$

$$I_1 = \int_a^b \frac{H_1^{(1)}\left(k\sqrt{\delta^2+s'^2}\right)}{(\delta^2+s'^2)^{1/2}} ds' , \tag{D-20a}$$

$$I_2 = \int_a^b \frac{s' H_1^{(1)}\left(k\sqrt{\delta^2+s'^2}\right)}{(\delta^2+s'^2)^{1/2}} ds' , \tag{D-20b}$$

$$I_3 = \int_a^b \frac{s'^2 H_1^{(1)}\left(k\sqrt{\delta^2+s'^2}\right)}{(\delta^2+s'^2)^{1/2}} ds', \tag{D-20c}$$

$$I_4 = \int_a^b \frac{s'^3 H_1^{(1)}\left(k\sqrt{\delta^2+s'^2}\right)}{(\delta^2+s'^2)^{1/2}} ds'. \tag{D-20d}$$

Introducing equation (3-27) into equation (D-20a) and carrying out the integration, we find that

$$I_1 \sim \frac{k}{2}\left\{ \left(1-\frac{k^2\delta^2}{8}\right)(b-a) - \frac{k^2}{24}(b^3-a^3) - \frac{2i}{\pi}\left[\frac{2}{k^2\delta}\left(\tan^{-1}\frac{b}{\delta} - \tan^{-1}\frac{a}{\delta}\right)\right.\right.$$

$$\left. + \frac{1}{2}\left(1-\frac{5k^2\delta^2}{16}\right)(b-a) - \frac{5k^2}{96}(b^3-a^3)\right]$$

$$+ \frac{2i}{\pi}\left[b\left(1-\frac{k^2\delta^2}{8}-\frac{k^2b^2}{24}\right)\ln\frac{\gamma k}{2}\left(b^2+\delta^2\right)^{1/2} - a\left(1-\frac{k^2\delta^2}{8}-\frac{k^2a^2}{24}\right)\ln\frac{\gamma k}{2}\left(a^2+\delta^2\right)^{1/2}\right.$$

$$\left.\left. + \frac{k^2}{72}(b^3-a^3) - \left(1-\frac{k^2\delta^2}{12}\right)\left(b-a-\delta\left(\tan^{-1}\frac{b}{\delta}-\tan^{-1}\frac{a}{\delta}\right)\right)\right]\right\}. \tag{D-21}$$

Equation (D-20b) can be integrated analytically for all values of the argument, and is given by

$$I_2 = -\frac{1}{k}\int_a^b \frac{d}{ds'}\left[H_0^{(1)}\left(k\sqrt{\delta^2+s'^2}\right)\right] ds' = \frac{1}{k}\left[H_0^{(1)}\left(k\sqrt{a^2+\delta^2}\right) - H_0^{(1)}\left(k\sqrt{b^2+\delta^2}\right)\right]. \tag{D-22}$$

Equations (D-20c) and (D-20d) can be rewritten in terms of equations (D-8a) and (D-8b) through integration by parts. Thus,

$$I_3 = -\frac{1}{k}\int_a^b s'\frac{d}{ds'}\left[H_0^{(1)}\left(k\sqrt{\delta^2+s'^2}\right)\right] ds',$$

$$= \frac{1}{k}\left\{ a H_0^{(1)}\left(k\sqrt{a^2+\delta^2}\right) - b H_0^{(1)}\left(k\sqrt{b^2+\delta^2}\right) + \int_a^b H_0^{(1)}\left(k\sqrt{s'^2+\delta^2}\right) ds'\right\}, \tag{D-23}$$

and

$$I_4 = -\frac{1}{k}\int_a^b s'^2 \frac{d}{ds}\left[H_0^{(1)}\left(k\sqrt{\delta^2+s'^2}\right)\right] ds',$$

$$= \frac{1}{k}\left\{a^2 H_0^{(1)}\left(k\sqrt{a^2+\delta^2}\right) - b^2 H_0^{(1)}\left(k\sqrt{b^2+\delta^2}\right) + 2\int_a^b s' H_0^{(1)}\left(k\sqrt{\delta^2+s'^2}\right) ds'\right\}. \quad \text{(D-24)}$$

The remaining integrals in equations (D-23) and (D-24) have been estimated previously by equations (D-13) and (D-14).

D-2 Perfectly Conducting Scatterers: H_y-Polarization

In estimating the surface current density on a perfectly conducting scatterer assuming H_y-polarization, the expression

$$H_y^i(\bar{\rho}'') = -\frac{K_s(\bar{\rho}'')}{2} - \frac{ik}{4}\int_a^b K_s(\bar{\rho}')\cos(\beta''-\alpha) H_1^{(1)}\left(k|\bar{\rho}''-\bar{\rho}'|\right) ds' \quad \text{(D-25)}$$

must be evaluated for $|k||\bar{\rho}''-\bar{\rho}'| << 1$. Since

$$\cos(\beta''-\alpha) = \frac{-\delta}{\sqrt{\delta^2+s'^2}}, \quad \text{(D-26)}$$

and $K_s(\bar{\rho}')$ is given by equation (D-6), equation (D-25) can be rewritten as

$$H_y^i(\bar{\rho}'') = -\frac{K_s(\bar{\rho}'')}{2} + i\frac{\delta k}{4} B \quad \text{(D-27)}$$

where B is given by (D-19b).

The magnetic field intensity scattered by perfectly conducting cylinders assuming H_y-polarization is given by an expression similar to equation (D-25):

$$H_y^{sc}(\bar{\rho}) = \frac{ik}{4}\int_c K_s(\bar{\rho}')\cos(\beta-\alpha)\,H_1^{(1)}(k|\bar{\rho}-\bar{\rho}'|)\,ds'. \qquad \text{(D-28)}$$

As a result, it is evident that the integration across the jth interval for points of observation close to the contour can be written as

$$H_y^{sc}(\bar{\rho}) = -i\,\frac{\delta k_1}{4}\,B. \qquad \text{(D-29)}$$

D-3 Scatters with Low Surface Impedance: E_y-Polarization

The integrals that are necessary to evaluate the electric field intensity for points of observation near the surface of a highly conducting scatterer assuming E_y-polarization have been estimated also. The expression

$$E_y^i(\bar{\rho}'') = \frac{Z_{2y}(\bar{\rho}'')\,K_y(\bar{\rho}'')}{2} + \frac{\mu\omega}{4}\int_a^b K_y(\bar{\rho}')\,H_0^{(1)}(k|\bar{\rho}''-\bar{\rho}'|)\,ds'$$
$$+ \frac{ik}{4}\int_a^b Z_{2y}(\bar{\rho}')\,K_y(\bar{\rho}')\cos(\beta''-\alpha)\,H_1^{(1)}(k|\bar{\rho}''-\bar{\rho}'|)\,ds', \qquad \text{(D-30)}$$

must be evaluated for $|k||\bar{\rho}''-\bar{\rho}'| << 1$. The first integral has been estimated by equation (D-7) and the second integral is just $Z_{2y}(\bar{\rho}')$ times the integral of equation (D-28) across the jth interval.

However, a rather complex expression results when we wish to estimate the scattered magnetic field intensity close to the contour of highly

conducting scatterers. The expression

$$\vec{H}_{th}(\bar{\rho}) = \frac{ik}{4}\int_a^b K_y(\bar{\rho}')\,H_1^{(1)}(k|\bar{\rho}-\bar{\rho}'|)\left[\sin\beta\,\hat{x} - \cos\beta\,\hat{z}\right]ds'$$

$$+ \frac{k^2}{4\mu\omega}\int_a^b Z_{2y}(\bar{\rho}')K_y(\bar{\rho}')\left\{\left[\cos(\beta-\alpha)\sin\beta\,H_0^{(1)}(k|\bar{\rho}-\bar{\rho}'|) - \frac{H_1^{(1)}(k|\bar{\rho}-\bar{\rho}'|)}{k|\bar{\rho}-\bar{\rho}'|}\sin(2\beta-\alpha)\right]\hat{x}\right.$$

$$\left. - \left[\cos(\beta-\alpha)\cos\beta\,H_0^{(1)}(k|\bar{\rho}-\bar{\rho}'|) - \frac{H_1^{(1)}(k|\bar{\rho}-\bar{\rho}'|)}{k|\bar{\rho}-\bar{\rho}'|}\cos(2\beta-\alpha)\right]\hat{z}\right\}ds' \,, \qquad \text{(D-31)}$$

must be evaluated for $|k||\bar{\rho}-\bar{\rho}'| \ll 1$. Since the first integral has been estimated by equation (D-18), we will consider only the second integral of equation (D-31). Once the trigonometric functions are expressed in the $(s';\delta)$ coordinate system as

$$\sin\beta = -\frac{(s'\cos\alpha + \delta\sin\alpha)}{(\delta^2+s'^2)^{1/2}} \,, \qquad \text{(D-17a)}$$

$$\cos\beta = \frac{s'\sin\alpha - \delta\cos\alpha}{(\delta^2+s'^2)^{1/2}} \,, \qquad \text{(D-17b)}$$

$$\cos(\beta-\alpha) = \cos\beta\cos\alpha + \sin\beta\sin\alpha = \frac{-\delta}{(\delta^2+s'^2)^{1/2}} \,, \qquad \text{(D-26)}$$

$$\sin(\beta-\alpha) = \sin\beta\cos\alpha - \cos\beta\sin\alpha = \frac{-s'}{(\delta^2+s'^2)^{1/2}} \,, \qquad \text{(D-32a)}$$

$$\sin(2\beta-\alpha) = \sin\beta\cos(\beta-\alpha) + \cos\beta\sin(\beta-\alpha) = \frac{(\delta^2-s'^2)\sin\alpha + 2s'\delta\cos\alpha}{(\delta^2+s'^2)} \,, \qquad \text{(D-32b)}$$

$$\cos(2\beta-\alpha) = \cos\beta\cos(\beta-\alpha) - \sin\beta\sin(\beta-\alpha) = \frac{(\delta^2-s'^2)\cos\alpha - 2s'\delta\sin\alpha}{(\delta^2+s'^2)} \,, \qquad \text{(D-32c)}$$

the second integral of equation (D-31) can be written in the form

$$\frac{k^2}{4\mu\omega}\int_a^b Z_{zy}(\bar{\rho}')K_y(\bar{\rho}')\left\{\left[\delta\,(s'\cos\alpha+\delta\sin\alpha)\frac{H_0^{(1)}\left(k\sqrt{\delta^2+s'^2}\right)}{\delta^2+s'^2}-\left((\delta^2-s'^2)\sin\alpha+2s'\delta\cos\alpha\right)\frac{H_1^{(1)}\left(k\sqrt{\delta^2+s'^2}\right)}{k\,(\delta^2+s'^2)^{3/2}}\right]\hat{x}\right.$$

$$\left.+\left[\delta\left(s'\sin\alpha-\delta\cos\alpha\right)\frac{H_0^{(1)}\left(k\sqrt{\delta^2+s'^2}\right)}{\delta^2+s'^2}+\left((\delta^2-s'^2)\cos\alpha-2s'\delta\sin\alpha\right)\frac{H_1^{(1)}\left(k\sqrt{\delta^2+s'^2}\right)}{k\,(\delta^2+s'^2)^{3/2}}\right]\hat{z}\right\}ds'. \tag{D-33}$$

Thus, introducing equation (D-6) into equation (D-33), our solution is

$$\frac{k^2}{4\mu\omega}Z_y(\bar{\rho}')\left\{\left[\delta\left(C\cos\alpha+\delta D\sin\alpha\right)-\frac{1}{k}\left((\delta^2E-F)\sin\alpha+2\delta G\cos\alpha\right)\right]\hat{x}\right.$$

$$\left.+\left[\delta\left(C\sin\alpha-\delta D\cos\alpha\right)+\frac{1}{k}\left((\delta^2E-F)\cos\alpha-2\delta G\sin\alpha\right)\right]\hat{z}\right\}, \tag{D-34}$$

where

$$C=\left[I_6-\frac{(1-\lambda_j)}{\Delta_j}(I_7-c_jI_6)-\frac{(I_8-2c_jI_7+c_j^2I_6}{\tau_j}\right]K_{y_j}$$

$$+\frac{K_{y_{j+1}}}{1+\lambda_j}\left[\frac{I_7-c_jI_6}{\Delta_j}+\frac{I_8-2c_jI_7+c_j^2I_6}{\tau_j}\right]$$

$$-\frac{K_{y_{j-1}}\lambda_j}{1+\lambda_j}\left[\frac{\lambda_j(I_7-c_jI_6)}{\Delta_j}-\frac{I_8-2c_jI_7+c_j^2I_6}{\tau_j}\right], \tag{D-35a}$$

$$D=\left[I_5-\frac{(1-\lambda_j)}{\Delta_j}(I_6-c_jI_5)-\frac{(I_7-2c_jI_6+c_j^2I_5)}{\tau_j}\right]K_{y_j}$$

$$+\frac{K_{y_{j+1}}}{1+\lambda_j}\left[\frac{I_6-c_jI_5}{\Delta_j}+\frac{I_7-2c_jI_6+c_j^2I_5}{\tau_j}\right]$$

$$-\frac{\lambda_jK_{y_{j-1}}}{1+\lambda_j}\left[\frac{\lambda_j(I_6-c_jI_5)}{\Delta_j}-\frac{I_7-2c_jI_6+c_j^2I_5}{\tau_j}\right]K_{y_{j-1}}, \tag{D-35b}$$

$$E = \left[I_9 - \frac{(1-\lambda_j)(I_{10} - c_j I_9)}{\Delta_j} - \frac{(I_{11} - 2c_j I_{10} + c_j^2 I_9)}{\tilde{\tau}_j} \right] K_{y_j}$$

$$+ \frac{K_{y_{j+1}}}{1+\lambda_j} \left[\frac{I_{10} - c_j I_9}{\Delta_j} + \frac{I_{11} - 2c_j I_{10} + c_j^2 I_9}{\tilde{\tau}_j} \right]$$

$$- \frac{\lambda_j K_{y_{j-1}}}{1+\lambda_j} \left[\frac{\lambda_j (I_{10} - c_j I_9)}{\Delta_j} - \frac{I_{11} - 2c_j I_{10} + c_j^2 I_9}{\tilde{\tau}_j} \right], \qquad \text{(D-35c)}$$

$$F = \left[I_{11} - \frac{(1-\lambda_j)(I_{12} - c_j I_{11})}{\Delta_j} - \frac{(I_{13} - 2c_j I_{12} + c_j^2 I_{11})}{\tilde{\tau}_j} \right] K_{y_j}$$

$$+ \frac{K_{y_{j+1}}}{1+\lambda_j} \left[\frac{I_{12} - c_j I_{11}}{\Delta_j} + \frac{I_{13} - 2c_j I_{12} + c_j^2 I_{11}}{\tilde{\tau}_j} \right]$$

$$- \frac{\lambda_j K_{y_{j-1}}}{1+\lambda_j} \left[\frac{\lambda_j (I_{12} - c_j I_{11})}{\Delta_j} - \frac{I_{13} - 2c_j I_{12} + c_j^2 I_{11}}{\tilde{\tau}_j} \right], \qquad \text{(D-35d)}$$

$$G = \left[I_{10} - \frac{(1-\lambda_j)(I_{11} - c_j I_{10})}{\Delta_j} - \frac{(I_{12} - 2c_j I_{11} + c_j^2 I_{10})}{\tilde{\tau}_j} \right] K_{y_j}$$

$$+ \frac{K_{y_{j+1}}}{1+\lambda_j} \left[\frac{I_{11} - c_j I_{10}}{\Delta_j} + \frac{I_{12} - 2c_j I_{11} + c_j^2 I_{10}}{\tilde{\tau}_j} \right]$$

$$- \frac{\lambda_j K_{y_{j-1}}}{1+\lambda_j} \left[\frac{\lambda_j (I_{11} - c_j I_{10})}{\Delta_j} - \frac{I_{12} - 2c_j I_{11} + c_j^2 I_{10}}{\tilde{\tau}_j} \right], \qquad \text{(D-35e)}$$

and

$$I_5 = \int_a^b \frac{H_0^{(1)}(k\sqrt{\delta^2+s'^2})}{\delta^2+s'^2} ds', \qquad \text{(D-36a)}$$

$$I_6 = \int_a^b \frac{s' H_0^{(1)}(k\sqrt{\delta^2+s'^2})}{\delta^2+s'^2} ds', \qquad \text{(D-36b)}$$

$$I_7 = \int_a^b \frac{s'^2 H_0^{(1)}(k\sqrt{\delta^2+s'^2})}{\delta^2+s'^2} ds', \qquad \text{(D-36c)}$$

$$I_8 = \int_a^b \frac{s'^3 H_0^{(1)}(k\sqrt{\delta^2+s'^2})}{\delta^2+s'^2} ds', \qquad \text{(D-36d)}$$

$$I_9 = \int_a^b \frac{H_1^{(1)}(k\sqrt{\delta^2+s'^2})}{(\delta^2+s'^2)^{3/2}} ds', \qquad \text{(D-37a)}$$

$$I_{10} = \int_a^b \frac{s' H_1^{(1)}(k\sqrt{\delta^2+s'^2})}{(\delta^2+s'^2)^{3/2}} ds', \qquad \text{(D-37b)}$$

$$I_{11} = \int_a^b \frac{s'^2 H_1^{(1)}(k\sqrt{\delta^2+s'^2})}{(\delta^2+s'^2)^{3/2}} ds', \qquad \text{(D-37c)}$$

$$I_{12} = \int_a^b \frac{s'^3 H_1^{(1)}(k\sqrt{\delta^2+s'^2})}{(\delta^2+s'^2)^{3/2}} ds', \qquad \text{(D-37d)}$$

$$I_{13} = \int_a^b \frac{s'^4 H_1^{(1)}\left(k\sqrt{\delta^2+s'^2}\right)}{(\delta^2+s'^2)^{3/2}} ds' \,. \tag{D-37e}$$

Before equations (D-36) and (D-37) can be evaluated, the following integrals will be required:

$$\int \frac{\ln \frac{\gamma k}{2} (\delta^2+s'^2)^{1/2}}{\delta^2+s'^2} ds' = \frac{1}{\delta}\left(\ln \frac{\gamma k}{2}\right)\tan^{-1}\frac{s'}{\delta} + \frac{1}{2}\int \frac{\ln(\delta^2+s'^2)}{\delta^2+s'^2} ds' + C, \tag{D-38}$$

and

$$\int \frac{s' \ln \frac{\gamma k}{2} (\delta^2+s'^2)^{1/2}}{\delta^2+s'^2} = \frac{\ln(\delta^2+s'^2)}{2}\left\{\ln\frac{\gamma k}{2} + \frac{1}{4}\ln(\delta^2+s'^2)\right\} + C, \tag{D-39}$$

where equation (D-39) has been obtained through integration by parts.

We can show that the remaining integral in equation (D-38) does not possess a closed form solution by transforming variables according to $s' = \delta x$. Thus,

$$\int_a^b \frac{\ln(\delta^2+s'^2)}{\delta^2+s'^2} ds' = \int_{a/\delta}^{b/\delta} \frac{\ln \delta^2(1+x^2)}{\delta(1+x^2)} dx = \frac{\ln\delta^2}{\delta}\tan^{-1}x\Big|_{a/\delta}^{b/\delta} + \frac{1}{\delta}\int_{a/\delta}^{b/\delta} \frac{\ln(1+x^2)dx}{1+x^2} \,. \tag{D-40}$$

The last term of equation (D-40) is given by Gröber and Hofreiter (1961, p. 112) as

$$\int \frac{\ln(1+x^2)}{1+x^2} dx = \frac{1}{2}\ln 4(1+x^2)\cdot\tan^{-1}x\Big|_{a/\delta}^{b/\delta} + \frac{i}{2}\left[\mathcal{L}_2\left(\frac{1+ix}{2}\right) - \mathcal{L}_2\left(\frac{1-ix}{2}\right)\right]\Bigg|_{a/\delta}^{b/\delta} \tag{D-41}$$

where $$\mathcal{L}_2(x) = -\int_0^x \frac{\ln(1-t)}{t}\,dt = \int_0^1 \frac{\ln u}{u-\frac{1}{x}}\,du \;,$$
$$= \sum_{\delta=1}^{\infty} \frac{x^\delta}{\delta^2} \qquad \text{for } |x| \le 1 \tag{D-42}$$

Since the evaluation of (D-41) would involve the numerical calculation of four integrals, the quickest numerical solution would be to evaluate equation (D-38) as it is written. However, by rewriting the integral of (D-38) as

$$\int_a^{\delta/30} \frac{\ln(s'^2+\delta^2)}{s'^2+\delta^2}\,ds' + \int_{\delta/30}^{30\delta} \frac{\ln(s'^2+\delta^2)}{s'^2+\delta^2}\,ds' + \int_{30\delta}^{b} \frac{\ln(s'^2+\delta^2)}{s'^2+\delta^2}\,ds'$$

$$\sim \frac{1}{\delta^2}(\ln\delta)\left(\frac{\delta}{30}-a\right) + \int_{\delta/30}^{30\delta} \frac{\ln(s'^2+\delta^2)}{s'^2+\delta^2}\,ds' - 2\left[\frac{\ln b+1}{b} - \frac{\ln 30\delta+1}{30\delta}\right] \;,$$

where we have assumed that $a < \delta < b$, the numerical integration is performed over the smallest width necessary.

Introducing equation (3-26) into equation (D-36a) and carrying out the integration, we find that

$$I_5 \sim \frac{1}{\delta}\left(\tan^{-1}\frac{b}{\delta} - \tan^{-1}\frac{a}{\delta}\right) - \frac{k^2}{4}(b-a)\left(1-\frac{2i}{\pi}\right)$$

$$+ \frac{2i}{\pi}\left\{\frac{1}{\delta}\ln\frac{\gamma k}{2}\left(\tan^{-1}\frac{b}{\delta} - \tan^{-1}\frac{a}{\delta}\right) + \frac{1}{2}I(a,b)\right.$$

$$\left. - \frac{k^2}{4}\left[b\ln\frac{\gamma k}{2}(b^2+\delta^2)^{1/2} - a\ln\frac{\gamma k}{2}(a^2+\delta^2)^{1/2} - \left(b-a-\delta\left(\tan^{-1}\frac{b}{\delta} - \tan^{-1}\frac{a}{\delta}\right)\right)\right]\right\}, \tag{D-43}$$

where

$$I(a,b) = \int_a^b \frac{\ln(s'^2+\delta^2)}{s'^2+\delta^2}\,ds' \;. \tag{D-44}$$

Similarly, introducing equation (3-26) into equation (D-36b), we find that

$$I_6 \sim \frac{1}{2}\ln\frac{b^2+\delta^2}{a^2+\delta^2} - \frac{k^2}{8}(b^2-a^2)\left(1-\frac{2i}{\pi}\right) + \frac{i}{\pi}\left\{\ln\frac{\gamma k}{2}\cdot\ln\frac{b^2+\delta^2}{a^2+\delta^2}\right.$$

$$+\frac{1}{4}\left(\ln^2(b^2+\delta^2) - \ln^2(a^2+\delta^2)\right) - \frac{k^2}{4}\left[b^2\ln\frac{\gamma k}{2}(b^2+\delta^2)^{1/2}\right.$$

$$\left.\left. - a^2\ln\frac{\gamma k}{2}(a^2+\delta^2)^{1/2} - \frac{1}{2}\left(b^2-a^2-\delta^2\ln\frac{b^2+\delta^2}{a^2+\delta^2}\right)\right]\right\}. \qquad \text{(D-45)}$$

By rewriting equations (D-36c) and (D-36d) in terms of proper fractions, we obtain integrals that have been estimated already. Thus,

$$I_7 = \int_a^b H_0^{(1)}\left(k\sqrt{\delta^2+s'^2}\right)ds' - \delta^2\int_a^b \frac{H_0^{(1)}\left(k\sqrt{\delta^2+s'^2}\right)ds'}{\delta^2+s'^2}, \qquad \text{(D-46)}$$

where the first integral has been estimated by equation (D-13) and the second integral has been estimated by equation (D-43).

Similarly, equation (D-36d) becomes

$$I_8 = \int_a^b s' H_0^{(1)}\left(k\sqrt{\delta^2+s'^2}\right)ds' - \delta^2\int_a^b \frac{s' H_0^{(1)}\left(k\sqrt{\delta^2+s'^2}\right)ds'}{\delta^2+s'^2}, \qquad \text{(D-47)}$$

where the integrals have been estimated by equations (D-14) and (D-45) respectively.

Introducing equation (3-27) into equation (D-37a) and carrying out the integration, we find that

$$I_9 \sim \frac{k}{2}\left[\frac{1}{\delta}\left(\tan^{-1}\frac{b}{\delta} - \tan^{-1}\frac{a}{\delta}\right) - \frac{k^2}{8}(b-a) - \frac{2i}{\pi}\left\{\frac{1}{k^2\delta^2}\left(\frac{b}{b^2+\delta^2} - \frac{a}{a^2+\delta^2}\right)\right.\right.$$

$$+ \frac{1}{\delta}\left(\frac{1}{k^2\delta^2} + \frac{1}{2} - \ln\frac{\gamma k}{2}\right)\left(\tan^{-1}\frac{b}{\delta} - \tan^{-1}\frac{a}{\delta}\right) - \frac{5k^2}{32}(b-a)\Bigg\}$$

$$+ \frac{i}{\tilde{\pi}}\left\{ I(a,b) - \frac{k^2}{4}\left[b\ln\frac{\gamma k}{2}(b^2+\delta^2)^{1/2} - a\ln\frac{\gamma k}{2}(a^2+\delta^2)^{1/2} \right.\right.$$

$$\left.\left. - \left(b-a-\delta\left(\tan^{-1}\frac{b}{\delta} - \tan^{-1}\frac{a}{\delta}\right)\right)\right]\right\}\Bigg], \qquad \text{(D-48)}$$

where I(a,b) is given by equation (D-44).

Equation (D-37b) can be rewritten in terms of integrals already estimated if it is integrated by parts. Thus

$$I_{10} = -\int_a^b \frac{s' H_1^{(1)}(k\sqrt{\delta^2+s'^2})}{(\delta^2+s'^2)^{3/2}}ds' = -\int_a^b H_1^{(1)}(k\sqrt{\delta^2+s'^2})\frac{d}{ds'}\left[\frac{1}{(\delta^2+s'^2)^{1/2}}\right]ds'$$

$$= -\left\{ \frac{H_1^{(1)}(k\sqrt{\delta^2+s'^2})}{(\delta^2+s'^2)^{1/2}}\Bigg|_a^b - k\int_a^b \frac{s' H_0^{(1)}(k\sqrt{\delta^2+s'^2})}{\delta^2+s'^2}ds' + \int_a^b \frac{s' H_1^{(1)}(k\sqrt{\delta^2+s'^2})}{(\delta^2+s'^2)^{3/2}}ds' \right\},$$

or

$$I_{10} = \frac{1}{2}\left\{ \frac{H_1^{(1)}(k\sqrt{a^2+\delta^2})}{(a^2+\delta^2)^{1/2}} - \frac{H_1^{(1)}(k\sqrt{b^2+\delta^2})}{(b^2+\delta^2)^{1/2}} + k\int_a^b \frac{s' H_0^{(1)}(k\sqrt{\delta^2+s'^2})}{\delta^2+s'^2}ds' \right\}, \qquad \text{(D-49)}$$

where the remaining integral has been estimated by equation (D-45).

The remaining three integrals, equations (D-37c), (D-37d) and (D-37e) can be written in terms of estimated integrals by expressing them as proper fractions. Thus, equation (D-37c) becomes

$$I_{11} = \int_a^b \frac{H_1^{(1)}\left(k\sqrt{\delta^2+s'^2}\right)ds'}{(\delta^2+s'^2)^{1/2}} - \delta^2 \int_a^b \frac{H_1^{(1)}\left(k\sqrt{\delta^2+s'^2}\right)ds'}{(\delta^2+s'^2)^{3/2}}, \qquad \text{(D-50)}$$

where the integrals have been estimated by equations (D-21) and (D-48) respectively.

Similarly, equation (D-37d) becomes

$$I_{12} = \int_a^b \frac{s' H_1^{(1)}\left(k\sqrt{\delta^2+s'^2}\right)ds'}{(\delta^2+s'^2)^{1/2}} - \delta^2 \int_a^b \frac{s' H_1^{(1)}\left(k\sqrt{\delta^2+s'^2}\right)ds'}{(\delta^2+s'^2)^{3/2}}, \qquad \text{(D-51)}$$

where the integrals have been estimated by equations (D-22) and (D-49) respectively.

Finally, equation (D-37e) becomes

$$I_{13} = \int_a^b \frac{s'^2 H_1^{(1)}\left(k\sqrt{\delta^2+s'^2}\right)ds'}{(\delta^2+s'^2)^{1/2}} - \delta^2 \int_a^b \frac{s'^2 H_1^{(1)}\left(k\sqrt{\delta^2+s'^2}\right)ds'}{(\delta^2+s'^2)^{3/2}}, \qquad \text{(D-52)}$$

where the integrals have been estimated by equations (D-23) and (D-50) respectively.

APPENDIX E

EVALUATION OF AN INTEGRAL OF THE SONINE-GEGENBAUER TYPE

To obtain the desired integral, we will evaluate

$$\int_0^\infty J_\mu(bs') \frac{H_\nu^{(1)}\left(k\sqrt{s'^2+\delta^2}\right)}{(s'^2+\delta^2)^{\nu/2}} s'^{\mu+1}\, ds' \tag{E-1}$$

first. (E-1) can be rewritten in terms of the modified Bessel function K_ν since we have from Watson (1966, p. 78) that

$$K_\nu(z) = \frac{1}{2}\pi i e^{\frac{\nu}{2}\pi i} H_\nu^{(1)}(iz) \quad , \; -\pi < \arg z \leq \pi/2 \, , \tag{E-2}$$

or

$$H_\nu^{(1)}(z) = \frac{2}{\pi i} e^{-\frac{\nu}{2}\pi i} K_\nu(-iz) \, . \tag{E-3}$$

Consequently, (E-1) becomes

$$\frac{2e^{-\frac{\nu}{2}\pi i}}{\pi i} \int_0^\infty J_\mu(bs') \frac{K_\nu\left(-ik\sqrt{s'^2+\delta^2}\right)}{(s'^2+\delta^2)^{\nu/2}} s'^{\mu+1} ds' \, . \tag{E-4}$$

However, since (E-4) can be considered to be a Hankel transform, we find from formula (35) of Erdelyi et al (1954, p. 72, Vol. 2) that

$$\frac{2e^{-\frac{\nu}{2}\pi i}}{\pi i} \int_0^\infty J_\mu(bs') \frac{K_\nu\left(-ik\sqrt{s'^2+\delta^2}\right)}{(s'^2+\delta^2)^{\nu/2}} s'^{\mu+1} ds'$$

$$= \frac{2e^{-\frac{\nu}{2}\pi i}}{\pi i} \frac{b^\mu}{(-ik)^\nu} \left(\frac{\sqrt{b^2-k^2}}{\delta}\right)^{\nu-\mu-1} K_{\nu-\mu-1}\left(\delta\sqrt{b^2-k^2}\right) \, , \tag{E-5}$$

provided $b>0$, $\mathrm{Im}(k)>0$, $\mathrm{Re}(\delta)>0$, and $\mathrm{Re}(\mu)>-1$.

On rewriting (E-5) in terms of Hankel functions, we find that

$$\int_0^\infty J_\mu(bs')\frac{H_\nu^{(1)}\left(k\sqrt{s'^2+\delta^2}\right)s'^{\mu+1}}{(s'^2+\delta^2)^{\nu/2}}\,ds' = \frac{b^\mu}{k^\nu}\left(\frac{\sqrt{k^2-b^2}}{\delta}\right)^{\nu-\mu-1} H_{\nu-\mu-1}^{(1)}\left(\delta\sqrt{k^2-b^2}\right), \quad \text{(E-6)}$$

provided $b>0$, $\mathrm{Im}(k)>0$, $\mathrm{Re}(\delta)>0$, and $\mathrm{Re}(\mu)>-1$.

Although it is not obvious, it would seem that equation (E-6) is valid in the limit as $\mathrm{Im}(k)$ approaches zero and $\mathrm{Re}(k)$ is greater than zero. This is easy to demonstrate for the special case when all the parameters in (E-6) are real.

Watson (1966, p. 179) gives an integral representation for $H_\nu^{(1)}(z)$ as

$$\frac{1}{\pi i}\int_{0e^{i\omega}}^{\infty e^{i(\pi+\omega)}} u^{-\nu-1} e^{\frac{z}{2}\left(u-\frac{1}{u}\right)}\,du, \quad \text{(E-7)}$$

provided $-\pi<\omega<\pi$ and $|\omega-\arg z|<\pi/2$.

Setting ω equal to zero in (E-7), then (E-1) can be rewritten as

$$\frac{1}{\pi i}\int_0^\infty\int_0^{\infty e^{\pi i}} J_\mu(bs')s'^{\mu+1}\frac{u^{-\nu-1}}{(s'^2+\delta^2)^{\nu/2}} e^{\frac{k}{2}\sqrt{s'^2+\delta^2}\left(u-\frac{1}{u}\right)}\,du\,ds'. \quad \text{(E-8)}$$

On interchanging the order of integration and setting $u=\frac{x}{(s'^2+\delta^2)^{1/2}}$, (E-8) becomes

$$\frac{1}{\pi i}\int_0^{\infty e^{\pi i}} x^{-\nu-1} e^{\frac{k}{2}\left(x-\frac{\delta^2}{x}\right)}\int_0^\infty J_\mu(bs')s'^{\mu+1} e^{-\frac{ks'^2}{2x}}\,ds'\,dx. \quad \text{(E-9)}$$

The inner integral of (E-9) can be evaluated from equation (4) of Watson (1966, p. 394), so that (E-9) becomes

$$\frac{b^\mu}{k^{\mu+1}\pi i}\int_0^{\infty e^{\pi i}} x^{\mu-\nu} e^{\frac{1}{2}\left(\frac{k^2-b^2}{k}x-\frac{k\delta^2}{x}\right)}\,dx, \quad \text{(E-10)}$$

provided $\mathrm{Re}(\mu) > -1$, $\mathrm{Re}(k) > 0$.

Setting $x = \sqrt{k^2 - b^2}\,/\,\delta a$ and assuming for convenience that $k > b$, then (E-10) reduces to an integral representation of the form (E-7). Thus, we find that

$$\int_0^\infty J_\mu(bs') \frac{H_\nu^{(1)}\left(k\sqrt{s'^2+\delta^2}\right) s'^{\mu+1}}{(s'^2+\delta^2)^{\nu/2}}\, ds'$$

$$= \frac{b^\mu}{k^\nu}\left(\frac{\sqrt{k^2-b^2}}{\delta}\right)^{\nu-\mu-1} H_{\nu-\mu-1}^{(1)}\left(\delta\sqrt{k^2-b^2}\right), \qquad \text{(E-11)}$$

provided $k > b > 0$, $\delta > 0$ and $\mathrm{Re}(\mu) > -1$.

By assuming that $k > b$ and that all parameters are real, we have avoided the problem of considering the validity of deformed contours for the integral representation of $H_\nu(z)$ which otherwise would have arisen.

Consequently, it would seem that (E-6) is valid at least in the special case $\mathrm{Re}(k) > b > 0$, $\mathrm{Im}(k) = 0$, and $\mathrm{Re}(\delta) > 0$.

If we take the limit of equation (E-6) as $b \to 0$, we obtain the formula of interest to our scattering problem. Noting that

$$\lim_{b\to 0}\left(J_\mu(bs')\right) \sim \frac{(bs')^\mu}{2^\mu \Gamma(\mu+1)}, \qquad \text{(E-12)}$$

then equation (E-6) reduces to

$$\int_0^\infty \frac{H_\nu^{(1)}\left(k\sqrt{s'^2+\delta^2}\right)}{(s'^2+\delta^2)^{\nu/2}}\, s'^{2\mu+1}\, ds' = \frac{2^\mu \Gamma(\mu+1)}{k^{\mu+1}\delta^{\nu-\mu-1}} H_{\nu-\mu-1}^{(1)}(k\delta), \qquad \text{(E-13)}$$

provided $\mathrm{Re}(k) > 0$, $\mathrm{Im}(k) \geq 0$, $\mathrm{Re}(\delta) > 0$, and $\mathrm{Re}(\mu) > -1$.

It may seem difficult to justify using (E-12) for all s' since

at some point during the integration the product bs' will violate this small argument assumption. However, it can be shown by using a stationary phase argument (see Papoulis, 1962, p. 139) that if b is small enough so that (E-12) is accurate up to that value of s' where the large argument approximation

$$\frac{H_\nu^{(1)}\left(k\sqrt{s'^2+\delta^2}\right)}{\left(s'^2+\delta^2\right)^{\nu/2}}\, s'^{\mu+1} \longrightarrow \sqrt{\frac{2}{\pi k}}\; s'^{\mu-\nu+1/2}\, e^{i\left(ks'-\frac{\pi}{4}-\frac{\nu\pi}{2}\right)} \tag{E-14}$$

is valid, then that part of the integral for which (E-12) is inappropriate contributes a negligible amount to the integral.

It should be noted that (E-13) could have been established by rewriting (E-13) in terms of the modified Bessel function K_ν as was done for equation (E-1). Then, considering (-ik) to be a complex constant and setting $x = (s'^2 + \delta^2)^{1/2}$, the resulting integral can be treated as a K-transform and evaluated using formula (13) of Erdelyi et al (1954, p. 129, Vol. 2). However, since it would have been difficult to confirm the validity of (E-13) for Im(k) equal to zero using this approach, (E-13) was established through (E-1).